



รายงานวิจัยฉบับสมบูรณ์

โครงการ การจำลองโดยวิธีสนามประจุกลศาสตร์ควอนตัมของใอออน ประกอบในน้ำเพื่อศึกษาสมบัติทางโครงสร้างและพลศาสตร์

โดย ผู้ช่วยศาสตราจารย์ คร. วิวัฒน์ วชิรวงศ์กวิน

รายงานวิจัยฉบับสมบูรณ์

โครงการ การจำลองโดยวิธีสนามประจุกลศาสตร์ควอนตัมของใอออน ประกอบในน้ำเพื่อศึกษาสมบัติทางโครงสร้างและพลศาสตร์

คณะผู้วิจัย

สังกัด ผู้ช่วยศาสตราจารย์ ดร. วิวัฒน์ วชิรวงศ์กวิน ภาควิชาเคมี คณะวิทยาศาสตร์ จุฬาลงกรณ์ มหาวิทยาลัย

สนับสนุนโดยสำนักงานคณะกรรมการการอุดมศึกษา และสำนักงานกองทุนสนับสนุนการวิจัย (ความเห็นในรายงานนี้เป็นของผู้วิจัย สกอ. และ สกว. ไม่จำเป็นต้องเห็นด้วยเสมอไป)

กิตติกรรมประกาศ

ผู้วิจัยขอขอบพระคุณอาจารย์วิจัยที่ปรึกษา Prof. Dr. Bernd Michael Rode และ รองศาสตราจารย์ คร. วิทยา เรื่องพรวิสุทธิ์ ที่ให้คำปรึกษาและแนะนำทั้งเรื่องงานวิจัยและการเป็นนักวิจัย ซึ่งโครงการนี้จะ สำเร็จลุล่วงไม่ได้หากไม่มีท่านทั้งสอง

ขอขอบคุณ ผู้ช่วยศาสตราจารย์ คร. ชินพงษ์ กฤตยากรนุพงศ์ อาจารย์ประจำภาควิชาเคมี คณะ วิทยาศาสตร์ มหาวิทยาลัยเทคโนโลยีพระจอมเกล้าธนบุรี และ Prof. Dr. Shigeyoshi Sakaki และ Prof. Dr. Hirofumi Sato มหาวิทยาลัยเกียว โตประเทศญี่ปุ่น ที่ให้ความร่วมมือในการทำงานวิจัยภายใต้โครงการนี้ เป็นอย่างคื

ผู้วิจัยขอขอบพระคุณภาควิชาเคมี คณะวิทยาศาสตร์ จุฬาลงกรณ์มหาวิทยาลัย ที่สนับสนุนและ เอื้อเฟื้อสถานที่ทำงานวิจัย

สุดท้ายขอขอบพระคุณ สำนักงานคณะกรรมการการอุดมศึกษา และสำนักงานกองทุนสนับสนุน การวิจัย ซึ่งเป็นแหล่งทุนภายนอกแรกที่ผู้วิจัยได้รับ รหัสโครงการ: MRG5280241

ชื่อโครงการ: การจำลองโดยวิธีสนามประจุกลศาสตร์ควอนตัมของไอออนประกอบในน้ำเพื่อ

ศึกษาสมบัติทางโครงสร้างและพลศาสตร์

ชื่อนักวิจัย: ผู้ช่วยศาสตราจารย์ คร. วิวัฒน์ วชิรวงศ์กวิน ภาควิชาเคมี คณะวิทยาศาสตร์

จุฬาลงกรณ์มหาวิทยาลัย

Email Address: Viwat.V@Chula.ac.th

ระยะเวลาโครงการ: 16 มีนาคม 2552 – 15 มีนาคม 2554

งานวิจัยนี้ประยุกร์วิธีสนามประจุกลศาสตร์ควอนตัมเพื่อจำลองระบบสารละลายในน้ำของใบ
คาร์บอนเนต ใบซัลเฟต ใบซัลไฟด์ และ ไฮโครคลอริก การวิเคราะห์สมบัติเชิงโครงสร้างและพลศาสตร์ของ
แต่ละระบบให้ผลสอดคล้องกับผลสังเกตจากการทคลอง สเปกตรัมการสั่นของแต่ละระบบคำนวณจากวิธี
วิโลซิตีออโตคอร์ริเลชันฟังก์ชันเพื่อเปรียบเทียบกับผลที่ได้จากการตรวจวัดด้วย Raman และ IR งานวิจัยนี้
เสนอวิธีการตรวจวัดคุณสมบัติเชิงโครงสร้างสำหรับโครงสร้างซับซ้อนที่มีความยุ่งยากกว่าตัวละลายทรง
กลมเดี่ยว จำนวนพันธะไฮโครเจนเฉลี่ยที่เกิดขึ้นระหว่างโมเลกุลตัวละลายและตัวทำละลายเป็นข้อมูลที่
แสดงโครงสร้างการละลายอย่างชัดเจนสำหรับตัวละลายประกอบ วิธีแบบจำลองการอ้างอิงทิศทางของ
อันตรกิริยาภายในสนามการกระจายความหนาแน่นเชิงพื้นที่เป็นอีกวิธีการที่ศึกษาผลกระทบของตัวทำ
ละลายต่อสมบัติเชิงอิเลีกตรอนของตัวละลาย ซึ่งงานวิจัยนี้ประยุกต์วิธีดังกล่าวในการศึกษาการมีระนาบ
ของคาร์บอเนตและในเตรตไอออนในน้ำ ผลการศึกษาแสดงให้เห็นว่าการ์บอเนตไอออนสูญเสียสมมาตร
ของโครงสร้างขณะที่ในเตรตไอออนยังคงมีระนาบของโมเลกุลอยู่

คำสำคัญ: การจำลองโมเลกุลาร์ไคนามิกส์, QMCF, วิโลซิตีออโตคอร์ริเลชันฟังก์ชัน, ใบคาร์บอเนตใอออน, คาร์บอนเนตใอออน, ในเตรตใอออน, ใบซัลเฟตใอออน, ใบซัลไฟค์ใอออน, ไฮโครคลอริก, RISM-SCF-SEDD

Project Code: MRG5280241

Project Title: Quantum mechanical charge field simulation of hydrated composite ions:

Structural and dynamical properties

Investigator: Viwat Vchirawongkwin, Department of Chemistry, Faculty of Science,

Chulalongkorn University

Email Address: Viwat.V@Chula.ac.th

Project Period: 16^{th} March $2009 - 15^{th}$ March 2011

The *ab initio* quantum mechanical charge filed molecular dynamics (QMCF MD) formalism has been applied to simulate the bicarbonate, bisulfate, bisulfide and hydrochloric in aqueous solutions. The structural and dynamical properties of each system were analyzed resulting in a good agreement with the experimental observations. The vibrational spectra were also evaluated from each system by means of the velocity autocorrelation functions (VACFs) to compare with Raman and IR results. We also introduced a method to determine the structural properties for a composite structure that it is more difficult than a single sphere solute. The averaged number of hydrogen bonds between solute and solvent molecules is one of information that it clarifies the hydration shell for the composite solute. The reference interaction site model self-consistent field spatial electron density distribution (RISM-SCF-SEDD) method is another approach to acquire the effect of solvent on the electronic properties of the solute, which applied to study the planarity of carbonate and nitrate ions in aqueous solutions. The results of solution phase presented the symmetry breaking of carbonate ion, while the nitrate ion retains the planarity.

Keyword: Molecular dynamic simulation, QMCF, velocity autocorrelation functions, bicarbonate ion, carbonate ion, nitrate ion, bisulfate ion, bisulfate ion, HCl, RISM-SCF-SEDD

3

Table of Contents

1.	In	troduction	5
2.	М	ethods	6
	2.1.	QMCF MD	6
	2.2.	RISM-SCF-SEDD	7
3.	Re	sults and Discussion	8
	3.1.	Bicarbonate ion in aqueous solution	8
	3.2.	Bisulfate ion in aqueous solution	9
	3.3.	Bisulfide ion in aqueous solution	.0
	3.4.	Dilute aqueous HCl solution	.0
	3.5.	RISM-SCF-SEDD study on the symmetry breaking of carbonate and nitrate anions in	
	aque	ous solution	.1
4.	Co	onclusions	.1
5.	Re	ferences	.2
6.	Οι	ıtput	.6
Αŗ	pend	dix 1	.7

1. Introduction

The understanding of solution is the most important to explain the chemical reaction most of them occur in the liquid phase. The dynamic properties of solute in solvent atmosphere are the challenge subject, providing the information of nonequilibrium processed in solution^{1, 2}. Although the structural properties of hydrated solute are obtained by the diffraction techniques and simulation procedures, only the simulation technique gives the dynamic properties.

The molecular dynamics (MD) method has become a valuable tool in this area as this technique yields not only equilibrium structures of the system but also its dynamical behavior^{1, 3, 4}. The success of a computer simulation depends on a suitable treatment of the inter-particles forces which is related to the employed potential functions describing the interactions between particles. These potentials are often constructed by fitting an analytical formula to a set of ab initio calculation results. Because of the difficulty to construct higher interaction functions than three-body potential functions and the importance of many-body effects to describe the solution system⁵, quantum mechanics (QM) are employed in the MD simulation to treat N-body interactions as well as polarization and charge transfer effects. For a MD simulation containing a few thousand particles, the application of quantum mechanics to treat the entire system is beyond the present technical feasibility. Thus, the most relevant region for example the solute and its first hydration shell is treated by QM, while the rest of the system is treated by molecular mechanics (MM). This approach is referred to as hybrid quantum mechanical/molecular mechanical (QM/MM) method. Potential functions are still required by the conventional QM/MM MD to treat interaction in the MM region as well as to account for the coupling of QM and MM region. This limitation limits the conventional QM/MM MD methodology to solutes with a very simple composition. In this work, a new formalism named the quantum mechanical charge field molecular dynamics (QMCF MD) based on an electrostatic embedding scheme was developed to omit the time-consuming and tedious task of the construction of new potential functions. This method has been succeeded to acquire the structural and dynamical properties for the solute that it has a complicated structure e.g. sulfate 6-8, phosphate⁸ and perchlorate⁸ anions.

A method based on a hybrid method of integral equation theory in statistical mechanics, namely reference interaction site model self-consistent field (RISM-SCF), is an alternative method to the

 QM/MM^{9-13} . This method succeeded to investigate the structural properties of the solute and the solvation effects on the reactions in a solution phase $^{14-18}$.

In this project, we applied the QMCF MD formalism to investigate the properties of bicarbonate, bisulfate and bisulfide anions, and the hydrochloric solutions. The evaluation of structural properties for these composite solutes was introduced by means of the molecular approach. The RISM-SCF formalism was also applied to investigate the optimized geometry of carbonate and nitrate anions in aqueous solution. The classical electrostatic free energy calculation based on the multipole expansion was also utilized as a model to understand the true nature of the symmetry breaking caused by the solvation effect.

2. Methods

2.1. QMCF MD

The *ab initio* quantum mechanical charge field molecular dynamics (QMCF MD) formalism has been outlined in detail elsewhere²¹. Due to the inclusion of an additional quantum mechanically treated solvent *layer zone* located beyond the first hydration shell of the solute species, the QMCF method does not require the construction of potential functions between the solute and water molecules; i.e., it avoids a time-consuming and sometimes hardly manageable task necessary in the conventional quantum mechanical/molecular mechanical molecular dynamics (QM/MM MD) formalism²²⁻²⁵. A further advantage of the QMCF MD method is the inclusion of the point charges of the atoms in the MM region with their changing positions in the core Hamiltonian for the QM region via a perturbation term

$$V' = \sum_{i=1}^{n} \sum_{j=1}^{m} \frac{q_{j}^{\text{MM}}}{r_{ij}} \tag{1}$$

where n is the number of atoms in the QM region, m is the number of atoms in the MM region, q_j^{MM} is the partial charges of these atoms according to the selected water model, and r_{ij} refers to the distance between a pair of particles in the QM (i) and MM (j) regions. On the other hand, the dynamically changing charges of QM particles, q_i^{QM} , determined by population analysis contribute to the force on each atom j in the MM region as Coulombic forces

$$F_j^{\text{QM}\to \text{MM}} = \sum_{i=1}^n \frac{q_i^{\text{QM}} \cdot q_j^{\text{MM}}}{r_{ij}}$$
 (2)

As the conventional QM/MM MD formalism, the QMCF MD method allows the migration of water molecules between the QM and MM region. For this process, one has to apply a smoothing function ²⁶

$$S(r) = \begin{cases} 0 & for \quad r > r_{on} \\ \frac{\left(r_{off}^2 - r^2\right)^2 \left(r_{off}^2 + 2r^2 - 3r_{on}^2\right)}{\left(r_{off}^2 - r_{on}^2\right)^3} & for \quad r_{on} \le r \le r_{off} \\ 1 & for \quad r < r_{off} \end{cases}$$
(3)

where r is the distance of a given solvent molecule from the center of the simulation box, r_{off} is the radius of the QM region, and r_{on} is the inner border of the smoothing region. The formalism is applied to all atoms of molecules located in the smoothing region, ensuring a continuous transition and change of forces for these molecules according to

$$F_{i}^{\text{smooth}} = F_{i}^{\text{MM}} + \left(F_{i}^{\text{layer}} - F_{i}^{\text{MM}}\right) \times S(r)$$

$$\tag{4}$$

where F_j^{layer} is the force acting on a particle j located in the (outer QM) smoothing zone and F_j^{MM} is the force acting on a particle j in the MM region. In this context, it has to be mentioned that energy is not rigorously conserved, but the related error can be considered very minor due to the short simulation time and the large size of the quantum mechanical region.

The dynamical properties of a fluid system related to macroscopic transport coefficients can be evaluated from the velocity autocorrelation functions (VACFs), and their Fourier transformations can be interpreted as the vibrational spectra. The vibrational spectra of bisulfate ion were obtained from the VACFs using normal-coordinate analysis²⁷. The normalized VACF, C(t), is defined as

$$C(t) = \frac{\sum_{i}^{N_{t}} \sum_{j}^{N} v_{j}(t_{i}) v_{j}(t_{i} + t)}{N_{t} N \sum_{i}^{N_{t}} \sum_{j}^{N} v_{j}(t_{i}) v_{j}(t_{i})}$$
(5)

where N is the number of particles, N_t is the number of time origins t_i , and v_j denotes a certain velocity component of the particle j. A correlation length of 2.0 ps was used to obtain the power spectra with 4000 averaged time origins.

2.2. RISM-SCF-SEDD

The RISM-SCF method has been outlined in detail elsewhere ⁹⁻¹³. Similar to the QM/MM, this method evaluates the statistical solvent distribution consistent with the electronic structure of the solute, while the electronic structure of the solute is affected by the surrounding solvent distribution. Thus, both the RISM integral equation and ab initio molecular orbital (MO) calculation must be solved in a self-consistent manner. The statistical mechanics part of the RISM-SCF method was solved with the Kovalenko and

Hirata (KH) closure approximation to obtain the structure of the solvent on a grid of 2048 points on the radial direction, whereas the ab initio MO methods at Hartree-Fock (HF) and density functional theory, namely, Becke, three-parameter, Lee-Yang-Parr exchange-correlation functional (B3LYP), associated with the 6-311+G* basis set 30,31 , were utilized to evaluate the electronic structure of carbonate and nitrate ions in the SCF procedure, so-called RISM-SCF/HF and RISM-SCF/B3LYP, respectively. We further employed the CCSD(T) method coupled with solvation effect (RISM-SCF/CCSD(T)) to obtain highly accurate solvation energy. The SPC water model with the corrected Lennard-Jones parameters of hydrogen sites (σ) 1.0 Å and ε) 0.056 kcal mol⁻¹) was selected for solvent water in the RISM equation.

All solution-phase calculations were performed with the RISM-SCF-SEDD (spatial electron density distribution, SEDD) code¹² implemented in GAMESS program package³³ modified by us. In the theory, the total energy of the system (A) is defined as the sum of the solute potential energy and solvation free energy:

$$A = \left\langle \Psi^{\text{solute}} \middle| H_0 \middle| \Psi^{\text{solute}} \right\rangle + \Delta \mu \tag{6}$$

where H_0 is the standard Hamiltonian of solute in a gas phase, Ψ^{solute} is the wave function of the solute obtained by solving the equation with the modified Fock operator, and $\Delta\mu$ is the solvation free energy evaluated by the KH closure equations.

3. Results and Discussion

This project applied the QMCF MD to simulate bicarbonate, bisulfate, bisulfide and HCl in aqueous solution. The RISM-SCF-SEDD was also applied to study the effect of solvent to the planarity of carbonate and nitrate ions in aqueous solution. All details for each work in this project were presented in the Appendix section.

3.1. Bicarbonate ion in aqueous solution

The structural and dynamical properties of bicarbonate ion in aqueous solution were evaluated by means of specific radial distribution functions (RDFs), coordination number distributions (CNDs), angular distribution functions (ADFs), and ligand mean residence time (MRTs). The molecular aspect was also introduced to determine the hydration shell of the ion. The difference in coordination numbers obtained by summation over atoms (6.6) and for the solvent-accessible surface (5.4) indicates the sharing

of some water molecules between the individual atomic hydration shells. It also proved the importance to consider the hydration of the chemically different atoms individually for the evaluation of structural and dynamical properties of the ion. The mean residence time in the surroundings of the bicarbonate ion classify it generally as a structure-breaking ion, but the analysis of the individual ion-water hydrogen bonds revealed a more complex behavior of the different coordination sites. This work was published in *Journal of Computational Chemistry* ³⁷.

The further analysis of bicarbonate ion was determined by means of the VACFs to clarify the ambiguous assignments of the CO-H stretching (v_1) mode in Raman and IR spectra, published in *Journal* of Molecular Structure: THEOCHEM³⁶. The v_1 spectrum includes inter- and intra-molecular OH stretching modes of hydrated bicarbonate ion and is presented together with the other vibrations, namely the symmetric CO stretching (v_3) , the C-OH stretching (v_5) and the CO₃ out-of-plane deformation (v_8) , modes.

3.2. Bisulfate ion in aqueous solution

The structural and dynamical properties of hydrated bisulfate ion were evaluated from the QMCF MD simulations, published in *The Journal of Physical Chemistry B*³⁵. The averaged geometry of bisulfate ion supports the separation of six normal modes of the O*-SO3 unit with C_{3v} symmetry from three modes of the OH group in the evaluation of vibrational spectra obtained from the velocity autocorrelation functions (VACFs) with subsequent normal coordinate analyses. The calculated frequencies are in good agreement with the observations in Raman and IR experiments. The difference of the averaged coordination number obtained for the whole molecule (8.0) and the summation over coordinating sites (10.9) indicates some water molecules to be located in the overlapping volumes of individual hydration spheres. The averaged number of hydrogen bonds during the simulation period (5.8) indicates that some water molecules are situated in the molecular hydration shell with an unsuitable orientation to form a hydrogen bond with the ion. The mean residence time in the surroundings of the bisulfate ion classify it generally as a weak structure-making ion, but the analysis of the individual sites reveals a more complex behavior of them, in particular a strong interaction with a water molecule at the hydrogen site.

3.3. Bisulfide ion in aqueous solution

The hydration structure of the bisulfide (HS) ion in dilute aqueous solution was characterized by means of an ab initio quantum mechanical charge field (QMCF) molecular dynamics simulation at the Hartree-Fock level employing Dunning double- ζ plus polarization function (DZP) basis sets, also published in *The Journal of Physical Chemistry B*³⁹. An average H-S bond distance of 1.35 Å resulted from the simulation and a hydration shell located at 2.42 Å S_{HS} ····H_w and 3.97 Å HS distances, respectively. At the sulfur site, the average coordination number is 5.9 ± 1.1, while the value for the hydrogen site is 9.2 ± 1.6 . The calculated H_{HS} – S_{HS} stretching frequency of 2752 cm⁻¹ obtained from the QMCF MD simulation is in good agreement with that reported from the Raman spectrum (2570 cm⁻¹) only if a scaling factor of 0.89 is applied. The stability of the nondissociated HS structure is reflected by the force constants of 436.1 and 4.5 N/m determined for the H_{HS} – S_{HS} and H_{HS} ···O_w bonds, respectively. A weak structure-making effect of the hydrated HS- ion results from the mean residence times of 1.5 and 2.1 ps of coordinated water molecules at the sulfur and hydrogen sites of the HS ion, respectively.

3.4. Dilute aqueous HCl solution

Another QMCF MD simulation has been performed to study the structural and dynamical properties of a dilute aqueous HCl solution, published in *Journal of Computational Chemistry*³⁴. The solute molecule HCl and its surrounding water molecules were treated at Hartree-Fock level in conjunction with Dunning double- ζ plus polarization function basis sets. The simulation predicts an average H-Cl bond distance of 1.28 Å, which is in good agreement with the experimental value. The $H_{\text{HCl}} \cdots O_{\text{w}}$ and $Cl_{\text{HCl}} \cdots H_{\text{w}}$ distances of 1.84 and 3.51 Å were found for the first hydration shell. At the hydrogen site of HCl, a single water molecule is the most preferred coordination, whereas an average coordination number of 12 water molecules of the full first shell was observed for the chloride site. The hydrogen bonding at the hydrogen site of HCl is weakened by proton transfer reactions and an associated lability of ligand binding. Two proton transfer processes were observed in the QMCF MD simulation, demonstrating acid dissociation of HCl. A weak structure-making/breaking effect of HCl in water is recognized from the mean residence times of 2.1 and 0.8 ps for ligands in the neighborhood of Cl and H sites of HCl, respectively.

3.5. RISM-SCF-SEDD study on the symmetry breaking of carbonate and nitrate anions in aqueous solution

The planarity of carbonate and nitrate anions was investigated in the gas and solution phases by means of the reference interaction site model self-consistent field spatial electron density distribution (RISM-SCF-SEDD) method. The computed optimized geometries and solvation structures are compared with the diffraction data. In the solution phase, the symmetry of carbonate anion is changed from D_{3h} to C_{3v} , whereas the planarity of nitrate anion is still retained. These are fully consistent with experimental knowledge. The classical electrostatic model was also utilized to elucidate the mechanism of the symmetry breaking. It should be emphasized that the symmetry breaking occurs not only by a specific solvent molecule attaching to the ion but by an overall electrostatic interaction between the infinite number of solvent molecules and the ion. This work was also published in *The Journal of Physical Chemistry B*³⁸.

4. Conclusions

Our structural and dynamical properties obtained from the QMCF MD simulations of hydrated anions and HCl are well compatible with the experimental data. The molecular evaluation of structural properties gives better results than the classical method that it determines such properties on each site of solute molecule. The molecular RDFs show the advantage of this method clarifying the hydration shell comparison to the atomic RDFs, which are unable to characterize the shell. The defined vector projection for each vibration mode coupling with the VACF calculation gives the vibrational frequencies in good agreement with the Raman and IR experiments. With these results, it indicates that the QMCF formalism is suitable to simulate the aqueous solution consisting of composite solute.

The RISM-SCF is another method that it can describe the solvent effect on the electronic structure of solute molecule in the statistical sense. The RDFs were also obtained from the calculations, presenting an excellent agreement with the diffraction results. The symmetry breaking occurs in the carbonate anion in an aqueous solution from D_{3h} to C_{3v} (or lower), while the nitrate anion still retains the planarity in the solution phase. The dynamic picture is also interested for these anion, however; the RISM-SCF is unable to present these properties. This work will be complemented with the QMCF MD simulation for both systems.

5. References

- 1. Ohtaki, H.; Radnai, T., Structure and Dynamics of Hydrated Ions. *Chem. Rev.* **1993**, 93, 1157-1204.
- 2. Helm, L.; Merbach, A. E., Inorganic and Bioinorganic Solvent Exchange Mechanisms. *Chem. Rev.* **2005**, 105, 1923-1959.
- 3. Marcus, Y., Ionic Radii in Aqueous Solutions. Chem. Rev. 1988, 88, 1475-1498.
- 4. Bagchi, B., Water Dynamics in the Hydration Layer around Proteins and Micelles. *Chem. Rev.* **2005**, 105, 3197-3219.
- 5. Allen, M. P.; Tildesley, D. J., Computer Simulation of Liquids. Oxford University Press: 1987.
- Vchirawongkwin, V.; Rode, B. M., Solvation energy and vibrational spectrum of sulfate in water
 An *ab initio* quantum mechanical simulation. *Chem. Phys. Lett.* 2007, 443, 152-157.
- 7. Vchirawongkwin, V.; Rode, B. M.; Persson, I., Structure and Dynamics of Sulfate Ion in Aqueous Solution An ab initio QMCF MD Simulation and Large Angle X-ray Scattering Study. *J. Phys. Chem. B* **2007**, 111, 4150-4155.
- 8. Pribil, A. B.; Hofer, T. S.; Vchirawongkwin, V.; Randolf, B. R.; Rode, B. M., Quantum mechanical simulation studies of molecular vibrations and dynamics of oxo-anions in water. *Chem. Phys.* **2008**, 346, 182-185.
- 9. Ten-no, S.; Hirata, F.; Kato, S., A hybrid approach for the solvent effect on the electronic structure of a solute based on the RISM and Hartree-Fock equations. *Chem. Phys. Lett.* **1993**, 214, (3-4), 391-396.
- 10. Ten-no, S.; Hirata, F.; Kato, S., Reference interaction site model self-consistent field study for solvation effect on carbonyl compounds in aqueous solution. *J. Chem. Phys.* **1994**, 100, (10), 7443-7453.
- 11. Sato, H.; Hirata, F.; Kato, S., Analytical energy gradient for the reference interaction site model multiconfigurational self-consistent-field method: Application to 1,2-difluoroethylene in aqueous solution. *J. Chem. Phys.* **1996**, 105, (4), 1546-1551.
- 12. Yokogawa, D.; Sato, H.; Sakaki, S., New generation of the reference interaction site model self-consistent field method: Introduction of spatial electron density distribution to the solvation theory. *J. Chem. Phys.* **2007**, 126, (24), 244504.

- 13. Yoshida, N.; Ishizuka, R.; Sato, H.; Hirata, F., Ab Initio Theoretical Study of Temperature and Density Dependence of Molecular and Thermodynamic Properties of Water in the Entire Fluid Region: Autoionization Processes. *J. Phys. Chem. B* **2006**, 110, (16), 8451-8458.
- 14. Sato, H.; Hirata, F., Theoretical Study for Autoionization of Liquid Water: Temperature Dependence of the Ionic Product (pKw). *J. Phys. Chem. A* **1998**, 102, (15), 2603–2608.
- 15. Sato, H.; Hirata, F., The syn-/anti-conformational equilibrium of acetic acid in water studied by the RISM-SCF/MCSCF method *J. Mol. Struct. (Theochem)* **1999**, 461-462, 113-120
- 16. Sato, H.; Sakaki, S., Comparison of Electronic Structure Theories for Solvated Molecules: RISM-SCF versus PCM. *J. Phys. Chem. B* **2004**, 108, (9), 1629–1634.
- 17. Iida, K.; Yokogawa, D.; Sato, H.; Sakaki, S., The barrier origin on the reaction of CO2 + OH[—] in aqueous solution *Chem. Phys. Lett.* **2007**, 443, (4-6), 264-268
- 18. Hayaki, S.; Yokogawa, D.; Sato, H.; Sakaki, S., Solvation effects in oxidative addition reaction of Methyliodide to Pt(II) complex: A theoretical study with RISM–SCF method *Chem. Phys. Lett.* **2008**, 458, (4-6), 329-332
- 19. Kirkwood, J. G., Theory of Solutions of Molecules Containing Widely Separated Charges with Special Application to Zwitterions. *J. Chem. Phys.* **1934**, 2, (7), 351-361.
- 20. Kirkwood, J. G.; Westheimer, F. H., The Electrostatic Influence of Substituents on the Dissociation Constants of Organic Acids. I. J. Chem. Phys. 1938, 6, (9), 506-512.
- 21. Rode, B. M.; Hofer, T. S.; Randolf, B. R.; Schwenk, C. F.; Xenides, D.; Vchirawongkwin, V., Ab initio quantum mechanical charge field (QMCF) molecular dynamics: a QM/MM-MD procedure for accurate simulations of ions and complexes. *Theor. Chem. Acc.* **2006**, 115, 77-85.
- 22. Warshel, A.; Levitt, M., Theoretical studies of enzymic reactions: Dielectric, electrostatic and steric stabilization of the carbonium ion in the reaction of lysozyme. *J. Mol. Biol.* **1976**, 103, 227-249.
- 23. Field, M. J.; Bash, P. A.; Karplus, M., A combined quantum mechanical and molecular mechanical potential for molecular dynamics simulations. *J. Comput. Chem.* **1990**, 11, 700-733.
- 24. Gao, J., Potential of mean force for the isomerization of DMF in aqueous solution: a Monte Carlo QM/MM simulation study. *J. Am. Chem. Soc.* **1993,** 115, (7), 2930–2935.
- 25. Bakowies, D.; Thiel, W., Hybrid Models for Combined Quantum Mechanical and Molecular Mechanical Approaches. *J. Phys. Chem.* **1996**, 100, (25), 10580–10594.

- 26. Brooks, B. R.; Bruccoleri, R. E.; Olafson, B. D.; States, D. J.; Swaminathan, S.; Karplus, M., CHARMM: A program for macromolecular energy, minimization, and dynamics calculations. *J. Comput. Chem* **1983**, **4**, (2), 187-217.
- 27. Bopp, P., A study of the vibrational motions of water in an aqueous CaCl2 solution *Chem. Phys.* **1986,** 106, (2), 205-212
- 28. Kovalenko, A.; Hirata, F., Self-consistent description of a metal—water interface by the Kohn–Sham density functional theory and the three-dimensional reference interaction site model. *J. Chem. Phys.* **1999**, 110, 10095-10112.
- 29. Kovalenko, A.; Hirata, F., First-principles realization of a van der Waals–Maxwell theory for water *Chem. Phys. Lett.* **2001**, 349, (5-6), 496-502
- 30. Krishnan, R.; Binkley, J. S.; Seeger, R.; Pople, J. A., Self-consistent molecular orbital methods. XX. A basis set for correlated wave functions. *J. Chem. Phys.* **1980**, 1980, 650-654.
- 31. Clark, T.; Chandrasekhar, J.; Spitznage, G. W.; Schleyer, P. V. R., Efficient diffuse function-augmented basis sets for anion calculations. III. The 3-21+G basis set for first-row elements, Li–F. *J. Comput. Chem* **1983**, 4, (3), 294–301.
- 32. Berendsen, H. J. C., Biophysical applications of molecular dynamics. *Comput. Phys. Commum.* **1987**, 44, (3), 233-242.
- 33. Schmidt, M. W.; Baldridge, K. K.; Boatz, J. A.; Elbert, S. T.; Gordon, M. S.; Jensen, J. H.; Koseki, S.; Matsunaga, N.; Nguyen, K. A.; Su, S.; Windus, T. L.; Dupuis, M.; Jr, J. A. M., General atomic and molecular electronic structure system. *J. Comput. Chem.* **1993**, 14, (11), 1347-1363.
- 34. Kritayakornupong, C.; Vchirawongkwin, V.; Rode, B. M., Ab Initio quantum mechanical charge field molecular dynamics simulation of a dilute aqueous HCl solution. *J. Comput. Chem.* **2010**, 31, 1785-1792.
- 35. Vchirawongkwin, V.; Kritayakornupong, C.; Rode, B. M., Structural and Dynamical Properties and Vibrational Spectra of Bisulfate Ion in Water: A Stady by Ab Initio Quantum Mechanical Charge Field Molecular Dynamics. *J. Phys. Chem. B* **2010**, 114, 11561-11569.
- 36. Vchirawongkwin, V.; Kritayakornupong, C.; Ruangpornvisuti, V.; Rode, B. M., Inter- and intra-molecular OH stretching modes of bicarbonate in aqueous solution. *J. Mol. Struct. (Theochem)* **2009**, 2009, (913), 236-239.

- 37. Vchirawongkwin, V.; Pribil, A. B.; Rode, B. M., Ab Initio quantum mechanical charge field study of hydrated bicarbonate ion: Structural and dynamical properties. *J. Comput. Chem.* **2010,** 31, (2), 249-257.
- 38. Vchirawongkwin, V.; Sato, H.; Sakaki, S., RISM-SCF-SEDD Study on the Symmetry Breaking of Carbonate and Nitrate Anions in Aqueous Solution. *J. Phys. Chem. B* **2010**, 114, 10513-10519.
- 39. Kritayakornupong, C.; Vchirawongkwin, V.; Rode, B. M., Determination of Structure and Dynamics of the Solvated Bisulfide (HS[—]) Ion by ab Initio QMCF Molecular Dynamics. *J. Phys. Chem. B* **2010**, 114, (40), 12883–12887.

6. Output

- 6.1. "Inter- and intra-molecular OH stretching modes of bicarbonate in aqueous solution", Vchirawongkwin, Viwat; Kritayakornupong, Chinapong; Ruangpornvisuti, Vithaya; Rode, Bernd M.; J. Mol. Struct. (Theochem) 2009, 913, 236-239.
- 6.2. "Ab Initio quantum mechanical charge field study of hydrated bicarbonate ion: Structural and dynamical properties", <u>Vchirawongkwin, Viwat</u>; Pribil, Andreas B.; Rode, Bernd M.; *J. Comput. Chem.* 2010, 31, 249-257.
- 6.3. "Ab Initio quantum mechanical charge field molecular dynamics simulation of a dilute aqueous HCl solution", Kritayakornupong, Chinapong; <u>Vchirawongkwin, Viwat</u>; Rode, Bernd M.; *J. Comput. Chem.* 2010, 31, 1785-1792.
- 6.4. "RISM-SCF-SEDD Study on the Symmetry Breaking of Carbonate and Nitrate Anions in Aqueous Solution", <u>Vchirawongkwin</u>, <u>Viwat</u>; Sato, Hirofumi; Sakaki, Shigeyoshi; *J. Phys. Chem. B* 2010, 114, 10513-10519.
- 6.5. "Structural and Dynamical Properties and Vibrational Spectra of Bisulfate Ion in Water: A Study by Ab Initio Quantum Mechanical Charge Field Molecular Dynamics", <u>Vchirawongkwin</u>, <u>Viwat</u>; Kritayakornupong, Chinapong; Rode, Bernd M.; *J. Phys. Chem. B* **2010**, *114*, 11564-11569.
- 6.6. "Determination of Structure and Dynamics of the Solvated Bisulfide (HS-) Ion by ab initio QMCF Molecular Dynamics", Kritayakornupong, Chinapong; <u>Vchirawongkwin, Viwat</u>; Rode, Bernd M.; *J. Phys. Chem. B* 2010, *114*, 12883-12887.

Appendix

Author's personal copy

Journal of Molecular Structure: THEOCHEM 913 (2009) 236-239



Contents lists available at ScienceDirect

Journal of Molecular Structure: THEOCHEM

journal homepage: www.elsevier.com/locate/theochem



Inter- and intra-molecular OH stretching modes of bicarbonate in aqueous solution

Viwat Vchirawongkwin a.*, Chinapong Kritayakornupong b, Vithaya Ruangpornvisuti a, Bernd M. Rode c

- ^a Department of Chemistry, Faculty of Science, Chulalongkorn University, Phyathai Road, Prathumwan, Bangkok 10330, Thailand
- pepartment of Chemistry, Faculty of Science, King Mongkut's University of Technology Thonburi, Bangkok 10140, Thailand
- ^c Theoretical Chemistry Division, Institute of General, Inorganic and Theoretical Chemistry, University of Innsbruck, Innrain 52a, A-6020 Innsbruck, Austria

ARTICLE INFO

Article history: Received 9 July 2009 Received in revised form 28 July 2009 Accepted 3 August 2009 Available online 11 August 2009

Keywords:
Bicarbonate ion
QMCF molecular dynamics
Vibrational spectrum
Velocity autocorrelation functions

ABSTRACT

The ambiguous assignments of the CO-H stretching (ν_1) mode of bicarbonate ion in Raman and IR spectra were clarified based on a careful investigation of hydrogen bonding and its influence on the power spectra evaluated from the velocity autocorrelation functions obtained by an ab initio QMCF MD simulation. The ν_1 spectrum includes inter- and intra-molecular OH stretching modes of hydrated bicarbonate ion and is presented together with the other vibrations, namely the symmetric CO stretching (ν_3) , the C-OH stretching (ν_3) and the CO₃ out-of-plane deformation (ν_8) , modes.

© 2009 Elsevier B.V. All rights reserved.

1. Introduction

The bicarbonate ion, plays important roles in chemical and biological processes. This ion is generated as the major product by the dissolution of carbon dioxide in water in the pH range of 8-10 [1], and also produced by the human carbonic anhydrase II [2,3] to maintain the blood pH at the level suitable for tissues and enzymes activities. Several spectroscopic techniques have been utilised to obtain experimentally quantitative and structural information about the bicarbonate anion dissolved in water [4]. The vibrational frequencies of bicarbonate ion in aqueous solution have been investigated by Raman and infrared (IR) spectroscopy and presented in many publications [4-12]. The deviations of normal frequencies between Raman spectra and theoretical results based on density functional theory (DFT) were less than 150 cm $^{-1}$, except the CO-H stretching mode which differed by ~ 1000 cm $^{-1}$ [10]. The CO-H stretching mode of bicarbonate ion was assigned to a band located around 2600 cm $^{-1}$ in Raman and IR spectra [4–6,10], while the DFT calculation employing the B3LYP/6-31+G * method for bicarbonate ion in a cluster with three water molecules gave the frequency of 3596.5 cm-1 [10]. This significant difference was attributed to the influence of strong anharmonicity [10], implying a scaling factor of 0.723 for correcting the overestimation of this frequency. However, it is well-known that the scaling factors for the B3LYP method are larger than 0.96 [13-15], thus making ambiguous the assignment of this vibrational frequency.

0166-1280/\$ - see front matter © 2009 Elsevier B.V. All rights reserved. doi:10.1016/j.theochem.2009.08.001

Computer simulations have become an alternative tool to elucidate the microscopic solvate properties helpful for the interpretation of experimental observations [16–18]. A recently proposed simulation protocol, namely the *ab initio* quantum mechanical charge field (QMCF) molecular dynamics (MD) formalism [19], has succeeded to determine the vibrational frequencies of tetrahedral sulphate ion [20] and analogous oxo-anions [21]. Here we report the vibrational frequencies of the stretching modes evaluated by means of the velocity autocorrelation functions (VACFs) of the bicarbonate ion in aqueous solution obtained from a QMCF MD simulation [22], associated with the influence of hydrogen-bonds (H-bonds), aiming at clarifying the OH stretching frequency assignments of bicarbonate ion in aqueous solution.

2. Computational details

The QMCF MD simulation protocol has been reported previously [22]. The QMCF MD formalism is based on the conventional quantum mechanical/molecular mechanical (QM/MM) MD method, increasing the size of the QM region by adding a further QM region containing only solvent molecules (layer zone), thus allowing the non-Coulombic interactions between the solute in the inner QM region (core zone) and solvent molecules in the MM region to be neglected. Therefore, the only potential function needed is the one for interaction between solvent molecules. The Coulombic interaction from the point charges of solvent molecules in the MM region to all atoms in the QM region are incorporated via a perturbation term in the core Hamiltonian, while the charges of the atoms in the QM region obtained from population analysis are

^{*} Corresponding author. Fax: +66 (0) 2218 7598. E-mail address: Viwat. V@Chula.ac.th (V. Vchirawongkwin).

V. Vchirawongkwin et al. /Journal of Molecular Structure: THEOCHEM 913 (2009) 236-239

utilised to evaluate the Coulombic interactions with the atoms in the MM part. The simulation was performed in the NVT ensemble using a general predictor-corrector algorithm with a time step of 0.2 fs. The system temperature was maintained at 298.16 K by the Berendsen temperature-scaling algorithm [23] with a relaxation time of 100 fs. The simulation system consisted of one bicarbonate ion and 496 water molecules in a cubic box of 24.65 Å with periodic boundary conditions. The density of the simulation box was $0.997~{\rm g~cm^{-3}}$, i.e. the experimental value of pure water at 298 K. The calculation of forces for the most relevant region, the QM region extended to 5.4 Å with the core radius of 3.2 Å, was performed by means of Hartree-Fock (HF) method with the Dunning double- ζ plus polarisation and diffuse functions (DZP+) basis sets [24-26] for hydrogen, carbon, and oxygen atoms of the bicarbonate ion, and Dunning double-\(\zeta \) plus polarisation function (DZP) basis sets [24-26] for hydrogen and oxygen atoms of water, respectively. The thickness of the smoothing region was chosen as 0.2 Å with the values of r_{on} and r_{off} as 5.2 and 5.4 Å, respectively, according to the radial distribution function (RDF) obtained from the equilibrated simulation. The selected water model applied to calculate the interactions between pairs of water in the MM region was the flexible BJH-CF2 model [27,28], with the cutoff distances of 3.0 and 5.0 Å for non-Coulombic interactions between H atoms and between O and H atoms, respectively. The reaction field method combined with the shifted-force potential technique were applied to account for long-range electrostatic potentials and forces, with a spherical cutoff limit of 12.350 Å. The system was initially equilibrated by performing the QMCF MD simulation for 10 ps (50,000 steps), and a further 10 ps (50,000 steps) were utilised for data sampling [22].

Because of the low symmetry of bicarbonate anion, the number of water molecules within the first hydration shell was evaluated firstly by the determination of the radius of hydration according to the RDFs for each atomic site. These radii were then utilised to determine the coordination number based on the solvent-accessible surface to avoid double-counting of some water molecules within the overlap zone of individual hydration shells, as presented in our previous work, resulting in an average total coordination number of 5.41 [22].

The dynamical properties of a fluid system related to macroscopic transport coefficients can be evaluated from the VACFs, and their Fourier transformations can be interpreted as the vibrational spectra. The vibrational spectra of bicarbonate ion were obtained from the VACFs using normal-coordinate analysis [29]. The normalised VACF, $\mathcal{C}(t)$, is defined as

$$C(t) = \frac{\sum_{i}^{N_{t}} \sum_{j}^{N} v_{j}(t_{i}) v_{j}(t_{i} + t)}{N_{t} N \sum_{i}^{N_{t}} \sum_{j}^{N} v_{j}(t_{i}) v_{j}(t_{i})}$$
(1)

where N is the number of particles, N_t is the number of time origins t_i , and v_j denotes a certain velocity component of the particle j. In order to obtain the vibrational frequencies corresponding to the vibrational motions, the instantanous velocities of hydrogen, carbon and three oxygen atoms of the bicarbonate ion were analysed on the basis of the Raman and IR active harmonic normal modes according to the C1 symmetry. All nine modes of bicarbonate are infrared and Raman active. Due to the main goal of the present work, only four vibrational modes were explicitly defined. The CO-H stretching (v_1) mode is the main target of this work, while the symmetric CO stretching (ν_3), C-OH stretching (ν_5) and CO $_3$ out-of-plane deformation (v_8) modes are employed to determine the ability of QMCF MD formalism to elucidate the dynamical properties of hydrated bicarbonate ion. The atomic motions of these modes are schematically depicted in Fig. 1. The instantaneous H, C and O velocities were decomposed into the necessary smallest fragments. The O velocity was projected onto a unit vector parallel

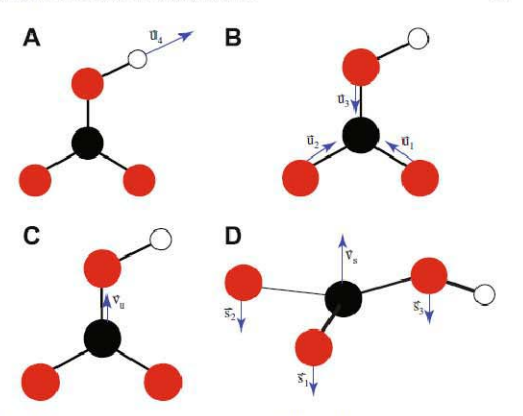


Fig. 1. The defined normal vectors of (A) CO–H stretching (v_1) , (B) symmetric CO stretching (v_3) , (C) C–OH stretching (v_3) and (D) CO₃ out-of-plane deformation (v_8) modes for the bicarbonate ion.

to the corresponding C–O bond ($\vec{u_i}$, i=1 to 3) and a unit vector perpendicular to a normal vector of the O–C–O plane ($\vec{s_i}$, i=1 to 3). The H velocity was projected onto a unit vector parallel to the O–H bond ($\vec{u_i}$). The C velocity was also projected onto a unit vector parallel to the bond between C and O adjacent hydrogen ($\vec{v_u}$) and a unit vector perpendicular to a normal vector of the bicarbonate plane ($\vec{v_s}$). $\vec{U_i}$, $\vec{S_i}$, $\vec{V_u}$ and $\vec{V_s}$ are used to denote the projection of the H, C and O velocity onto the unit vectors $\vec{u_i}$, $\vec{S_i}$, $\vec{v_u}$ and $\vec{v_s}$, respectively. The relevant four vibrational modes are defined as following

$$v_1 = U_4$$

$$v_3 = \sum_{i=1}^3 U_i$$

$$v_5 = V_u$$

$$v_8 = V_s + \sum_{i=1}^3 S_i$$

The v_3 , v_5 and v_8 modes present the mixing states due to the flexible movement of atoms within the simulation period.

As the bicarbonate ion exhibits structure-breaking effects in aqueous solution [9,22], the number of H-bonds between the ion and the hydration shell fluctuates during the simulation period. The number of H-bonds was estimated by different definitions on the basis of energetic and geometric criteria [30,31], as shown in Fig. 2, employing a structural criterion depending on the cutoff parameters (distance $R_{\rm HO}^{(c)}$, $R_{\rm OO}^{(c)}$ and angle $\phi^{(c)}$) in analogy to water–dimethyl sulphoxide mixtures [32]. The cutoff distances $R_{\rm HO}^{(c)}$ and $R_{\rm HO}^{(c)}$ were obtained from the radial distribution functions for the bicarbonate's hydrogen and water oxygen atoms $(H_b - O_w)$ and for the bicarbonate's oxygen and adjacent hydrogen and water oxygen atoms $(O_3 - O_w)$, presenting the boundary of the first coordination

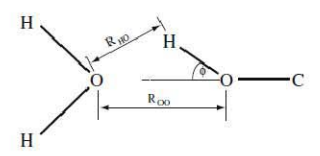


Fig. 2. The hydrogen-bond definition according to the geometrical relation between the hydrogen atom of bicarbonate ion and water molecule.

shell at 2.6 Å and 3.8 Å, respectively [22]. The angle $\phi^{(c)}$ was set to 30° [32].

For the CO-H stretching (v₁) frequency comparison between the experimental assignments and theoretical investigation, we also performed the frequency calculation with Gaussian 03 [33] for small water clusters of bicarbonate ion, employing the Hartree-Fock (HF), second-order Møller-Plesset (MP2) and Becke, three-parameter, Lee-Yang-Parr (B3LYP) methods associated with the double-c plus polarisation and diffuse functions (DZP+) basis set. Rudolph et al. suggested the cluster having three water molecules calculated with the B3LYP/6-31+C* method providing the best agreement of the calculated peak positions with the measured Raman data [10]. Thus, we extended the cluster size including the forth water molecule and also including electron correlation effects at MP2 level, to determine its effect on the v₁ frequency.

3. Results and discussion

The power spectra predicted by applying the Fourier transformation to the VACFs employing a correlation length of 1.0 ps with 1800 averaged time origins (10 ps) of the symmetric CO stretching (v_3) , C-OH stretching (v_5) and CO₃ out-of-plane deformation (v_8) modes, and CO-H stretching (v_1) mode in the bicarbonate ion are displayed in Fig. 3. The dominant peak at 1498 cm-1 of v₃ (Fig. 3A, spectrum a) differs from the Raman data (1312 cm⁻¹) [10] by 134 cm⁻¹, while two weak peaks located at 1075 and 700 cm⁻¹ superimpose with the strong peak of v₅ (Fig. 3A, spectrum b) and v_8 (Fig. 3A, spectrum c), respectively. These two modes were assigned in Raman experiment to 1015 and 673 cm⁻¹, respectively. [10] The acceptable deviation of vibrational frequencies for these three modes in Fig. 3A indicates the success of QMCF MD methodology to supply good dynamical data of hydrated bicarbonate ion [22]. The CO - H stretching spectrum in Fig. 3B consists of a strong peak located at 4023 cm $^{-1}$ and a weak broad band, shown in the insert, with its peak at 2687 cm⁻¹. We also performed the frequency calculation with Gaussian 03 [33] for small water clusters of bicarbonate ion (HCO₃ · nH₂O, n = 1, 2, 3, 4) [22], employing the Hartree-Fock (HF), second-order Møller-Plesset (MP2) and Becke, three-parameter, Lee-Yang-Parr (B3LYP) methods associated with DZP+ basis sets [24-26]. The v_1 frequencies are shown in Table 1, corresponding to the frequency of the strong peak in Fig. 3B. If one accepts that the MP2 level represents the best quality (although MP2 can also overestimate correlation influence), the obtained results confirm the common observation from many similar simulations including DFT-based Car-Parrinello MD simulations that DFT overestimates the strength and thus the rigidity of H bonds, while ab initio simulations at HF level tend to underestimate hydrogen bond strength. The peak of the observed weak band corresponds to the frequency found in the Raman and IR experi-

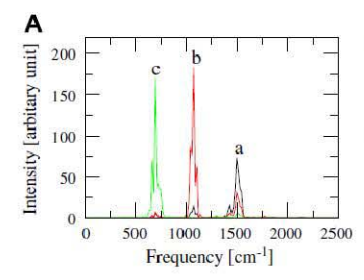
Table 1 Vibrational frequencies (cm $^{-1}$) of CO-H stretch (ν_1) within the bicarbonate ion in four hydrated forms (HCO $_3$ -nH₂O, n=1,2,3,4) obtained from HF, MP2 and B3LYP calculations with DZP+ basis sets [24-26].

Method	Frequencies (cm ⁻¹)					
	H ₂ O	2H₂O	3H ₂ O	4H ₂ O		
HF	4196	4182	4162	4146		
B3LYP	3692	3653	3609	3582		
MP2	3812	3782	3744	3719		

ments at ca. $2600\,$ cm $^{-1}$ [4–6,10]. The characterisation of this weak band requires further details for an interpretation, which are presented below.

The number of H-bonds between the hydrogen atom of bicarbonate ion and water molecules within the hydration shell was counted throughout the simulation time as shown in Fig. 4. Further, we investigated the effect of H-bonding on the vibrational spectrum of the v_1 vibration. We chose three short intervals located from 0.5 to 2.5 ps (few H-bonds), 6.0 to 8.0 ps (numerous H-bonds) and 8.6 to 10.0 ps (no H-bonds), and evaluated the spectrum for each period by means of the VACFs employing a correlation length of 1.0 ps with 200 and 80 averaged time origins for time intervals 2.0 ps and 1.4 ps, respectively. The power spectra are shown in Fig. 5. In the spectrum of the few H-bonds period (Fig. 5A), the strong peak is located at 4007 cm⁻¹ and a weak band from 2394 to 2736 cm⁻¹ reaches 3.0% of the strong peak's height. The strong presence of H-bonds affects the frequencies and intensities of strong and weak band, as shown in Fig. 5B. The strong peak is lowered and redshifted, while the weak band is less well structure and starts at 2525 cm⁻¹ and extends to 2899 cm⁻¹ implying a blueshift of this band. At the same time the intensity of the weak peak increases to 12.0% of that of the strong one, apparently due to the more intense H-bonding. The absence of H-bonds shifts the strong peak (cf. Fig. 5C) to 4039 cm-1, which means a blueshift compared to the peak in Fig. 5A. The weak band peak is redshifted by 81 cm⁻¹, and amounts to only 1.6% of the strong peak height. These results clearly reflect the influence of H-bonds on the interand intra-molecular OH stretching modes of bicarbonate ion. An increasing number of H-bonds redshifts the strong peak and blueshifts the weak band, also rising the relative intensity of the weak band. Our results show that the strong peak represents the intramolecular OH stretch, while the weak band corresponds to the intermolecular OH interactions due to the H-bonds. The shape of this peaks shows the wide varieties of H-bonds realised in solution.

The frequency of the strong peak agrees with the value obtained by the quantum mechanical calculations of the CO-H stretching within the bicarbonate ion. The location of the weak band corresponds to the peak assignment of CO-H stretch in the Raman



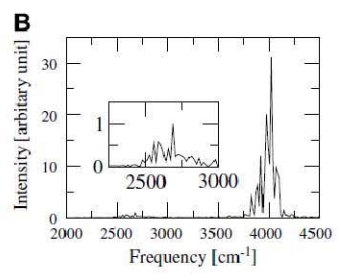


Fig. 3. Power spectra of (A) symmetric CO stretching (a), C-OH stretching (b) and CO₃ out-of-plane deformation (c) modes, and (B) CO-H stretch of the hydrated bicarbonate ion with the insert presenting the weak band located from 2250 to 3000 cm⁻¹ obtained from the 10 ps QMCF MD simulation [22].

V. Vchirawongkwin et al. /Journal of Molecular Structure: THEOCHEM 913 (2009) 236-239

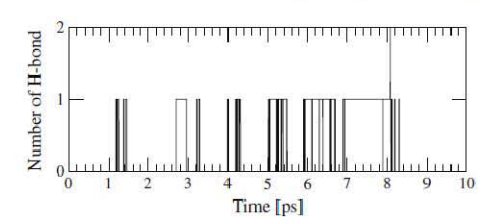


Fig. 4. Number of hydrogen-bonds between the hydrogen atom of bicarbonate ion and water molecules within the hydration shell during 10 ps of QMCF MD simulation [22].

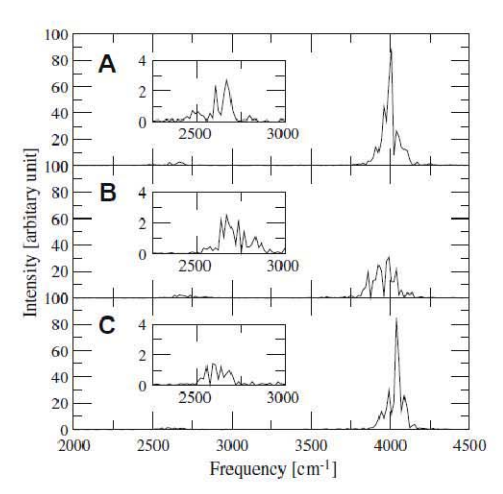


Fig. 5. Power spectra of v_1 obtained from the QMCF MD simulation [22] evaluated during (A) 0.5–2.5 ps, (B) 6.0–8.0 ps, and (C) 8.6–10.0 ps with the inserts showing the weak band located from 2250 to $3000\,\mathrm{cm}^{-1}$.

and IR experiments [4-6.10], but it has to be assigned to the intermolecular OH stretching mode involving hydrogen bonds between ion and water molecules.

4. Conclusion

The successful application of the ab initio QMCF MD approach for the unambiguous assignment of the experimentally observed vibrational frequencies, in particular of the CO-H stretching frequency, can be seen as a strong indication that this methodology is suitable for simulations of composite solutes of low symmetry in water. Previous simulations of phosphate, sulphate and perchlorate in water [20,34-36] have already shown that the method is well suited to treat hydrogen bonded, weakly interacting anions and thus let us expect in connection with the results presented here that this applicability is of rather general character and should be valid for neutral hydrogen bonding solutes as well.

Acknowledgments

Generous financial support by the Austrian Science Foundation (FWF), The Thailand Research Fund and Thailand Commission on Higher Education (fellowships for V.V. and C.K.) are gratefully acknowledged.

References

- D.M. Kern, J. Chem. Educ. 37 (1960) 14–23.
 D.N. Silverman, S.H. Vincent, CRC Crit. Rev. Biochem. 14 (1983) 207–255.
 D.N. Silverman, S. Lindskog, Acc. Chem. Res. 21 (1988) 30–36.
 A.R. Davis, B.C. Oliver, J. Solution Chem. 1 (1972) 239–339.
 B.G. Oliver, A.R. Davis, Can. J. Chem. 51 (1973) 698–702.
 W. Hage, A. Hallbrucker, E. Mayer, J. Am. Chem. Soc. 115 (1993) 8427–8431.
 N. Wen, M.H. Brooker, J. Phys. Chem. 99 (1995) 359–368.
 B.I. D. Frantz, Chem. Geol. 152 (1998) 211–225

- J.D. Frantz, Chem. Geol. 152 (1998) 211–225.
 J.S. Frantz, Chem. Geol. 152 (1998) 211–225.
 Z.S. Nickolov, O. Ozcan, J.D. Miller, Colloids Surf. A 224 (2003) 231–239.
 W.W. Rudolph, D. Fischer, G. Irmer, Appl. Spectrosc. 60 (2006) 130–144.
 O. Ozdemir, M.S. Çelik, Z.S. Nickolov, J.D. Miller, J. Colloids Interface Sci. 314 (2007) 545–551.
 W.W. Rudolph, G. Irmer, E. Königsberger, Dalton Trans. (2008) 900–908.
 G. Rajbur, P. Pullay, J. Phys. Chem. 90 (1995) 3093–3100.

- K. Rubutt, P. Pulay, J. Phys. Chem. 99 (1995) 3093–3100.
 K. Rubutt, P. Pulay, J. Phys. Chem. 99 (1995) 3093–3100.
 A. P. Scott, L. Radom, J. Phys. Chem. 100 (1996) 16502–16513.
 M.P. Andersson, P. Uvdal, J. Phys. Chem. A 109 (2005) 2937–2941.
 R.W. Impey, P.A. Madden, I.R. McDonald, J. Phys. Chem. 87 (1983) 5071–5083.
 S. Obst, H. Bradaczek, J. Phys. Chem. 100 (1996) 15677–15687.
 S. Koneshan, J.C. Rasaiah, R.M. Lynden-Bell, S.H. Lee, J. Phys. Chem. B 102 (1998) 4193–4204.
 B.M. Rode, T.S. Hofer, B.R. Randolf, C.F. Schwenk, D. Xenides, V.

- (1998) 4193–4204. [19] B.M. Rode, T.S. Hofer, B.R. Randolf, C.F. Schwenk, D. Xenides, V. Vchirawongkwin, Theor. Chem. Acc. 115 (2006) 77–85. [20] V. Vchirawongkwin, B.M. Rode, Chem. Phys. Lett. 443 (2007) 152–157. [21] A.B. Phibli, T.S. Hofer, V. Vchirawongkwin, B.R. Randolf, B.M. Rode, Chem. Phys. 346 (2008) 182–185.
- [22] V. Vchirawongkwin, A.B. Pribil, B.M. Rode, Ab initio quantum mechanical
- [22] V. Vchirawongkwin, A.B. Pribil, B.M. Rode, Ab initio quantum mechanical charge field study of hydrated bicarbonate ion: structural and dynamical properties, 2009. doi:10.1002/jc.c21308.
 [23] H.J.C. Berendsen, J.P.M. Postma, W.F. van Gunsteren, A. DiNola, J.R. Haak, J. Chem. Phys. 81 (1984) 3684–3690.
 [24] T.H. Dunning Jr., P.J. Hay, Gaussian basis sets for molecular calculations, in: H.F. Schaefer III (Ed.), Modern Theoretical Chemistry: Methods of Electronic Structure Theory, Ch. 1, vol. 3, Plenum Press, New York, 1977, pp. 1–27.
 [25] T.H. Dunning Jr., J. Chem. Phys. 53 (7) (1970) 2823–2833.
 [26] E. Magnusson, H.F. Schaefer III, J. Chem. Phys. 83 (1985) 5721–5726.
 [27] F.H. Stillinger, A. Rahman, J. Chem. Phys. 68 (2) (1978) 666–670.
 [28] P. Bopo, G. Jansoč, K. Heinzinger, Chem. Phys. Lett. 98 (2) (1983) 129–133.

- E. Magnusson, H.F. Schaeler III., J. Chem. Phys. 83 (1985) 5721–572b.
 F.H. Stillinger, A. Rahman, J. Chem. Phys. 68 (2) (1978) 666–670.
 P. Bopp, C., Janscó, K. Heinzinger, Chem. Phys. Lett. 98 (2) (1983) 129–133.
 P. Bopp, Chem. Phys. 106 (1986) 205–212.
 M.G. Sceats, S.A. Rice, J. Chem. Phys. 72 (1980) 3236–3247.
 M. Mezei, D.L. Beveridge, J. Chem. Phys. 72 (1981) 622–632.
 A. Luzar, D. Chandler, J. Chem. Phys. 89 (1993) 8160–8173.
 M.J. Frisch, G.W. Trucks, H.B. Schlegel, G.E. Scuseria, M.A. Robb, J.R. Cheeseman, J.A. Montgomery, T. Vreven, K.N. Kudin, J.C. Burant, J.M. Millam, S.S. Iyengar, J. Tomasi, V. Barone, B. Mennucci, M. Cossi, G. Scalmani, N. Rega, G.A. Petersson, H. Nakatsuji, M. Hada, M. Ehara, K. Toyota, R. Fukuda, J. Hasegawa, M. Ishida, T. Nakajima, Y. Honda, O. Kitao, H. Nakai, M. Klene, X. Li, J.E. Knox, H.P. Hratchian, J.B. Cross, V. Bakken, C. Adamo, J. Jaramillo, R. Gomperts, R.E. Stratmann, O. Yazyev, A.J. Austin, R. Cammi, C. Pomelli, J.W. Ochterski, P.Y. Ayala, K. Morokuma, C.A. Voth, P. Salvador, J.J. Dannenbeng, V.G. Zakrzewski, S. Dapprich, A.D. Daniels, M.C. Strain, O. Farkas, D.K. Malick, A.D. Rabuck, K. Raghavachari, J.B. Foresman, J.V. Ortic, Q. Cui, A.G. Baboul, S. Clifford, J. Cioslowski, B.B. Stefanov, G. Liu, A. Liashenko, P. Piskorz, I. Komaromi, R.L. Martin, D.J. Fox, T. Keith, A.M.A. Laham, C.Y. Peng, A. Nanayakkara, M. Challacombe, P.M.W. Gill, B. Johnson, W., Chen, M.W. Wong, C. Gonzalez, J.A. Pople, Gaussian 03, Revision E.O1, Gaussian, Inc., Wallingford, CT, 2004. Pople, Gaussian 03, Revision E.01, Gaussian, Inc., Wallingford, CT, 2004. V. Vchirawongkwin, B.M. Rode, I. Persson, J. Phys. Chem. B 111 (2007) 4150–
- [35] A.B. Pribil, V. Vchirawongkwin, T.S. Hofer, B.R. Randolf, Structure and dynamics of composite anions in aqueous solution, in: T.E. Simos, G. Maroulis (Eds.),
 Computation in Modern Science and Engineering, Proceedings of the
 International Conference on Computational Methods in Science and
 Engineering, vol. 2, Part B, 2007, pp. 921–923.

 [36] A.B. Pribil, T.S. Hofer, B.R. Randolf, B.M. Rode, J. Comput. Chem. 29 (2008)
 2330–2334.

Ab Initio Quantum Mechanical Charge Field Study of Hydrated Bicarbonate Ion: Structural and Dynamical Properties

VIWAT VCHIRAWONGKWIN, ANDREAS B. PRIBIL, BERND M. RODE²

 Department of Chemistry, Faculty of Science, Chulalongkorn University, Phyathai Road, Prathumwan, Bangkok 10330, Thailand
 Theoretical Chemistry Division, Institute of General, Inorganic and Theoretical Chemistry, University of Innsbruck, Innrain 52a, A-6020 Innsbruck, Austria

Received 14 August 2008; Revised 1 March 2009; Accepted 23 March 2009 DOI 10.1002/jcc.21308 Published online 11 May 2009 in Wiley InterScience (www.interscience.wiley.com).

Abstract: The *ab initio* quantum mechanical charge field molecular dynamics (QMCF MD) formalism was applied to simulate the bicarbonate ion, HCO_3^- , in aqueous solution. The difference in coordination numbers obtained by summation over atoms (6.6) and for the solvent-accessible surface (5.4) indicates the sharing of some water molecules between the individual atomic hydration shells. It also proved the importance to consider the hydration of the chemically different atoms individually for the evaluation of structural and dynamical properties of the ion. The orientation of water molecules in the hydration shell was visualized by the θ -tilt surface plot. The mean residence time in the surroundings of the HCO_3^- ion classify it generally as a structure-breaking ion, but the analysis of the individual ion-water hydrogen bonds revealed a more complex behavior of the different coordination sites.

© 2009 Wiley Periodicals, Inc. J Comput Chem 31: 249-257, 2010

Key words: QM/MM MD simulation; QMCF simulation; bicarbonate ion

Introduction

The bicarbonate ion, HCO_3^- , is one of the most commonly found anions. Dissolution of carbon dioxide in water in the pH range of 8 to 10 generates the HCO_3^- ion as the major product.¹ The HCO_3^- ion is also produced by human carbonic anhydrase II (HCA II), ^{2.3} which catalyzes the hydration of CO_2 . This ion also maintains the pH of blood at the level suitable for tissues and enzyme activities.

The structural parameters of HCO_3^- ion have been investigated by X-ray diffraction of sodium bicarbonate crystals. 4.5 Jönsson et al. reported the optimized geometry with an unusually long C–OH distance in the HCO_3^- ion based on a Hartree-Fock level calculation with a double- ζ basis set augmented by diffuse s and p functions. 6 Keesee et al. used high-pressure mass spectrometry to determine the hydration enthalpy of HCO_3^- ion as -95 kcal mol $^{-1}$ in the gas phase. 7 Leung et al. employed molecular dynamics based on density functional theory (DFT) to simulate a hydrated HCO_3^- system containing 63 water molecules and one ion. 8 They obtained an average coordination number of 6.9 water molecules from the summation of coordination numbers of individual atoms.

The structural and dynamical properties of hydrated bicarbonate ion are of great significance for the detailed understanding of all chemical processes of this ion in aqueous solution, in particular its

role in biology. However, the bicarbonate ion is a composite structure difficult to access by a conventional QM/MM method, because of the complicated and asymmetric potential energy hypersurface describing the interaction between the HCO3 ion and water. The ab initio quantum mechanical charge field molecular dynamics (QMCF MD) formalism,9 however, does not require a constructed analytical potential and hence this method has already been successfully employed to investigate the structural and dynamical properties of the hydrated composite anions sulfate, 10,11 phosphate, 12,13 and perchlorate.12 In this work, the QMCF MD method was used to simulate the hydrated HCO3 ion in order to obtain its structure and some dynamical properties. The structural properties were obtained via radial distribution functions (RDFs), coordination number distributions (CNDs), and angular distribution functions (ADFs). The dynamics were characterized by means of ligand mean residence times (MRTs). We also introduce the "solvent-accessible surface" to evaluate the additional structural and dynamical features of the hydration shell. The θ and tilt angles are characteristic properties

Correspondence to: V. Vchirawongkwin; e-mail: viwat.v@chula.ac.th Contract/grant sponsors: Austrian Science Foundation (FWF), The Thailand Research Fund, Thailand Commission on Higher Education

© 2009 Wiley Periodicals, Inc.

of hydrating water and were thus depicted by means of surface and contour plots to interpret the orientation of water molecules within the hydration shell.

Methods

The *ab initio* quantum mechanical charge field molecular dynamics (QMCF MD) formalism has been outlined in detail previously. Because of the inclusion of an additional quantum mechanically treated solvent *layer zone* located beyond the first hydration shell of the solute species, the QMCF method does not require the construction of potential functions between the solute and water molecules, i.e., it avoids a time-consuming and sometimes hardly manageable task necessary in the conventional quantum mechanical/molecular mechanical molecular dynamics (QM/MM MD) formalism. ^{14–17} A further advantage of the QMCF MD method is the inclusion of the point charges of the atoms in the MM region in their changing positions in the core Hamiltonian for the QM region via a perturbation term,

$$V' = \sum_{i=1}^{n} \sum_{i=1}^{m} \frac{q_j^{\text{MM}}}{r_{ij}}$$
 (1)

where n is the number of atoms in the QM region, m the number of atoms in the MM region, q_j^{MM} the partial charges of these atoms according to the selected water model, and r_{ij} refers to the distance between a pair of particles in the QM (i) and MM (j) regions. On the other hand, the dynamically changing charges of QM particles, q_i^{QM} , contribute to the force on each atom j in the MM region as Coulombic forces,

$$F_j^{\text{QM}\to \text{MM}} = \sum_{i=1}^n \frac{q_i^{\text{QM}} \cdot q_j^{\text{MM}}}{r_{ij}}.$$
 (2)

As the conventional QM/MM MD formalism, the QMCF MD method allows the migration of water molecules between the QM and MM region. For this process, one has to apply a smoothing function. ¹⁸

$$S(r) = \begin{cases} 0 & \text{for } r > r_{\text{on}}, \\ \frac{\left(r_{\text{off}}^2 - r^2\right)^2 \left(r_{\text{off}}^2 + 2r^2 - 3r_{\text{on}}^2\right)}{\left(r_{\text{off}}^2 - r_{\text{on}}^2\right)^3} & \text{for } r_{\text{on}} \le r \le r_{\text{off}}, \\ 1 & \text{for } r < r_{\text{off}} \end{cases}$$
(3)

where r is the distance of a given solvent molecule from the center of the simulation box, $r_{\rm off}$ is the radius of the QM region, and $r_{\rm on}$ is the inner border of the smoothing region. The formalism is applied to all atoms of molecules located in the smoothing region, ensuring a smooth transition and continuous change of forces for these molecules according to

$$F_j^{\text{smooth}} = F_j^{\text{MM}} + \left(F_j^{\text{layer}} - F_j^{\text{MM}}\right) \times S(r) \tag{4}$$

where $F_j^{\rm layer}$ is the force acting on a particle j located in the (outer QM) smoothing zone and $F_j^{\rm MM}$ is the force acting on a particle j in the MM region. In this context, it has to be mentioned that energy is not rigorously conserved, but the related mistake can be considered very minor due to the short simulation time and the large size of the quantum mechanical region.

The bicarbonate solution consisted of one bicarbonate ion and 496 water molecules in a cubic box of 24.65 Å with periodic boundary condition. The separate zones of this system according to the QMCF scheme are shown in Figure 1. The density of the simulation box was 0.997 g cm⁻³, i.e., the experimental value of pure water at 298 K. The simulation was performed in the NVT ensemble using a general predictor-corrector algorithm with a time step of 0.2 fs. The system temperature was maintained at 298.16 K by the Berendsen temperature-scaling algorithm19 with a relaxation time of 100 fs. The QM subregions, namely the core and layer zone, extended to 3.2 and 5.4 Å, respectively. The quantum mechanical calculation was performed by means of the Hartree-Fock (HF) method with the Dunning double-ζ plus polarization and diffuse functions 20,21 basis sets for hydrogen, carbon, and oxygen atoms of the HCO3 ion, and Dunning double-ζ plus polarization function^{20,21} basis sets for hydrogen and oxygen atoms of water, respectively. The thickness of the smoothing region was chosen as 0.2 Å with the values of ron and roff as 5.2 and 5.4 Å, respectively, according to the radial distribution function (RDF) obtained from the equilibrated simulation. The selected water model applied to calculate the interactions between pairs of water in the MM region was the flexible BJH-CF2 model, 22,23 with the cutoff distances of 3.0 and 5.0 Å for non-Coulombic interactions between H atoms and between O and H atoms, respectively. The partial charges for oxygen and hydrogen atoms in the water molecule according to the BJH-CF2 model are -0.65996 and +0.32983. This water model supports the fully flexible molecular geometries of water molecule within the QM region. Whenever a water molecule migrates to the MM region it can retain its geometry as initial configuration in the MM region. The Coulombic interactions between the Mulliken charges on the atoms within the QM region and the point charges of water molecules according to the BJH-CF2 model are evaluated providing an electrostatic description by a dynamically charging field of point charges, which changes according to the movements of atoms inside the QM region and water molecules in the MM region in the course of the simulation. This ensures the continuous adaptation of the Coulombic interactions to all polarization and charge-transfer effects within solute and surrounding solvent layers.9 In addition, the reaction field method combined with the shifted-force potential technique were applied to account for long-range electrostatic potentials and forces, with a spherical cutoff limit of 12.350 Å. The system was equilibrated with the QMCF MD method for 50,000 steps (10 ps), and a further 50,000 steps (10 ps) were collected as data sampling for analyzing the structural and dynamical properties.

One problem to elucidate the structural and dynamical properties of the hydration shell of composite ions is the identification of water molecules coordinating to individual atoms of the solute species on the hand, and the general properties of the whole ion in solution. For the latter, one can define a "solvent-accessible surface," calculating all distances between the oxygen atoms of all water molecules and each atom within the carbonate ion and searching for each

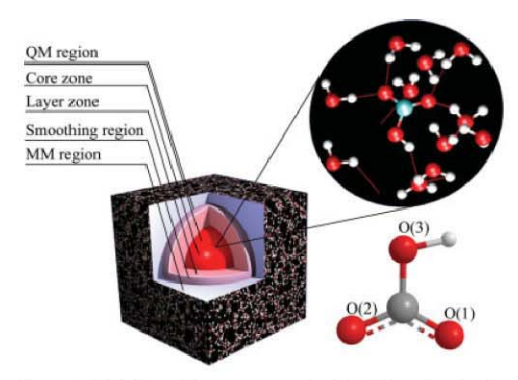


Figure 1. Definition of the quantum mechanical (QM) and molecular mechanical (MM) regions in the QMCF formalism: the QM region is separated into the core zone and the layer zone (the picture is not in scale). The numbering of oxygen atoms is also outlined.

shortest distance to define the coordination. Another method to solve this problem has been proposed based on allowing/removing double counting of solvent molecules. ²⁴ The solvent-accessible surface can be applied to evaluate both structural and dynamical properties by means of specific radial distribution functions (RDFs), coordination number distributions (CNDs), angular distribution functions (ADFs), and ligand mean residence times (MRTs) of the bicarbonate ion. Figure 2 shows the shape of the solvent-accessible surface constructed with a probing water molecule around all sites of bicarbonate ion.

All MRT values were evaluated by the direct method,²⁵ counting the water exchange processes between hydration shell and bulk. The most appropriate time span to record a water displacement from its original coordination sphere as an exchange process is 0.5 ps,²⁵ which corresponds to the average lifetime of a hydrogen bond in the solvent.²⁶

Results

Structural Properties of HCO3 Ion

Taking into account the stretching motions of bonds within the bicarbonate ion during the simulation period, bond distances were collected and their variations determined. The most probable bond distances of C=O(1) and C=O(2) and their "bandwidth" are 1.243 \pm 0.085 Å and 1.248 \pm 0.090 Å, respectively. The O(3) linked to the hydrogen atom has a longer mean distance to carbon, C=O(3), of 1.370 \pm 0.145 Å, and the O(3)–H distance is 0.960 \pm 0.085 Å. These data show a high flexibility of the HCO $_3^-$ ion in water, which certainly has consequences for all of its properties.

A further important information in this context are the bond angles. The $\angle O(1)CO(2), \angle O(1)CO(3),$ and $\angle CO(3)H$ angles were collected in the form of angular distribution functions (ADFs). The most probable angles for $\angle O(1)CO(2)$ and $\angle O(1)CO(3)$ are $129^{\circ}\pm12^{\circ}$ and $115^{\circ}\pm10^{\circ}$, respectively. The $\angle CO(3)H$ ADF shows an even stronger flexibility of this angle along the simulation. The most

probable angles were analyzed decomposing the ADF to a linear combination of three Gaussian functions (average absolute residual of fitting was 0.00663). The maxima of these functions are located at 100.5° , 106.3° , and 113.3° , with a probability of 1.58%, 5.81%, and 3.57%, respectively.

The dihedral angle measured between the plane defined by the oxygen atoms of HCO_3^- ion and the hydrogen atom is one of its characteristic structural properties. The distribution of this angle within the simulation period is presented in Figure 3, showing two peaks located at -7° and 7° with the probability of 9.49% and 8.31%, respectively. The left peak appears in the range between -22° and -1° , while the right peak extends from 1° to 22° . The symmetric shape of these peaks show an average dihedral angle of 7° . This angle distribution represents the flexibility of the HCO_3^- ion in water, H being located either above or below the oxygens' plane.

Structural Properties of the First Hydration Shell

In the simulation period, the average number of solvent molecules within the total QM region is 16.40, which are almost all located in the layer zone. Figures $4a_1-4c_1$ and Figures $4a_2-4c_2$ present the radial distribution functions (RDFs) of individual oxygen atoms within the bicarbonate ion with oxygen and hydrogen atoms of water molecules. The O(1) RDFs in Figures 4a1 and 4a2 show the average distances of O(1)-Owater and O(1)-Hwater as 2.855 and 1.895 Å, respectively. The well-defined hydration shell of O(2) represented by Figures 4b1 and 4b2 has the main peaks for O(2)-Owater and O(2)-Hwater at 2.865 and 1.895 Å. The average distance of O(3)-O_{mator} is considerably higher than either O₁- and O₂-O_{mator} with 3.385 Å [Fig. 4c₁], and the O(3)-H_{water} RDF smoothly increases, starting from ~1.7 Å [Fig. 4c2] without forming a distinct first-shell peak. The integration numbers are 1.80 (O(1)-Owater RDF), 2.45 (O(2)-O_{water} RDF), and 1.98 (O(3)-O_{water} RDF), referring to the average number of water molecules within the first hydration shells of individual atoms. However, because of the less-defined minimum of the O3-Owater RDF and the lack of a first-shell minimum in the O3-Hwater RDF the water in the neighborhood of O3 cannot be considered as regular hydrating ligands. Figures 4d1 and 4d2 show the H-water RDFs. The first peak of the H-Owater RDF extends from 1.559 to 2.585 Å with the integration number of 0.33. This indicates



Figure 2. The solvent-accessible surface of HCO₃⁻ ion showing the allocated spheres around the individual atoms with the intersection volume causing multicounts of water molecules in the analysis of hydration shell properties.

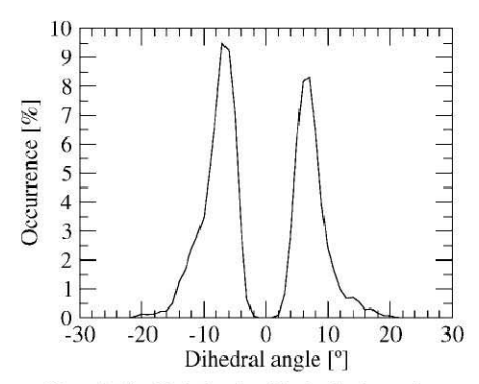


Figure 3. The dihedral angle within the bicarbonate ion.

a very weak interaction between the hydrogen of the O-H group with the solvent.

The calculated solvent-accessible surface leads to the RDFs between HCO_3 and water molecules shown in Figure 5. The HCO_3^- -O_{water} RDF has its maximum at 2.855 Å with some sidepeaks hidden under the main peak. The distance of 3.485 Å was chosen as the criterion to determine the integration number of HCO_3^- -O_{water} RDF, because the value of function at this distance is the lowest one. The integration number according to this condition results as 6.13. For the HCO_3^- -H_{water} RDF, the dominant peak is located at 1.905 Å and the minimum limiting the first hydration shell is found at 2.775 Å. Integration up to this point gives a value of 6.13 as well.

The first minimum of O(1)-Owater (3.265 Å), O(2)-Owater (3.515 Å), O(3)-Owater (3.595 Å), and H-Owater (2.585 Å) RDFs were utilized as the boundary of atom-specific hydration shells to evaluate the coordination number distributions (CNDs) for each site, shown in Figure 6. The coordination number of O(1) varies from 0 to 3 with the occurrence of 3.2, 31.9, 46.4, and 18.5%, respectively. The O(2) CND in Figure 6b shows the most probable coordination number at 3 with the occurrence of 42.3% and other possibilities of 0 (0.4%), 1 (12.3%), 2 (37.5%), 4 (6.9%), and 5 (0.6%). For the O(3) CND, the coordination number is distributed in the range of 0 to 5 similar to the O(2) CND, but the most probable occurrence of 35.6% occurs at the coordination number of 2, the other percentages are 5.9, 27.1, 25.7, 5.3, and 0.4 for the coordination numbers 0, 1, 3, 4, and 5, respectively. The H CND in Figure 6d delivers a probability of 32.8% for the coordination number 1, while 67.2% of the simulation time no water is found linked to H (OH). The average coordination numbers obtained for the O(1), O(2), O(3), and H are 1.80, 2.45, 1.98, and 0.33, respectively, summing upto 6.56, which is slightly higher than the value obtained for the solvent-accessible surface.

Thus, the solvent-accessible surface was also utilized to evaluate the CND for the HCO_3^- ion using the identical criterion as in the evaluation of individual CNDs. Figure 7 shows a dominant coordination number for the whole surface of 6 with the occurrence of 34.4%. Other coordination numbers are 2 (0.1%), 3(4.5%), 4 (15.6%), 5 (31.2%), 7 (11.4%), 8 (2.5%), and 9 (0.3%), presenting the average coordination number of 5.41.

The angle between the O(X)- O_{water} (X=1 to 3) or H- O_{water} connecting vector and the normal vector produced by O-H vectors of water molecule defines the tilt angle, and the angle between the O(X)- O_{water} vector and the vector sum of O-H vectors within the water molecule defines the θ angle. Their evaluation was again based

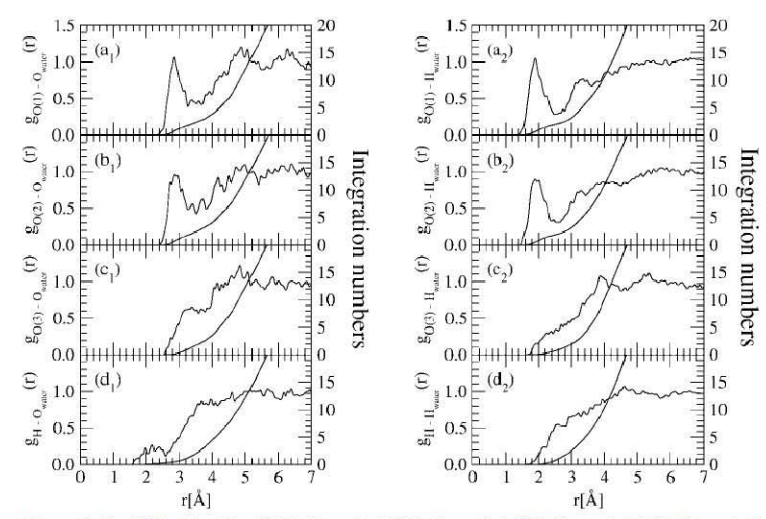


Figure 4. The RDF plots of (a_1) O(1)–O_{water}, (a_2) O(1)–H_{water}, (b_1) O(2)–O_{water}, (b_2) O(2)–H_{water}, (c_1) O(3)–O_{water}, (c_2) O(3)–H_{water}, (d_1) H–O_{water}, and (d_2) H–H_{water}, and their running integration numbers.

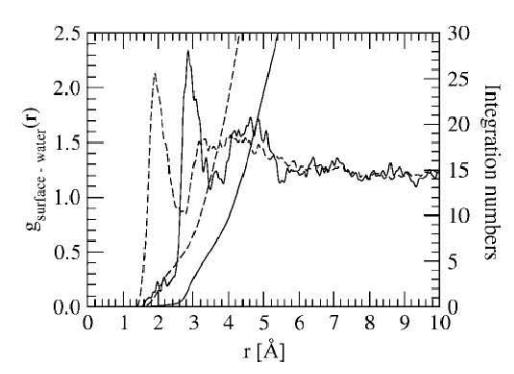


Figure 5. The RDF plots of HCO_3^- with their running integration numbers obtained from the QMCF MD simulation evaluated by means of the solvent-accessible surface. Solid and dashed lines refer to the RDFs for the O and H atoms of water, respectively.

on the solvent-accessible surface, i.e., the shortest distance between the center of mass of water molecules and individual oxygen or hydrogen atom within the HCO3 ion was the criterion of allocated hydration shell. Figure 8 shows the θ -tilt surface, distribution of θ angle, and distribution of tilt angle plots for the hydration shell of HCO₃ ion. The θ -tilt surface plot shows the probable orientation of water molecules in the hydration shell. The large number of peaks in the θ -tilt surface plot are located in the range of from 90.0° to 175.0° (θ) and from -40.0° to 40.0° (tilt). However, we found two significant peaks located at the $(\theta, tilt)$ coordinates of $(60.0^{\circ}, -59.0^{\circ})$ and $(60.0^{\circ}, -30.0^{\circ})$. The projections of θ -tilt surface plot onto the θ and tilt plane are equivalent to the distribution of separated θ and tilt angle evaluated from the QMCF simulation, respectively. The main peaks of the distribution of θ angle at 124° and the distribution of tilt angle at 8° and -6° represent the orientation of water molecules, pointing with one of hydrogen atom to the surface of HCO3 ion without the information of the orientation of water molecules within the hydration shell of bicarbonate's hydrogen atom.

Dynamical Properties of the Hydration Shell

Table 1 summarizes the ligand mean residence time (MRT) results evaluated by the direct method 25 for individual oxygen atoms and hydrogen and for the solvent-accessible surface of HCO $_3^-$ ion with $t^*=0.0$ and 0.5 ps to account an exchange event. The total number of water molecules counted for individual exchange processes of the oxygens and hydrogen of HCO $_3^-$ ion were 83 and 29, being larger than those obtained for the solvent-accessible surface (34 and 18). The total number of attempted exchange processes of individual atoms evaluated at $t^*=0.0$ ps (477 events) is identical to the value of the surface (480 events), while the total value of individual atoms obtained at $t^*=0.5$ ps is 62 and thus higher than the 31 events counted for the surface of the ion. The total number of processes needed for one successful water exchange, $R_{\rm ex}$, for individual atoms within the HCO $_3^-$ ion is 34.4, compared to 15.3 evaluated for the solvent-accessible surface. With the standard relaxation time used

in the direct method with $t^*=0.5\,\mathrm{ps}$, 25 the mean residence time (MRT) of a water ligand at a coordination site results as 1.04, 1.05, 1.36, 0.82, and 1.62 ps for O(1), O(2), O(3), H atom, and the whole HCO $_3^-$ ion, respectively. Hydrogen bond life-times can be evaluated with $t^*=0.0\,\mathrm{ps}$ and result as 0.15, 0.18, 0.12, 0.07, and 0.10, respectively. The corresponding value obtained for pure water by a simulation based on the QM/MM MD formalism is 0.33 ps; these values account for each hydrogen bond making/breaking process. 27 Both mean residence times and hydrogen bond life-times for the individual atoms and the whole ion prove the HCO $_3^-$ ion to weaken the solvent's structure in its vicinity. This effect is not evenly distributed, however, to all sites of the anion, and most pronounced near the H atom.

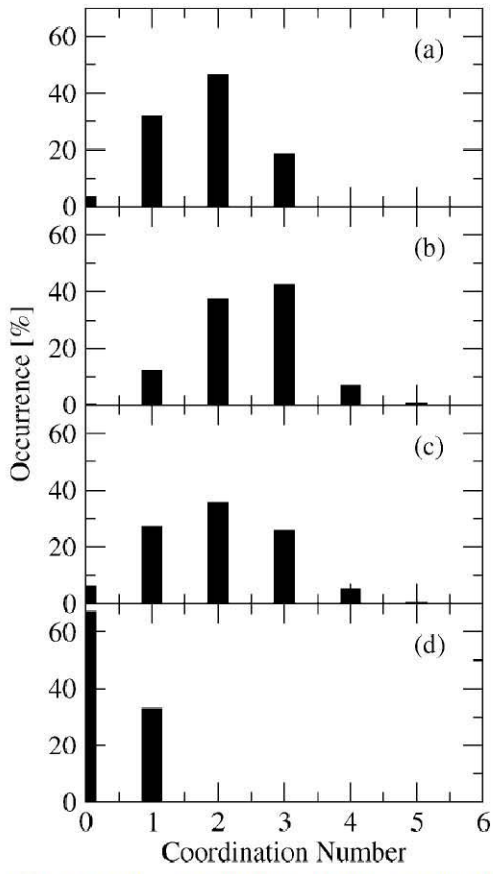


Figure 6. First shell coordination number distributions of (a) O(1), (b) O(2), (c) O(3), and (d) H atoms of bicarbonate ion obtained from the QMCF MD simulation.

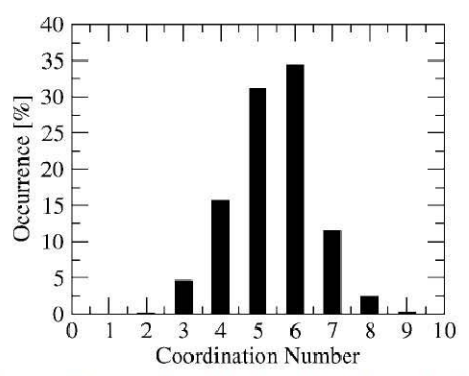


Figure 7. The first shell coordination number distribution for the solvent-accessible surface of bicarbonate ion.

Discussion and Conclusion

Assessment of the Usage of Methodological Level

The Hartree-Fock (HF) level with the selected basis sets used within the QM region of the QMCF formalism was assessed by comparing the predicted structure of the HCO3 ion in terms of bond distances and bond angles to the available experimental data. Table 2 summarizes the structural properties of HCO₃ ion obtained from our QMCF simulation in comparison to the structures of NaHCO3 obtained from X-ray crystallography, 4,5 a previous gasphase theoretical study⁶ and our optimized structures obtained at Hartree-Fock (HF), second-order Møller-Plesset (MP/2), coupledcluster singles and doubles (CCSD), and density functional levels (B3LYP and B3PW91), associated with Dunning double- ζ plus polarization function (DZP+)^{20,21} and aug-cc-pVXZ (X = D, T, Q, and 5)28,29 basis sets. All bond distances between carbon and oxygens of HCO3 ion of our QMCF simulation are very similar to those obtained from X-ray crystallography, while our distance of O(3)-H is significantly shorter. However, X-ray diffraction cannot determine the location of hydrogen atom well and we, therefore, consider our value for the liquid reliable. The similar distance reported by Jönsson et al. for the gas-phase, calculated with (9s5p)/[4s2p] basis set6 seems to support our viewpoint. Our gas-phase structures of bicarbonate ion optimized with and without inclusion of electron correlation predict an O(3)-H distance in the range of 0.94 to 0.97 Å, indicating the influence of correlation to be rather minor, and also indicating the reliability of our QMCF result for the ion in water. For the angles within the HCO3 ion, the peak of our angular distributions coincides with the optimized gas-phase structure reported by Jönsson et al., but the angles from our optimized structures in the gas phase show significant deviations from the values obtained in solution. Considering the high flexibility and thus variability of these angles, the solution values are also in fair agreement with the crystal structure. The structural parameters obtained from the QMCF simulation represent the ion in aqueous solution and are expected, therefore, to differ to some extent from both gas and solid state, due to the influence of hydration on the structure of ion. The fair agreement of the HCO_3^- structure obtained by our calculation level with the crystal structure of $NaHCO_3^{-5}$ can be seen as a good indication toward the reliability of the HF method with the Dunning double- ζ plus polarization and diffuse functions $(DZP+)^{20,21}$ basis sets for the investigation of structural properties of hydrated anions.

Structural Properties of the Hydration Shell

Table 3 presents the average binding energy with the percentage of basis set superposition error (BSSE) according to Boys-Bernardi procedure 30,31 for the $[HCO_3(H_2O)_n]^-$ (n=1 to 4) clusters obtained from HF, B3LYP, MP2, and CCSD levels with DZP+basis set. The corresponding structures are shown in Figure 9. The binding energy obtained from the HF calculations are close to the values of correlated methods (MP2 and CCSD), comparing to the overestimated energy calculated by the density functional method (B3LYP) showing again a significant weakness of the density functional theory approach for solvated ions. $^{32-34}$ QM/MM simulations for hydrated metal ions by both HF and DFT methods have shown the advantage of ab initio HF as far as structure and coordination numbers are concerned. 33,35 The percentages of BSSE also indicate the suitability of HF level associated with DZP+ basis set to investigate the aqueous bicarbonate system.

The dihedral angles determined between the hydrogen atom and three oxygen atoms within the HCO_3^- ion obtained from the optimized structures of $[HCO_3(H_2O)_n]^-$ (n=1 to 4) in Figure 9 are presented in Table 4. These dihedral angle values indicate that the number of water molecules has an influence in distorting the planarity of bicarbonate structure. The dihedral angle distribution in Figure 3 shows the absolute variation of this angle and also represents the dynamical movement of the hydrogen atom between both sides of oxygen plane agrees according to solvent effects. Our results differ from the hydrated planar HCO_3^- structure resulting from a DFT simulation using the RPBE functional. 8 One reason for the deviation could be the small number of water molecules in

Table 1. Mean Ligand Residence Time τ in ps, Number of Accounted Ligand Exchange Events N, and Sustainability of Migration Processes to/from the First Hydration Shell $S_{\rm ex}$ Obtained from the QMCF Simulation.

	$t^* = 0.0 \text{ ps}$			$t^* = 0.5 \text{ps}$			
	N _{inv} ^a	$N_{\rm ex}^{0.0}/10{\rm ps^b}$	$ au_D^{0.0\mathrm{c}}$	N _{inv} a	$N_{\rm ex}^{0.5}/10{\rm ps^b}$	$\tau_D^{0.5\mathrm{c}}$	$R_{\rm ex}^{\rm d}$
O(1)	22	124	0.15	8	19	1.04	6.5
O(2)	26	143	0.18	11	24	1.05	6.0
O(3)	26	166	0.12	8	15	1.36	11.1
Н	9	44	0.07	2	4	0.82	10.8
Surface	34	480	0.10	18	31	1.62	15.3
H ₂ O ^e		269 ²⁵	$0.2,^{25}, 0.33,^{27}$ 0.55^{26}	24 ²⁵	1.7, ²⁵ 1.51 ²⁷	11.225	

^aNumber of ligand involved in the MRT evaluation according to the value of t*.

bNumber of accounted exchange events per 10 ps lasting at least 0.0 and 0.5 ps, respectively.

^cMean residence time determined by the direct method²⁵ in ps.

^dAverage number of processes needed for one successful ligand exchange.

eValues obtained from a QM/MM-MD simulation of pure water²⁵ in ps.

Table 2. Comparison of Bond Distances and Bond Angles within HCO $_3^-$ Ion Obtained from the QMCF Simulation with the Structural Parameters Obtained from X-ray Crystallography, 4.5 the Optimized Structure of Hartree-Fock Calculations, 6 and the Optimized Structures Obtained at Hartree-Fock (HF), Second-Order Møller-Plesset (MP/2), Coupled-Cluster Singles and Doubles (CCSD), and Density Functional Levels (B3LYP and B3PW91), Associated with Various Basis Sets. 20 , 21, 28, 29

Method	$r_{\text{C-O(1)}}$ (Å)	$r_{\text{C-O(2)}}$ (Å)	$r_{\text{C-O(3)}}$ (Å)	$r_{\mathrm{O(3)-H}}$ (Å)	∠O(1)CO(2)(°)	∠O(1)CO(3)(°)	∠CO(3)H(°)
QMCF	1.24 ± 0.08	1.25 ± 0.09	1.37 ± 0.14	0.96 ± 0.08	129 ± 12	115 ± 10	106 ± 15
X-ray4,5	1.25	1.28	1.35	1.07	126	120	103
HF ⁶	1.25	1.25	1.43	0.98	129	115	106
				HF			
DZP+	1.22	1.24	1.40	0.94	132	114	104
aug-cc-pVDZ	1.22	1.24	1.40	0.94	131	114	104
aug-cc-pVTZ	1.22	1.23	1.39	0.94	131	114	105
aug-cc-pVQZ	1.21	1.23	1.39	0.94	131	114	105
aug-cc-pV5Z	1.21	1.23	1.39	0.94	131	114	105
				B3LYP			
DZP+	1.24	1.25	1.45	0.97	132	113	102
aug-cc-pVDZ	1.24	1.26	1.45	0.97	132	114	102
aug-cc-pVTZ	1.23	1.25	1.45	0.96	132	113	102
aug-cc-pVQZ	1.23	1.25	1.45	0.96	132	114	102
aug-cc-pV5Z	1.23	1.25	1.45	0.96	132	114	102
				B3PW91			
DZP+	1.24	1.26	1.44	0.97	132	113	101
aug-cc-pVDZ	1.24	1.26	1.44	0.97	132	114	102
aug-cc-pVTZ	1.23	1.25	1.44	0.96	132	113	102
aug-cc-pVQZ	1.23	1.25	1.44	0.96	132	114	102
aug-cc-pV5Z	1.23	1.25	1.44	0.96	132	114	102
				MP/2			
DZP+	1.25	1.27	1.45	0.97	133	113	101
aug-cc-pVDZ	1.25	1.26	1.46	0.97	133	114	101
aug-cc-pVTZ	1.24	1.26	1.44	0.96	132	113	101
aug-cc-pVQZ	1.24	1.25	1.44	0.96	132	113	101
				CCSD			
DZP+	1.24	1.26	1.44	0.97	132	113	102
aug-cc-pVDZ	1.24	1.26	1.44	0.96	132	114	102
aug-cc-pVTZ	1.23	1.25	1.43	0.96	132	114	102

Car-Parrinello type simulations, which does not provide a proper embedding in a larger amount of solvent.

Because of the low symmetry of HCO₃, the individual RDFs of each oxygen and hydrogen atom were evaluated to determine the boundary of individual hydration shells and to compare them to the data obtained for the solvent-accessible surface. The summation of the individual coordination numbers gives a value of 6.56, which is close to the coordination number of 6.9 reported by Leung et al.8 However, the integration and the coordination number obtained for the solvent-accessible surface of 6.13 and 5.41, respectively, are lower than the sum of individual coordination numbers (6.56), showing the location of some water molecules within the overlap zone of individual hydration shells. The inequality of coordination number obtained from the solvent-accessible surface RDF and CND arises from the asymmetric geometry of solvent-accessible surface and the different evaluation procedures. The integration number from HCO₃ RDF was obtained by counting the water molecules referring to all oxygens and thus to somewhat larger distance from hydrogen. The volume with the solvent-accessible radius of 3.485 Å, therefore, includes some extra water molecules beyond the hydration shell of

Table 3. Average Binding Energies in kcal/mol with the Percentage of Basis Set Superposition Error (BSSE) According to Boys-Bernardi Procedure 30,31 in Parentheses for [HCO $_3$ (H $_2$ O $_n$ l) $^-$ Clusters Obtained from HF, B3LYP, MP2, and CCSD Calculations with DZP+ Basis Set.

		E _{bond} (kcal/mol)				
Structure	HF	B3LYP	MP2	CCSD		
		[HCO ₃ (H ₂ O) ₁]=			
1	-18.4(8.7)	-20.3(14.3)	-18.7(19.2)	-18.7(17.6)		
2	-14.7(10.2)	-19.7(17.2)	-15.4(27.3)	-15.3(24.2)		
3	-16.6(9.6)	-18.8(15.4)	-17.0(20.6)	-17.0(18.2)		
		[HCO ₃ (H ₂ O) ₂]_			
4	-17.0(9.1)	-18.9(15.6)	-17.4(20.4)	-17.4(18.4)		
4 5	-16.5(9.4)	-20.0(16.2)	-17.1(23.4)	-17.0(21.2)		
6	-15.1(9.9)	-18.6(17.2)	-15.6(25.0)	-15.6(22.4)		
		[HCO ₃ (H ₂ O) ₃				
7	-16.0(10.0)	-18.8 (16.8)	-16.4(23.8)	-16.4(21.3)		
		[HCO ₃ (H ₂ O) ₄	1-			
8	-14.8(9.8)	-17.1 (16.5)	-15.2 (23.4)	-15.2(21.2)		

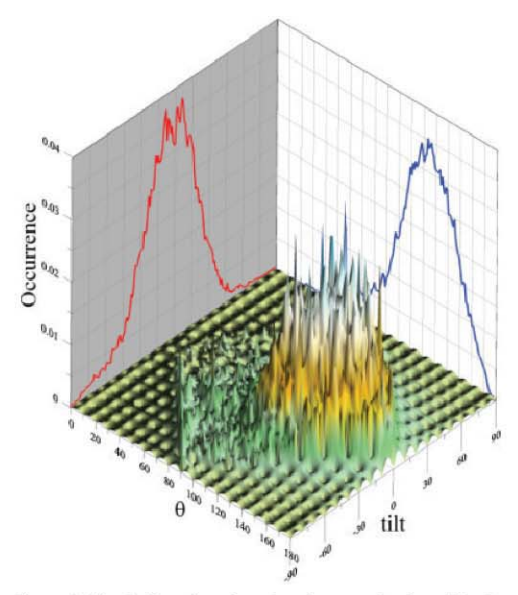


Figure 8. The θ -tilt angle surface plot of water molecules within the hydration shell of HCO_3^- ion based on the solvent-accessible surface. The projections of the surface plot onto the θ and tilt plane refer to the distribution functions of θ and tilt angle, respectively.

hydrogen atom. In the CND case, the radii of individual hydration shells were assigned in the evaluation process, and hence the coordination number obtained from the CND evaluation is slightly smaller.

The $\theta-$ tilt surface plot (Fig. 8) shows the major configuration of water molecules within the first hydration shell, utilizing one of the hydrogen atom to coordinate with the oxygen atoms of HCO_3^- ion. This plot also reveals a further orientation of water molecules with the $(\theta,$ tilt) coordinates at $(60.0^\circ, -59.0^\circ)$ and $(60.0^\circ, -30.0^\circ)$, representing the oxygen atom of water molecules coordinating to the hydrogen atom of HCO_3^- ion. This information is lost in the investigation of separated θ and tilt angle distribution. The different number of peaks for the orientation of water molecule suggests a weak hydration shell for the hydrogen atom of HCO_3^- ion compared with the oxygen atoms of this ion, corresponding to the coordination numbers of 0.33 for hydrogen and $\sim\!\!2$ for the oxygen atoms.

Dynamical Properties of the Hydration Shell

The difference of water molecules involved in the exchange processes between the sum over individual atoms (29 molecules) and the HCO_3^- ion as an entity (18 molecules) again indicates the location of water molecules within the intersection of individual hydration shells. The corresponding difference in exchange processes (62 and 31, respectively) shows that half of the exchange

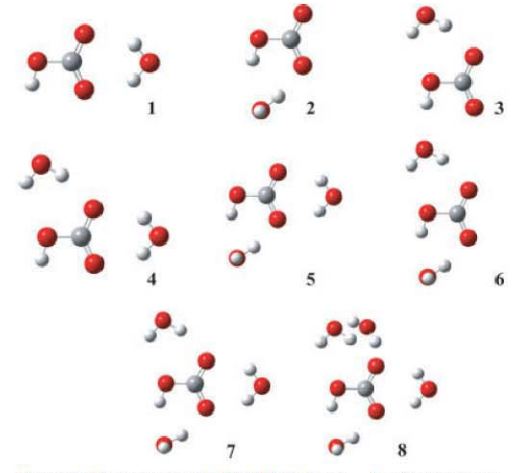


Figure 9. The structure of $[HCO_3(H_2O)_n]^-$ (n=1 to 4) clusters correspond to the structures employing as the starting configuration for the optimization with the selected theoretical levels to determine the binding energy and structural parameter.

events are migrations of water molecules between coordination sites of the HCO₃ ion. All MRT values of oxygen atoms are larger than the values for the hydrogen atom, indicating the easiest exchange of water at this site of the ion. On the other hand, the smaller number of water molecules involved in the exchange processes is an evidence for a local fluctuation of hydrogen bonds to the oxygens without producing ligand exchanges in every case. This can be well recognized from a visualization provided as a short video clip (http://www.molvision.com/video clips). Although the Berendsen temperature-scaling algorithm ¹⁹ requires in principle a long simulation period to sufficiently describe the phase space, a large number

Table 4. The Dihedral Angle Measured Between the Hydrogen Atom and the Plane of Three Oxygen Atoms within the HCO_3^- Ion, Corresponding to the $[HCO_3(H_2O)_n]^-$ Clusters Presented Earlier.

	Dihedral angle (°)					
Structure	HF	B3LYP	MP2	CCSD		
	1	HCO ₃ (H ₂ O) ₁]				
1	0.000	0.000	0.000	0.000		
2	-0.628	-0.735	-0.757	-0.772		
3	0.000	-0.145	-0.510	-0.025		
	1	HCO ₃ (H ₂ O) ₂]-				
4	0.004	-0.003	-0.009	-0.023		
5	-0.518	-0.459	-0.102	-0.255		
5 6	-0.606	-0.651	-0.908	-0.731		
	T	HCO ₃ (H ₂ O) ₃]				
7	-0.314	-0.400	0.875	0.230		
	1	HCO ₃ (H ₂ O) ₄] ⁻				
8	0.224	0.289	1.109	1.036		

of successful simulations published indicate that our simulation time of 10 ps is adequate to investigate the properties of hydrated ions, and thus also of the bicarbonate ion. Comparing results for exchange dynamics and H-bond life times for simulations of pure water²⁷ and experimental results, 26 the HF method seems to be the best compromise between accuracy and affordable computational effort to estimate dynamical effects as well. Although HF and the methodical problems associated with the thermostatization probably lead to slightly underestimated values, the associated errors are probably within a 10-20% range.

Summarizing all results, HCO3 is clearly characterized as a structure-breaking ion in water. Compared with other hydrated anions studied by the same simulation technique, the simultaneous presence of different hydration sites in the low symmetry of HCO₃ ion and the higher vicinity of coordination sites distinguishes it clearly from anions with tetrahedral symmetry such as sulfate, phosphate, and perchlorate, in particular if one compares the range of mean residence times of water ligands at these hydration sites (0.82 to 1.36) with those for the aforementioned anions $(PO_4^{3-} 3.9,$ SO₄²⁻, 2.1, and ClO₄⁻ 1.5 ps). 12 The flexibility of the HCO₃⁻ hydration structure is not only reflected in the weak and thus rapidly changing solvent binding, but it also shows a clear dependence on the location of the solvent molecules in the surrounding of the anion. To describe these effects by classical or conventional QM/MM molecular dynamics would be a most difficult task. Conventional QM/MM MD simulations would have required the construction of analytical interaction potential functions taking into account all the asymmetry of the interaction between solute and solvent, which in the case of bicarbonate would be extremely difficult and subject to many possible error sources and inaccuracies.

References

- 1. Kern, D. M. J Chem Educ 1960, 37, 14.
- Silverman, D. N.; Vincent, S. H. CRC Crit Rev Biochem 1983, 14, 207.
- Silverman, D. N.; Lindskog, S. Acc Chem Res 1988, 21, 30.
 Sass, R. L.; Scheuerman, R. F. Acta Crystallogr 1962, 15, 77.
- 5. Sharma, B. D. Acta Crystallogr 1965, 18, 818.
- 6. Jönsson, B.; Karlström, G.; Wennerström, H. J Am Chem Soc 1978, 100, 1658.
- 7. Keesee, R. G.; Lee, N.; Castleman, A. W., Jr. J Am Chem Soc 1979, 101, 2599

- 8. Leung, K.; Nielsen, I. M. B.; Kurtz, I. J Phys Chem B 2007, 111, 4453.
- 9. Rode, B. M.; Hofer, T. S.; Randolf, B. R.; Schwenk, C. F.; Xenides, D.; Vchirawongkwin, V. Theor Chem Acc 2006, 115, 77.
- 10. Vchirawongkwin, V.; Rode, B. M.; Persson, I. J Phys Chem B 2007, 111, 4150.
- 11. Vchirawongkwin, V.; Rode, B. M. Chem Phys Lett 2007, 443, 152.
- 12. Pribil, A. B.; Vchirawongkwin, V.; Hofer, T. S.; Randolf, B. R. In Computation in Modern Science and Engineering, Proceedings of the International Conference on Computational Methods in Science and Engineering, Vol. 2, Part B; Simos, T. E.; Maroulis, G., Eds.; American Institute of Physics: New York, 2007; pp. 921.
- 13. Pribil, A. B.; Hofer, T. S.; Randolf, B. R.; Rode, B. M. J Comput Chem 2008, 29, 2330.
- 14. Warshel, A.; Levitt, M. J Mol Bio 1976, 103, 227.
- Field, M. J.; Bash, P. A.; Karplus, M. J Comput Chem 1990, 11, 700.
 Gao, J. J Am Chem Soc 1993, 115, 2930.
- 17. Bakowise, D.; Thiel, W. J Phys Chem 1996, 100, 10580.
- Brooks, B. R.; Bruccoleri, R. E.; Olafson, B. D.; States, B. D.; Swaminathan, S.; Karplus, M. J Comput Chem 1983, 4, 187.
- 19. Berendsen, H. J. C.; Postma, J. P. M.; van Gunsteren, W. F.; DiNola, A.; Haak, J. R. J Chem Phys 1984, 81, 3684.
- Dunning, T. H., Jr.; Hay, P.J. In Modern Theoretical Chemistry: Methods of Electronic Structure Theory; Schaefer, H. F., III, Ed.; Plenum Press; New York, 1977; Vol. 3; Chapter 1, pp. 1.
- 21. Dunning, T. H., Jr. J Chem Phys 1970, 53, 2823.
- 22. Stillinger, F. H.; Rahman, A. J Chem Phys 1978, 68, 666.
- Bopp, P.; Janscó, G.; Heinzinger, K. Chem Phys Lett 1983, 98, 129.
- 24. Leung, K. Biophys Chem 2006, 124, 222.
- 25. Hofer, T. S.; Tran, H. T.; Schwenk, C. F.; Rode, B. M. J Comput Chem 2004, 25, 211,
- 26. Lock, A. J.; Woutersen, S.; Bakker, H. J. J Phys Chem A 2001, 105, 1238.
- 27. Xenides, D.: Randolf, B. R.: Rode, B. M. J Chem Phys 2005, 122, 174506.
- 28. Dunning, T. H., Jr. J Chem Phys 1989, 90, 1007.
- 29. Kendall, R. A.; Dunning, T. H., Jr.; Harrison, R. J. J Chem Phys 1992, 96,6796
- Boys, S. F.; Bernardi, F. Mol Phys 1970, 19, 553.

DOI 10.1002/jcc

- 31. Simon, S.; Duran, M.; Dannenberg, J. J. J Chem Phys 1996, 105, 11024.
- 32. Schwenk, C. F.; Loeffler, H. H.; Rode, B. M. J Chem Phys 2001, 115,
- 33. Schwenk, C. F.; Rode, B. M. J Chem Phys 2003, 119, 9523.
- 34. Schwenk, C. F.; Hofer, T. S.; Rode, B. M. J Phys Chem A 2004, 108, 1509.
- 35. Schwenk, C. F.; Hofer, T. S.; Rode, B. M. J Am Chem Soc 2004, 126, 12786

An Ab Initio Quantum Mechanical Charge Field Molecular Dynamics Simulation of a Dilute Aqueous HCl Solution

CHINAPONG KRITAYAKORNUPONG,1 VIWAT VCHIRAWONGKWIN,2 BERND M. RODE3

¹Faculty of Science, Department of Chemistry, King Mongkut's University of Technology,
Thonburi, Bangkok 10140, Thailand

²Faculty of Science, Department of Chemistry, Chulalongkorn University,
Bangkok 10330, Thailand

³Theoretical Chemistry Division, Institute of General, Inorganic and Theoretical Chemistry,
University of Innsbruck, Innrain 52a, Innsbruck A-6020, Austria

Received 19 June 2009; Revised 14 September 2009; Accepted 20 October 2009 DOI 10.1002/jcc.21469 Published online 17 December 2009 in Wiley InterScience (www.interscience.wiley.com).

Abstract: An *ab initio* quantum mechanical charge field (QMCF) molecular dynamics simulation has been performed to study the structural and dynamical properties of a dilute aqueous HCl solution. The solute molecule HCl and its surrounding water molecules were treated at Hartree-Fock level in conjunction with Dunning double- ζ plus polarization function basis sets. The simulation predicts an average H—Cl bond distance of 1.28 Å, which is in good agreement with the experimental value. The $H_{\rm HGC}$ -O_w and $C_{\rm HGC}$ -H_w distances of 1.84 and 3.51 Å were found for the first hydration shell. At the hydrogen site of HCl, a single water molecule is the most preferred coordination, whereas an average coordination number of 12 water molecules of the full first shell was observed for the chloride site. The hydrogen bonding at the hydrogen site of HCl is weakened by proton transfer reactions and an associated lability of ligand binding. Two proton transfer processes were observed in the QMCF MD simulation, demonstrating acid dissociation of HCl. A weak structure-making/breaking effect of HCl in water is recognized from the mean residence times of 2.1 and 0.8 ps for ligands in the neighborhood of Cl and H sites of HCl, respectively.

© 2009 Wiley Periodicals, Inc. J Comput Chem 31: 1785-1792, 2010

Key words: hydrogen chloride; hydration structure; dynamical properties; hydrogen bond; acid dissociation; proton transfer; simulation; QMCF

Introduction

It is well known that hydrogen bond formation and proton transfer of hydrogen halides in aqueous solution play an important role in a wide range of chemical and biological processes.1 Hydrogen chloride is a strong acid with $pK_a = -7$, indicating a dissociated form of hydrogen chloride in dilute aqueous solution. There are very few experiments related to the hydration structure of HCl in aqueous solution.2-6 Matrix isolation spectroscopy of HCl(H2O)n complexes was performed, showing the nondissociated structure of HCl with $n \leq 3$, whereas proton transfer is achieved from the complex with n = 4.2 X-ray and neutron diffraction techniques were applied to evaluate the structure of the aqueous HCl acid solution at 20°C and it was found that four water molecules were required to solvate each hydronium and Cl ions in solution.3 Concentrated HCl solutions were also studied using spectroscopic and diffraction techniques, suggesting a pentagonal ring structures of HCl(H2O)6 and (HCl)2(H2O)6 in solution. A Ragout-jet Fourier transform infrared spectroscopy was used to evaluate the proton vibrational dynamics in $(HCl)_{m^-}(H_2O)_n$ clusters, reporting that HCl complexes with three or more water molecules could not be assigned in the IR spectrum. Recently, X-ray absorption of aqueous HCl solution was investigated. It was found that the addition of HCl to liquid water leads to a decrease in intensity of the X-ray absorption spectrum. In addition, neutron diffraction of a highly concentrated HCl solution has been performed to determine the Eigen or Zundel complexes, but its results are not comparable to the species formation in dilute HCl solution. Numerous theoretical techniques have been applied to describe the characteristics of

Correspondence to: C. Kritayakomupong; e-mail: chinapong.kri@kmutt.

Contract/grant sponsors: Thailand Research Fund (TRF), Thailand Commission on Higher Education, Austrian Science Foundation (FWF)

© 2009 Wiley Periodicals, Inc.

HCl in aqueous solution. 4-6,8-25 An MP2/6-31+G* calculation in the continuum model of water confirmed the nondissociation of monohydrated and dihydrated HCl complexes.8 HCl on an ice surface at 190 K was studied using molecular dynamics simulations, indicating that ionic solvation processes are thermodynamically feasible. 9,10 A calculation using BLYP level of approximation with an extended basis set showed that the proton transfer takes place without transition state in the case of $HCl(H_2O)_4$. Using the MP2 method, a nondissociated HCl complex was observed with a cyclic three-water cluster, indicating a red-shift in the HCl stretching frequency, dissociated form appears to be possible when the HCl molecule was surrounded by four water molecules. ¹⁵ The MP2/ 6-311++G(d,p) level of theory was applied to describe the nondissociated form of HCl with four water molecules. 18 Upon extension of the cluster size to five water molecules, proton transferred type was shown to exist. The nondissociated form was determined as the most stable structure for the HCl(H₂O). (n=1-3) clusters evaluated by the B3LYP/D95++(d,p) method.¹⁹ The HCl(H₂O)₄ cluster resulted as an intermediate with both nondissociated and dissociated structures obtained from both the B3LYP and the MP2 method. 19,22 Car-Parrinello molecular dynamics (CPMD) simulations were performed to evaluate the dissociation and vibrational dynamics of DCl in D_2O molecules. $^{12,16,23-25}$ Concentrated HCl solutions (2.7 and 5.3 M) where complete dissociation has already been assumed by the composition of the system (protons, CI ions, and water) have also been studied by CPMD simulations,26 in which the gradient-corrected BLYP functional has been used that usually leads to too rigid H-bonds and thus to too slow dynamics. The amount of solvent considered further does not provide sufficient water molecules for a full hydration of ions. Monte Carlo simulations were applied to investigate the mechanism of HCl ionization in water. ^{17,20} Furthermore, the vibrational spectra of aqueous HCl were evaluated in both experimental and theoretical studies. 4,5,13,19-25 The results obtained thereby showed that the number of water molecules surrounding HCl and the accuracy of approximation methods utilized play a significant role on characteristics and stability of proton transferred and proton nontransferred HCl forms in aqueous solution. Summarizing all of these results, therefore, our intentions were (i) To investigate HCl in very dilute aqueous solution, providing the possibility of full hydration (498 water molecules for one HCl molecule). (ii) To utilize an ab initio HF method in an extended QM region with the new quantum mechanical charge field (QMCF) methodology. HF is known to lead to slightly too weak H-bonds, but proved more suitable than DFT in many systems.^{27,28} (iii) To start with undissociated HCl to see, whether dissociation would occur readily.

To answer these questions, in this study, we have performed an *ab initio* QMCF molecular dynamics simulation of HCl in aqueous solution. The structure of aqueous HCl solution was evaluated in terms of radial distribution functions, coordination numbers, angular distributions, θ -angle, and tilt angle distributions. To describe the dynamical properties, the mean ligand residence times for ligand exchange processes between hydration shell of HCl and bulk and the vibrational frequency of H—Cl were also determined.

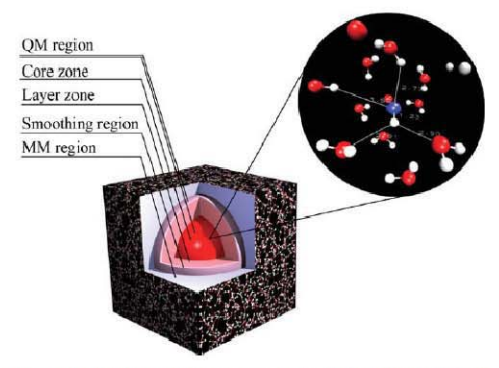


Figure 1. Definition of the quantum mechanical (QM) and molecular mechanical (MM) regions in the QMCF approach.

OMCF MD Simulation

The *ab initio* QMCF molecular dynamics technique²⁹ is similar to conventional QM/MM MD methods^{30–32} in which the system is separated into two regions, namely QM and MM regions. In the QMCF method, the QM region is enlarged to include the second hydration shell and consists of two subregions, the so-called "core region" (inner QM subregion) and the "layer region" (outer QM subregion), as shown in Figure 1. By using the QMCF method, no solute–solvent potentials are required, and an improved handling of Coulombic interactions is introduced. The calculated forces between the core region and the MM region are the major difference between the QM/MM MD and the QMCF MD simulation. In the QMCF MD simulation, the forces acting on each particle in the different regions are defined as

$$F_j^{\text{core}} = F_j^{\text{QM}} + \sum_{i=1}^{M} \frac{q_j^{\text{QM}} q_i^{\text{MM}}}{r_{ij}^2}$$
 (1)

$$F_{j}^{\text{layer}} = F_{j}^{\text{QM}} + \sum_{i=1}^{M} \frac{q_{j}^{\text{QM}} q_{i}^{\text{MM}}}{r_{ij}^{2}} + \sum_{i=1}^{M} F_{ij}^{\text{BJHnC}}$$
 (2)

$$F_{j}^{\text{MM}} = \sum_{\substack{i=1\\i\neq j}}^{M} F_{ij}^{\text{BJH}} + \sum_{i=1}^{N_{1}+N_{2}} \frac{q_{i}^{\text{QM}} \cdot q_{j}^{\text{MM}}}{r_{ij}^{2}} + \sum_{i=1}^{N_{2}} F_{ij}^{\text{BJHnC}}$$
(3)

where $F_j^{\rm core}$ is the quantum mechanical force acting on the particle j in the core region, $F_j^{\rm layer}$ is the forces acting on particle j located in the solvation layer, $F_j^{\rm MM}$ represents the forces acting on the particle j in the MM region, and M is the number of atoms in the MM region. In each simulation step, the forces in the core and layer region ($F_j^{\rm core}$, $F_j^{\rm layer}$) are calculated from the ab initio quantum mechanical treatment plus the Coulombic forces obtained from all MM atoms, whereas the forces in the

MM region (F_j^{MM}) are obtained from the BJH-CF2 water model^{33,34} augmented by the Coulombic forces exerted by all atoms in the core region (N_1) and the layer region (N_2) , and the noncoulombic forces generated by the atoms in the layer region (N_2) . Consequently, the QM forces in the layer (F_j^{layer}) are supplemented by the noncoulombic forces of particles in the MM region evaluated from the BJH-CF2 water model.^{33,34} The Coulombic interactions are calculated with the point charges of the atoms in the MM region and the quantum chemically evaluated partial charges on the atoms in the QM region. The charges of the particles in the MM region are incorporated via a perturbation term into the core Hamiltonian:

$$H_{\rm CF} = H_{\rm HF} + V_i'$$

$$V_i' = \sum_{j=1}^M \frac{q_j}{r_{ij}} \tag{4}$$

where q_j are the partial charges of each MM atoms obtained by Mulliken population analysis, which proved to be best compatible with the BJH-CF2 water model. The oxygen and hydrogen charges are -0.65996 and +0.32983, according to the charges of the BJH-CF2 water model utilized in the MM region. 33,34

In the QMCF MD simulation, solvent molecules can freely migrate between the QM and MM region. A smoothing function 35 is applied between the radii r_0 (5.7 Å) and r_1 (5.5 Å), corresponding to an interval of 0.2 Å, to ensure a continuous transition of forces at the boundary. The forces acting on each particle in the system can be defined as:

$$F_i^{\text{Smooth}} = F_i^{\text{MM}} + (F_i^{\text{layer}} - F_i^{\text{MM}}) \cdot S_m(r)$$
 (5)

where $F_j^{\rm MM}$ represents the force acting on the particle j in the MM region, $F_j^{\rm layer}$ is the force acting on the particle j located in the solvation layer, r is the distance of the water molecule from the chlorine atom of the solute molecule, and $S_{\rm m}$ a smoothing function.³⁵

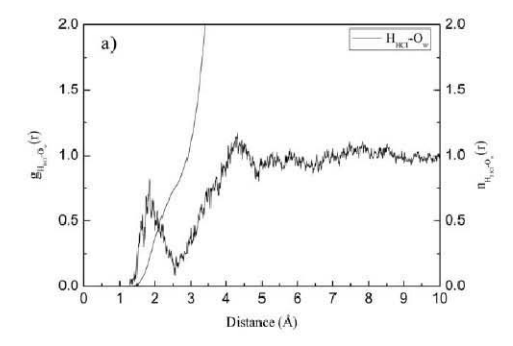
$$\begin{split} S_{\rm m}(r) &= 1, & \text{for } r \leq r_1 \\ S_{\rm m}(r) &= \frac{\left(r_0^2 - r^2\right)^2 \left(r_0^2 + 2^2 - 3r_1^2\right)}{\left(r_0^2 - r_1^2\right)^3}, & \text{for } r_1 < r \leq r_0 \\ S_{\rm m}(r) &= 0, & \text{for } r > r_0, \end{split} \tag{6}$$

where r_1 is the inner border of the smoothing region and r_0 is the radius of the QM region. Further details of this method are given in ref. 31.

This simulation protocol used in the present work is similar to that applied in a previous simulation of aqueous HF solution³⁶ and has been successfully applied to investigate characteristics of several composite chemical species in solution.^{29,36–39} The QMCF MD simulation was performed in a periodic boundary cubic box with a side length of 24.65 Å, containing one hydrogen chloride molecule plus 498 water molecules. Temperature was controlled by the Berendsen temperature-scaling algorithm⁴⁰ with a relaxation time of 100 fs to maintain 298.15 K. The

density of the simulation was fixed at 0.997 g/cm³, corresponding to the experimental value of pure water. A predictor-corrector algorithm was used to integrate the Newtonian equations of motion with the chosen time step of 0.2 fs. The flexible BJH-CF2 water model^{33,34} including an intramolecular potential was used to elucidate the interactions between pairs of water molecules in the MM region, as it allows explicit hydrogen movements, and thus, also a smooth transition of water molecules from the QM to the MM region and vice versa. The reaction field⁴¹ was applied to correct for longrange Coulombic interactions. Cutoff distances of 5 and 3 Å were used for noncoulombic O-H and H-H interactions, respectively. The radial cutoff limit for Coulombic interactions was set to half the box length. The values of 6.0 and 11.0 Å were chosen for the diameters of the core and the layer region, respectively, and hence, the full first hydration shell and a part of the second hydration shell are included in the QM region, according to the radial distribution functions (RDF) in the equilibrated state. The TURBOMOLE 5.9 program⁴²⁻⁴⁴ was used to evaluate the forces in the QM region calculated at the restricted Hartree-Fock level. Dunning dou-ble- ζ plus polarization function (DZP) basis sets^{45,46} were applied for chlorine, oxygen, and hydrogen atoms. These basis sets were chosen as a suitable compromise between accuracy of the results and computational effort. Many test calculations with the DZP basis sets comparing solvent clusters with one to six water molecules by HF, B3LYP, MP2, and CSSD have shown that the error by neglecting electron correlation is very minor. 47-50 Moreover, the QM/MM simulation using the B3LYP functional have revealed deviating descriptions such as too rigid structures for solvates and H-bonded systems. 51-53 In addition, the influence of the basis set super position error (BSSE) for HCl monohydrate was also determined at several levels of theory. The lowest BSSE energy of 0.2 kcal/mol was obtained from the HF method, whereas the values of 0.5, 0.9, and 0.8 kcal/mol were evaluated from the B3LYP, MP2, and CCSD methods, respectively. These indicate that the effects of electron correlation and BSSE should have only a minor influence on quality of the QMCF simulation results. The QMCF MD simulation was equilibrated for 2 ps and total of 10 ps was performed for sampling. Simulation time had to be limited to 50,000 steps of 0.2 fs (needed to appropriately describe hydrogen movements) as these 10 ps already consume 5 months of CPU time on a 4 AMD Opteron 2.8 GHz processors high performance computer.

Velocity autocorrelation functions (VACFs) were used to determine the dynamical properties of HCl in aqueous solution. With $C_{\infty v}$ symmetry of the HCl molecule, the vibrational motion of the HCl molecule is both infrared active and Raman active. The velocities of the hydrogen atom of HCl and the oxygen atom of H₂O were projected onto a unit vector parallel to the corresponding Cl—H bond $(\bar{\mathbf{u}}_1)$ and $H_{\text{HCl}} \cdots O_{\mathbf{w}}$ direction $(\bar{\mathbf{u}}_2)$, respectively, thus the vibrational modes are the projections of the hydrogen and oxygen velocities onto the unit vectors $\bar{\mathbf{u}}_1$ and $\bar{\mathbf{u}}_2$, respectively. The vibrational frequencies of the normal mode and the intermolecular $H_{\text{HCl}} \cdots O_{\mathbf{w}}$ interactions were calculated by their Fourier transformations of the VACFs. The normalized VACF, C(t), is defined by



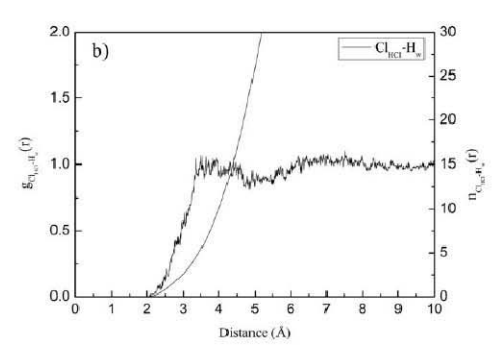


Figure 2. (a) $H_{HCl}\cdots O_w,$ and (b) $Cl_{HCl}\cdots H_w$ RDFs and their corresponding integration numbers.

$$C(t) = \frac{\sum_{i}^{N_t} \sum_{j}^{N} v_j(t_i) v_j(t_i + t)}{N_t N \sum_{i}^{N_t} \sum_{j}^{N} v_j(t_i) v_j(t_i)},$$
(7)

where N is the number of particles, N_t is the number of time origins t_i , and v_j denotes a certain velocity component of the particle j.

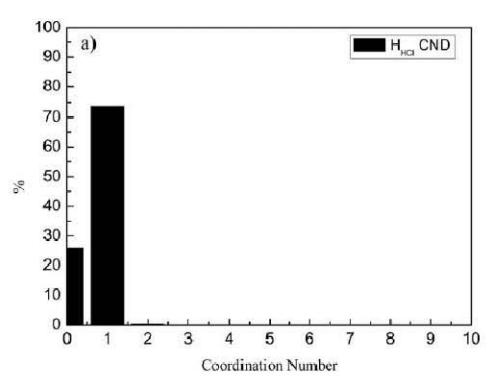
Results and Discussion

Structural Properties

The hydration structure of the HCl in aqueous solution was evaluated in terms of RDF, coordination numbers, and angular distributions. In the QMCF MD simulation, The H—Cl distance varies in the range of 1.2–1.5 Å, with an averaged value of 1.28 Å, which is in good agreement with the experimental value of 1.274 Å. S4.55 Figure 2 shows the radial distribution functions for each atom of HCl and its neighboring water molecules together with their corresponding integration numbers evaluated

from the QMCF MD simulation. The first peak in the H_{HCI} ···O_w RDF characterizes the first hydration shell, located between 1.5 and 2.5 Å with a maximum value of 1.84 Å. This value is larger than that determined in the case of an aqueous HF solution (1.62 Å).³⁶ The second peak corresponding to the water ligands near the Cl atom in the first hydration shell is located at 4.30 Å. The Cl_{HCI} ···H_w RDF and the corresponding integration are depicted in Figure 2b. The first Cl_{HCI} ····H_w peak lies within the range of 2.0-4.0 Å, showing its maximum at 3.51 Å with additional peaks at 3.36, 3.62, and 3.93 Å. The Cl_{HCI} ····H_w second peak is situated at 4.40 Å, covering distances of 4.0-4.7 Å, and corresponds to the second H atom of coordinated water molecules.

The coordination number distributions of the first hydration shell determined from the $H_{\rm HCI}$... $O_{\rm w}$ and $Cl_{\rm HCI}$... $O_{\rm w}$ interactions of the aqueous HCI solution are displayed in Figure 3. According to Figure 3a, a single water molecule bound to the H site of the HCI molecule is the most dominant coordination with 74%



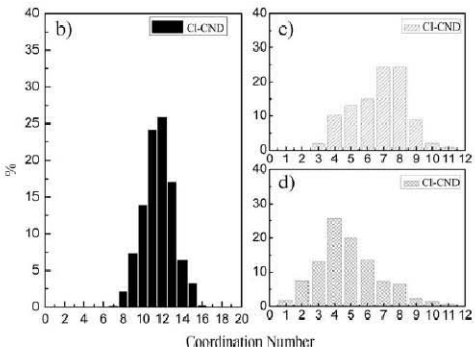


Figure 3. Coordination number distributions of (a) H and (b) Cl atoms in the first hydration shell of HCl, (c) Cl atom in immediate first shell from 0.0 to 4.2 Å, and (d) Cl atom in extended first hydration shell from 4.2 to 4.8 Å.

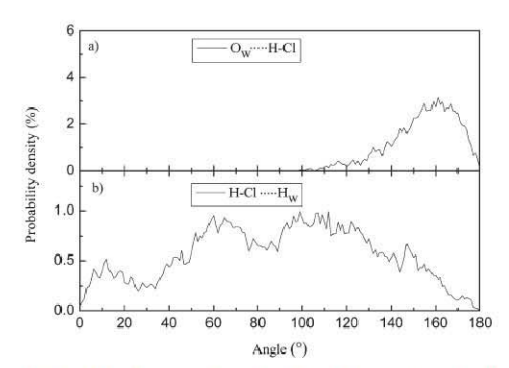


Figure 4. Distributions of (a) $O_w \cdots H_{HCI} - Cl_{HCI}$ angles and (b) $H_{HCI} - Cl_{HCI} \cdots H_w$ angles, obtained from the QMCF MD simulation.

occurrence. The ClHCI ... Ow RDF displays two distinguished parts of the first hydration shell, one representing an extended first hydration shell located between 4.2 and 4.8 Å. Therefore, the coordination number distributions of the water molecules in the substructure near the CI atom were examined and depicted in Figures 3b-3d. As shown in Figure 3c, the coordination number distribution integrated up to the distance of 4.2 Å of the first part of the ClHCI...Ow peak covers a wide range of 3-11, giving an average value of 6.7. For the extended first hydration shell, an average coordination number of 4.9 was found with a large variation in the hydration numbers ranging from 1 to 11. These findings indicate almost seven water molecules to be directly bound to the CI site of the HCl molecule, while in average five water molecules are located in the extended first hydration shell. This shows that the frequent ligand exchange processes must occur at the Cl site, whereas the one water molecule bound to the H atom seems to be more stably coordinated.

The hydrogen bond angle between HCl and water molecule can be determined in terms of the angular distribution functions of the O_w — $H_{\rm HCl}$ — $Cl_{\rm HCl}$ and $H_{\rm HCl}$ — $Cl_{\rm HCl}$ — H_w angles in the first hydration shell. According to Figure 4a the O_w — $H_{\rm HCl}$ — $Cl_{\rm HCl}$ angular distribution has its maximum at 161° with tailing until 100°, proving the preference for linear O_w — $H_{\rm HCl}$ — $Cl_{\rm HCl}$ hydrogen bond arrangements. However, considerably less linearity of this hydrogen bond in the case of HCl was observed in comparison with HF, where the O_w — $H_{\rm HF}$ — $F_{\rm HF}$ angular distribution is situated at 170° with variation down to 100° . ³⁶ The presence of nonlinear, weak, and flexible hydrogen bonds between water and the Cl site of HCl is recognized from three dominant $H_{\rm HCl}$ — $Cl_{\rm HCl}$ — H_w peaks at 12°, 60°, and 112°, respectively. The low angle value of 12° reflects the arrangement of two hydrogen bonds in the intermediate HCl monohydrate ($Cl_{\rm HCl}$ — H_w and $H_{\rm HCl}$ — O_w).

To further characterize the flexibility and orientation of the water molecules surrounding HCl in the first hydration shell, angle θ and tilt angle are introduced. The angle θ is the angle between the vector pointing along $C_{\mathbf{g}}$ — $O_{\mathbf{w}}$ ($C_{\mathbf{g}}$ is the center of mass of the HCl molecule) and the dipole vector of water

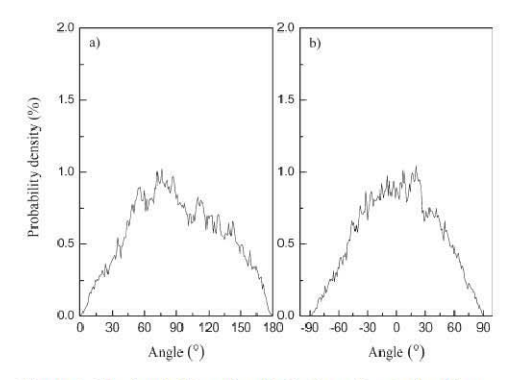


Figure 5. The θ and tilt angular distributions of water ligands near the HCl molecule.

molecule. The tilt angle is the angle between the $H_{HCI}-Cl_{HCI}$ axis and the plane defined by the O_w-H_w vectors. Figure 5 presents the θ and tilt angular distributions in the first hydration shell of HCl. The broad peak of the angle θ distribution obtained from the QMCF MD simulation has its maximum at 76° , covering a wide range of $0\text{--}180^\circ$. A similar result was also observed in the case of HF. 36 However, the maximum value of 136° evaluated for HF is much larger than that determined from HCl. The maximum value of the tilt angle for the first shell is located at 20° , and the distribution reaches 0 at $\pm 90^\circ$. Both angle distributions prove a very high flexibility of the first shell ligands' orientation.

Dynamical Properties

The vibrational frequencies of the normal mode H_{HCI} — Cl_{HCI} and the intermolecular H_{HCI} — O_w interactions were examined using the VACFs and their Fourier transformations. Figure 6

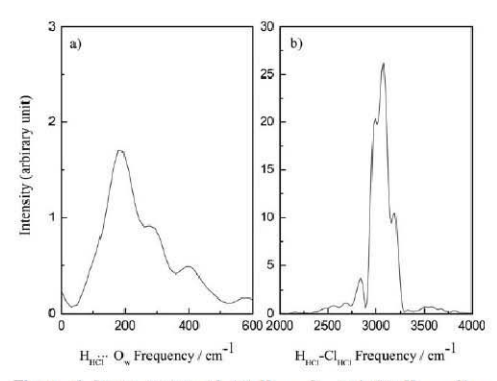


Figure 6. Power spectra of (a) $H_{HCl} \cdots O_w$ and (b) $H_{HCl} - Cl_{HCl}$ stretching modes in the first hydration shell.

Journal of Computational Chemistry DOI 10.1002/jcc

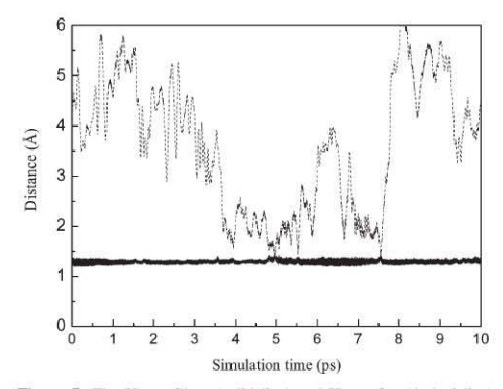


Figure 7. The $H_{\rm HCI} \cdots Cl_{\rm HCI}$ (solid line) and $H_{\rm HCI} \cdots O_{\rm w}$ (dashed line) distances as a function of time in the first hydration shell evaluated for the proton transfer processes.

illustrates the power spectra of the HHCI...Ow and HHCI-ClHCI vibrational motions in the first hydration shell obtained from the QMCF MD simulation. In Figure 6a, the maximum frequency of the HHCI...Ow vibrational mode in the first hydration shell is situated at 179 cm⁻¹, with two shoulder peaks at 277 and 390 cm⁻¹. The force constant of 1.8 N/m was calculated for this frequency of the HHCI...Ow peak, which is much weaker than that obtained for the HHF...Ow interaction (5.9 N/m),36 but slightly stronger than the value of 1.6 N/m retrieved from the experimental O_w — H_w — O_w stretching (170 cm $^{-1}$). 56 This demonstrates that the acid dissociation of HCl is much more facilitated than that of HF, since the HHCI···Ow hydrogen bond interaction is almost equally weak as the $O_w - H_w \cdots O_w$ interaction in pure water. For the H_{HCl}—Cl_{HCl} stretching motion, the highest value of this mode is centered at 3078 cm⁻¹, with two shoulder peaks at 2997 and 3192 cm⁻¹. The force constants evaluated for these peaks are 547.1, 518.7, and 588.4 N/m, respectively. The H_{HCI}-Cl_{HCI} stretching frequency calculated from the QMCF simulation is in reasonable agreement with the experimental harmonic vibrational frequency of 2990 cm^{-1,57,58} In addition, the

Table 1. The Energy Parameters for the $HCl(H_2O)_4$ Clusters Calculated by Different Levels of Theory.

Method	HCl(H ₂ O) ₄ undissociated form (Hartree)	HCl(H ₂ O) ₄ dissociated form (Hartree)	ΔE (kcal/mol) ^a
HF/DZP	-764.2932329	-764.2869273	3.96
BLYP/DZPb	We to be 40 to	-766.5469201	-
B3LYP/DZPb	-	-766.6512601	1 - 0
MP2/DZP	-765.2326384	-765.2291570	2.18
CCSD/DZP	-765.2784585	-765.2715970	4.31

^aThe relative energies of the dissociated form with that of the undissoci-

Table 2. Mean Ligand Residence Times and Sustainability of Migration Processes to and from the First Hydration Shell of Chlorine and Hydrogen Atoms of the Hydrogen Chloride Molecule.

		$t^* = 0 \text{ ps}$		$t^* = 0.5 \text{ ps}$			
Solute t _{si}	$t_{ m sim}$	$N_{\rm ex}^0$	$\tau_{H_2O}^0$	$N_{\rm ex}^{0.5}$	$\tau_{\rm H_2O}^{0.5}$	S_{ex}	1/S _{ex}
Cl _{HCI}	10.0	392	0.3	56	2.1	0.14	7.1
H _{HCI}	10.0	80	0.1	9	0.8	0.11	9.1
Bulka	10.0	269	0.2	24	1.7	0.09	11.2

^aValues obtained from a QM/MM MD simulation of pure water.⁵²

gas-phase value of 3153 cm $^{-1}$ for the H_{HCI} – Cl_{HCI} stretching frequency was also evaluated from the HF/DZP method to confirm that this agreement is not a coincidence. The value of 547.1 N/m estimated for the force constant in the case of HCI is much weaker than that observed for HF (819.1 N/m), 36 proving less stability of the nondissociated form of HCI. It was further found that the ligand exchange processes in the H site of HCI causes the shoulder peaks in the H_{HCI} – Cl_{HCI} stretching mode.

To characterize the acid dissociation of HCI, the ionization structure of this acid has been evaluated. Figure 7 shows distributions of the $H_{\rm HCI}{}^{\dots}{}^{\text{Cl}}_{\rm HCI}$ and $H_{\rm HCI}{}^{\dots}{}^{\text{O}}_{\rm W}$ distances in the first hydration shell, exhibiting the proton migration from the chlorine atom of hydrogen chloride to oxygen of a neighboring water. The first proton migration takes place around 4.9–5.0 ps and the second one occurs during the simulation time of 7.5–7.6 ps. Another dissociation attempt observed at 5.5 ps is not completed, but almost successful. It is seen that the proton coming from HCI bound to the neighboring water forming H_3O^+ species comes back to the CI atom reforming the HCI molecule within the femtosecond scale. Despite the short simulation time of 10 ps, three proton migration processes were observed, which shows that dissociation can occur already on the picosecond scale in very dilute solution. In the previous CPMD simulation, for corresponding to a higher concentration, a number of

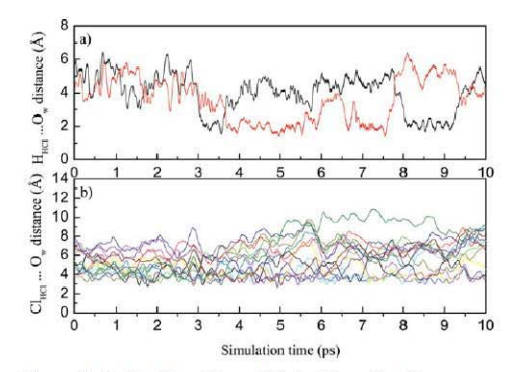


Figure 8. (a) The H_{HCl} \cdots O_w and (b) the Cl_{HCl} \cdots O_w distances as a function of time in the first hydration shell obtained from the QMCF MD simulation.

Journal of Computational Chemistry DOI 10.1002/jcc

bOnly the dissociated forms were observed.

error sources can be identified, partly due to the early time it has been performed, such as the use of DCl and D2O and the functionals being used, for which several problems have been identified in the meantime.⁵⁹ As previous cluster calculations (DFT and MP2)^{19,22} have already shown that DFT overrates the stability of the dissociated state, it seemed appropriate to perform new cluster calculations including HF, MP2, CCSD, and the more modern B3LYP density functional, and the results, shown in Table 1, clearly prove that DFT leads to an unjustified preference for the dissociated state. It should be emphasized, however, that the frequent attempts of proton transfer in our simulation within a few picoseconds are a clear indication that over a longer time period a number of them will be successful thus creating a sufficient number of hydronium ions. For study of full dissociation, i.e., separation of Cl⁻ and hydrated hydronium ion, a longer simulation time would have been required but on the basis of the results obtained for 10 ps one can easily predict such a dissociation process to happen.

The dynamics of ligand exchange processes at each atom of HCl were also determined by the mean residence times (MRTs) using the "direct" method. 60 The time parameters t^* of 0.0 and 0.5 ps were used, reflecting to the minimum duration of a ligand's displacement from its original coordination shell to be accounted. The number of ligand exchange processes, the MRTs, and the sustainability of migration processes from the first hydration shell are summarized in Table 2. The variations of the HHCI···Ow and ClHCI···Ow distances obtained at t* 0.5 ps in the first hydration shell are presented in Figure 8. As shown in Figure 8a, there are three exchange processes occurring at the H atom of HCl, the first one taking place at 3.5 ps and the second and the third one observed in the range of 6-7 and 7-8 ps, respectively. For the Cl site, several ligand exchange processes were found during the simulation time of 10 ps, as shown in Figure 8b. The calculated MRT values with respect to $t^* = 0.0$ and 0.5 ps for the first hydration shell located around the CI atom are 0.3 and 2.1 ps, which are the same as those estimated for the F site of HF. 36 The values of 0.1 and 0.8 ps for $t^*=0.0$ ps and $t^*=0.5$ ps, respectively, were determined for the H site of HCl. These values are smaller in comparison with the aqueous HF solution (0.8 ps for $t^* = 0.0$ ps and 2.5 ps for t^* 0.5~ps), 36 and also smaller than that obtained from QM/MM (1.51 ps) 53 simulation of pure water. In the QMCF MD, hydrogen bond life times of 1.1 and 0.31 ps were evaluated for the Cl_{HC1}—H_{HC1}···O_w and H_{HC1}—Cl_{HC1}···H_w hydrogen bonds, respectively, suggesting a very different stability of these Hbonds. The average lifetime of the Cl_{HCI}-H_{HCI}...O_w hydrogen bond is higher than that observed in pure water by experiment (0.55 ps), and a QM/MM MD simulation (0.33 ps),⁵³ confirming the stability of this H bond. The value of 0.31 ps obtained for the HHCI-ClHCI-Hw hydrogen bond is almost the same as the value of 0.36 determined for the F site of the HF molecule. The MRT values and the hydrogen bond lifetimes predicted from the QMCF MD simulation reveal that HCl in aqueous solution is simultaneously a weak structure-making and a weak structure breaking species. The sustainability coefficients $S_{\rm ex}$ were computed by comparing the number of all exchanges through the border of the hydration shell $(N_{\rm ex}^{0.0})$ to the number of exchanges processes lasting at least 0.5 ps $(N_{\rm ex}^{0.5})$, resulting in 0.11 and 0.14 for H and Cl sites of hydrogen chloride. The corresponding 1/Sex values are 9.1 and 7.1, suggesting that one lasting exchange process in the neighborhood of H and Cl is achieved by about nine and seven attempts to cross a shell boundary, respectively.

Conclusions

We have performed a QMCF molecular dynamics simulation to investigate the hydration structure and dynamics of the aqueous HCl solution. The calculated H-Cl bond distance and its vibrational frequency are in good agreement with the experimental observation. A relatively strong hydrogen bond at the H site of hydrogen chloride was detected, whereas weak hydrogen bonding dominates at the Cl site. The coordination number of \sim 7 is prevailing in the first hydration shell, augmented by about five water molecules of an extended first shell. The acid dissociation of HCl is visible from the proton transfer events observed in the QMCF MD simulation. The QMCF MD simulation shows several ligand exchange processes in the first hydration shell, which occur more frequently at the Cl site of the molecule.

Acknowledgments

Financial support for this work by the Thailand Research Fund (TRF) and Thailand Commission on Higher Education (ASEA-UNINET fellowships for C.K. and V.V.) are gratefully acknowledged and B.M.R. acknowledges support by the Austrian Science Foundation (FWF).

References

- 1. Kirk, K. L. Biochemistry of Halogens and Inorganic Halides; Plenum Press: New York, 1991.
- 2. Amirand, C.; Maillard, D. J Mol Struct 1988, 176, 181.
- 3. Triolo, R.; Narten, A. H. J Chem Phys 1975, 63, 3624.
- 4. Agmon, N. J Phys Chem A 1998, 102, 192,
- 5. Fámík, M.; Weimann, M.; Suhm, M. A. J Chem Phys 2003, 118, 10120
- 6. Cappa, C. D.; Smith, J. D.; Messer, B.; Cohen, R. C.; Saykally, R. J. J Phys Chem B 2006, 110, 1166.
- 7. Botti, A.; Bruni, F.; Ricci, M. A.; Soper, A. K. J Chem Phys 2006, 125, 14508.
- Chipot, C.; Gorb, L. G.; Rivail, J. L. J Phys Chem 1994, 98, 1601. 9. Robertson, S. H.; Clary, D. C. Faraday Discuss 1995, 100, 309.
- 10. Gertner, B. J.; Hynes, J. T. Science 1996, 271, 1563.
- 11. Planas, M.; Lee, C.; Novoa, J. J. J Phys Chem 1996, 100, 16495.
- 12. Laasonen, K.; Klein, M. L. J Am Chem Soc 1994, 116, 11620.
- Packer, M. J.; Clary, D. C. J Phys Chem 1995, 99, 14323.
 Balbuena, P. B.; Johnston, K. P.; Rossky, P. J. J Phys Chem 1996, 100, 2716.
- 15. Lee, C.; Sosa, C.; Planas, M.; Novoa, J. J Chem Phys 1996, 104,
- Laasonen, K.; Klein, M. L. J Phys Chem A 1997, 101, 98.
- Ando, K.; Hynes, J. T. J Phys Chem B 1997, 101, 10464.
 Geiger, F. M.; Hicks, J. M.; de Dios, A. C. J Phys Chem A 1998, 102, 1514.
- 19. Re, S.; Osamura, Y.; Suzuki, Y. J Chem Phys 1998, 109, 973.

Journal of Computational Chemistry DOI 10.1002/jcc

- 20. Bacelo, D. E.; Binning, R. C.; Ishikawa, Y. J Phys Chem A 1999, 103, 4631
- 21. Chaban, G. M.; Gerber, R. B.; Janda, K. C. J Phys Chem A 2001, 105, 8323.
- 22. Cabaleiro-lago, E. M.; Hermida-Ramón, J. M.; Rodríguez-Otero, J. J Chem Phys 2002, 117, 3160.
- Masia, M.; Forbert, H.; Marx, D. J Phys Chem A 2007, 111, 12181.
 Buch, V.; Dubrovskiy, A.; Mohamed, F.; Parrinello, M.; Sadlej, J.; Hammerich, A. D.; Devlin, J. P. J Phys Chem A 2008, 112, 2144.
- Lee, H.-S.; Tuckerman, M. E. J. Phys Chem A 2009, 113, 2144.
 Heuft, J. M.; Meijer, E. J. Phys Chem Chem Phys 2006, 8, 3116.
- 27. Rode, B. M.; Schwenk, C. F.; Tongraar, A. J Mol Liq 2003, 110, 105.
- 28. Rode, B. M.; Schwenk, C. F.; Hofer, T. S.; Randolf, B. R. Coord Chem Rev 2005, 249, 2993.
- Rode, B. M.; Hofer, T. S.; Randolf, B. R.; Schwenk, C. F.; Xenides, D.; Vchirawongkwin, V. Theor Chem Acc 2006, 115, 77.
- 30. Field, M. J.; Bash, P. A.; Karplus, M. J Comput Chem 1990, 11, 700.
- 31. Gao, J. J Am Chem Soc 1993, 115, 2930.
- 32. Bakowies, D.; Thiel, W. J Phys Chem 1996, 100, 10580.
- 33. Stillinger, F. H.; Rahman, A. J Chem Phys 1978, 68, 666. 34. Bopp, P.; Janscó, G.; Heinzinger, K. Chem Phys Lett 1983, 98, 129.
- 35. Brooks, B. R.; Bruccoleri, R. E.; Olafson, B. D.; States, D. J.; Swaminathan, S.; Karplus, M. J Comput Chem 1983, 4, 187.
- Kritayakomupong, C.; Vchirawongkwin, V.; Hofer, T. S.; Rode, B. M. J Phys Chem B 2008, 112, 12032.
- 37. Vchirawongkwin, V.; Rode, B. M.; Persson, I. J Phys Chem B 2007, 111, 4150,
- 38. Fatmi, M. Q.; Hofer, T. S.; Randolf, B. R.; Rode, B. M. J Comput Chem 2007, 28, 1704.
- 39. Hofer, T. S.; Randolf, B. R.; Shah, S. A. A.; Rode, B. M.; Persson, I. Chem Phys Lett 2007, 445, 193.
- Berendsen, H. J. C.; Postma, J. P. M.; van Gunsteren, W. F.; DiNola, A.; Haak, J. R. J Chem Phys 1984, 81, 3684.
- 41. Adams, D. J.; Adams, E. H.; Hills, G. J Mol Phys 1979, 38, 387.
- 42. Ahlrichs, R.; Bär, M.; Häser, M.; Horn, H.; Kölmel, C. Chem Phys Lett 1989, 162, 165.

- 43. Ahlrichs, R.; von Arnim, M. Methods and Techniques in Computa-
- tional Chemistry: METECC-95; Cagliari: Sardinia, 1995. 44. von Amim, M.; Ahlrichs, R. J Comput Chem 1998, 19, 1746
- Dunning, T. H., Jr.; Wadt, W. R. J Chem Phys 1989, 90, 1007.
 Dunning, T. H., Jr.; Hay, P. J. Modern Theoretical Chemistry: Methods of Electronic Structure Theory, Vol. 3; Schaefer, H. F., III, Ed.;
- Plenum Press: New York, 1977. 47. D'Incal, A.; Hofer, T. S.; Randolf, B. R.; Rode, B. M. Phys Chem Chem Phys 2006, 8, 2841.
- Hofer, T. S.; Pribil, A. B.; Randolf, B. R.; Rode, B. M. J Am Chem Soc 2005, 127, 14231.
- 49. Hofer, T. S.; Randolf, B. R.; Rode, B. M. Phys Chem Chem Phys 2005, 7, 1382,
- 50. Hofer, T. S.; Rode, B. M.; Randolf, B. R. Chem Phys 2005, 312,
- 51. Schwenk, C. F.; Hofer, T. S.; Rode, B. M. J Phys Chem A 2004,
- 52. Schwenk, C. F.; Löfffler, H. H.; Rode, B. M. J Chem Phys 2001, 115, 10808.
- 53. Xenides, D.; Randolf, B. R.; Rode, B. M. J Chem Phys 2005, 122, 174506.
- 54. Herzberg, G.; Spink, J. W. T. Z. Phys 1934, 89, 474.
- 55. Huber, K. P.; Herzberg, G.Molecular Spectra and Molecular Structure, Vol. 37; Van Nostrand Reinhold: New York, 1979.
- 56. Franks, F. Water: A Comprehensive Treatise, Vol. 1; Plenum Press: New York, 1972.
- 57. Shimanouchi, T. Tables of Molecular Vibrational Frequencies, Vol. 37; National Bureau of Standards: Washington, D.C., 1972.
- Chase, M. W.; Davies, C. A.; Downey, J. R.; Frurip, D. J.; McDonald, R. A.; Syverud, A. N. J Phys Chem Ref Data Suppl 1985, 14.
- 59. Yoo, S.; Zeng, X. C.; Xantheas, S. S. J Chem Phys 2009, 130, 221102
- 60. Hofer, T. S.; Tran, H. T.; Schwenk, C. F.; Rode, B. M. J Comput Chem 2004, 25, 211.
- 61. Lock, A. J.; Woutersen, S.; Bakker, H. J. J Phys Chem A 2001, 105, 1238.

DOI 10.1002/jcc

RISM-SCF-SEDD Study on the Symmetry Breaking of Carbonate and Nitrate Anions in **Aqueous Solution**

Viwat Vchirawongkwin,† Hirofumi Sato,*** and Shigeyoshi Sakaki**

Department of Chemistry, Faculty of Science, Chulalongkorn University, Phyathai Road, Prathumwan, Bangkok 10330, Thailand, Department of Molecular Engineering, and Fukui Institute for Fundamental Chemistry, Kyoto University, Kyoto, 615-8510, Japan

Received: February 25, 2010; Revised Manuscript Received: July 1, 2010

The planarity of carbonate and nitrate anions was investigated in the gas and solution phases by means of the reference interaction site model self-consistent field spatial electron density distribution (RISM-SCF-SEDD) method. The computed optimized geometries and solvation structures are compared with the diffraction data. In the solution phase, the symmetry of carbonate anion is changed from D_{3h} to C_{3v} , whereas the planarity of nitrate anion is still retained. These are fully consistent with experimental knowledge. The classical electrostatic model was also utilized to elucidate the mechanism of the symmetry breaking. It should be emphasized that the symmetry breaking occurs not only by a specific solvent molecule attaching to the ion but by an overall electrostatic interaction between the infinite number of solvent molecules and the ion.

Introduction

Carbonate and nitrate anions are abundant and important in biological systems as well as in environmental systems. Carbonate is a ubiquitous and reactive anion that can be found in groundwater and reacts to form aqueous and solid-state complexes with the majority of metals in the periodic table. 1 Nitrate is the most fully oxidized compound of nitrogen and is therefore stable to oxidation, regarded as a potentially strong oxidizing agent. It can also be generated in the human body through the oxidation of nitric oxide, which is produced by nitric oxide synthases from L-arginine.²³

The structures of these two compounds are very similar, normally planar possessing D_{3h} symmetry with six normal modes: symmetric stretch (ν_1) , out-of-plane deformation (ν_2) , two doubly degenerate modes, i.e., antisymmetric stretch (ν_3) and in-plane deformation (ν_4). Rudolph and co-workers observed the ν_2 mode and its overtone of carbonate ion in an aqueous solution using Raman spectroscopy, suggesting the symmetry breaking in the concentrated4 and dilute5 solutions. They also optimized the water cluster, a carbonate with two water molecules, by employing the density functional theory in the gas phase, showing the C_{2v} symmetry.⁴ On the other hand, the far-ultraviolet resonance Raman spectroscopy indicates the planarity of nitrate ion in several polar solvents, though a very broad band of v_3 suggests that the symmetry is lowered from D_{3h} to C_{2v} or to C_{s} . The results of photoelectron spectroscopy suggested the first hydration consisting of three water molecules with the C_{3h} symmetry as the geometry of nitrate ion in aqueous solution.7 Raman results have been reported that the splitting of v_3 vanishes for the dilute nitrate solutions.⁸⁻¹⁰ The recent infrared multiple photon photodissociation experiment on the $NO_3^-(H_2O)_n$ clusters (n = 1-6) observed the splitting of the v_3 band due to the perturbation of water molecules, showing the possibility of symmetry lowering to C_1 . Pathak et al.

The optimization of carbonate ion in aqueous solution (dielectric media) with the generalized conductor-like screening model indicates a slight effect on the geometry compared with the gaseous state.¹³ An empirical force field for the carbonate ion including the out-of-plane displacement of the carbon atom was developed to investigate the phase transition of calcite.14 The potential function with increasing the stiffness of the carbonate ion was adopted to the classical molecular dynamics (MD) simulation of calcium carbonate. 15 The recent investigations based on Car-Parrinello (CP) MD simulation provided the structural properties of hydration shell, but the symmetry breaking was not discussed. ^{16,17} The inclusion of an anharmonic force field in the classical MD simulation¹⁸ and a combined quantum mechanics/molecular mechanics (QM/MM) MD simulation 19 of hydrated nitrate ion presented the splitting of ν_3 that agrees with the spectroscopic results.

At the same time, there is no wonder that nonsymmetric solvation structure around the ion breaks its symmetry; the symmetry of the cluster model is inevitably lowered by the specific hydrating molecule. The question that we would like to raise here is whether the symmetry of the anions in aqueous solution is inherently broken or not, under an isotropic environment. If so, what is the driving force of the breaking? It should be stressed that the issue is deeply related to both the electronic structure of the anion and solvation structure around it. OM/ MM or an equivalent treatment is essentially needed.

Here we present an alternative method to the QM/MM, RISM-SCF, which is a hybrid method of integral equation theory in statistical mechanics (reference interaction site model selfconsistent field, RISM-SCF) and an ab initio electronic structure theory. 20-24 This method succeeded to investigate the structural properties of the solute and the solvation effects on the reactions in a solution phase.²⁵⁻²⁹ In particular, the symmetry breaking in the solvated I3 system was precisely discussed.30 In this work, we applied the RISM-SCF formalism to investigate the optimized geometries of carbonate and nitrate anions in aqueous solutions. The classical electrostatic free energy calculation

computed an effect of explicit water molecules on the lowering symmetry of carbonate and nitrate anion clusters.11

^{*} To whom correspondence should be addressed. E-mail: hirofumi@

moleng.kyoto-u.ac.jp.

† Chulalongkorn University.

† Department of Molecular Engineering, Kyoto University.

† Fukui Institute for Fundamental Chemistry, Kyoto University.

TABLE 1: Lennard-Jones Parameters for the ${\rm CO_3^{2-}}$ and ${\rm NO_3^-}$ Anions and Water Molecule

σ/Å		ε/kcal mol
	Solute	
C	3.296	0.1200
N	3.150	0.1700
O	2.850	0.2000
	H_2O	
H	1.000	0.0560
0	3.166	0.1550

based on the multipole expansion^{31,32} was also utilized as a model to understand the true nature of the symmetry breaking caused by the solvation effect.

Method

The RISM-SCF method has been outlined in detail elsewhere.20-24 Similar to the QM/MM, this method evaluates the statistical solvent distribution consistent with the electronic structure of the solute, while the electronic structure of the solute is affected by the surrounding solvent distribution. Thus, both the RISM integral equation and ab initio molecular orbital (MO) calculation must be solved in a self-consistent manner. The statistical mechanics part of the RISM-SCF method was solved with the Kovalenko and Hirata (KH) closure approximation 33,34 to obtain the structure of the solvent on a grid of 2048 points on the radial direction, whereas the ab initio MO methods at Hartree-Fock (HF) and density functional theory, namely, Becke, three-parameter, Lee-Yang-Parr exchange-correlation functional (B3LYP), associated with the 6-311+G* basis set, 35,36 were utilized to evaluate the electronic structure of carbonate and nitrate ions in the SCF procedure, so-called RISM-SCF/ HF and RISM-SCF/B3LYP, respectively. We further employed the CCSD(T) method coupled with solvation effect (RISM-SCF/ CCSD(T)) to obtain highly accurate solvation energy. The SPC water model³⁷ with the corrected Lennard-Jones parameters of hydrogen sites ($\sigma = 1.0 \text{ Å}$ and $\varepsilon = 0.056 \text{ kcal mol}^{-1}$) was selected for solvent water in the RISM equation. Table 1 lists all parameters^{21,38,39} employed in the solution-phase calculations. The density of solvent water was set to 1 g cm⁻³ at 298.15 K.

All solution-phase calculations were performed with the RISM-SCF-SEDD (spatial electron density distribution, SEDD)²³ code implemented in GAMESS program package⁴⁰ modified by us. In the theory, the total energy of the system (A) is defined as the sum of the solute potential energy and solvation free energy:

$$\mathcal{A} = \langle \Psi^{\text{solute}} | H_0 | \Psi^{\text{solute}} \rangle + \Delta \mu \tag{1}$$

where H_0 is the standard Hamiltonian of solute in a gas phase, Ψ^{solute} is the wave function of the solute obtained by solving the equation with the modified Fock operator, and $\Delta\mu$ is the solvation free energy evaluated by the KH closure equations. ^{33,34}

In order to understand the solvation effects on the symmetry breaking of anions, we also calculated the classical electrostatic free energy based on the multipole expansion with the spherical model 31,32 of radius b from the center of mass of solute immersed in a solvent with a dielectric constant D, which was set to 80 for the solvent water.

Results and Discussion

Optimized Structures of Carbonate and Nitrate Anions in the Solution Phase. The initial geometries of carbonate and nitrate anions in both gas and solution phases were set as an

TABLE 2: Optimized Geometries of CO₃²⁻ and NO₃⁻ Anions in the Gas and Solution Phases Obtained from HF, B3LYP, RISM-SCF/HF, and RISM-SCF/B3LYP Calculations with the 6-311+G* Basis Set

	gas phase		solution	n phase
	HF	B3LYP	RISM-SCF/ HF	RISM-SCF/ B3LYP
		CO ₃ 2-		
C-O ₁ (Å)	1.282	1.308	1.267	1.288
C-O ₂ (Å)	1.282	1.308	1.267	1.288
C-O ₃ (Å)	1.282	1.308	1.267	1.288
C- torsion (deg)	0.00	0.00	7.45	7.79
		NO ₃		
$N-O_1$ (Å)	1.224	1.261	1.217	1.253
$N-O_2$ (Å)	1.224	1.261	1.217	1.253
$N-O_3$ (Å)	1.224	1.261	1.217	1.253
N- torsion (deg)	0.00	0.00	0.02	0.00

nonsymmetric structure and optimized without any symmetry constraint. Table 2 summaries the optimized geometries of carbonate and nitrate anions in the isolated state evaluated with the standard HF and B3LYP and the solution phase with the RISM-SCF/HF and RISM-SCF/B3LYP methods. The C- and N- torsion angles are defined to investigate the planarity of the solute as the $C-O_1-O_2-O_3$ and $N-O_1-O_2-O_3$ dihedral angles, respectively.

The geometries of both anions obtained from the HF and B3LYP optimizations in the gas phase show the equivalence of three bonds and the molecular plane described with the Cand N- torsion angles to be equal to 0.00°, possessing the D3h symmetry. However, the situation is different when these anions are dissolved in water. The symmetry of carbonate ion was lowered to nonplanar structure. The C- torsions were increased to 7.45° and 7.79° for the optimized geometry obtained from the RISM-SCF/HF and RISM-SCF/B3LYP, respectively. The N- torsion of nitrate ion obtained from the RISM-SCF/HF was hardly changed by 0.02°, and the ion has retained the planarity for the RISM-SCF/B3LYP optimization. All bonds within each anion remain the equivalence in the solution phase, but they are slightly shorter than those in the gas phase by 0.015 and 0.020 Å for carbonate ion, and 0.007 and 0.008 Å for nitrate, obtained from the RISM-SCF/HF and RISM-SCF/B3LYP, respectively. These results indicate the symmetry of carbonate ion is changed from D_{3h} to C_{3v} , but nitrate ion is still as D_{3h} . Our intramolecular distances of carbonate and nitrate anions, namely, C-O_C and N-O_N, obtained from the RISM-SCF optimizations show a good agreement with the recent neutron diffraction experiments of K2CO3 solutions that reported the C-Oc distance of 1.3 Å41 and with the NaNO3 solutions in which the N-O $_{N}$ distances vary between 1.21 \pm 0.02 and 1.24 \pm 0.02 Å, 42 respectively.

The radial distribution functions (RDFs) of solvent molecules around the solute are also obtained from the computations as shown in Figures 1 and 2. The positions of the first peaks for each anion obtained from the RISM-SCF/HF summarized in Table 3 are slightly shorter than those of RISM-SCF/B3LYP within the maximum deviation of 0.03 Å. The positions of the first hydration peaks represent the stronger interactions of water molecules with the carbonate ion than those of the nitrate ion. This result corresponds to the neutron diffraction with isotopic substitution (NDIS) of $\rm Cs_2CO_3$ and $\rm CsNO_3$ in an aqueous solution, indicating that the stronger hydrogen bonds are formed between the solvent water and carbonate ion than those formed in the nitrate ion. 43 Our results in Table 3 are also in an

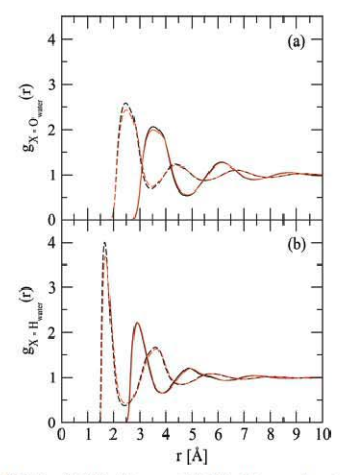


Figure 1. RDFs of (a) $X-O_{water}$ and (b) $X-H_{water}$, where X stands for the C and O sites of CO_3^{-2} ion. The black and red lines refer to the RDFs obtained from RISM-SCF/HF for the C (the black solid lines) and O (the black dashed lines) sites and RISM-SCF/B3LYP for the C (the red solid lines) and O (the red dashed lines) sites, respectively.

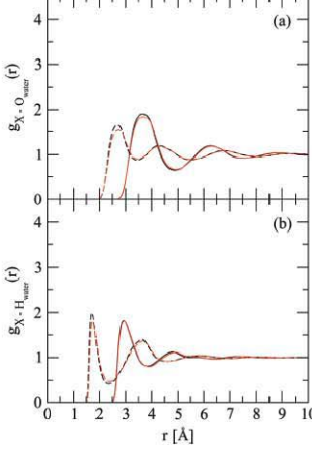


Figure 2. RDFs of (a) $X-O_{water}$ and (b) $X-H_{water}$, where X stands for the N and O sites of NO_3^- ion. The black and red lines refer to the RDFs obtained from RISM-SCF/HF for the N (the black solid lines) and O (the black dashed lines) sites and RISM-SCF/B3LYP for the N (the red solid lines) and O (the red dashed lines) sites, respectively.

agreement with the $\text{C}\cdots\text{O}_w$ of 3.35 Å and $\text{N}\cdots\text{O}_w$ of approximately 3.7 Å estimated by the neutron diffraction and X-ray diffraction and x-ray

Comparison of Energy Surfaces between the Gas and Solution Phases. The potential energy surfaces (PESs) in the gas phase and free energy surfaces (FESs) in the aqueous solution of carbonate and nitrate anions are plotted as a function of C- or N- torsion at the same theoretical levels employed

TABLE 3: Distance of First Hydration Peaks Obtained from the RISM-SCF Optimizations of ${\rm CO_3}^{2-}$ and ${\rm NO_3}^-$ Anions in the Solution Phase

	RISM-SCF/HF	RISM-SCF/B3LYF
	CO ₃ ²⁻	
C···O _w	3.53	3.53
$C \cdots H_w$	2.90	2.91
$O_C \cdots O_w$	2.48	2.49
$O_C \cdots H_w$	1.67	1.69
	NO ₃	
N···O _w	3.66	3.68
$N \cdots H_w$	2.92	2.94
$O_N \cdots O_w$	2.70	2.73
$O_N \cdots H_w$	1.72	1.75

in the previous section (Figure 3). The FESs of the solution phase were constructed by moving the carbon or nitrogen atom along the principal axis, retaining the $C_{3\nu}$ symmetry, and the optimization for the rest of geometrical parameters was performed to evaluate the total energy according to eq 1. The energy points of PESs in the gas phase were obtained by the single-energy calculations at the geometries adopted from each point in the FESs of the solution phase. Each relative energy with respect to the minimum is plotted in the figure.

The minimum for the carbonate and nitrate anions in the gasphase PES is located at 0.00° , corresponding to the D_{3h} symmetry structure. Whereas the FESs of nitrate anion in the solution phase have a minimum at the N- torsion of 0.00° , those of carbonate anion show double minima situated at $\pm 7.39^\circ$ and $\pm 7.49^\circ$ obtained from the RISM-SCF/HF and RISM-SCF/B3LYP calculations, respectively. Furthermore, the RISM-SCF/CCSD(T) method was also employed to construct the FESs at the geometry of each point on the FES of RISM-SCF/B3LYP calculations. The FES of hydrated nitrate anion showed the minimum at the N- torsion of 0.00° , whereas those of the carbonate anion again exhibited double minima located at the C-

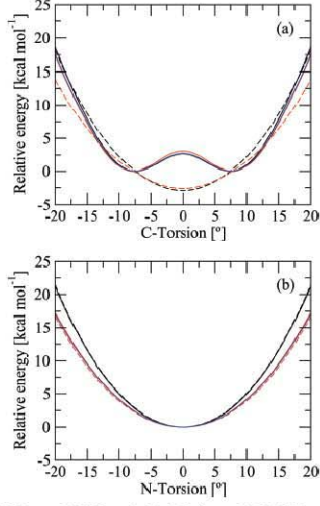


Figure 3. PESs and FESs of (a) CO₃²⁻ and (b) NO₃⁻ anions as a function of dihedral angle obtained by HF (the black dashed lines) and B3LYP (the red dashed lines) in the gas phase and by RISM-SCF/HF (the black solid lines), RISM-SCF/B3LYP (the red solid lines), and RISM-SCF/CCSD(T) (the blue solid lines) in aqueous solution.

TABLE 4: Harmonic Frequencies of CO₃²⁻ and NO₃ Anions in Gas Phases

	frequency (cm ⁻¹)				
	ν_1	ν_2	ν_3	v_4	
		CO ₃ ²⁻			
HF	1125	991	1498	722	
B3LYP	1011	856	1311a	643	
exptl ^b	1066	884	1385	684	
		NO ₃			
HF	1228	989	1567	792	
B3LYP	1066	842	1378a	704	
exptl ^b	1048	832	1348	718	

^a Averaged values. ^b In aqueous solution (ref 4).

TABLE 5: Harmonic Force Constant and Frequency of the Out-of-Plane Mode for CO₃²⁻ and NO₃⁻ Anions

		$k \text{ (kcal mol}^{-1} \text{ Å}^{-2}\text{)}$	$\nu_{\rm g}$ or $\nu_{\rm s}$ (cm ⁻¹)
		CO3 ²⁻	
gas	HF	1420.02	991
B3LYP	B3LYP	1124.17	856
aqueous	RISM-SCF/HF	3461.29	1591
	RISM-SCF/B3LYP	3548.21	1521
		NO ₃ -	
gas	HF	1474.78	989
	B3LYP	1078.94	842
aqueous	RISM-SCF/HF	1391.22	960
500 1 00 / 500 000	RISM-SCF/B3LYP	1141.02	866

torsion of $\pm 7.57^{\circ}$. The local maximum points on the FESs of hydrated carbonate anion are located at the C- torsion = 0.00°, showing the barrier of 2.71 (RISM-SCF/HF), 3.12 (RISM-SCF/B3LYP), and 2.76 (RISM-SCF/CCSD(T)) kcal mol $^{-1}$. These results strongly indicate that the statistical optimal geometry of carbonate is inherently C_{3v} symmetry in the solution phase. It is noted that the present result does not deny the possibility of further lowering of symmetry caused by a specific hydration of water solvents.

The fundamental frequencies are usually obtained from the Hessian method, i.e., the second-order energy gradient with respect to the nuclear coordinates, implemented in the standard ab initio MO program packages. Table 4 list the fundamental frequencies of carbonate and nitrate anions for the optimized geometries corresponding to the PESs (Figure 3). On the other hand, FES is not directly connected to the frequencies of solvated ions (ν_s) , but still it might be meaningful to estimate the frequency from the curvature, especially for the out-of-plane motion (ν_s) in the solution phase.

$$v_{\rm s} = \sqrt{\frac{k_{\rm s}}{k_{\rm o}}} v_{\rm g} \tag{2}$$

was employed to evaluate the frequency from the FES curvature, where $k_{\rm g}$ and $k_{\rm s}$ are, respectively, the harmonic force constant obtained from the curve-fitting of gas and solution energy surfaces, and $v_{\rm g}$ is the frequency in the gas phase. These are summarized in Table 5. The significant changing of energy surfaces and k values shows a large effect on the solvation of carbonate anion and introduces strong anharmonicity. The similarity of PESs and FESs in Figure 3b for the nitrate ion in the gas and solution phase shows a moderate effect of water on the solvation.

Origin of the Symmetry Breaking. The present result suggests that the symmetry breaking of carbonate anion does

TABLE 6: Molecular Radius (b) and Atomic Charge Sets of $\mathrm{CO_3}^{2-}$ and $\mathrm{NO_3}^-$ Anions Obtained from the RISM-SCF Calculations at the D_{3h} Symmetry in the Solution Phase

	CO_3^2	!- ion	NO ₃ ⁻ ion		
	HF	B3LYP	HF	B3LYP	
b (Å)	2.408	2.417	2.377	2.391	
e_1	1.753	1.686	1.248	1.120	
e_2	-1.251	-1.229	-0.749	-0.706	
e_3	-1.251	-1.229	-0.749	-0.706	
e_4	-1.251	-1.229	-0.749	-0.706	

occur even without specific water molecules attaching to the ion, whereas the nitrate anion does not. What is the difference between the two anions? The classical electrostatic free energy, \mathcal{W} , based on the multipole expansion with the spherical model, 31,32 is introduced here to clarify the difference. The expression of \mathcal{W} is

$$\mathcal{W} = \sum_{k=1}^{\nu-1} \sum_{b k}^{\nu} \frac{e_k e_l}{D_i | \mathbf{r}_k - \mathbf{r}_i |} + \sum_{n=0}^{\infty} \frac{-(D - D_i)(n+1)G_n}{D_i b^{2n+1} [(n+1)D + nD_i]} \quad (\nu = 4) \quad (3)$$

where G_n is defined as

$$G_n = \sum_{k=1}^{\nu-1} \sum_{l=k}^{\nu} e_k e_l |\mathbf{r}_k|^n |\mathbf{r}_l|^n P_n(\cos \vartheta_{kl})$$
 (4)

The set of point charge $\{e_v\}$ denotes the atomic charges evaluated by the Gill et al. procedure⁴⁴ at the RISM-SCF optimized D_{3h} structure for the carbonate and nitrate anions, \mathbf{r}_k is a position vector with respect to the center of mass, and ϑ_{kl} is the angle between \mathbf{r}_k and \mathbf{r}_l . The D_i is the internal dielectric constant of molecule that equals to 1, whereas D=80 represents water solvent. $P_n(\cos\vartheta_{kl})$ are the ordinary Legendre functions. The molecular radius b was determined from the polarizable continuum model (PCM). All these parameters obtained from the RISM-SCF/HF and RISM-SCF/B3LYP are summarized in Table 6.

The computed \mathcal{W} 's for the carbonate anion are plotted in Figure 4, parts a and b. The calculations were performed with different maximum orders of Legendre functions (n=0,1,2,3,4,5,10, and 20). As shown in the figures, eqs 3 and 4 properly reproduce the double-minima character corresponding to the FESs obtained from the RISM-SCF-SEDD calculations (Figure 3a). The dipole moment (n=1), represented with the red lines in the figure, seems dominate the height of the barrier in the FESs of carbonate ion. \mathcal{W} 's for the nitrate (Figure 4, parts e and f) are again identical with the FESs obtained from the RISM-SCF-SEDD calculations (Figure 3b). These results indicate this simple classical model is reasonably representing the solvation free energy profile obtained from the higher-level, coupled electronic/classical RISM-SCF-SEDD method.

In this simplified model, both of the atomic charges and geometrical coordinates are taken from the RISM-SCF-SEDD computations. A hypothetical model is thus introduced to check which contribution is responsible to the difference between the anions. W's were computed with the charge sets of the nitrate anion at the carbonate optimized geometry (Figure 4, parts c and d) and vice versa (Figure 4, parts g and h). The changing

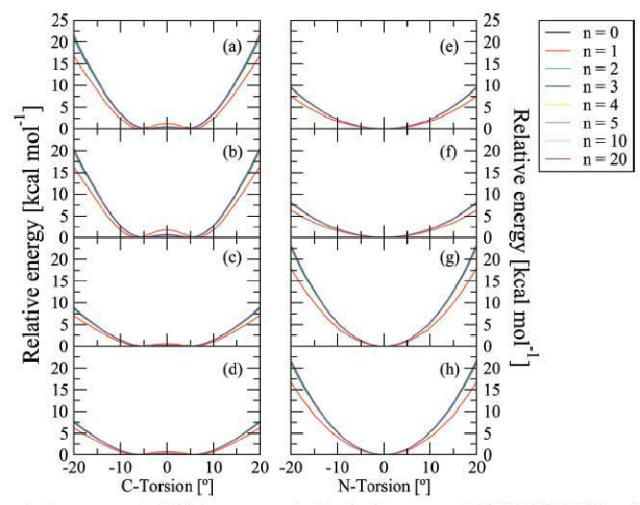


Figure 4. Classical electrostatic free energy of CO_3^{2-} ion computed with the charge sets of (a) RISM-SCF/HF and (b) RISM-SCF/B3LYP. The hypothetical sets were taken from NO_3^- ; (c) RISM-SCF/HF and (d) RISM-SCF/B3LYP (see the text). The classical electrostatic free energy of NO_3^- ion computed with the charge sets of (e) RISM-SCF/HF and (f) RISM-SCF/B3LYP. The hypothetical sets were taken from CO_3^{2-} ; (g) RISM-SCF/HF and (h) RISM-SCF/B3LYP. All of them are plotted with various multipole expansions (n = 0, 1, 2, 3, 4, 5, 10, and 20).

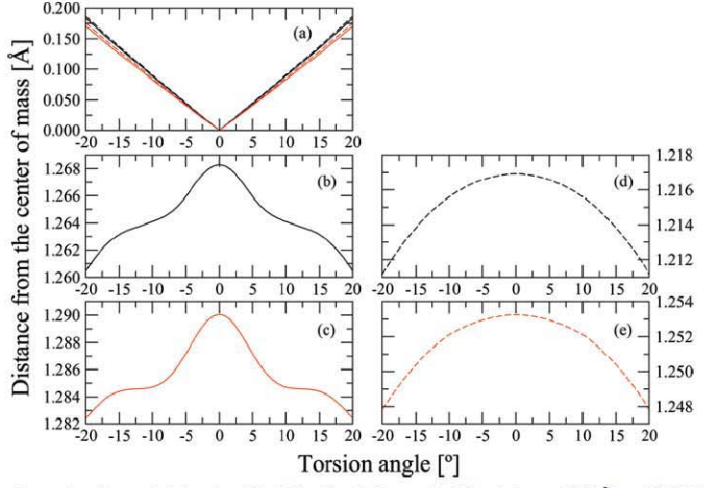


Figure 5. Distance from the center of mass to (a) carbon (black lines) and nitrogen (red lines) atoms of CO_3^{2-} and NO_3^- by RISM-SCF/HF (solid lines) and RISM-SCF/B3LYP (dashed lines). The same plots to oxygen of CO_3^{2-} anion by (b) RISM-SCF/HF (the black solid line) and (c) RISM-SCF/B3LYP (the black dashed line) and of NO_3^- anion by (b) RISM-SCF/HF (the red solid line) and (c) RISM-SCF/B3LYP (the red dashed line).

of total charge from -2 to -1 for the carbonate ion makes the curvature moderate. On the contrary, the changing of total charge from -1 to -2 for the nitrate anion raises the relative energies. But all of these figures still remain the similar pattern corresponding to the original FESs. These results suggest that the atomic and total charges are rather minor contributions on the peculiar properties of hydrated carbonate anion. The geometry of the anion is the parameter that emphasizes the contribution from the multipole expansion and makes the symmetry-broken structure stable.

To check the geometrical difference between the anions in detail, the distances between the central atom (carbon or

nitrogen) and the center of mass are plotted as a function of the torsion angles (C— and N— torsion) in Figure 5a. All of them are linear functions, representing the similar behavior with the slightly larger slope obtained from the carbonate anion than that of the nitrate. This means that the stabilization in carbonate anion due to the shift of the central atom (C) is more greater than that of nitrate (N) because the distances ($|r_{g}|$) are important to increase the attractive contribution according to the eq 4. However, the oxygen atoms play a more important role. The distance plots of oxygen with respect to the center of mass at the optimized geometry are shown for the carbonate (Figure 5, parts b and c) and for the nitrate (Figure 5, parts d and e) anions;

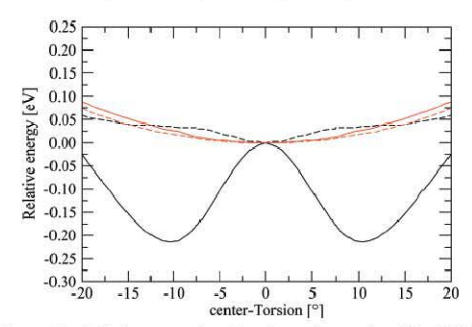


Figure 6. Orbital energy changing along the torsion. The HOMO energies are plotted with respect to the D_{3h} values: CO_3^{2-} in the gas phase (dotted black line) and in aqueous solution (solid black line) and NO3- in the gas phase (dotted red line) and in aqueous solution (solid red line).

obviously they look very different from each other. The drastic decreasing as increasing of C-O distances found in the carbonate anion around the C- torsion = 0.00° seems to be related to the character of carbonate FESs. In other words, the symmetry breaking in the carbonate is attributed to the peculiar character of the optimized geometry.

The orbital energy changing along the distortion (Walsh diagram) may provide a direct information for the present issue. Figure 6 plots the changing of the orbital energy of the highest occupied molecular orbital (HOMO) along the torsion angle. The optimized geometry in aqueous solution was adopted to plot both of the gas- and aqueous-phase values. Two nitrate curves are nondescriptive and increase as distorting from the highly symmetric geometry. However, the energy of carbonate in aqueous solution again shows a peculiar character with a minimum around 10°. It is interesting to note that the orbital energy in the gas phase monotonically increases although the same geometry was used. Hence, the above-mentioned peculiar character of the optimized geometry is attributed to the changing of orbital energy in aqueous solution. It is well-recognized that orbital energy in aqueous solution differs from the gas-phase one under the influence of the electric field from the polar solvent. Many of the deeper orbitals also show a similar trend for solvated carbonate. Presumably, the minimum is caused by an interplay between the two different contributions: one is an increasing in energy along the torsion corresponding to the gasphase behavior, the other is stabilization due to the enhancement of multipole interaction between solute and solvent.46

The carbonate and nitrate anions in an aqueous solution were investigated by means of the RISM-SCF-SEDD method. The computed bond distances and RDFs show an excellent agreement with the diffraction results. 41-43 The optimized geometries of nitrate anion are in a good agreement with the experimental results, meaning that the structure retains planarity in both gas and solution phases. On the contrary, the symmetry breaking occurs in the carbonate anion in an aqueous solution from D_{3h} to C_{3v} (or lower) losing the planarity. This phenomenon has been detected by IR and Raman spectra4 but has not been discussed in other theoretical studies. Our calculations suggest the strong anharmonicity of hydrated carbonate anion. It is important to emphasize that the symmetry is inherently broken even under the isotropic and uniform field generated by the solvent. We also employed a simple model based on the classical electrostatic free energy calculations to clarify the effect. Although the changing of the atomic charge gives only a small effect on the profile of FESs, geometrical changing considerably affects the contribution from the multipole moments, especially the dipole moment, resulting in the main reason to break the molecular planarity of carbonate ion.

Acknowledgment. The authors express their thanks to Professor Keiji Morokuma for many helpful discussions about this work. We are also grateful to the JENESYS (Japan-East Asia Network of Exchange for Students and Youths) Programme. The Thailand Research Fund and Thailand Commission on Higher Education (MRG5280241, fellowships for V.V.) are gratefully acknowledged. The work is also financially supported in part by the Grant-in-Aid for Scientific Research on Priority Areas "Ionic Liquids" (452-20031014) and "Molecular Science of Fluctuations" (2006-21107511) as well as by the Grant-in-Aid for Scientific Research (C) (20550013).

References and Notes

- Bargar, J. R.; Kubicki, J. D.; Reitmeyer, R.; Davis, J. A. Geochim. Cosmochim. Acta 2005, 69 (6), 1527–1542.
 Mitchell, H. H.; Shonle, H. A.; Grindley, H. S. J. Biol. Chem. 1916,
- 24, 461-490.
- Benjamin, N. Ann. Zootech. 2000, 49 (3), 207–216.
 Rudolph, W. W.; Fischer, D.; Irmer, G. Appl. Spectrosc. 2006, 60
- (5) Rudolph, W. W.; Irmer, G.; Königsberger, E. Dalton Trans. 2008, (7),900-908
- (6) Waterland, M. R.; Kelley, A. M. J. Chem. Phys. 2000, 113 (16), 6760-6773.
- Wang, X.-B.; Yang, X.; Wang, L.-S.; Nicholas, J. B. J. Chem. Phys. 2002, 116 (2), 561–570.
 Chang, T. G.; Irish, D. E. J. Phys. Chem. 1973, 77 (1), 52–57.
- (9) Zhang, Y.-H.; Choi, M. Y.; Chan, C. K. J. Phys. Chem. A 2004, 108 (10), 1712–1718.
- (10) Wahab, A.; Mahiuddin, S.; Hefter, G.; Kunz, W.; Minofar, B.; ngwirth, P. *J. Phys. Chem. B* **2005**, *109* (50), 24108–24120. (11) Goebbert, D. J.; Garand, E.; Wende, T.; Bergmann, R.; Meijer, Asmis, K. R.; Neumark, D. M. *J. Phys. Chem. A* **2009**, *113* (26), 7584–
- (12) (a) Pathak, A. K.; Mukherjee, T.; Maity, D. K. J. Phys. Chem. A (12) (a) Pathak, A. K.; Mukherjee, T.; Maity, D. K. J. Phys. Chem. A 2008, 1/2 (15), 3399–3408. (b) Pathak, A. K.; Maity, D. K. J. Phys. Chem. A 2009, 1/3 (48), 13443–13447.
 (13) Stefanovich, E. V.; Boldyrev, A. I.; Truong, T. N.; Simons, J. J. Phys. Chem. B 1998, 1/02 (21), 4205–4208.
 (14) Archer, T. D.; Birse, S. E. A.; Dove, M. T.; Redfern, S. A. T.; Gale, J. D.; Cygan, R. T. Phys. Chem. Miner. 2003, 30 (7), 416–424.
 (15) Bruneval, F.; Donadio, D.; Parrinello, M. J. Phys. Chem. B 2007, 1/1 (42), 12219–12227.
 (16) Transpare, D. P.; de Legury, N. H. J. Blys. Chem. B 2008, 1/2 (16).

- (16) Tommaso, D. D.; de Leeuw, N. H. J. Phys. Chem. B 2008, 112 (23), 6965-6975 (17) Kumar, P. P.; Kalinichev, A. G.; Kirkpatrick, R. J. J. Phys. Chem.
- B 2009, 113 (3), 794-802. (18) Ebner, C.; Sansone, R.; Hengrasmee, S.; Probst, M. Int. J. Quantum Chem. 1999, 75 (4-5), 805-814.
- (19) Tongraar, A.; Tangkawanwanit, P.; Rode, B. M. J. Phys. Chem. A 2006, 110 (47), 12918–12926.
- (20) Ten-no, S.; Hirata, F.; Kato, S. Chem. Phys. Lett. 1993, 214 (3-
- (21) Ten-no, S.; Hirata, F.; Kato, S. J. Chem. Phys. 1994, 100 (10),
- 7443-7453 (22) Sato, H.; Hirata, F.; Kato, S. J. Chem. Phys. 1996, 105 (4), 1546-
- (23) Yokogawa, D.; Sato, H.; Sakaki, S. J. Chem. Phys. 2007, 126 (24), 244504.
- (24) Yoshida, N.; Ishizuka, R.; Sato, H.; Hirata, F. J. Phys. Chem. B
- 2006, 110 (16), 8451–8458. (25) Sato, H.; Hirata, F. J. Phys. Chem. A 1998, 102 (15), 2603–2608.
- (26) Sato, H.; Hirata, F. J. Mol. Struct. (THEOCHEM) 1999, 461-462, (27) Sato, H.; Sakaki, S. J. Phys. Chem. A 2004, 108 (9), 1629-1634.
- (28) Iida, K.; Yokogawa, D.; Sato, H.; Sakaki, S. Chem. Phys. Lett. 2007, 443 (4-6), 264-268.
- (29) Hayaki, S.; Yokogawa, D.; Sato, H.; Sakaki, S. Chem. Phys. Lett. 2008, 458 (4-6), 329-332.

- (30) Sato, H.; Hirata, F.; Myers, A. B. J. Phys. Chem. A 1998, 102 (11),
- (30) Saturday (31) Saturday (32) Kirkwood, J. G. J. Chem. Phys. 1934, 2 (7), 351–361. (32) Kirkwood, J. G.; Westheimer, F. H. J. Chem. Phys. 1938, 6 (9),
- (33) Kovalenko, A.; Hirata, F. J. Chem. Phys. 1999, 110 (20), 10095-10112
- (34) Kovalenko, A.; Hirata, F. Chem. Phys. Lett. 2001, 349 (5-6), 496-
- (35) Krishnan, R.; Binkley, J. S.; Seeger, R.; Pople, J. A. J. Chem. Phys. 1980, 72 (1), 650-654.
- 1980, 72 (1), 650-654.
 (36) Clark, T.; Chandrasekhar, J.; Spitznagel, G. W.; Schleyer, P. V. R. J. Comput. Chem. 1983, 4 (3), 294-301.
 (37) Berendsen, H. J. C.; Postma, J. P. M.; van Gunsteren, W. F.; Hermans, J. In Intermolecular Forces; Pullman, B., Ed.; Reidel Publishing Company: Boston, MA, 1981; pp 331-342.
 (38) Weiner, S. J.; Kollman, P. A.; Case, D. A.; Singh, U. C.; Ghio, C.; Alagona, G.; Profeta, S.; Weiner, P. J. Am. Chem. Soc. 1984, 106 (3), 765-784.
- (39) Weiner, S. J.; Kollman, P. A.; Nguyen, D. T.; Case, D. A. J. Comput. Chem. 1986, 7 (2), 230–252.
- J. Comput. Chem. 1980, 7 (2), 230–292. (40) Schmidt, M. W.; Baldridge, K. K.; Boatz, J. A.; Elbert, S. T.; Gordon, M. S.; Jensen, J. H.; Koseki, S.; Matsunaga, N.; Nguyen, K. A.; Su, S.; Windus, T. L.; Dupuis, M.; Montgomery, J. A., Jr. J. Comput. Chem. 1993, 14 (11), 1347–1363.
- (41) Kanneda, Y.; Sasaki, M.; Hino, S.; Amo, Y.; Usuki, T. Physica B (Amsterdam, Neth.) 2006, 385–386 (Part 1), 279–281.

- (42) Megyes, T.; Bálint, S.; Peter, E.; Grósz, T.; Bakó, I.; Krienke, H.;

- (42) Megyes, T.; Bálint, S.; Peter, E.; Grósz, T.; Bakó, I.; Krienke, H.; Bellissent-Funel, M.-C. *J. Phys. Chem. B* 2009, *113* (13), 4054–4064. (43) Mason, P. E.; Neilson, G. W.; Dempsey, C. E.; Brady, J. W. *J. Am. Chem. Soc.* 2006, *128* (47), 15136–15144. (44) Gill, P. M. W.; Johnson, B. G.; Pople, J. A.; Taylor, S. W. *J. Chem. Phys.* 1992, 96 (9), 7178–7179. (45) Frisch, M. J.; Trucks, G. W.; Schlegel, H. B.; Scuseria, G. E.; Robb, M. A.; Cheesseman, J. R.; Montgomery, J. A., Jr.; Vreven, T.; Kudin, K. N.; Burant, J. C.; Millam, J. M.; Iyengar, S. S.; Tomasi, J. J.; Barone, V.; Mennucci, B.; Cossi, M.; Scalmani, G.; Rega, N.; Petersson, G. A.; Nakatsuji, H.; Hada, M.; Ehara, M.; Toyota, K.; Fukuda, R.; Hasegawa, J.; Ishida, M.; Nakajima, T.; Honda, Y.; Kitao, O.; Nakai, H.; Klene, M.; Li, X.; Knox, J. E.; Hratchian, H. P.; Cross, J. B.; Adamo, C.; Jaramillo, J.; Gomperts, R.; Stratmann, R. E.; Yazyev, O.; Austin, A. J.; Cammi, R.; Pomelli, C.; Ochterski, J. W.; Ayala, P. Y.; Morokuma, K.; Voth, A.; Salvador, P.; Dannenberg, J. J.; Zakrzewski, V. G.; Dapprich, S.; Daniels, A. D.; Strain, M. C.; Farkas, O.; Malick, D. K.; Rabuck, A. D.; Raghavachari, K.; Foresman, J. B.; Ortiz, J. V.; Cui, Q.; Baboul, A. G.; Clifford, S.; Cioslowski, J.; Stefanov, B. B.; Liu, G.; Liashenko, A.; Piskorz, P.; Komaromi, I.; Martin, R. L.; Fox, D. J.; Keith, T.; Al-Laham, M. A.; Peng, C. Y.; Nanayakkara, A.; Challacombe, M.; Gill, P. M. W.; Johnson, B.; Chen, W.; Wong, M. W.; Gonzalez, C.; Pople, J. A. Gaussian 03, revision D.02; Gaussian Inc.; Wallingford, C.T., 2004. (46) Iida, K.; Sato, H.; Sakaki, S. *J. Chem. Phys.* 2009, *130*, 044107.

JP101700D

Structural and Dynamical Properties and Vibrational Spectra of Bisulfate Ion in Water: A Study by Ab Initio Quantum Mechanical Charge Field Molecular Dynamics

Viwat Vchirawongkwin,*,† Chinapong Kritayakornupong,† and Bernd M. Rode8

Department of Chemistry, Faculty of Science, Chulalongkorn University, Phayathai Road, Patumwan, Bangkok 10330, Thailand, Department of Chemistry, Faculty of Science, King Mongkut's University of Technology Thonburi, Bangkok 10140, Thailand, and Theoretical Chemistry Division, Institute of General, Inorganic and Theoretical Chemistry, University of Innsbruck, Innrain 52a, A-6020 Innsbruck, Austria

Received: June 6, 2010; Revised Manuscript Received: August 2, 2010

The ab initio quantum mechanical charge field molecular dynamics (QMCF MD) formalism was applied to simulate the bisulfate ion, HSO₄-, in aqueous solution. The averaged geometry of bisulfate ion supports the separation of six normal modes of the O*-SO₃ unit with C_{3y} symmetry from three modes of the OH group in the evaluation of vibrational spectra obtained from the velocity autocorrelation functions (VACFs) with subsequent normal coordinate analyses. The calculated frequencies are in good agreement with the observations in Raman and IR experiments. The difference of the averaged coordination number obtained for the whole molecule (8.0) and the summation over coordinating sites (10.9) indicates some water molecules to be located in the overlapping volumes of individual hydration spheres. The averaged number of hydrogen bonds (Hbonds) during the simulation period (5.8) indicates that some water molecules are situated in the molecular hydration shell with an unsuitable orientation to form a hydrogen bond with the ion. The mean residence time in the surroundings of the bisulfate ion classify it generally as a weak structure-making ion, but the analysis of the individual sites reveals a more complex behavior of them, in particular a strong interaction with a water molecule at the hydrogen site.

Introduction

Bisulfate ion is produced by the first deprotonation of sulfuric acid, playing an important role to form hygroscopic aerosols in the atmosphere. 1-4 The vibrational spectra of bisulfate ion were investigated by in situ Fourier transform infrared (FTIR) spectroscopy of molecular adsorption on the surface of Pt single crystal electrodes,5 producing anomalous peaks from the adsorption and desorption of submonolayers of strongly bound hydrogen. $^{6.7}\,\rm The$ fundamental vibrational frequencies of $\rm HSO_4^$ ion were also assigned within the infrared spectra of concentrated solution in the spectral region of 600-1500 cm⁻¹.8 The Raman studies of aqueous NH4HSO4 solutions over a broad concentration and temperature range indicate that the bisulfate ion is the dominant species above 250 °C and possesses C_{3v} symmetry in dilute solutions. 9,10 The phase diagram for the NH₄HSO₄/H₂O system presented a low-temperature crystalline phase composed of NH4HSO4 with eight water molecules.11 Although the properties of bisulfate ion have been investigated in many experiments, most theoretical treatments were only interested in the system of hydrated sulfuric acid. 12-17 This motivated our interest to investigate the vibrational spectra and the structural and dynamical properties for the HSO₄ ion and its hydration shell in aqueous solution.

The specific investigation of an aqueous bisulfate system is difficult by experiment, due to a mixture of sulfate and hydronium ions produced by the second dissociation of sulfuric acid. Computer simulations have become an alternative tool to gain access to solvate microspecies properties needed for the

interpretation of experimental observations and the chemical behavior. The structural and dynamical properties of hydrated bisulfate ion are of great significance for the detailed understanding of all chemical processes of this ion in aqueous solution. However, the bisulfate ion is a composite structure difficult to access by a conventional QM/MM method, because of the complicated and asymmetric potential energy hypersurface describing the interaction between the HSO4 ion and water. An *ab initio* quantum mechanical charge field molecular dynamics (QMCF MD) formalism, ^{18,19} however, does not require an analytical solute-solvent potential, and hence, this method has already been successfully employed to investigate the structural and dynamical properties of the hydrated sulfate, ^{20,21} phosphate, ^{22,23} perchlorate, ^{22,24} and bicarbonate ^{25,26} anions. In this work, the QMCF MD method was used to simulate the hydrated HSO4 ion in order to obtain its structure and some dynamical properties, and also the vibrational spectra of all normal modes evaluated by means of the velocity autocorrelation functions (VACFs). The structural properties for each hydration site and the overall molecular shell were obtained via radial distribution functions (RDFs), coordination number distributions (CNDs), and angular distribution functions (ADFs). The dynamics were characterized by means of ligand mean residence times (MRTs). We also evaluated structural and dynamical properties by means of the molecular approach equivalent to the "solventaccessible surface" referred to in previous work.2

Methods

The ab initio quantum mechanical charge field molecular dynamics (QMCF MD) formalism has been outlined in detail elsewhere. 18,19 Due to the inclusion of an additional quantum mechanically treated solvent layer zone located beyond the first hydration shell of the solute species, the QMCF method does

10.1021/jp105181n © 2010 American Chemical Society Published on Web 08/13/2010

^{*} To whom correspondence should be addressed. E-mail: Viwat.V@ Chula.ac.th.

Chulalongkorn University.

^{*} King Mongkut's University of Technology Thonburi. * University of Innsbruck.

not require the construction of potential functions between the solute and water molecules; i.e., it avoids a time-consuming and sometimes hardly manageable task necessary in the conventional quantum mechanical/molecular mechanical molecular dynamics (QM/MM MD) formalism.^{27–30} A further advantage of the QMCF MD method is the inclusion of the point charges of the atoms in the MM region with their changing positions in the core Hamiltonian for the QM region via a perturbation term

$$V' = \sum_{i=1}^{n} \sum_{j=1}^{m} \frac{q_j^{\text{MM}}}{r_{ij}} \tag{1}$$

where n is the number of atoms in the QM region, m is the number of atoms in the MM region, q_j^{MM} is the partial charges of these atoms according to the selected water model, and r_{ij} refers to the distance between a pair of particles in the QM (i) and MM (j) regions. On the other hand, the dynamically changing charges of QM particles, q_i^{QM} , determined by population analysis contribute to the force on each atom j in the MM region as Coulombic forces

$$F_j^{\text{QM} \to \text{MM}} = \sum_{i=1}^n \frac{q_i^{\text{QM}} \cdot q_j^{\text{MM}}}{r_{ij}}$$
 (2)

As the conventional QM/MM MD formalism, the QMCF MD method allows the migration of water molecules between the QM and MM region. For this process, one has to apply a smoothing function³¹

$$\begin{split} S(r) &= & & \text{for } r > r_{\text{on}} \\ &\frac{\left(r_{\text{off}}^2 - r^2\right)^2 \left(r_{\text{off}}^2 + 2r^2 - 3r_{\text{on}}^2\right)}{\left(r_{\text{off}}^2 - r_{\text{on}}^2\right)^3} & \text{for } r_{\text{on}} \le r \le r_{\text{off}} \\ 1 & & \text{for } r < r_{\text{off}} \end{split} \tag{3}$$

where r is the distance of a given solvent molecule from the center of the simulation box, $r_{\rm off}$ is the radius of the QM region, and $r_{\rm on}$ is the inner border of the smoothing region. The formalism is applied to all atoms of molecules located in the smoothing region, ensuring a continuous transition and change of forces for these molecules according to

$$F_j^{\text{smooth}} = F_j^{\text{MM}} + (F_j^{\text{layer}} - F_j^{\text{MM}}) \times S(r)$$
 (4)

where $F_j^{\rm layer}$ is the force acting on a particle j located in the (outer QM) smoothing zone and $F_j^{\rm MM}$ is the force acting on a particle j in the MM region. In this context, it has to be mentioned that energy is not rigorously conserved, but the related error can be considered very minor due to the short simulation time and the large size of the quantum mechanical region.

The bisulfate solution consisted of one bisulfate ion and 496 water molecules in a cubic box of 24.67 Å with the periodic boundary condition. The density of the simulation box was 0.997 g cm $^{-3}$, i.e., the experimental value of pure water at 298 K. The simulation was performed in the *NVT* ensemble using a general predictor-corrector algorithm with a time step of 0.2 fs. The system temperature was maintained at 298.16 K by the

Berendsen temperature-scaling algorithm32 with a relaxation time of 100 fs. The OM subregions, namely, the core and layer zone, extended to 3.5 and 6.0 Å, respectively. The quantum mechanical calculation was performed by means of the Hartree-Fock (HF) method with the Dunning double-ζ plus polarization (DZP)33,34 basis sets for hydrogen, sulfur, and oxygen atoms in the QM region, i.e., the same theoretical level employed in our previous study of the hydrated sulfate ion.20 The thickness of the smoothing region was chosen as 0.2 Å with the values of $r_{\rm on}$ and $r_{\rm off}$ as 5.8 and 6.0 Å, respectively, according to the radial distribution function (RDF) obtained from the equilibrated simulation. The selected water model applied to calculate the interactions between pairs of water in the MM region was the flexible BJH-CF2 model, 35,36 with cutoff distances of 3.0 and 5.0 Å for non-Coulombic interactions between H atoms and between O and H atoms, respectively. The partial charges for oxygen and hydrogen atoms in the water molecule according to the BJH-CF2 model are -0.65966 and +0.32983. This water model supports the fully flexible molecular geometries of water molecules transiting between the OM and MM region. The Coulombic interactions between the Mulliken charges on the atoms within the QM region and the point charges of water molecules according to the BJH-CF2 model are evaluated providing an electrostatic description by a dynamically charging field of point charges, which change according to the movements of atoms inside the QM region and water molecules in the MM region in the course of the simulation. This ensures the continuous adaptation of the Coulombic interactions to all polarization and charge-transfer effects within solute and surrounding solvent layers. 18,19 In addition, the reaction field method combined with the shifted-force potential technique were applied to account for long-range electrostatic potentials and forces, with a spherical cutoff limit of 12.350 Å. The system was equilibrated with the QMCF MD method for 50 000 steps (10 ps), and a further 50 000 steps (10 ps) were collected as data sampling for analyzing the structural and dynamical properties. On average, 24.8 water molecules were present in the OM region.

The structural and dynamical properties for the hydration shell of HSO₄ ion were not only evaluated for individual atoms but also in a molecular manner. The molecular hydration shell of bisulfate ion was constructed by the combination of all atomic hydration spheres of the ion. The coordinating site for each water molecule to the bisulfate ion was defined by searching for the shortest distance between the oxygen atom of the water molecule and each atom within the ion.25 The molecular radial distribution functions (RDFs), molecular coordination number distributions (CNDs), and molecular ligand mean residence times (MRTs) for the hydration shell of bisulfate ion are thus presented in this Article. All MRT values were evaluated by the direct method,37 counting the water exchange processes between hydration shell and bulk. The most appropriate time span to record a water displacement from its original coordination sphere as an exchange process is 0.5 ps, 37,38 which corresponds to the average lifetime of a hydrogen bond in the solvent.39

The dynamical properties of a fluid system related to macroscopic transport coefficients can be evaluated from the velocity autocorrelation functions (VACFs), and their Fourier transformations can be interpreted as the vibrational spectra. The vibrational spectra of bisulfate ion were obtained from the VACFs using normal-coordinate analysis. 40 The normalized VACF, C(t), is defined as

Bisulfate Ion in Water

$$C(t) = \frac{\sum_{i}^{N_{t}} \sum_{j}^{N} v_{j}(t_{i})v_{j}(t_{i} + t)}{N_{t}N \sum_{i}^{N_{t}} \sum_{j}^{N} v_{j}(t_{i})v_{j}(t_{i})}$$
(5)

where N is the number of particles, N_t is the number of time origins t_i , and v_j denotes a certain velocity component of the particle j. A correlation length of 2.0 ps was used to obtain the power spectra with 4000 averaged time origins.

Results and Discussion

Structural and Dynamical Properties of HSO₄⁻ Ion. Due to the dynamic motion of all atoms within the system during the simulation period, all structural parameters such as bonds, angles, and dihedral angles within the bisulfate ion required to construct the geometry of the ion were collected with their statistical deviation listed in Table 1. The averaged geometry of HSO₄ ion constructed from the structural parameters in Table 1 is shown in Figure 1. The average S=O distances vary within 0.070 Å and are slightly shorter than those in the SO42 ion²⁰ by 0.02 Å, while the single bond of S to O(4) is significantly longer with 1.585 Å. The average O-H distance of 0.975 Å for the HSO₄ ion is slightly longer than the distance of the analogous bond in the HCO₃ ion²⁵ by ~0.02 Å. The bond and dihedral angles were collected in the form of angular distribution functions (ADFs). The average bond angles around the sulfur atom again indicate the similarity of terminal oxygens and the unique property of O(4). In contrast to the strong flexibility of the ∠CO(3)H angle of the HCO3⁻ ion,²⁵ the ∠SO(4)H ADF shows a deviation of only 9°. Our selected theoretical level, HF/DZP, for the QMCF MD simulation was validated by comparing the structural parameters with those obtained from various methods evaluated in the gas phase and solution using the polarizable continuum model (PCM).42 The hybrid B3LYP exchange-correlation functional coupling with the tzvp+ basis set43 was employed to verify the interpretation of the spectra of photoelectron spectroscopy for the HSO₄ ion;⁴¹ thus, we also utilized this basis set coupling with the Hartree-Fock (HF), B3LYP, and quadratic CI calculation including single and double substitutions (QCISD) levels to optimized the geometry of HSO₄ in both phases. The HF/DZP level was also performed to investigate the effect of isotropic and uniform field generated by the PCM to the geometry of HSO₄ ion. All optimized geometries in gas and solution phase were found to have C_s symmetry. The effect of PCM on the geometry of HSO₄ ion presents slightly longer bonds of terminated oxygen and O(4)-H bond, and a slightly shorter S-O(4) bond. The structural parameters obtained from the QMCF MD simulation show a similar changing pattern to the PCM model but presenting a slightly stronger effect of explicit water molecules on the HSO₄ ion compared with the HF/DZP results. Due to the fact that the structural parameters from the QCISD/tzvp+ optimization are within the deviation of those obtained from the QMCF MD simulation, this presents a suitability of the HF/DZP level to investigate the structural and dynamical properties of hydrated HSO₄ ion.

The dihedral angle measured between the plane defined by the O(4)-S-O(1) and the hydrogen atom is one of the interesting structural characteristics, with a large deviation as shown in Table 1. The distribution of this angle within the simulation period is presented in Figure 2, showing a broad band with a main peak situated at 60° and an average dihedral

angle of 40° . This angle distribution represents the ease of rotation for the hydrogen atom around the S–O(4) bond. This result agrees with the experimental result of a free rotation of OH group, treating the bisulfate ion with the $C_{3\nu}$ symmetry. We also utilized this approximation to separate three modes of the OH group, namely, O–H stretching (ν (OH)), S–O–H bending (δ (OH)), and S–O–H torsional (γ (OH)), from nine normal modes of the O*–SO₃ unit. The nine normal modes of the O*–SO₃ unit in $C_{3\nu}$ symmetry will span the following representation:

$$\Gamma(C_{3v}) = 3a_1(R, ir) + 3e(R, ir)$$
 (6)

In the Raman and infrared spectra under C_{3v} symmetry, the spectra will be predicted as only six bands, three of them becoming doubly degenerate modes. The power spectra of these normal modes for the HSO₄ ion predicted by the QMCF MD simulation are displayed in Figure 3, and the frequencies of peaks for each mode are listed in Table 2. The ν_1 and ν_2 modes seemed to identify the characteristic of the O*-SO3 unit in the HSO4 ion when it was investigated by Raman and IR experiments. 8-10 The calculated frequencies of these modes are in good agreement with the experimental data, again showing the reliability of QMCF MD simulation analyzing via VACFs the vibration modes of the solute. 21,26,44,45 It is interesting that the peak at 593 cm⁻¹⁸ was only assigned as a characteristic frequency of HSO₄ ion by Miller et al. 46 The peak of our calculation for the δ_6 mode located at 603 cm⁻¹ corresponds to the observed data, 8,46 and hence, we assigned this mode to the characteristic frequency of HSO4 ion found in the cesium bromide region.46 We also classified the frequency at 1341 cm reported by Walrafen et al. as δ_4 , as the other two totally symmetric (a₁) modes at 1050 and 885 cm⁻¹ were identified as the v_1 and v_3 modes, respectively.⁸ However, the peak of the δ_4 mode calculated by our VACF method at 635 cm⁻¹ agrees with the assignment by Dawson et al. for this mode at 585

Our calculated spectra for the OH group present very broad bands, as shown in Figure 3B. The power spectrum of the $\nu(OH)$ mode also presents the frequency band coinciding with the the δ(OH) mode, due to the different orientation of the O-H bond for each time origin included in the evaluation of the $\nu(OH)$ mode producing the mixed modes. By our vector projection, the frequency bands of the $\nu(OH)$, $\delta(OH)$, and $\gamma(OH)$ modes are found in the region of 2573-4039, 1075-1645, and 179-928 cm⁻¹, respectively. The $\nu(OH)$ mode shows the highest peak as a strong band at 3795 cm-1 and a weak band in the region 2573-3339 cm⁻¹ in agreement with the assignment by the experiments. 8,10 The $\delta(OH)$ mode again is identified as characteristic of the OH group by the Raman and IR investigations, 8-10 and our calculated band with the peak at 1384 cm-1 for this mode is in good agreement with that. The projection of H's velocities onto a unit vector perpendicular to the S-O(4)-H plane for the γ (OH) mode presents two bands with peaks at 179 and 733 cm⁻¹ for a weak and a strong band, respectively; this corresponds well with the assignment by Walrafen et al.8

The self-diffusion coefficient (D) of bisulfate ion was calculated from the center-of-mass VACF using the Green-Kubo relation⁴⁷

$$D = \frac{1}{3} \lim_{t \to \infty} \int_0^t C(t) dt$$
 (7)

TABLE 1: Structural Parameters for the Geometry of HSO₄⁻ Ion Obtained from the Averaging of Their Distributions with Their Variations

		HF/	DZP	HF/tzvp+		B3LYP/tzvp+		QCISD/tzvp+	
structural parameter	QMCF MD	gas	PCM	gas	PCM	gas ⁴¹	PCM	gas	PCM
S-O(1) (Å)	1.453 ± 0.062	1.441	1.444	1.446	1.449	1.483	1.485	1.477	1.479
S-O(2) (Å)	1.455 ± 0.064	1.432	1.440	1.436	1.445	1.473	1.480	1.467	1.475
S-O(3) (Å)	1.454 ± 0.067	1.441	1.444	1.446	1.449	1.483	1.485	1.477	1.479
S-O(4) (Å)	1.585 ± 0.076	1.619	1.579	1.626	1.585	1.709	1.655	1.682	1.635
O(4)-H (Å)	0.975 ± 0.064	0.946	0.969	0.947	0.970	0.968	0.993	0.969	0.993
∠O(1)SO(2) (deg)	113 ± 7	115	114	115	114	116	114	116	114
∠O(1)SO(3) (deg)	113 ± 7	113	113	113	113	114	113	114	113
∠O(1)SO(4) (deg)	106 ± 7	104	106	104	106	104	106	104	106
∠SO(4)H (deg)	113 ± 9	108	112	107	110	104	108	104	108
O(3)SO(1)O(2) dihedral (deg)	-131 ± 7	-136	-132	-136	-132	-137	-133	-137	-133
O(4)SO(1)O(2) dihedral (deg)	114 ± 8	112	112	112	112	110	111	110	111
HO(4)SO(1) dihedral (deg)	40 ± 49	59	60	59	60	60	60	59	60

The calculated D value obtained from the QMCF MD simulation is 1.584×10^{-5} cm 2 s $^{-1}$, which is in good agreement with the experimental value of 1.385×10^{-5} cm 2 s $^{-1}$. 48 This again presents the success of the QMCF MD formalism to acquire the dynamical properties of hydrated composite solute.

Structural and Dynamical Properties of the Hydration Shell. With the QM radius of 6.0 Å, the average number of solvent molecules inside this region was 24.8 ± 6.3 , during the simulation period. The coordinating sites of bisulfate ion consist of five atoms, namely, O(1) to O(4) and H, interacting with water molecules, and thus producing the hydration shell around this molecular solute. The structural property for each site was first evaluated by means of the radial distribution functions

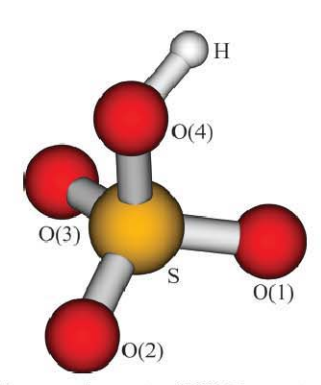


Figure 1. The averaged geometry of HSO_4^- ion constructed from the structural parameters of QMCF MD simulation presenting with the labels.

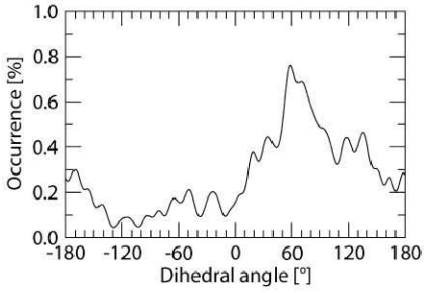


Figure 2. The distribution of H-O(4)-S-O(1) dihedral angle.

(RDFs) shown in Figure 4. The maximum and minimum distances of the hydration shell for each coordinating site obtained from the (site)– O_{water} and (site)– H_{water} are listed in Table 3. The shorter distances of a maximum and minimum for each Os-Hwater RDF compared to each related Os-Owater RDF correspond to the orientation of water molecules pointing with hydrogen to the coordinating oxygens. Although the geometry analysis in the previous section has shown that the S-O bonds for the terminal oxygens O(1) to O(3) are almost identical, the hydration shells for each site present a different structure reflected by some variations of maximal and minimal distances in their RDFs. The RDFs of the hydration shell of O(2) represent a slightly more compact structure than those of the other two sites. With respect to the averaged geometry of HSO₄ ion (see Figure 1), the O(2) site is far from the hydrogen atom so that the water molecules can hydrate this site with less perturbation from the hydrogen atom. The RDFs of O(4) atom show a more flexible hydration shell than the terminal oxygens,

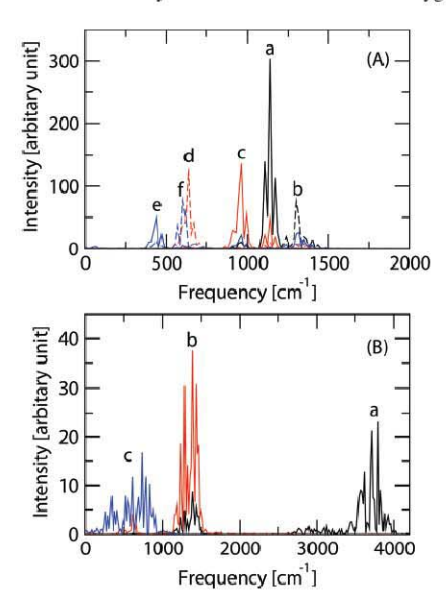


Figure 3. Power spectra of (A) the O*-SO₃ unit consisting of (a) ν_1 , (b) ν_2 , (c) ν_3 , (d) δ_4 , (e) δ_5 , and (f) δ_6 modes and (B) three modes for the OH group consisting of (a) ν (OH), (b) δ (OH), and (c) γ (OH) modes

TABLE 2: Vibration Frequencies (cm⁻¹) of Highest Peak for Each Normal Mode of HSO₄⁻ Ion Evaluated by the VACFs of QMCF MD Simulation, Given as Values Scaled by the Factor 0.902²¹ in Parentheses

vibration mode	QMCF MD	Raman and IR
ν ₁ symmetric SO ₃ stretch, a ₁	1140 (1028)	1050, ^a 1052, ^b 1050 ^c
ν ₂ asymmetric SO ₃ stretch, e	1303 (1175)	1191, ^a 1230 ^c
ν ₃ S -(OH) stretch, a ₁	961 (867)	899, ^a 898, ^b 885 ^c
δ ₄ symmetric SO ₃ deformation, a ₁	635 (573)	585, ^a 1341 ^c
δ ₅ asymmetric SO ₃ deformation, e	440 (397)	422,ª 417°
δ_6 SO ₂ bending, e	603 (544)	593°
ν (OH)	3795 (3423)	2900,a 3000c
δ (OH)	1384 (1248)	1340, ^a 1240, ^b 1175-1250, ^c 1800 ^c
γ(OH)	733 (661)	675-740°

 $[^]a$ Raman data of 3.8 mol kg $^{-1}$ NH₄HSO₄ solution at 25 $^{\circ}$ C. 10 b Raman data of 0.876 mol kg $^{-1}$ NH₄HSO₄ solution at 22 $^{\circ}$ C. 9 c IR data of concentrated aqueous solutions of sulfuric acid in the region 290–4000 cm $^{-1.8}$

indicated by the flat shape and lower maximum of the O(4)– H_{water} RDF in the region assigned as hydration shell. The RDFs of H atom indicate the direction of the oxygen atom of water pointing to this site, and represent a well-defined structure by a strong peak in the H– O_{water} RDF.

The distances of the minima for each (site)-Owater RDF were employed to evaluate the coordination number distribution (CND) for the sites, as shown in Figure 5. Their averaged coordination numbers are also listed in Table 3 in the last column. The O(2) atom located in the far position from the hydrogen atom has the smallest coordination number among the oxygens and a significantly large average CND of O(3), again illustrating the different hydration structure for these oxygen atoms. The reasons for small deviations of the coordination numbers of the three terminated oxygen atoms are to be seen in slight deviations from the C_{3v} symmetry in the course of the simulation and the short sampling time, which would not cover sufficient orientations to include all possible configurations. Hence, the difference of 0.3 water molecules cannot be considered statistically significant. The actual effect of water molecules to each oxygen site requires further details as the average number of H-bonds, presented with the following analysis. The minimum of the O(4)-Owater RDF at 3.46 Å utilized to evaluate its CND also includes a part of the hydration shell of hydrogen atom. This leads to an overcounting of the coordination number for the composite molecular solute. 20,25 To clarify this problem, we again evaluated the RDF and CND for the molecular structure employing the distances of minimum for each (site)-O_{water} RDF as the criterion to assign the coordinating site for each water molecule shown in Figure 6. The characteristic values of molecular hydration shell and its averaged coordination number obtained from the molecular surface-water RDFs and CND are also listed in Table 3 in the last row.

The surface– O_{water} RDF presents two peaks at 1.80 and 2.90 Å in the region of 0.00–3.72 Å, corresponding to the hydration spheres of hydrogen and all oxygen atoms. The peak of O_s – O_{water} within the molecular RDF is well-defined and stronger than that in the individual O_s – O_{water} RDFs, representing more water molecules confined in the molecular hydration shell than those in the individual hydration spheres. However, the total average coordination number of 10.9 for all individual sites is larger than the average coordination number of 8.0 for the

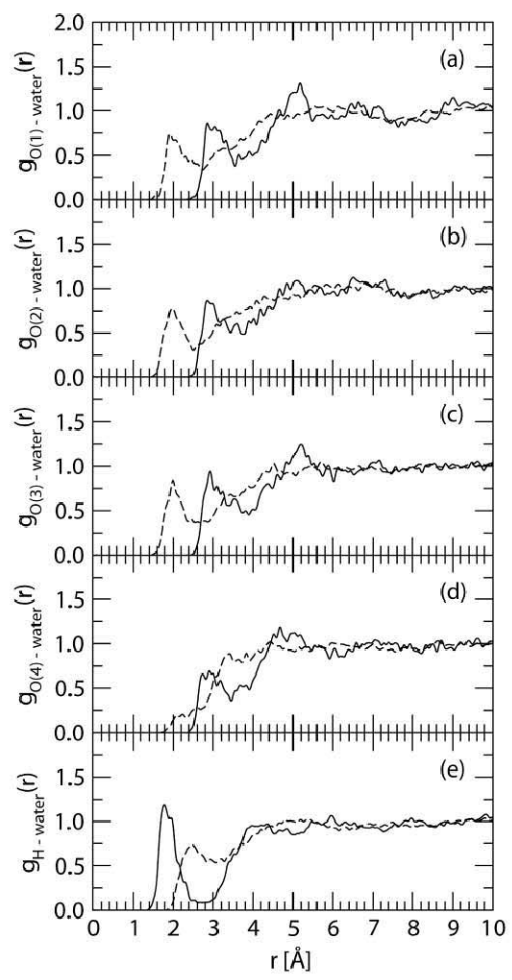


Figure 4. RDF plots of (a) O(1)-water, (b) O(2)-water, (c) O(3)-water, (d) O(4)-water, and (e) H-water; solid and dashed lines refer to the RDFs for the O and H atoms of water, respectively.

TABLE 3: Characteristic Values of the Radial Distribution Function $g_{\alpha\beta}(r)$ for Each Site of ${\rm HSO_4}^-$ Ion in the Hydration Shell Determined by the QMCF MD Simulation

coordinating site	$r_{\max}(O_{\mathrm{w}})^a$	$r_{\min}(O_{\mathrm{w}})^a$	$r_{\rm max}(H_{\rm w})^a$	$r_{\min}(H_{\mathrm{w}})^a$	n^a
O(1)	2.86	3.56	1.92	2.72	2.4
O(2)	2.86	3.44	1.98	2.52	2.1
O(3)	2.92	3.88	1.98	2.68	3.5
O(4)	2.90	3.46	2.22	3.34	1.9
H	1.78	2.64	2.48	3.08	1.0
surface	1.80, 2.90	2.42, 3.72	2.10	3.72	8.0

 $[^]a r_{\max}$ and r_{\min} are the distances of the maximum and minimum of $g_{\alpha\beta}(r)$ for the hydration shell in Å, and n is the averaged coordination number of the shell, respectively.

molecular hydration shell, showing an overcounting of $\sim\!\!3$ water molecules, due to the overlap of individual hydration spheres as observed also in the hydration structures of sulfate^{20} and bicarbonate^{25} ions.

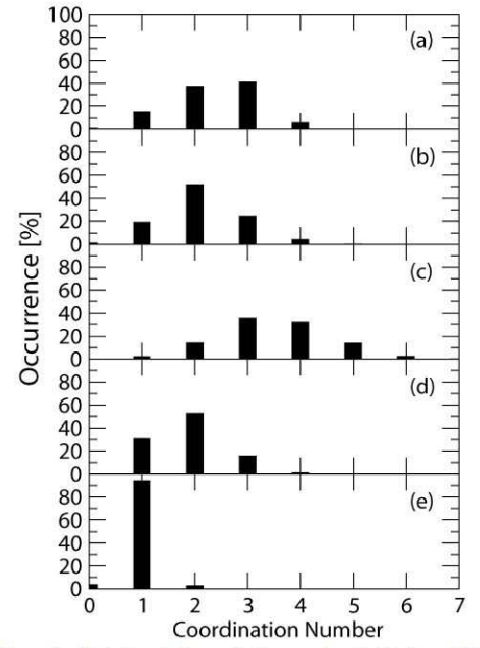


Figure 5. Hydration shell coordination number distributions of (a) O(1), (b) O(2), (c) O(3), (d) O(4), and (e) H atom of bisulfate ion.

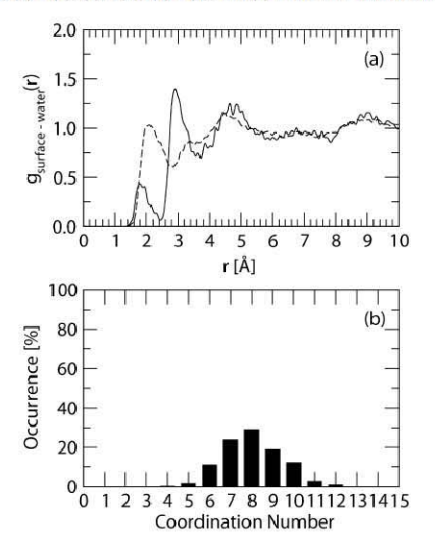


Figure 6. (a) Molecular RDF plots of HSO_4^- ion obtained from the QMCF MD simulation evaluated by means of the combination of spheres; solid and dashed lines refer to the RDFs for the O and H atoms of water, respectively. (b) The molecular hydration shell coordination number distribution of the HSO_4^- ion.

The orientation of water molecules in the individual hydration spheres was investigated by means of the angular distribution function (ADF) of O_w - H_w -··(site) angles, shown in Figure 7. These ADFs show a similar pattern with two peaks located at ca. 60 and 160° , corresponding to the two hydrogens of

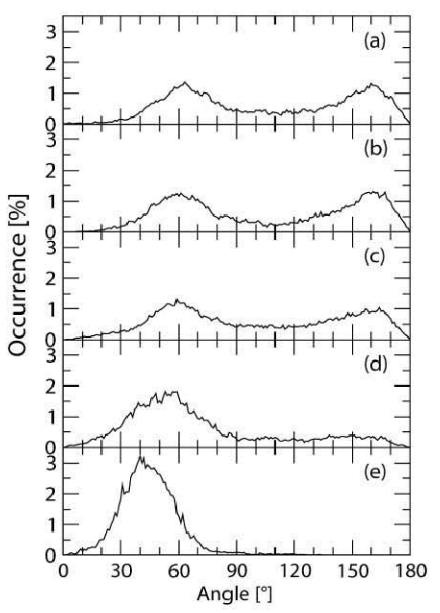


Figure 7. O_w-H_w ··· (site) ADFs for (a) O(1), (b) O(2), (c) O(3), (d) O(4), and (e) H atom of HSO_4^- ion.

hydrating water molecules. The H_{water} atom pointing to the terminal oxygen sites is represented by the large angles. The ADF of O(4) displays a different orientation of hydrating water molecules with a high probability of small angles and very low probability of large angles, indicating that most of the H_{water} atoms do not point to this site.

According to the dynamical movements of all atoms within the system, the number of H-bonds between the bisulfate ion and the hydrating water molecules fluctuates during the simulation period. Since the definition of H-bond has been expressed in two different ways, namely, an energetic and a geometric criterion, 49,50 we utilized the structural criterion depending on the cutoff parameters (distances $R_{\rm HO}^{\rm (c)}$ and $R_{\rm OO}^{\rm (c)}$ and angle $\phi^{\rm (c)}$) in analogy to water—dimethyl sulfoxide mixtures⁵¹ and hydrated bicarbonate ion.²⁶ The cutoff distances $R_{HO}^{(c)}$ and $R_{OO}^{(c)}$ for each oxygen site were obtained from the corresponding (Os-Hwater and Os-Owater) RDFs, while the cutoff parameters for the hydrogen site employed the distances of the first boundary in the H-Owater and O(4)-Owater RDFs, respectively. The angle $\phi^{(c)}$ was set to 30°. ⁵¹ The number of H-bonds as a function of time for each site is shown in Figure 8, presenting an average number of H-bonds of 1.5 \pm 0.8, 1.5 \pm 0.8, 1.6 \pm 0.8, 0.4 \pm 0.5, and 0.9 \pm 0.3 for the O(1), O(2), O(3), O(4), and H sites, respectively. The smaller average number of H-bonds compared with the corresponding average coordination number for each hydration site indicates that some water molecules located in the hydration shell actually coordinate with the bisulfate ion, while others have an unsuitable orientation to form an H-bond. The slight difference of the average number of H-bonds for the O(1), O(2), and O(3) again presents the identical characteristics of these sites, corresponding to the C_{3v} symmetry. This difference for the O(4) site (ca. 1.5 molecules) clarifies the inclusion of extra water molecules from the hydration shell of the H site, and proves a weak interaction with water molecules at this site. The average number of H-bonds (5.8) compared

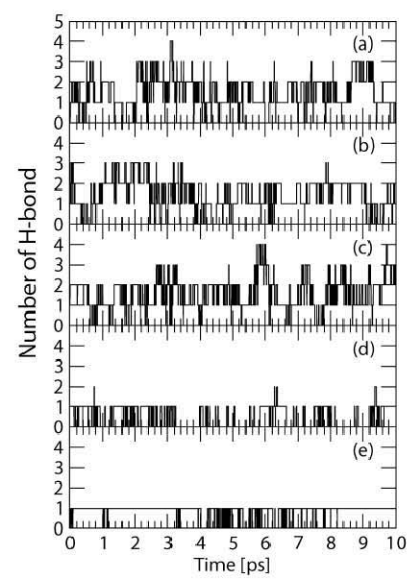


Figure 8. Number of hydrogen bonds between (a) O(1), (b) O(2), (c) O(3), (d) O(4), and (e) H atom of ${\rm HSO_4}^-$ ion and water molecules within the hydration shell during 10 ps of the QMCF MD simulation.

with the average coordination number (8.0) for the molecular ion shows that $\sim\!2$ water molecules are located in the molecular hydration shell without forming H-bonds to the bisulfate ion, however.

The dynamical properties of water molecules hydrating the bisulfate ion were investigated by the ligand mean residence time (MRT) evaluated by the direct method,37 from the average number of water molecules in the hydration shell during the simulation and from the number of exchange events for two time parameters $t^* = 0.0$, defined as the minimum duration of a ligand displacement from its original shell to account for an exchange process. t^* was set to 0.5 ps in accordance with the average lifetime of a hydrogen bond, ³⁹ whereas $t^* = 0.0$ counts all exchange attempts. All MRT values for individual oxygen and hydrogen sites were summarized in Table 4. The total number of water molecules counted for individual exchange processes of all oxygens and hydrogen were 90 and 37, being larger than those counted for the molecular hydration shell (33 and 19). The total number of attempted and lasting exchange processes of individual atoms evaluated at $t^* = 0.0$ ps (576 events) and $t^* = 0.5$ ps (73 events), respectively, are also higher than the 410 and 39 events counted by the molecular approach, which avoids counting water molecules within the intersection of individual hydration spheres. The difference in exchange processes (73 and 39, respectively) shows that half of the exchange events are actually migrations of water molecules between the coordinating sites of ${\rm HSO_4}^-$ ion, similar to the HCO₃⁻ system.²⁵ The number of processes needed for one successful water exchange, Rex, for the terminal oxygen atoms indicates a weak interaction with the water molecules in their vicinity compared to the hydrogen site. The peculiar value of $R_{\rm ex}$ for the O(4) site stems from the partial inclusion of the hydration sphere of the hydrogen site. The standard relaxation time used in the direct method with $t^* = 0.5$ ps leads to the MRT of water ligands at the coordination sites, while the

TABLE 4: Mean Ligand Residence Time τ in ps, Number of Accounted Ligand Exchange Events N, and Total Number of Processes Needed for One Successful Water Exchange $R_{\rm ex}$ Obtained from the QMCF Simulation

	$t^* = 0.0 \text{ ps}$).5 ps		
	N'inv	$N_{\rm ex}^{0.0}/10 {\rm ps}^b$	τ _D 0.0 °	$N'_{\rm inv}$	$N_{\rm ex}^{0.5}/10~{\rm ps}^b$	τ _D 0.5 °	$R_{\rm ex}^{d}$
O(1)	17	118	0.20	10	19	1.27	6.2
O(2)	19	131	0.17	8	21	1.04	6.2
O(3)	25	160	0.22	12	24	1.47	6.7
O(4)	22	110	0.17	5 2	7	2.72	15.7
H	7	57	0.17	2	2	4.95	28.5
surface	33	410	0.19	19	39	2.02	10.5
H ₂ O ^e H ₂ O ^f		269 ³⁷ 131 ⁵²	$0.2,^{37}, 0.33^{38}, 0.2,^{52}, 0.55^{39}$		24 ³⁷ 20 ⁵²	$1.7,^{37}$ 1.51^{38} 1.3^{52}	11.2 ³⁷ 6.5 ⁵²

^a Number of ligands involved in the MRT evaluation according to the value of t*. ^b Number of accounted exchange events per 10 ps lasting at least 0.0 and 0.5 ps, respectively. ^c Mean residence time determined by the direct method³⁷ in ps. ^d Average number of processes needed for one successful ligand exchange. ^e Values obtained from a QM/MM-MD simulation of pure water^{57,28} in ps. ^f Values obtained from a QMCF MD simulation of pure water⁵² in ps.

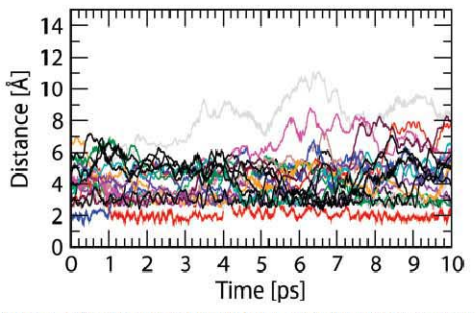


Figure 9. Distance plot of the molecular anion sites and oxygen atom of water as a function of time during the QMCF MD simulation period.

hydrogen bond lifetimes can be estimated with $t^* = 0.0 \text{ ps.}^{25,37}$ The corresponding value obtained from the simulation of the pure water system based on the QM/MM MD formalism is 0.33 ps; the $t^* = 0.0$ values account for each hydrogen bond making/ breaking process.38 Both mean residence times and hydrogen bond lifetimes for the individual sites and the molecular ion as a whole prove HSO₄⁻ as a weak structure-making ion. This effect is not evenly distribution to all sites of the ion but most pronounced near the hydrogen site, as shown in Figure 9. This plot presents the distances of all water molecules within the molecular hydration shell measured from each coordinating site. After an exchange of water molecules binding to the hydrogen site at 1.0 ps, the water molecule retained the interaction with this site until the end of sampling time. Structure breaking/ making is commonly regarded as a property related to the dynamics of the water molecules in the surrounding of a solute. If it was defined only as a structural effect, any kind of solute would break some H bonds of the solvent and hence its structure. However, in a dynamical sense, structure making means the formation of a layer of solvent molecules around the solute with lower mobility, while structure breaking would mean that the surrounding solvent molecules are more mobile than the solvent molecules in the bulk. Although the Berendsen temperaturescaling algorithm32 requires in principle a long simulation period to sufficiently describe the phase space, a large number of

successful simulations published indicate that our simulation time of 10 ps is adequate to reproduce well the properties of hydrated ions, and thus also of the bisulfate ion. Comparing results for exchange dynamics and H-bond life times for simulations of pure water38 and experimental results39 the HF method seems to be a good compromise between accuracy and affordable computational effort to estimate dynamical effects as well. Although HF and the methodical problems associated with the thermostatisation probably lead to slightly underestimated values, the associated errors are probably within a 10 -20% range.

As HSO4 ion is still a fairly strong acid in water, a dissociation process could be expected to be observable. However, this is a function not only of the thermodynamics but also of the kinetics, and even in the case of a much stronger acid, namely, HCl, despite a number of attempted proton transfers within 10 ps of simulation, no full proton transfer could be observed.45 There is no doubt that, over a much longer simulation time, such a process would occur, however.

Our OMCF MD simulation results for hydrated bisulfate ion are well compatible with the Raman and IR experiments, assuming C_{3v} symmetry. 9.10 The vector projection of each vibration mode coupling with the VACF calculations gives the vibrational frequencies in good agreement with the experimental observations, especially of the characteristic modes. $^{8-10}$ These results again indicate the success and reliability of our approach to investigate the properties of composite hydrated anions.2 The HSO₄ ion is characterized as a weakly structure-making ion in aqueous solution, slightly weaker than the sulfate ion. The hydrogen site forms a significant hydration structure characterized by a strong H-bond with one water. This stronger interaction of the hydrogen site of the HSO4 on compared to that of the HCO3- ion reflected by the mean residence times of water ligands at the hydrogen site of 4.95 for the HSO_4^- and 0.82 for HCO_3^{-25} clearly demonstrates the higher acidity of HSO₄. The water molecules hydrating the bisulfate ion have a high mobility, reflected by rapidly changing binding sites and orientations while forming and breaking H-bonds with the ion. To describe these effects by classical or conventional QM/MM molecular dynamics would be a most difficult task, as it would have required the construction of analytical interaction potential functions taking into account all the asymmetry of the interaction between solute and solvent, which in the case of bisulfate would be difficult and subject to many possible error sources and inaccuracies.

Acknowledgment. Generous financial support by the Austrian Science Foundation (FWF) and ASEA-UNINET, the Thailand Research Fund and Thailand Commission on Higher Education (fellowships for V.V. and C.K.), Faculty of Science, Chulalongkorn University (RES A1 B1-19 for V.V.), and Center for Petroleum, Petrochemicals and Advanced Materials, Chulalongkorn University are gratefully acknowledged.

References and Notes

- (1) Calhoun, J. A.; Charlson, R. J.; Bates, T. S. Geophys. Res. Lett. 1991. 18. 1877-1880.
- 1991, 18, 1877–1880.
 Charlson, R. J.; Schwartz, S. E.; Hales, J. M.; Cess, R. D.; Coakley,
 J. A., Jr.; Hansen, J. E.; Hofmann, D. J. Science 1992, 255, 423–430.
 Laaksonen, A.; Talanquer, V.; Oxtoby, D. W. Annu. Rev. Phys. Chem. 1995, 46, 489–524.
 Bianco, R.; Hynes, J. T. Acc. Chem. Res. 2006, 39, 159–165.
- (5) Faguy, P. W.; Marinković, N. S.; Adžić, R. R. Langmuir 1996, 12, 243–247.

- (6) Clavilier, J. J. Electroanal. Chem. 1980, 107, 211-216.
- (7) Faguy, P. W.; Marinkovic, N.; Adzic, R. R.; Fierro, C. A.; Yeager, E. B. J. Electroanal. Chem. 1990, 298, 245–262.
- (8) Walrafen, G. E.; Dodd, D. M. Trans. Faraday Soc. 1961, 57, 1286-
- (9) Rudolph, W. Z. Phys. Chem. 1996, 194, 73–95.
 (10) Dawson, B. S. W.; Irish, D. E.; Toogood, G. E. J. Phys. Chem. 1986, 90, 334-341.
- (11) Imre, D. G.; Xu, H.; Tang, I. N.; McGraw, R. J. Phys. Chem. A 1997, 101, 4191–4195.
- (12) Re, S.; Osamura, Y.; Morokuma, K. J. Phys. Chem. A 1999, 103, 3535-3547
- (13) Ding, C.-G.; Laasonen, K. Chem. Phys. Lett. 2004, 390, 307-313. (14) Choe, Y.-K.; Tsuchida, E.; Ikeshoji, T. J. Chem. Phys. 2007, 126,
- (15) Anderson, K. E.; Siepmann, J. I.; McMurry, P. H.; VandeVondele,
 J. Am. Chem. Soc. 2008, 130, 14144–14147.
 (16) Hammerich, A. D.; Buch, V.; Mohamed, F. Chem. Phys. Lett. 2008,
- 460, 423-431.
- (17) Kakizaki, A.; Motegi, H.; Yoshikawa, T.; Takayanagi, T.; Shiga, M.; Tachikawa, M. THEOCHEM 2009, 901, 1–8.
- (18) Rode, B. M.; Hofer, T. S.; Randolf, B. R.; Schwenk, C. F.; Xenides,
- (16) ROUE, B. M., FIDICI, I. S., RABIDOII, D. R., SCHWEIN, C. F., ACHIUCS,
 D.; Vchirawongkwin, V. Theor. Chem. Acc. 2006, 115, 77–85.
 (19) Hofer, T. S.; Pribil, A. B.; Randolf, B. R.; Rode, B. M. Ab Initio Quantum Mechanical Charge Field Molecular Dynamics: A Nonparametrized First-Principle Approach to Liquids and Solutions. In Combining Quantum Mechanics and Molecular Mechanics. Some Recent Progresses in QM/MM Methods; Sabin, J. R., Brändas, E., Eds.; Academic Press: San
- Diego, 2010; Vol. 59, pp 213–246. (20) Vchirawongkwin, V.; Rode, B. M.; Persson, I. *J. Phys. Chem. B* 2007, 111, 4150–4155.
- (21) Vchirawongkwin, V.; Rode, B. M. Chem. Phys. Lett. 2007, 443, 4152-157
- (22) Pribil, A. B.; Vchirawongkwin, V.; Hofer, T. S.; Randolf, B. R. Structure and Dynamics of Composite Anions in Aqueous Solution. Computation in Modern Science and Engineering, Proceedings of the International Conference on Computational Methods in Science and Engineering; American Institute of Physics (AIP): New York, 2007; pp
- (23) Pribil, A. B.; Hofer, T. S.; Randolf, B. R.; Rode, B. M. J. Comput. Chem. 2008, 29, 2330-2334.
- (24) Pribil, A. B.; Hofer, T. S.; Vchirawongkwin, V.; Randolf, B. R.;
- Rode, B. M. Chem. Phys. 2008, 346, 182–185.
 (25) Vchirawongkwin, V.; Pribil, A. B.; Rode, B. M. J. Comput. Chem. 2010, 31, 249–257.
- (26) Vchirawongkwin, V.; Kritayakornupong, C.; Ruangpornvisuti, V.; Rode, B. M. *THEOCHEM* 2009, *913*, 236–239.
 - (27) Warshel, A.; Levitt, M. J. Mol. Biol. 1976, 103, 227-249.
- (28) Field, M. J.; Bash, P. A.; Karplus, M. J. Comput. Chem. 1990, 11,
- (29) Gao, J. J. Am. Chem. Soc. 1993, 115, 2930-2935.
- (30) Bakowise, D.; Thiel, W. J. Phys. Chem. 1996, 100, 10580-10594.
- (31) Brooks, B. R.; Bruccoleri, R. E.; Olafson, B. D.; States, B. D.; Swaminathan, S.; Karplus, M. *J. Comput. Chem.* 1983, 4, 187–217. (32) Berendsen, H. J. C.; Postma, J. P. M.; van Gunsteren, W. F.; DiNola,
- (32) Bereinssen, H. J. C., Fostina, J. F., Van Guisseten, W. F., Dilvola, A.; Haak, J. R. J. Chem. Phys. 1984, 81, 3684–3690.

 (33) Dunning, T. H., Jr.; Hay, P. J. In Gaussian Basis Sets for Molecular Calculations; Schaefer, H. F., III, Ed.; Plenum Press: New York, 1977; Vol. 3, Chapter 1, pp 1–27.
 - (34) Dunning, T. H., Jr. J. Chem. Phys. 1970, 53, 2823–2833.
 (35) Stillinger, F. H.; Rahman, A. J. Chem. Phys. 1978, 68, 666–670.
- (36) Bopp, P.; Janscó, G.; Heinzinger, K. Chem. Phys. Lett. 1983, 98,
- (37) Hofer, T. S.; Tran, H. T.; Schwenk, C. F.; Rode, B. M. J. Comput. Chem. 2004, 25, 211–217.
- (38) Xenides, D.; Randolf, B. R.; Rode, B. M. J. Chem. Phys. 2005,
- (39) Lock, A. J.; Woutersen, S.; Bakker, H. J. J. Phys. Chem. A 2001, 105, 1238–1243.
 - (40) Bopp, P. Chem. Phys. 1986, 106, 205-212
- (41) Wang, X.-B.; Nicholas, J. B.; Wang, L.-S. J. Phys. Chem. A 2000, 104, 504–508.
- (42) Frisch, M. J. et al. Gaussian 03, revision E.01; Gaussian, Inc.: Wallingford, CT, 2004.
- (43) Godbout, N.; Salahub, D. R.; Andzelm, J.; Wimmer, E. Can. J. Chem. 1992, 70, 560–571.
 (44) Kritayakornupong, C.; Vchirawongkwin, V.; Hofer, T. S.; Rode, B. M. J. Phys. Chem. B 2008, 112, 12032–12037.
- (45) Kritayakornupong, C.; Vchirawongkwin, V.; Rode, B. M. J. Comput. Chem. 2010, 31, 1785–1792.

Bisulfate Ion in Water

- (46) Miller, F. A.; Carlson, G. L.; Bentley, F. F.; Jones, W. H. Spectrochim. Acta 1960, 16, 135–235.
 (47) McQuarrie, D. A. Statistical Mechanics; Harper & Row: New York, 1976.
 (48) CRC Handbook of Chemistry and Physics, 90th ed.; Lide, D. R., Ed.; CRC Press/Taylor and Francis: Boca Raton, FL, 2010.
- (49) Sceats, M. G.; Rice, S. A. J. Chem. Phys. 1980, 72, 3236–3247.
 (50) Mezei, M.; Beveridge, D. L. J. Chem. Phys. 1981, 74, 622-632.
 (51) Luzar, A.; Chandler, D. J. Chem. Phys. 1993, 98, 8160–8173.
 (52) Randolf, B. R.; Hofer, T. S.; Rode, B. M. Unpublished results.

Determination of Structure and Dynamics of the Solvated Bisulfide (HS-) Ion by ab Initio **QMCF Molecular Dynamics**

Chinapong Kritayakornupong,*,† Viwat Vchirawongkwin,‡ and Bernd M. Rode8

Department of Chemistry, Faculty of Science, King Mongkut's University of Technology Thonburi, Bangkok, 10140 Thailand, Department of Chemistry, Faculty of Science, Chulalongkorn University, Bangkok, 10330 Thailand, and Theoretical Chemistry Division, Institute of General, Inorganic and Theoretical Chemistry, University of Innsbruck, Innrain 52a, A-6020 Innsbruck, Austria

Received: May 27, 2010; Revised Manuscript Received: August 13, 2010

The hydration structure of the bisulfide (HS-) ion in dilute aqueous solution was characterized by means of an ab initio quantum mechanical charge field (QMCF) molecular dynamics simulation at the Hartree-Fock level employing Dunning double-ξ plus polarization function (DZP) basis sets. An average H-S bond distance of 1.35 Å resulted from the simulation and a hydration shell located at 2.42 Å S_{HS}····H_w and 3.97 Å HS distances, respectively. At the sulfur site, the average coordination number is 5.9 ± 1.1 , while the value for the hydrogen site is 9.2 ± 1.6 . The calculated H_{HS} - S_{HS} - stretching frequency of 2752 cm⁻¹ obtained from the QMCF MD simulation is in good agreement with that reported from the Raman spectrum (2570 cm⁻¹) only if a scaling factor of 0.89 is applied. The stability of the nondissociated HS⁻ structure is reflected by the force constants of 436.1 and 4.5 N/m determined for the H_{HS}--S_{HS}- and H_{HS}-···O_w bonds, respectively. A weak structure-making effect of the hydrated HS- ion results from the mean residence times of 1.5 and 2.1 ps of coordinated water molecules at the sulfur and hydrogen sites of the HS- ion, respectively.

1. Introduction

The chemistry of sulfide ions is an interesting area, not only in the fundamental chemistry and electrochemistry of numerous salts1 but also in atmospheric pollution as a constituent of the sulfur cycle,² petroleum hydrodesulfurization processes, as well as paper and pulp industries. In aqueous solution, bisulfide (HS-) ion can be obtained from the dissolved hydrogen sulfide (H2S) with a suggested pK_1 value of 7.01,³ while the subsequent dissociation of the bisulfide leads to the sulfide (S2-) ion, characterized by large experimental values of pK_2 in the wide range $12.5-18.5.^{4-11}$ For example, Stephens and Cobble⁵ presented a value of 13.78, Licht et al.⁸ reported a value of 17.1, and Migdisov et al.9 selected a value of 17.4 at 25 °C. All of these indicate that HS- exists as a major species in aqueous H₂S solution, while minor activities of S²⁻ only occur in extremely high ionic strength solutions.8 In general, HS- acts as a Lewis base, whereas H2S can behave as a Lewis base or acid. Due to the dominance of bisulfide ion in aqueous solution, several experiments confirmed that the bisulfide ion acts as the initial species to form metal hydrosulfide in the precipitation of metal sulfide from solution, which is of great environmental interest. 12,13 To our knowledge, no structural analysis of the HSion in aqueous solution has been performed by experimental techniques, only the H-S vibrational frequency of 2570 cm-1 was determined by Raman spectroscopy.7 For theoretical investigations, there have been a few calculations aimed at the structure and stability of [H₂S(H₂O)]_n clusters, 14-18 which are not directly relevant for the solvated HS- ion.

Recently, the quantum mechanical charge field (QMCF) molecular dynamics simulation approach has been developed, 19 presenting a suitable tool to investigate composite and asymmetrical ions in aqueous solution, $^{20-23}$ since the first and second hydration layers are included in the quantum mechanical treatment. In our previous publications, 21,22 structural and dynamical properties of aqueous HF and HCl solutions were successfully studied using this technique. Therefore, it was of great interest to characterize the hydration structure as well as the dynamical behavior of the analogous HS- compound with its extremely weak acid behavior in aqueous solution by employing the QMCF MD methodology.

In the present work, an ab initio quantum mechanical charge field molecular dynamics simulation at the Hartree-Fock level was performed for a system consisting of one HS- ion plus 498 water molecules. To characterize the hydration structure of the hydrated HS- ion, numerous structural parameters such as radial distribution functions, coordination numbers, angular distributions, θ angle, and tilt angle distributions were determined. The vibrational frequency of the H-S bond was determined to compare it with the experimental value, while the Hus-***O... vibrational mode was calculate to describe the hydrogen bond strength between solute and water molecules. Subsequently, dynamics of ligand exchange processes between hydration shell of the HS ion and bulk were analyzed on the basis of the mean residence times.

2. QMCF MD Simulation

The quantum mechanical charge field (QMCF) molecular dynamics simulation^{19,24} is a technique based on a partitioning scheme similar to conventional QM/MM MD methods, 25which divides the system into two parts (QM and MM regions) where different levels of theory are appropriately applied. In the QMCF technique, the QM region using the ab initio quantum mechanical calculation is extended to include the second hydration shell and also splits into two subregions, which are

10.1021/jp104856q © 2010 American Che Published on Web 09/21/2010 © 2010 American Chemical Society

^{*} Corresponding author. Fax: +66(2)470-8962. E-mail:chinapong.kri@ kmutt.ac.th

King Mongkut's University of Technology Thonburi.

[‡] Chulalongkorn University. [§] University of Innsbruck.

the core region containing the solute and the first solvation shell and the solvation layer containing only solvent molecules. In addition, the QMCF technique describes the Coloumbic interactions of the solute with bulk solvent molecules by quantum chemically evaluated partial charges of the atoms in the QM region and the point charges of the atoms in the MM region. The charges of the MM particles also enter as a perturbation term into the core Hamiltonian:

$$H_{\rm CF} = H_{\rm HF} + V_i \tag{1}$$

$$V_i = \sum_{j=1}^M \frac{q_j}{r_{ij}} \tag{2}$$

where q_j are the partial charges of each atom in the MM region as defined in the used water model BJH-CF2, ^{28,29} i.e., -0.65966 and +0.32983 for oxygen and hydrogen, respectively. Consequently, the forces acting on each particle in the different regions are defined as

$$F_{j}^{\text{core}} = F_{j}^{\text{QM}} + \sum_{i=1}^{M} \frac{q_{j}^{\text{QM}} q_{i}^{\text{MM}}}{r_{ij}^{2}}$$
(3)

$$F_{j}^{\text{layer}} = F_{j}^{\text{QM}} + \sum_{i=1}^{M} \frac{q_{j}^{\text{QM}} q_{i}^{\text{MM}}}{r_{ii}^{2}} + \sum_{i=1}^{M} F_{ij}^{\text{BJHnC}}$$
(4)

$$F_{j}^{\text{MM}} = \sum_{\substack{i=1\\i\neq j}}^{M} F_{ij}^{\text{BJH}} + \sum_{\substack{i=1}}^{N_{1}+N_{2}} \frac{q_{i}^{\text{QM}} \cdot q_{j}^{\text{MM}}}{r_{ij}^{2}} + \sum_{\substack{i=1\\i\neq j}}^{N_{2}} F_{ij}^{\text{BJHnC}}$$
(5

where F_j^{over} , F_j^{layer} , and F_j^{MM} are the forces acting on particle j situated in the core region, the solvation layer, and the MM region, respectively. M is the number of atoms in the MM region. In each simulation step, the ab initio quantum mechanical forces in core and layer regions (F_j^{pore} and F_j^{layer}) are evaluated in conjunction with the Coulombic forces obtained from all particles in the MM region. The non-Coulombic forces between the core particles and the MM particles are neglected, justified by the distance between the core and the MM region of at least 3 Å, while the QM forces in the layer (F_j^{layer}) are supplemented by the non-Coulombic forces of particles in the MM region according to the BJH-CF2 water model. ^{28,29} Consequently, the forces in the MM region (F_j^{MM}) are determined by the BJH-CF2 water model. ^{28,29} augmented by the Coulombic forces exerted by all particles in the core region (N_j) and the layer region (N_2), and the non-Coulombic forces (F_j^{BJHnC}) generated by the particles in the layer region (N_2).

During the QMCF MD simulation, the migration of solvent molecules between the QM and MM region can occur frequently. To ensure a continuous transition of forces at the boundary, the forces acting on each particle in the system can be defined as

$$F_j^{\text{Smooth}} = F_j^{\text{MM}} + (F_j^{\text{layer}} - F_j^{\text{MM}}) \cdot S_{\text{m}}(r)$$
 (6)

where F_j^{MM} and F_j^{layer} are the forces acting on the particle j in the MM region and located in the solvation layer, respectively,

r is the distance of the water molecule from the sulfur atom of the HS⁻ ion, and S_m is a smoothing function,³⁰

$$\begin{split} S_{\rm m}(r) &= 1 & \text{for } r \leq r_1 \\ S_{\rm m}(r) &= \frac{(r_0^2 - r^2)^2 (r_0^2 + 2r^2 - 3r_1^2)}{(r_0^2 - r_1^2)^3} & \text{for } r_1 < r \leq r_0 \\ S_{\rm m}(r) &= 0 & \text{for } r > r_0 \end{split}$$

where r_1 is the inner border of the smoothing region and r_0 is the radius of the QM region. Further details of the method are presented in refs 19 and 24.

The QMCF MD simulation of the bisulfide ion in aqueous solution was performed in a 24.7 Å × 24.7 Å × 24.7 Å periodic boundary cubic box, consisting of one HS- ion plus 498 water molecules. The canonical NVT ensemble was controlled by the Berendsen temperature-scaling algorithm31 using a relaxation time of 100 fs to keep the temperature at 298.15 K. The density of the simulation was fixed at 0.997 g cm⁻³, corresponding to the experimental value of pure water at this temperature. The time step of the predictor-corrector algorithm was set to 0.2 fs, enabling an explicit description of hydrogen movements. The flexible BJH-CF2 water model^{28,29} for the MM region also enables explicit hydrogen movements, thus ensuring a smooth transition of water molecules between QM and MM region. Cutoff distances of 5 and 3 Å were used for non-Coulombic O-H and H-H interactions, respectively. The radial cutoff limit for Coulombic interactions was set to half the box length and the reaction field32 was applied to correct for long-range Coulombic interactions. The radius of the core region was chosen as 3.0 Å with the layer region ranging from 3.0 to 5.7 Å in which the smoothing function³⁰ was applied between r_0 (5.7 Å) and r_1 (5.5 Å). The TURBOMOLE 5.9 program^{33–35} was employed to evaluate the forces in the QM region calculated at the restricted Hartree-Fock (RHF) level. Dunning double-ζ plus polarization function (DZP) basis sets³⁶⁻³⁸ were applied for sulfur, oxygen, and hydrogen atoms. A methodical test was performed for a comparison of the geometric parameters obtain from the HF method optimization of $[HS(H_2O)_n]^-$ (n = 0-6) clusters with and without diffuse functions of the DZP basis set. It was found that the average H-S distances determined by the HF/DZP+ method are slightly shorter by ~0.002 Å than those evaluated from the HF/DZP method. In addition, the H-S distance in the [HS(H2O)4] cluster is 1.3333 Å calculated from the HF/DZP method, which is in good agreement with that evaluated from the MP2/6-31+G(d,p) method (1.33 Å).16 These prove that the diffuse functions can be neglected. The initial configuration was taken from the simulation of the HF molecule. After equilibration of 6 ps, a 10 ps run was used for sampling. To ensure that true equilibrium had been established, the sampling trajectory was separately evaluated for the first and second 5 ps. The simulation protocol applied in this work is similar to that utilized in previous simulations of aqueous HF and HCl solutions.21,22

Similar to the HF and HCl molecules, the HS $^-$ ion has the $C_{\rm sev}$ symmetry, indicating that vibrational motion of the HS $^-$ ion is both infrared- and Raman-active. Velocity autocorrelation functions (VACFs) were evaluated to gain access to the vibrational spectrum of the HS $^-$ ion in aqueous solution. The velocity of the hydrogen atom was projected onto a unit vector parallel to the corresponding S-H bond (\tilde{u}_1), while the vibrational mode ν is the projection of the hydrogen velocity onto the unit vector \tilde{u}_1 . The vibrational frequencies of the normal

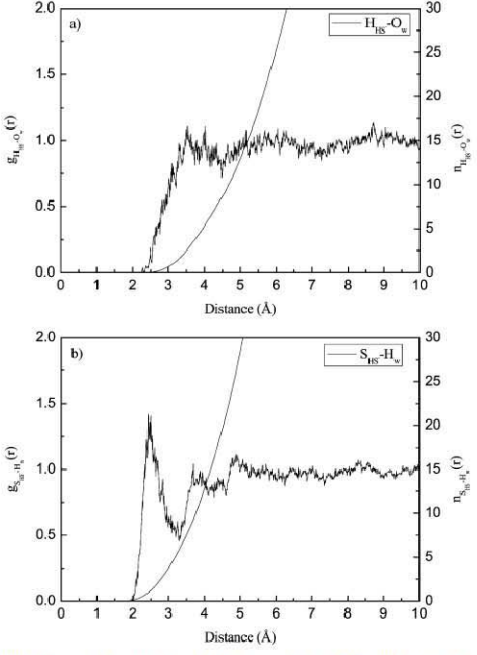


Figure 1. (a) $H_{HS}\hbox{-}\cdots O_w$ and (b) $S_{HS}\hbox{-}\cdots H_w$ RDFs and their corresponding integration numbers.

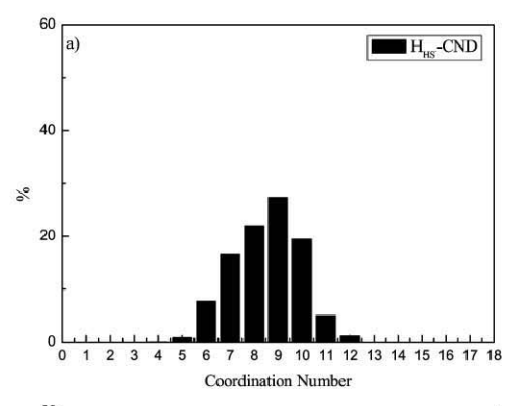
mode and the intermolecular H_{HS} —···O_w interactions were calculated by their Fourier transformations of the velocity autocorrelation functions (VACFs). The normalized VACF, C(t), is defined by

$$C(t) = \frac{\sum_{i}^{N_{t}} \sum_{j}^{N} \nu_{j}(t_{i}) \nu_{j}(t_{i} + t)}{N_{t}N \sum_{i}^{N_{t}} \sum_{j}^{N} \nu_{j}(t_{i}) \nu_{j}(t_{j})}$$
(7a)

where N is the number of particles, N_t is the number of time origins t_i , and v_j denotes a certain velocity component of the particle j. The power spectrum of C(t) was determined using a correlation length of 2.0 ps.

3. Results and Discussion

3.1. Structural Properties. To describe the structural properties of the HS $^-$ ion in aqueous solution, several hydration parameters such as radial distribution functions (RDF), coordination numbers, and angular distributions were determined. An averaged H $^-$ S bond distance of 1.35 Å was evaluated for HS $^-$ in water. Figure 1 illustrates the radial distribution functions for both atoms of the HS $^-$ ion and their neighboring water molecules together with the corresponding integration numbers. The first broad $H_{\rm HS}^{-\cdots}O_{\rm w}$ peak corresponding to the hydration shell is peaking $\sim\!\!4$ Å, covering a wide range of 2.1–4.6 Å. Weak intermediate peaks at 3.2 and 3.6 Å correspond to water molecules near the H of the HS $^-$ ion. As the mean $H_{\rm HS}^{-\cdots}O_{\rm w}$ distance $\sim\!\!4$ Å is much larger than the $H_{\rm HF}^{+\cdots}O_{\rm w}$ and $H_{\rm HCl}^{+\cdots}O_{\rm w}$ distances of 1.62 and 1.84 Å observed in aqueous



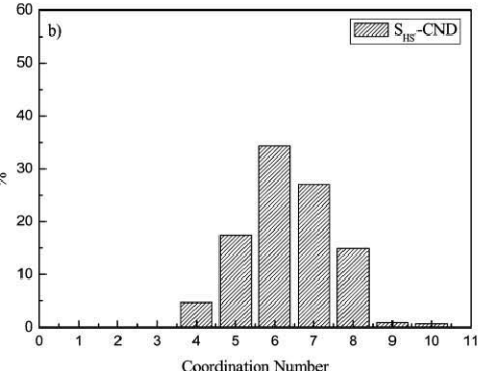


Figure 2. Coordination number distributions of (a) H (up to 4.5 Å) and (b) S (up to 4.0 Å) atoms in the first hydration shell of the HS-ion.

HF and HCl solutions, respectively, $^{21.22}$ the extremely weak acidity of the H atom and thus its inability to form stable hydrogen bonds is clearly recognized. As visible in Figure 1a, the minimum between the first shell and bulk is far from the baseline, indicating frequent water exchanges and a very weak separation of the hydration shell from bulk. Figure 1b presents the S_{HS} — \cdots H_w RDF and the corresponding integration. The first sharp S_{HS} — \cdots H_w peak is centered at 2.42 Å, reflecting that the water molecules in the first hydration shell bind much more strongly to the sulfur site than to the hydrogen site. According to Figure 1b, a second S_{HS} — \cdots H_w peak within the range 3.2–4.0 Å with its maximum at \sim 3.7 Å can be assigned to the distance between sulfur atom and the second hydrogen atom of coordinated water molecules in the hydration shell.

The hydration shell coordination number distribution determined from the $H_{\rm HS^{++}}\cdots O_w$ interactions of the HS $^-$ ion in aqueous solution is shown in Figure 2a. A variation between 5 and 12, with 9 being the most dominant species is obtained from the simulation. As shown in Figure 2b, the coordination number distribution of the $S_{\rm HS}^{-+}\cdots O_w$ interactions covers a narrower range of 4–10 with an average value of 5.9 \pm 1.1. These results confirm the assumption of a very weak water coordination at the hydrogen site of the HS $^-$ ion. To see whether a true equilibrium has been established, the first and the second half of the sampling trajectory were analyzed separately and listed in Table 1. The results prove that there is only a minor

TABLE 1: Coordination Numbers for the Hydration Shell of the HS⁻ Ion Evaluated for Sulfur and Hydrogen Sites, and in a Molecular Manner

simulation time (ps)	CND-S	CND-H	CND-HS	
0-5	5.9 ± 1.1	9.3 ± 1.6	10.2 ± 1.6	
5-10	5.8 ± 1.0	9.0 ± 1.5	9.9 ± 1.5	
0-10	5.9 ± 1.1	9.2 ± 1.6	10.0 ± 1.7	

difference between both parts, which also gives a confidence limit for the overall results.

To further detail the hydrogen bond interactions of the HS¯ ion in aqueous solution, the angular distribution functions of the $O_w\cdots H_{HS}-S_{HS}$ and $H_{HS}-S_{HS}\cdots H_w$ angles in the first hydration shell were examined as depicted in Figure 3. Both of these extend over almost the whole range from 0° to 180°, with a clear preference of nonlinear, almost rectangular H bonds. This result is in strong contrast to the cases of $O_w\cdots H-X$ bonds of HF (170°)²¹ and HCl (161°).²² The $H_{HS}-S_{HS}-\cdots H_w$ angle peaking at $\sim\!100^\circ$ is smaller but not so different from the $H_{HF}-F_{HF}\cdots H_w$ and $H_{HCl}-Cl_{HCl}\cdots H_w$ angles of 116° and $112^\circ.²1.2^\circ$

3.2. Dynamical Properties. On the basis of the velocity autocorrelation functions (VACFs) and their Fourier transformations, the vibrational frequencies of the normal mode H_{HS}-SHS- and the intermolecular HHS-...Ow interactions were analyzed. The power spectra of the HHS ... Ow and HHS -SHS vibrational modes of the hydrated ion obtained from the simulation are presented in Figure 4. As shown in Figure 4a, the maximum frequency of the HHS ... Ow vibrational mode in the first hydration shell is centered at 285 cm⁻¹, with two shoulder peaks at 204 and 383 cm⁻¹, corresponding to the force constants of 4.5, 2.3, and 8.2 N/m, respectively. The calculated force constant of 4.5 N/m obtained from the HHS ··· Ow frequency is slightly weaker than the value of 5.9 N/m determined from the HHF...Ow interaction.21 However, it is much stronger than that of 1.6 N/m evaluated from the experimental Ow-Hw ... Ow stretching frequency of 170 cm-1 in pure water.³⁹ This indicates a preference of the nondissociated structure of the HS ion, which was also observed in the case of HF.21 The intramolecular HHS--SHS- stretching mode obtained from the QMCF MD simulation is centered at 2752 cm (a value of 2449 cm⁻¹ is obtained, if the intramolecular frequency is scaled by the standard factor of 0.89^{40-42} for Hartree-Fock results), which is in reasonable agreement with the experimental evaluation by Raman spectroscopy (2570 cm⁻¹).7 The deviation can be explained by the high concentration

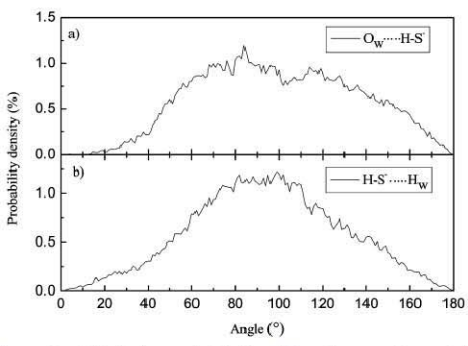


Figure 3. Distributions of (a) $O_w \cdots H_{HS} - S_{HS}$ angles and (b) $H_{HS} - S_{HS} \cdots H_w$ angles, obtained from the QMCF MD simulation.

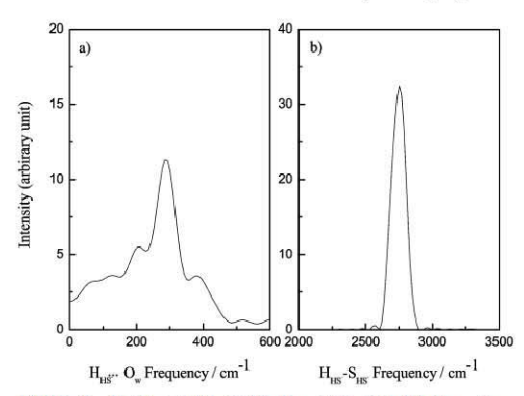


Figure 4. Power spectra of (a) $H_{HS}\cdots O_w$ and (b) $H_{HS}-S_{HS}$ stretching modes in the first hydration shell.

TABLE 2: Mean Ligand Residence Times and Sustainability of Migration Processes to and from the First Hydration Shell of Sulfur and Hydrogen atoms of the Bisulfide ion

		$t^* = 0 \text{ ps}$		$t^* = 0.5 \text{ ps}$			
solute	$t_{\rm sim}$	$N_{\rm ex}^{\rm O}$	$\tau_{\rm H_2O}^0$	$N_{\rm ex}^{0.5}$	$ au_{ m H_2O}^{0.5}$	$R_{\rm ex}$	
SHS	10.0	190	0.3	40	1.5	4.8	
H _{HS} -	10.0	900	0.1	43	2.1	20.0	
bulk ^a	10.0	131	0.2	20	1.3	6.5	

^a Values obtained from a QMCF MD simulation of pure water. ⁴⁴

of perchlorate solution employed in the Raman study 7 and/or the inaccuracy of the Hartree–Fock method and the relatively small basis set. The force constant of 436.1 N/m for the H_{HS} – S_{HS} -bond confirms the stability of the HS- ion in water.

Additional information about the solution dynamics was obtained in terms of the mean residence times (MRTs), corresponding to ligand exchange processes in the first hydration shell of the HS- ion and determined by the "direct" method43 for both sulfur and hydrogen sites of the HS- ion. The number of ligand exchange processes, the mean residence times, and the number of attempts needed for a sustainable ligand migrating from the hydration shell as revealed by the use of both time parameters t* 0.0 and 0.5 ps are listed in Table 2. As shown in Table 2, only 43 ligand exchange processes lasted longer than 0.5 ps at the hydrogen site of the HS⁻ ion during the simulation time of 10 ps, while 900 exchange attempts were recorded for $t^* = 0.0$ ps. The calculated MRT values for the hydrogen site are 0.1 ps and 2.1 for $t^* = 0.0$ and 0.5 ps, respectively. The MRT value of 2.1 ps is considerably larger than that of pure water determined from a QMCF simulation (1.3 ps)44 and HCl (0.8 ps),22 but it is slightly smaller than that of HF (2.5 ps).21 At the sulfur site, the MRT values of 0.3 and 1.5 ps for $t^* =$ 0.0 and 0.5 ps were obtained, corresponding to 190 and 40 exchange processes, respectively. As the result, the mean residence time for the water ligands located around the sulfur atom is shorter than that evaluated for the fluorine (2.1 ps) and chlorine (2.1 ps) sites of HF and HCl, respectively, 21,22 suggesting weak hydrogen bond interactions at the sulfur site of the HS- ion. For the evaluation of hydrogen bond, the distances of 4.0 and 4.5 Å for hydrogen and oxygen atoms of water molecules and angle of >120° were applied to define hydrogen bonds between HS- and water molecules. Hydrogen bond life times estimated for the SHS-HHS-...Ow and HHS-SHS-...Hw hydrogen bonds are 0.23 and 0.26 ps, respectively. The average

lifetime of the S_{HS}--H_{HS}-···O_w hydrogen bond is much smaller than that determined by experimental investigation of pure water (0.55 ps),45 and a QMCF MD simulation (0.33 ps).44 The value of 0.26 ps of the H_{HS}--S_{HS}····H_w hydrogen bond is also smaller than the corresponding values of 0.36 and 0.31 ps for HF and HCl. These results reflect once more a very weak hydrogen bond between the HS- ion and its neighboring water molecules in the hydration shell. According to the MRT values and the hydrogen bond lifetimes obtained from the QMCF MD simulation, the HS- ion in aqueous solution behaves as weak structuremaking species.

4. Conclusion

A detailed description on hydration structure and dynamics of the HS- ion in aqueous solution could be obtained using a QMCF MD simulation. The HHS--SHS- vibrational frequency predicted from the QMCF MD simulation is in reasonable agreement with the experiment, while very weak hydrogen bonding between the bisulfide ion and its neighboring water molecules was recognized. These data confirm the preference of nondissociated HS⁻ in aqueous solution. As expected, ligand exchange processes in the hydration shell occur frequently at both sites of the HS ion.

Acknowledgment. Financial support for this work by the Thailand Research Fund (TRF) and Thailand Commission on Higher Education (ASEA-UNINET fellowships for C.K. and V.V.) are gratefully acknowledged and B.M.R. acknowledges support by the Austrian Science Foundation (FWF). V.V. acknowledges additional support by Faculty of Science, Chulalongkorn University (Grant Number RES A1 B1-19).

References and Notes

- Light, T. S. *Ion-Selective Electrodes*; National Bureau Standards
 Special Publication no. 314; NBS: Washington, DC, 1969; p 371.
 Wayne, R. P. *Chemistry of Atmospheres*, 2nd ed.; Clarendon Press: Oxford, U.K., 1991; *Chapters 1 and 5*.
- (3) Barbero, J. A.; McCurdy, K. G.; Tremaine, P. R. Can. J. Chem.
- 60, 1872.
 Licht, S.; Manassen, J. J. Electrochem. Soc. 1987, 134, 918.
 Stephens, H. P.; Cobble, J. W. Inorg. Chem. 1971, 10, 619.
 Gigenbach, W. Inorg. Chem. 1971, 10, 1333.
 Meyer, B.; Ward, K.; Koshlap, K.; Peter, L. Inorg. Chem. 1983, 2345. 22, 2345.
- Licht, S.; Forouzan, F.; Longo, K. Anal. Chem. 1990, 62, 1356.
 Migdisov, A. A.; Williams, A. E.; Lakshtanov, L. Z.; Alekhin, Y. V. Geochim. Cosmoschim. Acta 2002, 66, 1713.
 Schoonen, M. A.; Barnes, H. L. Geochim. Cosmoschim. Acta 1988,
- - (11) Eckert, W. J. Electrochem. Soc. 1998, 145, 77.

- (12) Kolthoff, L.; Moltzau, D. Chem. Rev. 1935, 17, 293.
- (12) KOHROH, L.; MORIZAU, D. Chem. Rev. 1935, 17, 293.
 (13) Luther, I., G. W.; Richard, D. T.; Theberge, S.; Olroyd, A. Environ.
 Sci. Technol. 1996, 30, 671.
 (14) McCarthy, V. N.; Jordan, K. D. Chem. Phys. Lett. 2006, 429, 166.
 (15) Joshi, R.; Ghanty, T. K.; Naumov, S.; Mukherjee, T. J. Phys. Chem.
 A 2007, 111, 2362.
- (16) Lee, C.; Sosa, C.; Planas, M.; Novoa, J. J. Chem. Phys. 1996, 104,
- (17) Planas, M.; Lee, C.; Novoa, J. J. J. Phys. Chem. 1996, 100, 16495. (18) Smith, A.; Vencent, M. A.; Hillier, I. H. J. Phys. Chem. 1999, 103,
- (19) Rode, B. M.; Hofer, T. S.; Randolf, B. R.; Schwenk, C. F.; Xenides,
- D.; Vchirawongkwin, V. Theor. Chem. Acc. 2006, 115, 77.
 (20) Vchirawongkwin, V.; Pribil, A. B.; Rode, B. M. J. Comput. Chem. 2010, 37, 249,
- (21) Kritayakomupong, C.; Vchirawongkwin, V.; Hofer, T. S.; Rode, B. M. *J. Phys. Chem. B* **2008**, *112*, 12032.
- (22) Kritayakornupong, C.; Vchirawongkwin, V.; Rode, B. M. *J. Comput. Chem.* 2010, 31, 1785.
 (23) Frick, R. J.; Hofer, T. S.; Pribil, A. B.; Randolf, B. R.; Rode, B. M.
- (23) Files, A. J., Rullet, T. S., Fillot, A. B., Randolf, B. R., Rode, B. M. J. Phys. Chem. A 2009, 113, 12496.
 (24) Hofer, T. S.; Pribil, A. B.; Randolf, B. R.; Rode, B. M. Ab Initio Quantum Mechanical Charge Field Molecular Dynamics-A Nonparameterized First-Principle Approach to Liquids and Solutions; Academic Press, Elsevier Inc.; Amsterdam, 2001; Vol. 59.
- (25) Field, M. J.; Bash, P. A.; Karplus, M. J. Comput. Chem. 1990, 11,
 - (26) Gao, J. J. Am. Chem. Soc. 1993, 115, 2930.
- (27) Bakowies, D.; Thiel, W. J. Phys. Chem. 1996, 100, 10580.
 (28) Stillinger, F. H.; Rahman, A. J. Chem. Phys. 1978, 68, 666
- (29) Bopp, P.; Janscó, G.; Heinzinger, K. Chem. Phys. Lett. 1983, 98,
- (30) Brooks, B. R.; Bruccoleri, R. E.; Olafson, B. D.; States, D. J.;
- Swaninathan, S.; Karplus, M. J. Comput. Chem. 1983, 4, 187.
 (31) Berendsen, H. J. C.; Postma, J. P. M.; van Gunsteren, W. F.; DiNola,
 A.; Haak, J. R. J. Chem. Phys. 1984, 81, 3684.
 (32) Adams, D. J.; Adams, E. H.; Hills, G. J. Mol. Phys. 1979, 38, 387.
- (33) Ahlrichs, R.; Bär, M.; Häser, M.; Hom, H.; Kölmel, C. Chem. Phys. Lett. 1989, 162, 165.

- Lett. 1989, 162, 165.
 (34) Ahlrichs, R.; von Arnim, M. Methods and Techniques in Computational Chemistry: METECC-95; Cagliari: Sardinia, 1995.
 (35) von Arnim, M.; Ahlrichs, R. J. Comput. Chem. 1998, 19, 1746.
 (36) Magnusson, E.; Schaefer, H. F., III. J. Chem. Phys. 1985, 83, 5721.
 (37) Dunning, T. H., Jr.; Wadt, W. R. J. Chem. Phys. 1989, 90, 1007.
 (38) Dunning, T. H., Jr.; Hay, P. J. Modern Theoretical Chemistry: Methods of Electronic Structure Theory; Schaefer, H. F., III, Ed.; Plenum Press: New York, 1977; Vol. 3.
 (39) Franks, F. Water: a Comprehensive Treatise; Plenum Press: New York, 1972; Vol. 1.
- York, 1972; Vol. 1. (40) Scott, A. P.; Random, L. J. Phys. Chem. 1996, 100, 16502.
- (41) Grev, R. S.; Janssen, C. L.; Schaefer, H. F., III. J. Chem. Phys. 1991, 95, 5128.
- (42) DeFrees, D. J.; McLean, A. D. J. Chem. Phys. 1985, 82, 333.
 (43) Hofer, T. S.; Tran, H. T.; Schwenk, C. F.; Rode, B. M. J. Comput. Chem. 2004, 25, 211.
- (44) Randolf, B. R.; Hofer, T. S.; Rode, B. M. Unpublished results.
 (45) Lock, A. J.; Woutersen, S.; Bakker, H. J. J. Phys. Chem. A 2001, 105, 1238.

JP1048560

Author's personal copy

Journal of Molecular Structure: THEOCHEM 913 (2009) 236-239



Contents lists available at ScienceDirect

Journal of Molecular Structure: THEOCHEM

journal homepage: www.elsevier.com/locate/theochem



Inter- and intra-molecular OH stretching modes of bicarbonate in aqueous solution

Viwat Vchirawongkwin a,*, Chinapong Kritayakornupong b, Vithaya Ruangpornvisuti a, Bernd M. Rode c

- ^a Department of Chemistry, Faculty of Science, Chulalongkorn University, Phyathai Road, Prathumwan, Bangkok 10330, Thailand
- ^b Department of Chemistry, Faculty of Science, King Mongkut's University of Technology Thonburi, Bangkok 10140, Thailand
- ^cTheoretical Chemistry Division, Institute of General, Inorganic and Theoretical Chemistry, University of Innsbruck, Innrain 52a, A-6020 Innsbruck, Austria

ARTICLE INFO

Article history: Received 9 July 2009 Received in revised form 28 July 2009 Accepted 3 August 2009 Available online 11 August 2009

Keywords:
Bicarbonate ion
QMCF molecular dynamics
Vibrational spectrum
Velocity autocorrelation functions

ABSTRACT

The ambiguous assignments of the CO–H stretching (ν_1) mode of bicarbonate ion in Raman and IR spectra were clarified based on a careful investigation of hydrogen bonding and its influence on the power spectra evaluated from the velocity autocorrelation functions obtained by an ab initio QMCF MD simulation. The ν_1 spectrum includes inter- and intra-molecular OH stretching modes of hydrated bicarbonate ion and is presented together with the other vibrations, namely the symmetric CO stretching (ν_3), the C–OH stretching (ν_5) and the CO₃ out-of-plane deformation (ν_8), modes.

© 2009 Elsevier B.V. All rights reserved.

1. Introduction

The bicarbonate ion, plays important roles in chemical and biological processes. This ion is generated as the major product by the dissolution of carbon dioxide in water in the pH range of 8-10 [1], and also produced by the human carbonic anhydrase II [2,3] to maintain the blood pH at the level suitable for tissues and enzymes activities. Several spectroscopic techniques have been utilised to obtain experimentally quantitative and structural information about the bicarbonate anion dissolved in water [4]. The vibrational frequencies of bicarbonate ion in aqueous solution have been investigated by Raman and infrared (IR) spectroscopy and presented in many publications [4-12]. The deviations of normal frequencies between Raman spectra and theoretical results based on density functional theory (DFT) were less than 150 cm⁻¹, except the CO-H stretching mode which differed by ${\sim}1000\,\text{cm}^{-1}$ [10]. The CO–H stretching mode of bicarbonate ion was assigned to a band located around 2600 cm⁻¹ in Raman and IR spectra [4-6,10], while the DFT calculation employing the B3LYP/6-31+G* method for bicarbonate ion in a cluster with three water molecules gave the frequency of $3596.5\ cm^{-1}$ [10]. This significant difference was attributed to the influence of strong anharmonicity [10], implying a scaling factor of 0.723 for correcting the overestimation of this frequency. However, it is well-known that the scaling factors for the B3LYP method are larger than 0.96 [13-15], thus making ambiguous the assignment of this vibrational frequency.

Computer simulations have become an alternative tool to elucidate the microscopic solvate properties helpful for the interpretation of experimental observations [16–18]. A recently proposed simulation protocol, namely the *ab initio* quantum mechanical charge field (QMCF) molecular dynamics (MD) formalism [19], has succeeded to determine the vibrational frequencies of tetrahedral sulphate ion [20] and analogous oxo-anions [21]. Here we report the vibrational frequencies of the stretching modes evaluated by means of the velocity autocorrelation functions (VACFs) of the bicarbonate ion in aqueous solution obtained from a QMCF MD simulation [22], associated with the influence of hydrogen-bonds (H-bonds), aiming at clarifying the OH stretching frequency assignments of bicarbonate ion in aqueous solution.

2. Computational details

The QMCF MD simulation protocol has been reported previously [22]. The QMCF MD formalism is based on the conventional quantum mechanical/molecular mechanical (QM/MM) MD method, increasing the size of the QM region by adding a further QM region containing only solvent molecules (layer zone), thus allowing the non-Coulombic interactions between the solute in the inner QM region (core zone) and solvent molecules in the MM region to be neglected. Therefore, the only potential function needed is the one for interaction between solvent molecules. The Coulombic interaction from the point charges of solvent molecules in the MM region to all atoms in the QM region are incorporated via a perturbation term in the core Hamiltonian, while the charges of the atoms in the QM region obtained from population analysis are

^{*} Corresponding author. Fax: +66 (0) 2218 7598. E-mail address: Viwat.V@Chula.ac.th (V. Vchirawongkwin).

utilised to evaluate the Coulombic interactions with the atoms in the MM part. The simulation was performed in the NVT ensemble using a general predictor-corrector algorithm with a time step of 0.2 fs. The system temperature was maintained at 298.16 K by the Berendsen temperature-scaling algorithm [23] with a relaxation time of 100 fs. The simulation system consisted of one bicarbonate ion and 496 water molecules in a cubic box of 24.65 Å with periodic boundary conditions. The density of the simulation box was 0.997 $\mathrm{g}\,\mathrm{cm}^{-3}$, i.e. the experimental value of pure water at 298 K. The calculation of forces for the most relevant region, the QM region extended to 5.4 Å with the core radius of 3.2 Å, was performed by means of Hartree-Fock (HF) method with the Dunning double-ζ plus polarisation and diffuse functions (DZP+) basis sets [24-26] for hydrogen, carbon, and oxygen atoms of the bicarbonate ion, and Dunning double-ζ plus polarisation function (DZP) basis sets [24-26] for hydrogen and oxygen atoms of water, respectively. The thickness of the smoothing region was chosen as 0.2 Å with the values of r_{on} and r_{off} as 5.2 and 5.4 Å, respectively, according to the radial distribution function (RDF) obtained from the equilibrated simulation. The selected water model applied to calculate the interactions between pairs of water in the MM region was the flexible BJH-CF2 model [27,28], with the cutoff distances of 3.0 and 5.0 Å for non-Coulombic interactions between H atoms and between O and H atoms, respectively. The reaction field method combined with the shifted-force potential technique were applied to account for long-range electrostatic potentials and forces, with a spherical cutoff limit of 12.350 Å. The system was initially equilibrated by performing the QMCF MD simulation for 10 ps (50,000 steps), and a further 10 ps (50,000 steps) were utilised for data

Because of the low symmetry of bicarbonate anion, the number of water molecules within the first hydration shell was evaluated firstly by the determination of the radius of hydration according to the RDFs for each atomic site. These radii were then utilised to determine the coordination number based on the solvent-accessible surface to avoid double-counting of some water molecules within the overlap zone of individual hydration shells, as presented in our previous work, resulting in an average total coordination number of 5.41 [22].

The dynamical properties of a fluid system related to macroscopic transport coefficients can be evaluated from the VACFs, and their Fourier transformations can be interpreted as the vibrational spectra. The vibrational spectra of bicarbonate ion were obtained from the VACFs using normal-coordinate analysis [29]. The normalised VACF, C(t), is defined as

$$C(t) = \frac{\sum_{i}^{N_t} \sum_{j}^{N} v_j(t_i) v_j(t_i + t)}{N_t N \sum_{i}^{N_t} \sum_{j}^{N} v_j(t_i) v_j(t_i)}$$
(1)

where N is the number of particles, N_t is the number of time origins t_i , and v_j denotes a certain velocity component of the particle j. In order to obtain the vibrational frequencies corresponding to the vibrational motions, the instantanous velocities of hydrogen, carbon and three oxygen atoms of the bicarbonate ion were analysed on the basis of the Raman and IR active harmonic normal modes according to the C_1 symmetry. All nine modes of bicarbonate are infrared and Raman active. Due to the main goal of the present work, only four vibrational modes were explicitly defined. The CO-H stretching (v_1) mode is the main target of this work, while the symmetric CO stretching (v_3) , C-OH stretching (v_5) and CO₃ out-of-plane deformation (v_8) modes are employed to determine the ability of QMCF MD formalism to elucidate the dynamical properties of hydrated bicarbonate ion. The atomic motions of these modes are schematically depicted in Fig. 1. The instantaneous H, C and O velocities were decomposed into the necessary smallest fragments. The O velocity was projected onto a unit vector parallel

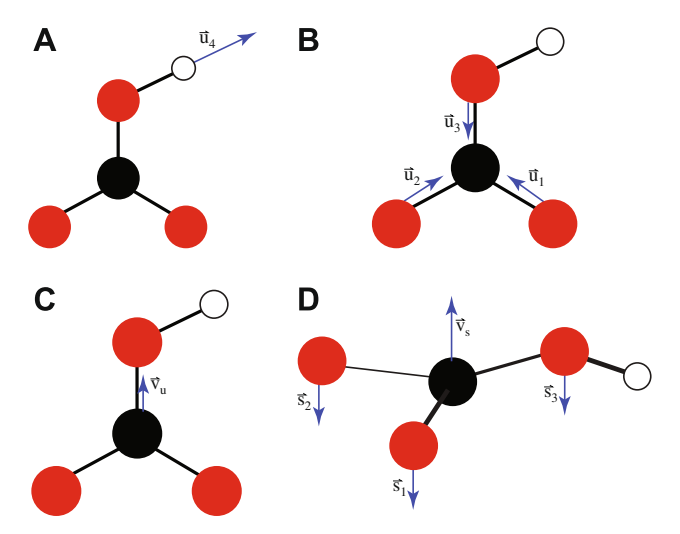


Fig. 1. The defined normal vectors of (A) CO–H stretching (v_1) , (B) symmetric CO stretching (v_3) , (C) C–OH stretching (v_5) and (D) CO₃ out-of-plane deformation (v_8) modes for the bicarbonate ion.

to the corresponding C–O bond (\vec{u}_i , i=1 to 3) and a unit vector perpendicular to a normal vector of the O–C–O plane (\vec{s}_i , i=1 to 3). The H velocity was projected onto a unit vector parallel to the O–H bond (\vec{u}_4). The C velocity was also projected onto a unit vector parallel to the bond between C and O adjacent hydrogen (\vec{v}_u) and a unit vector perpendicular to a normal vector of the bicarbonate plane (\vec{v}_s). \vec{U}_i , \vec{S}_i , \vec{V}_u and \vec{V}_s are used to denote the projection of the H, C and O velocity onto the unit vectors \vec{u}_i , \vec{s}_i , \vec{v}_u and \vec{v}_s , respectively. The relevant four vibrational modes are defined as following

$$v_1 = U_4$$

$$v_3 = \sum_{i=1}^3 \mathbf{U}_i$$

$$v_5 = V_u$$

$$v_8 = V_s + \sum_{i=1}^3 S_i$$

The v_3 , v_5 and v_8 modes present the mixing states due to the flexible movement of atoms within the simulation period.

As the bicarbonate ion exhibits structure-breaking effects in aqueous solution [9,22], the number of H-bonds between the ion and the hydration shell fluctuates during the simulation period. The number of H-bonds was estimated by different definitions on the basis of energetic and geometric criteria [30,31], as shown in Fig. 2, employing a structural criterion depending on the cutoff parameters (distance $R_{\rm HO}^{(c)}, R_{\rm OO}^{(c)}$ and angle $\phi^{(c)}$) in analogy to water–dimethyl sulphoxide mixtures [32]. The cutoff distances $R_{\rm HO}^{(c)}$ and $R_{\rm OO}^{(c)}$ were obtained from the radial distribution functions for the bicarbonate's hydrogen and water oxygen atoms $(H_b - O_w)$ and for the bicarbonate's oxygen and adjacent hydrogen and water oxygen atoms $(O_3 - O_w)$, presenting the boundary of the first coordination

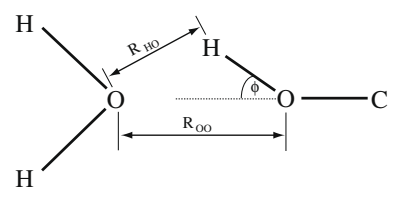


Fig. 2. The hydrogen-bond definition according to the geometrical relation between the hydrogen atom of bicarbonate ion and water molecule.

shell at 2.6 Å and 3.8 Å, respectively [22]. The angle $\phi^{(c)}$ was set to 30 $^{\circ}$ [32].

For the CO–H stretching (ν_1) frequency comparison between the experimental assignments and theoretical investigation, we also performed the frequency calculation with Gaussian 03 [33] for small water clusters of bicarbonate ion, employing the Hartree-Fock (HF), second-order Møller–Plesset (MP2) and Becke, three-parameter, Lee–Yang–Parr (B3LYP) methods associated with the double- ζ plus polarisation and diffuse functions (DZP+) basis set. Rudolph *et al.* suggested the cluster having three water molecules calculated with the B3LYP/6-31+G* method providing the best agreement of the calculated peak positions with the measured Raman data [10]. Thus, we extended the cluster size including the forth water molecule and also including electron correlation effects at MP2 level, to determine its effect on the ν_1 frequency.

3. Results and discussion

The power spectra predicted by applying the Fourier transformation to the VACFs employing a correlation length of 1.0 ps with 1800 averaged time origins (10 ps) of the symmetric CO stretching (v_3) , C-OH stretching (v_5) and CO₃ out-of-plane deformation (v_8) modes, and CO-H stretching (v_1) mode in the bicarbonate ion are displayed in Fig. 3. The dominant peak at 1498 cm $^{-1}$ of v_3 (Fig. 3A, spectrum a) differs from the Raman data (1312 cm⁻¹) [10] by 134 cm⁻¹, while two weak peaks located at 1075 and 700 cm $^{-1}$ superimpose with the strong peak of v_5 (Fig. 3A, spectrum b) and v_8 (Fig. 3A, spectrum c), respectively. These two modes were assigned in Raman experiment to 1015 and 673 cm⁻¹, respectively. [10] The acceptable deviation of vibrational frequencies for these three modes in Fig. 3A indicates the success of QMCF MD methodology to supply good dynamical data of hydrated bicarbonate ion [22]. The CO - H stretching spectrum in Fig. 3B consists of a strong peak located at 4023 cm⁻¹ and a weak broad band, shown in the insert, with its peak at 2687 cm⁻¹. We also performed the frequency calculation with Gaussian 03 [33] for small water clusters of bicarbonate ion (HCO $_3$ · nH $_2$ O, n = 1, 2, 3, 4) [22], employing the Hartree-Fock (HF), second-order Møller-Plesset (MP2) and Becke, three-parameter, Lee-Yang-Parr (B3LYP) methods associated with DZP+ basis sets [24–26]. The v_1 frequencies are shown in Table 1, corresponding to the frequency of the strong peak in Fig. 3B. If one accepts that the MP2 level represents the best quality (although MP2 can also overestimate correlation influence), the obtained results confirm the common observation from many similar simulations including DFT-based Car-Parrinello MD simulations that DFT overestimates the strength and thus the rigidity of H bonds, while ab initio simulations at HF level tend to underestimate hydrogen bond strength. The peak of the observed weak band corresponds to the frequency found in the Raman and IR experi-

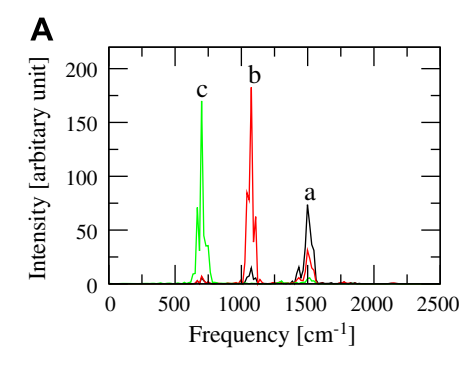
Table 1 Vibrational frequencies (cm $^{-1}$) of CO $^{-}$ H stretch (ν_1) within the bicarbonate ion in four hydrated forms (HCO $_3^-$ · nH $_2$ O, n=1,2,3,4) obtained from HF, MP2 and B3LYP calculations with DZP+ basis sets [24 $^{-}$ 26].

Frequencies (cm ⁻¹)					
H ₂ O	2H ₂ O	$3H_2O$	4H ₂ O		
4196 3692	4182 3653	4162 3609	4146 3582 3719		
	H ₂ O 4196	H ₂ O 2H ₂ O 4196 4182 3692 3653	H ₂ O 2H ₂ O 3H ₂ O 4196 4182 4162 3692 3653 3609		

ments at ca. 2600 cm⁻¹ [4–6,10]. The characterisation of this weak band requires further details for an interpretation, which are presented below.

The number of H-bonds between the hydrogen atom of bicarbonate ion and water molecules within the hydration shell was counted throughout the simulation time as shown in Fig. 4. Further, we investigated the effect of H-bonding on the vibrational spectrum of the v_1 vibration. We chose three short intervals located from 0.5 to 2.5 ps (few H-bonds), 6.0 to 8.0 ps (numerous H-bonds) and 8.6 to 10.0 ps (no H-bonds), and evaluated the spectrum for each period by means of the VACFs employing a correlation length of 1.0 ps with 200 and 80 averaged time origins for time intervals 2.0 ps and 1.4 ps, respectively. The power spectra are shown in Fig. 5. In the spectrum of the few H-bonds period (Fig. 5A), the strong peak is located at 4007 cm⁻¹ and a weak band from 2394 to 2736 cm⁻¹ reaches 3.0% of the strong peak's height. The strong presence of H-bonds affects the frequencies and intensities of strong and weak band, as shown in Fig. 5B. The strong peak is lowered and redshifted, while the weak band is less well structure and starts at 2525 cm⁻¹ and extends to 2899 cm⁻¹ implying a blueshift of this band. At the same time the intensity of the weak peak increases to 12.0% of that of the strong one, apparently due to the more intense H-bonding. The absence of H-bonds shifts the strong peak (cf. Fig. 5C) to 4039 cm⁻¹, which means a blueshift compared to the peak in Fig. 5A. The weak band peak is redshifted by 81 cm⁻¹, and amounts to only 1.6% of the strong peak height. These results clearly reflect the influence of H-bonds on the interand intra-molecular OH stretching modes of bicarbonate ion. An increasing number of H-bonds redshifts the strong peak and blueshifts the weak band, also rising the relative intensity of the weak band. Our results show that the strong peak represents the intramolecular OH stretch, while the weak band corresponds to the intermolecular OH interactions due to the H-bonds. The shape of this peaks shows the wide varieties of H-bonds realised in solution.

The frequency of the strong peak agrees with the value obtained by the quantum mechanical calculations of the CO-H stretching within the bicarbonate ion. The location of the weak band corresponds to the peak assignment of CO-H stretch in the Raman



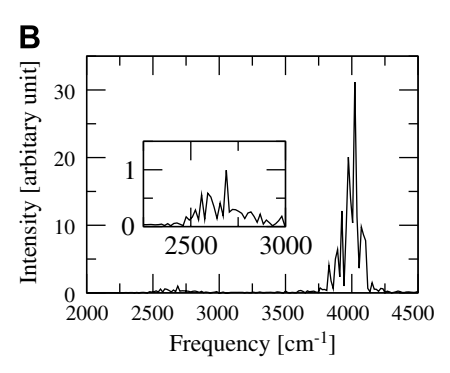


Fig. 3. Power spectra of (A) symmetric CO stretching (a), C-OH stretching (b) and CO_3 out-of-plane deformation (c) modes, and (B) CO-H stretch of the hydrated bicarbonate ion with the insert presenting the weak band located from 2250 to 3000 cm⁻¹ obtained from the 10 ps QMCF MD simulation [22].

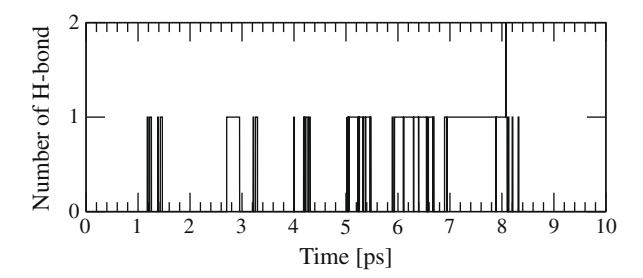


Fig. 4. Number of hydrogen-bonds between the hydrogen atom of bicarbonate ion and water molecules within the hydration shell during 10 ps of QMCF MD simulation [22].

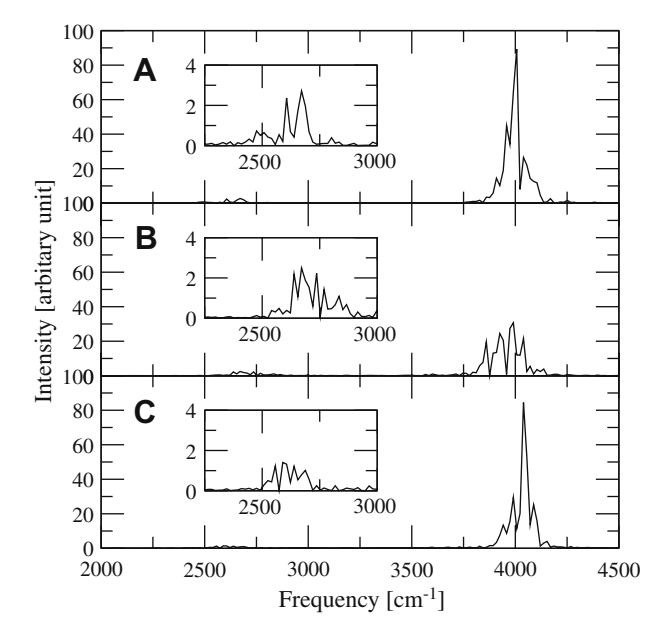


Fig. 5. Power spectra of v_1 obtained from the QMCF MD simulation [22] evaluated during (A) 0.5-2.5 ps, (B) 6.0-8.0 ps, and (C) 8.6-10.0 ps with the inserts showing the weak band located from 2250 to $3000\ cm^{-1}$.

and IR experiments [4-6,10], but it has to be assigned to the intermolecular OH stretching mode involving hydrogen bonds between ion and water molecules.

4. Conclusion

The successful application of the ab initio QMCF MD approach for the unambiguous assignment of the experimentally observed vibrational frequencies, in particular of the CO-H stretching frequency, can be seen as a strong indication that this methodology is suitable for simulations of composite solutes of low symmetry in water. Previous simulations of phosphate, sulphate and perchlorate in water [20,34-36] have already shown that the method is well suited to treat hydrogen bonded, weakly interacting anions and thus let us expect in connection with the results presented here that this applicability is of rather general character and should be valid for neutral hydrogen bonding solutes as well.

Acknowledgments

Generous financial support by the Austrian Science Foundation (FWF), The Thailand Research Fund and Thailand Commission on Higher Education (fellowships for V.V. and C.K.) are gratefully acknowledged.

References

- [1] D.M. Kern, J. Chem. Educ. 37 (1960) 14-23.
- [2] D.N. Silverman, S.H. Vincent, CRC Crit. Rev. Biochem. 14 (1983) 207-255.
- D.N. Silverman, S. Lindskog, Acc. Chem. Res. 21 (1988) 30-36.
- [4] A.R. Davis, B.G. Oliver, J. Solution Chem. 1 (1972) 329–339.
 [5] B.G. Oliver, A.R. Davis, Can. J. Chem. 51 (1973) 698–702.
- W. Hage, A. Hallbrucker, E. Mayer, J. Am. Chem. Soc. 115 (1993) 8427-
- N. Wen, M.H. Brooker, J. Phys. Chem. 99 (1995) 359-368.
- [8] J.D. Frantz, Chem. Geol. 152 (1998) 211-225.
- [9] Z.S. Nickolov, O. Ozcan, J.D. Miller, Colloids Surf. A 224 (2003) 231-239.
- [10] W.W. Rudolph, D. Fischer, G. Irmer, Appl. Spectrosc. 60 (2006) 130–144.
- [11] O. Ozdemir, M.S. Çelik, Z.S. Nickolov, J.D. Miller, J. Colloids Interface Sci. 314 (2007) 545-551.
- W.W. Rudolph, G. Irmer, E. Königsberger, Dalton Trans. (2008) 900-908.
- G. Rauhut, P. Pulay, J. Phys. Chem. 99 (1995) 3093-3100.
- [14] A.P. Scott, L. Radom, J. Phys. Chem. 100 (1996) 16502–16513.
- [15] M.P. Andersson, P. Uvdal, J. Phys. Chem. A 109 (2005) 2937–2941.
- [16] R.W. Impey, P.A. Madden, I.R. McDonald, J. Phys. Chem. 87 (1983) 5071-5083.
- [17] S. Obst, H. Bradaczek, J. Phys. Chem. 100 (1996) 15677-15687.
- [18] S. Koneshan, J.C. Rasaiah, R.M. Lynden-Bell, S.H. Lee, J. Phys. Chem. B 102 (1998) 4193–4204.
- [19] B.M. Rode, T.S. Hofer, B.R. Randolf, C.F. Schwenk, D. Xenides, V. Vchirawongkwin, Theor. Chem. Acc. 115 (2006) 77–85.
- V. Vchirawongkwin, B.M. Rode, Chem. Phys. Lett. 443 (2007) 152–157.
- [21] A.B. Pribil, T.S. Hofer, V. Vchirawongkwin, B.R. Randolf, B.M. Rode, Chem. Phys. 346 (2008) 182-185.
- V. Vchirawongkwin, A.B. Pribil, B.M. Rode, Ab initio quantum mechanical charge field study of hydrated bicarbonate ion: structural and dynamical properties, 2009. doi:10.1002/jcc.21308.
- [23] H.I.C. Berendsen, J.P.M. Postma, W.F. van Gunsteren, A. DiNola, J.R. Haak, J. Chem. Phys. 81 (1984) 3684-3690.
- [24] T.H. Dunning Jr., P.J. Hay, Gaussian basis sets for molecular calculations, in: H.F. Schaefer III (Ed.), Modern Theoretical Chemistry: Methods of Electronic Structure Theory, Ch. 1, vol. 3, Plenum Press, New York, 1977, pp. 1-27.
- [25] T.H. Dunning Jr., J. Chem. Phys. 53 (7) (1970) 2823-2833.
- [26] E. Magnusson, H.F. Schaefer III, J. Chem. Phys. 83 (1985) 5721-5726.
- F.H. Stillinger, A. Rahman, J. Chem. Phys. 68 (2) (1978) 666-670.
- [28] P. Bopp, G. Janscó, K. Heinzinger, Chem. Phys. Lett. 98 (2) (1983) 129-133.
- [29] P. Bopp, Chem. Phys. 106 (1986) 205–212.
- [30] M.G. Sceats, S.A. Rice, J. Chem. Phys. 72 (1980) 3236-3247.
- [31] M. Mezei, D.L. Beveridge, J. Chem. Phys. 74 (1981) 622–632.
 [32] A. Luzar, D. Chandler, J. Chem. Phys. 98 (1993) 8160–8173.
- [33] M.J. Frisch, G.W. Trucks, H.B. Schlegel, G.E. Scuseria, M.A. Robb, J.R. Cheeseman, J.A. Montgomery, T. Vreven, K.N. Kudin, J.C. Burant, J.M. Millam, S.S. Iyengar, J. Tomasi, V. Barone, B. Mennucci, M. Cossi, G. Scalmani, N. Rega, G.A. Petersson, H. Nakatsuji, M. Hada, M. Ehara, K. Toyota, R. Fukuda, J. Hasegawa, M. Ishida, T. Nakajima, Y. Honda, O. Kitao, H. Nakai, M. Klene, X. Li, J.E. Knox, H.P. Hratchian, J.B. Cross, V. Bakken, C. Adamo, J. Jaramillo, R. Gomperts, R.E. Stratmann, O. Yazyev, A.J. Austin, R. Cammi, C. Pomelli, J.W. Ochterski, P.Y. Ayala, K. Morokuma, G.A. Voth, P. Salvador, J.J. Dannenberg, V.G. Zakrzewski, S. Dapprich, A.D. Daniels, M.C. Strain, O. Farkas, D.K. Malick, A.D. Rabuck, K. Raghavachari, J.B. Foresman, J.V. Ortiz, Q. Cui, A.G. Baboul, S. Clifford, J. Cioslowski, B.B. Stefanov, G. Liu, A. Liashenko, P. Piskorz, I. Komaromi, R.L. Martin, D.J. Fox, T. Keith, A.M.A. Laham, C.Y. Peng, A. Nanayakkara, M. Challacombe, P.M.W. Gill, B. Johnson, W. Chen, M.W. Wong, C. Gonzalez, J.A. Pople, Gaussian 03, Revision E.01, Gaussian, Inc., Wallingford, CT, 2004.
- [34] V. Vchirawongkwin, B.M. Rode, I. Persson, J. Phys. Chem. B 111 (2007) 4150-
- [35] A.B. Pribil, V. Vchirawongkwin, T.S. Hofer, B.R. Randolf, Structure and dynamics of composite anions in aqueous solution, in: T.E. Simos, G. Maroulis (Eds.), Computation in Modern Science and Engineering, Proceedings of the International Conference on Computational Methods in Science and Engineering, vol. 2, Part B, 2007, pp. 921-923.
- A.B. Pribil, T.S. Hofer, B.R. Randolf, B.M. Rode, J. Comput. Chem. 29 (2008) 2330-2334.

Ab Initio Quantum Mechanical Charge Field Study of Hydrated Bicarbonate Ion: Structural and Dynamical Properties

VIWAT VCHIRAWONGKWIN,¹ ANDREAS B. PRIBIL,² BERND M. RODE²

¹Department of Chemistry, Faculty of Science, Chulalongkorn University, Phyathai Road,
Prathumwan, Bangkok 10330, Thailand

²Theoretical Chemistry Division, Institute of General, Inorganic and Theoretical Chemistry,
University of Innsbruck, Innrain 52a, A-6020 Innsbruck, Austria

Received 14 August 2008; Revised 1 March 2009; Accepted 23 March 2009 DOI 10.1002/jcc.21308 Published online 11 May 2009 in Wiley InterScience (www.interscience.wiley.com).

Abstract: The *ab initio* quantum mechanical charge field molecular dynamics (QMCF MD) formalism was applied to simulate the bicarbonate ion, HCO_3^- , in aqueous solution. The difference in coordination numbers obtained by summation over atoms (6.6) and for the solvent-accessible surface (5.4) indicates the sharing of some water molecules between the individual atomic hydration shells. It also proved the importance to consider the hydration of the chemically different atoms individually for the evaluation of structural and dynamical properties of the ion. The orientation of water molecules in the hydration shell was visualized by the θ -tilt surface plot. The mean residence time in the surroundings of the HCO_3^- ion classify it generally as a structure-breaking ion, but the analysis of the individual ion-water hydrogen bonds revealed a more complex behavior of the different coordination sites.

© 2009 Wiley Periodicals, Inc. J Comput Chem 31: 249–257, 2010

Key words: QM/MM MD simulation; QMCF simulation; bicarbonate ion

Introduction

The bicarbonate ion, HCO_3^- , is one of the most commonly found anions. Dissolution of carbon dioxide in water in the pH range of 8 to 10 generates the HCO_3^- ion as the major product. The HCO_3^- ion is also produced by human carbonic anhydrase II (HCA II), which catalyzes the hydration of CO_2 . This ion also maintains the pH of blood at the level suitable for tissues and enzyme activities.

The structural parameters of HCO_3^- ion have been investigated by X-ray diffraction of sodium bicarbonate crystals. ^{4,5} Jönsson et al. reported the optimized geometry with an unusually long C–OH distance in the HCO_3^- ion based on a Hartree-Fock level calculation with a double- ζ basis set augmented by diffuse s and p functions. ⁶ Keesee et al. used high-pressure mass spectrometry to determine the hydration enthalpy of HCO_3^- ion as -95 kcal mol^{-1} in the gas phase. ⁷ Leung et al. employed molecular dynamics based on density functional theory (DFT) to simulate a hydrated HCO_3^- system containing 63 water molecules and one ion. ⁸ They obtained an average coordination number of 6.9 water molecules from the summation of coordination numbers of individual atoms.

The structural and dynamical properties of hydrated bicarbonate ion are of great significance for the detailed understanding of all chemical processes of this ion in aqueous solution, in particular its role in biology. However, the bicarbonate ion is a composite structure difficult to access by a conventional QM/MM method, because of the complicated and asymmetric potential energy hypersurface describing the interaction between the HCO₃ ion and water. The ab initio quantum mechanical charge field molecular dynamics (QMCF MD) formalism, however, does not require a constructed analytical potential and hence this method has already been successfully employed to investigate the structural and dynamical properties of the hydrated composite anions sulfate, 10,11 phosphate, 12,13 and perchlorate.¹² In this work, the QMCF MD method was used to simulate the hydrated HCO₃ ion in order to obtain its structure and some dynamical properties. The structural properties were obtained via radial distribution functions (RDFs), coordination number distributions (CNDs), and angular distribution functions (ADFs). The dynamics were characterized by means of ligand mean residence times (MRTs). We also introduce the "solvent-accessible surface" to evaluate the additional structural and dynamical features of the hydration shell. The θ and tilt angles are characteristic properties

Correspondence to: V. Vchirawongkwin; e-mail: viwat.v@chula.ac.th Contract/grant sponsors: Austrian Science Foundation (FWF), The Thailand Research Fund, Thailand Commission on Higher Education of hydrating water and were thus depicted by means of surface and contour plots to interpret the orientation of water molecules within the hydration shell.

Methods

The *ab initio* quantum mechanical charge field molecular dynamics (QMCF MD) formalism has been outlined in detail previously. Because of the inclusion of an additional quantum mechanically treated solvent *layer zone* located beyond the first hydration shell of the solute species, the QMCF method does not require the construction of potential functions between the solute and water molecules, i.e., it avoids a time-consuming and sometimes hardly manageable task necessary in the conventional quantum mechanical/molecular mechanical molecular dynamics (QM/MM MD) formalism. ^{14–17} A further advantage of the QMCF MD method is the inclusion of the point charges of the atoms in the MM region in their changing positions in the core Hamiltonian for the QM region via a perturbation term,

$$V' = \sum_{i=1}^{n} \sum_{j=1}^{m} \frac{q_j^{\text{MM}}}{r_{ij}} \tag{1}$$

where n is the number of atoms in the QM region, m the number of atoms in the MM region, q_j^{MM} the partial charges of these atoms according to the selected water model, and r_{ij} refers to the distance between a pair of particles in the QM (i) and MM (j) regions. On the other hand, the dynamically changing charges of QM particles, q_i^{QM} , contribute to the force on each atom j in the MM region as Coulombic forces,

$$F_j^{\text{QM}\to\text{MM}} = \sum_{i=1}^n \frac{q_i^{\text{QM}} \cdot q_j^{\text{MM}}}{r_{ij}}.$$
 (2)

As the conventional QM/MM MD formalism, the QMCF MD method allows the migration of water molecules between the QM and MM region. For this process, one has to apply a smoothing function, ¹⁸

$$S(r) = \begin{cases} 0 & \text{for } r > r_{\text{on}}, \\ \frac{\left(r_{\text{off}}^2 - r^2\right)^2 \left(r_{\text{off}}^2 + 2r^2 - 3r_{\text{on}}^2\right)}{\left(r_{\text{off}}^2 - r_{\text{on}}^2\right)^3} & \text{for } r_{\text{on}} \le r \le r_{\text{off}}, \end{cases}$$

$$1 & \text{for } r < r_{\text{off}}$$

where r is the distance of a given solvent molecule from the center of the simulation box, $r_{\rm off}$ is the radius of the QM region, and $r_{\rm on}$ is the inner border of the smoothing region. The formalism is applied to all atoms of molecules located in the smoothing region, ensuring a smooth transition and continuous change of forces for these molecules according to

$$F_j^{\text{smooth}} = F_j^{\text{MM}} + \left(F_j^{\text{layer}} - F_j^{\text{MM}}\right) \times S(r) \tag{4}$$

where F_j^{layer} is the force acting on a particle j located in the (outer QM) smoothing zone and F_j^{MM} is the force acting on a particle j in the MM region. In this context, it has to be mentioned that energy is not rigorously conserved, but the related mistake can be considered very minor due to the short simulation time and the large size of the quantum mechanical region.

The bicarbonate solution consisted of one bicarbonate ion and 496 water molecules in a cubic box of 24.65 Å with periodic boundary condition. The separate zones of this system according to the QMCF scheme are shown in Figure 1. The density of the simulation box was 0.997 g cm⁻³, i.e., the experimental value of pure water at 298 K. The simulation was performed in the NVT ensemble using a general predictor-corrector algorithm with a time step of 0.2 fs. The system temperature was maintained at 298.16 K by the Berendsen temperature-scaling algorithm¹⁹ with a relaxation time of 100 fs. The QM subregions, namely the core and layer zone, extended to 3.2 and 5.4 Å, respectively. The quantum mechanical calculation was performed by means of the Hartree-Fock (HF) method with the Dunning double- ζ plus polarization and diffuse functions^{20,21} basis sets for hydrogen, carbon, and oxygen atoms of the HCO₃ ion, and Dunning double- ζ plus polarization function^{20,21} basis sets for hydrogen and oxygen atoms of water, respectively. The thickness of the smoothing region was chosen as 0.2 Å with the values of $r_{\rm on}$ and $r_{\rm off}$ as 5.2 and 5.4 Å, respectively, according to the radial distribution function (RDF) obtained from the equilibrated simulation. The selected water model applied to calculate the interactions between pairs of water in the MM region was the flexible BJH-CF2 model, ^{22,23} with the cutoff distances of 3.0 and 5.0 Å for non-Coulombic interactions between H atoms and between O and H atoms, respectively. The partial charges for oxygen and hydrogen atoms in the water molecule according to the BJH-CF2 model are -0.65996 and +0.32983. This water model supports the fully flexible molecular geometries of water molecule within the QM region. Whenever a water molecule migrates to the MM region it can retain its geometry as initial configuration in the MM region. The Coulombic interactions between the Mulliken charges on the atoms within the QM region and the point charges of water molecules according to the BJH-CF2 model are evaluated providing an electrostatic description by a dynamically charging field of point charges, which changes according to the movements of atoms inside the QM region and water molecules in the MM region in the course of the simulation. This ensures the continuous adaptation of the Coulombic interactions to all polarization and charge-transfer effects within solute and surrounding solvent layers.9 In addition, the reaction field method combined with the shifted-force potential technique were applied to account for long-range electrostatic potentials and forces, with a spherical cutoff limit of 12.350 Å. The system was equilibrated with the QMCF MD method for 50,000 steps (10 ps), and a further 50,000 steps (10 ps) were collected as data sampling for analyzing the structural and dynamical properties.

One problem to elucidate the structural and dynamical properties of the hydration shell of composite ions is the identification of water molecules coordinating to individual atoms of the solute species on the hand, and the general properties of the whole ion in solution. For the latter, one can define a "solvent-accessible surface," calculating all distances between the oxygen atoms of all water molecules and each atom within the carbonate ion and searching for each

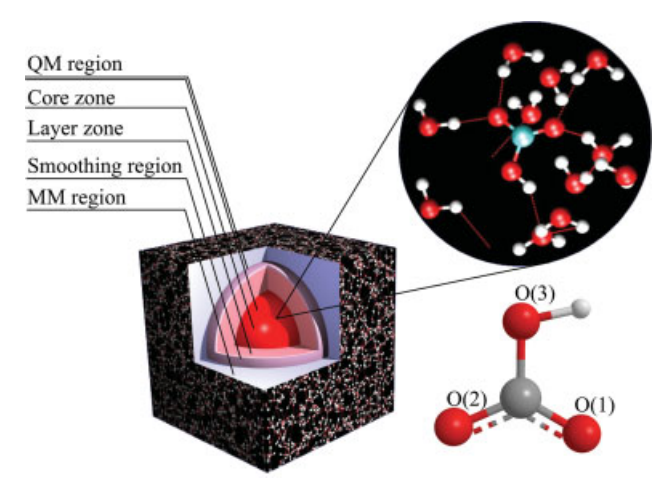


Figure 1. Definition of the quantum mechanical (QM) and molecular mechanical (MM) regions in the QMCF formalism: the QM region is separated into the core zone and the layer zone (the picture is not in scale). The numbering of oxygen atoms is also outlined.

shortest distance to define the coordination. Another method to solve this problem has been proposed based on allowing/removing double counting of solvent molecules. ²⁴ The solvent-accessible surface can be applied to evaluate both structural and dynamical properties by means of specific radial distribution functions (RDFs), coordination number distributions (CNDs), angular distribution functions (ADFs), and ligand mean residence times (MRTs) of the bicarbonate ion. Figure 2 shows the shape of the solvent-accessible surface constructed with a probing water molecule around all sites of bicarbonate ion.

All MRT values were evaluated by the direct method, ²⁵ counting the water exchange processes between hydration shell and bulk. The most appropriate time span to record a water displacement from its original coordination sphere as an exchange process is 0.5 ps, ²⁵ which corresponds to the average lifetime of a hydrogen bond in the solvent. ²⁶

Results

Structural Properties of HCO₃⁻ Ion

Taking into account the stretching motions of bonds within the bicarbonate ion during the simulation period, bond distances were collected and their variations determined. The most probable bond distances of C–O(1) and C–O(2) and their "bandwidth" are 1.243 ± 0.085 Å and 1.248 ± 0.090 Å, respectively. The O(3) linked to the hydrogen atom has a longer mean distance to carbon, C–O(3), of 1.370 ± 0.145 Å, and the O(3)–H distance is 0.960 ± 0.085 Å. These data show a high flexibility of the HCO $_3^-$ ion in water, which certainly has consequences for all of its properties.

A further important information in this context are the bond angles. The $\angle O(1)CO(2)$, $\angle O(1)CO(3)$, and $\angle CO(3)H$ angles were collected in the form of angular distribution functions (ADFs). The most probable angles for $\angle O(1)CO(2)$ and $\angle O(1)CO(3)$ are $129^{\circ}\pm12^{\circ}$ and $115^{\circ}\pm10^{\circ}$, respectively. The $\angle CO(3)H$ ADF shows an even stronger flexibility of this angle along the simulation. The most

probable angles were analyzed decomposing the ADF to a linear combination of three Gaussian functions (average absolute residual of fitting was 0.00663). The maxima of these functions are located at 100.5° , 106.3° , and 113.3° , with a probability of 1.58%, 5.81%, and 3.57%, respectively.

The dihedral angle measured between the plane defined by the oxygen atoms of HCO_3^- ion and the hydrogen atom is one of its characteristic structural properties. The distribution of this angle within the simulation period is presented in Figure 3, showing two peaks located at -7° and 7° with the probability of 9.49% and 8.31%, respectively. The left peak appears in the range between -22° and -1° , while the right peak extends from 1° to 22° . The symmetric shape of these peaks show an average dihedral angle of 7° . This angle distribution represents the flexibility of the HCO_3^- ion in water, H being located either above or below the oxygens' plane.

Structural Properties of the First Hydration Shell

In the simulation period, the average number of solvent molecules within the total QM region is 16.40, which are almost all located in the layer zone. Figures $4a_1$ – $4c_1$ and Figures $4a_2$ – $4c_2$ present the radial distribution functions (RDFs) of individual oxygen atoms within the bicarbonate ion with oxygen and hydrogen atoms of water molecules. The O(1) RDFs in Figures 4a₁ and 4a₂ show the average distances of O(1)-O_{water} and O(1)-H_{water} as 2.855 and 1.895 Å, respectively. The well-defined hydration shell of O(2) represented by Figures 4b₁ and 4b₂ has the main peaks for O(2)-Owater and O(2)-H_{water} at 2.865 and 1.895 Å. The average distance of O(3)-Owater is considerably higher than either O₁- and O₂-Owater with 3.385 Å [Fig. 4c₁], and the O(3)–H_{water} RDF smoothly increases, starting from \sim 1.7 Å [Fig. 4c₂] without forming a distinct first-shell peak. The integration numbers are 1.80 (O(1)-O_{water} RDF), 2.45 (O(2)-Owater RDF), and 1.98 (O(3)-Owater RDF), referring to the average number of water molecules within the first hydration shells of individual atoms. However, because of the less-defined minimum of the O₃-O_{water} RDF and the lack of a first-shell minimum in the O₃-H_{water} RDF the water in the neighborhood of O₃ cannot be considered as regular hydrating ligands. Figures 4d₁ and 4d₂ show the H-water RDFs. The first peak of the H-Owater RDF extends from 1.559 to 2.585 Å with the integration number of 0.33. This indicates

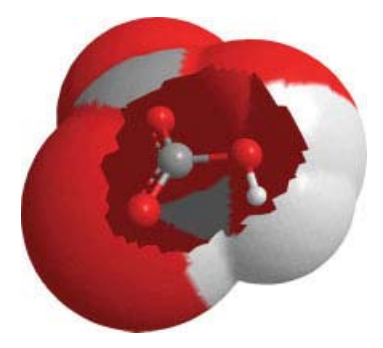


Figure 2. The solvent-accessible surface of HCO₃⁻ ion showing the allocated spheres around the individual atoms with the intersection volume causing multicounts of water molecules in the analysis of hydration shell properties.

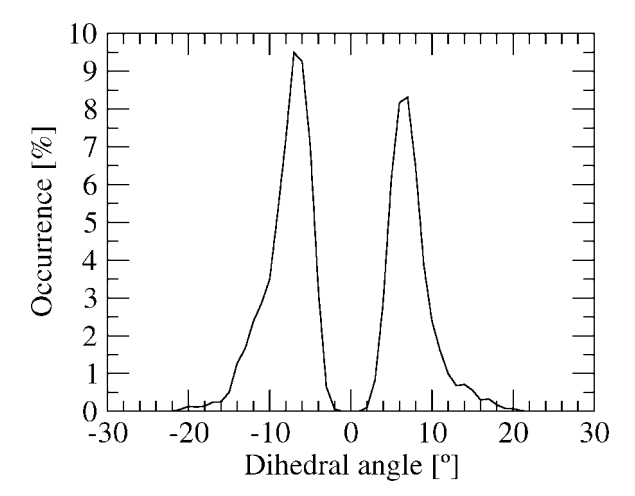


Figure 3. The dihedral angle within the bicarbonate ion.

a very weak interaction between the hydrogen of the O-H group with the solvent.

The calculated solvent-accessible surface leads to the RDFs between HCO_3^- and water molecules shown in Figure 5. The HCO_3^- -O_{water} RDF has its maximum at 2.855 Å with some side-peaks hidden under the main peak. The distance of 3.485 Å was chosen as the criterion to determine the integration number of HCO_3^- -O_{water} RDF, because the value of function at this distance is the lowest one. The integration number according to this condition results as 6.13. For the HCO_3^- -H_{water} RDF, the dominant peak is located at 1.905 Å and the minimum limiting the first hydration shell is found at 2.775 Å. Integration up to this point gives a value of 6.13 as well.

The first minimum of O(1)-O_{water} (3.265 Å), O(2)-O_{water} (3.515 Å), O(3)–O_{water} (3.595 Å), and H–O_{water} (2.585 Å) RDFs were utilized as the boundary of atom-specific hydration shells to evaluate the coordination number distributions (CNDs) for each site, shown in Figure 6. The coordination number of O(1) varies from 0 to 3 with the occurrence of 3.2, 31.9, 46.4, and 18.5%, respectively. The O(2) CND in Figure 6b shows the most probable coordination number at 3 with the occurrence of 42.3% and other possibilities of 0 (0.4%), 1 (12.3%), 2 (37.5%), 4 (6.9%), and 5 (0.6%). For the O(3) CND, the coordination number is distributed in the range of 0 to 5 similar to the O(2) CND, but the most probable occurrence of 35.6% occurs at the coordination number of 2, the other percentages are 5.9, 27.1, 25.7, 5.3, and 0.4 for the coordination numbers 0, 1, 3, 4, and 5, respectively. The H CND in Figure 6d delivers a probability of 32.8% for the coordination number 1, while 67.2% of the simulation time no water is found linked to H (OH). The average coordination numbers obtained for the O(1), O(2), O(3), and H are 1.80, 2.45, 1.98, and 0.33, respectively, summing upto 6.56, which is slightly higher than the value obtained for the solvent-accessible surface.

Thus, the solvent-accessible surface was also utilized to evaluate the CND for the HCO_3^- ion using the identical criterion as in the evaluation of individual CNDs. Figure 7 shows a dominant coordination number for the whole surface of 6 with the occurrence of 34.4%. Other coordination numbers are 2 (0.1%), 3(4.5%), 4 (15.6%), 5 (31.2%), 7 (11.4%), 8 (2.5%), and 9 (0.3%), presenting the average coordination number of 5.41.

The angle between the O(X)–O_{water} (X = 1 to 3) or H–O_{water} connecting vector and the normal vector produced by O–H vectors of water molecule defines the tilt angle, and the angle between the O(X)–O_{water} vector and the vector sum of O–H vectors within the water molecule defines the θ angle. Their evaluation was again based

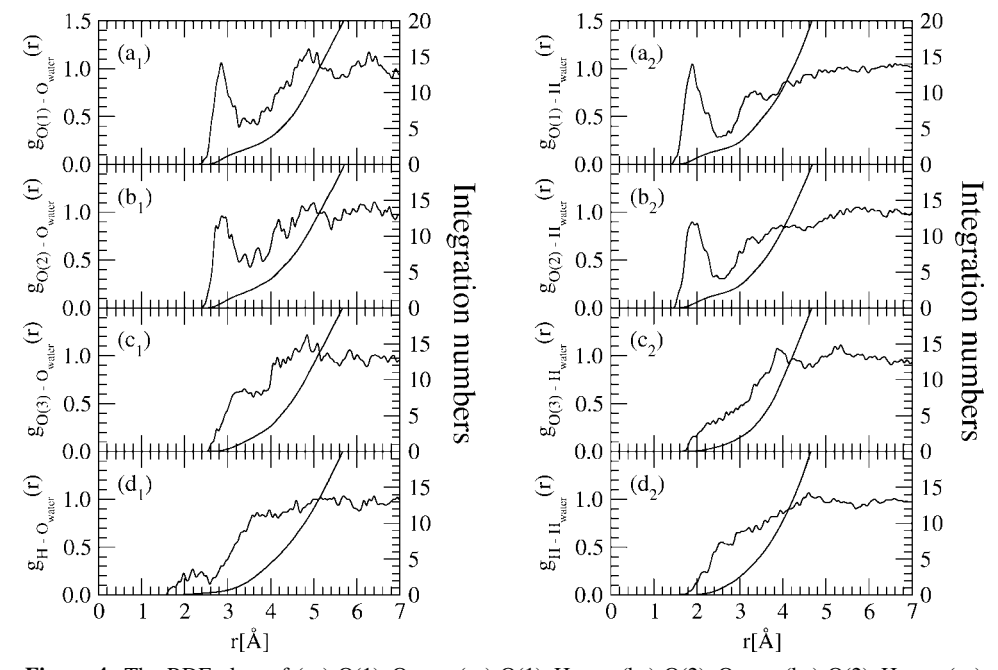


Figure 4. The RDF plots of (a₁) O(1)– O_{water} , (a₂) O(1)– H_{water} , (b₁) O(2)– O_{water} , (b₂) O(2)– H_{water} , (c₁) O(3)– O_{water} , (c₂) O(3)– H_{water} , (d₁) H– O_{water} , and (d₂) H– H_{water} , and their running integration numbers.

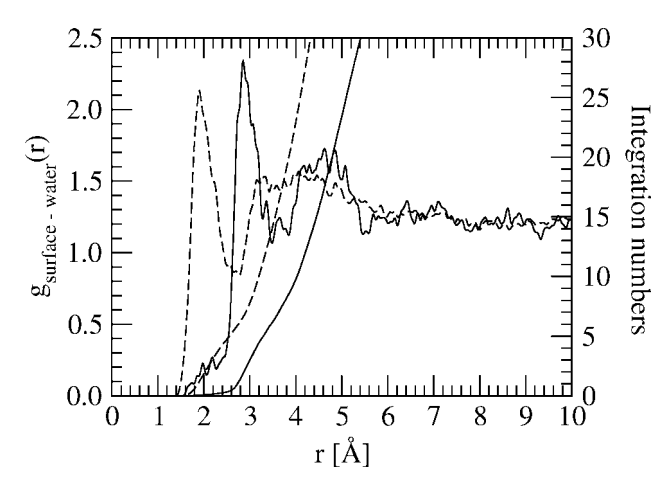


Figure 5. The RDF plots of HCO₃⁻ with their running integration numbers obtained from the QMCF MD simulation evaluated by means of the solvent-accessible surface. Solid and dashed lines refer to the RDFs for the O and H atoms of water, respectively.

on the solvent-accessible surface, i.e., the shortest distance between the center of mass of water molecules and individual oxygen or hydrogen atom within the HCO₃ ion was the criterion of allocated hydration shell. Figure 8 shows the θ -tilt surface, distribution of θ angle, and distribution of tilt angle plots for the hydration shell of HCO₃⁻ ion. The θ -tilt surface plot shows the probable orientation of water molecules in the hydration shell. The large number of peaks in the θ -tilt surface plot are located in the range of from 90.0° to 175.0° (θ) and from -40.0° to 40.0° (tilt). However, we found two significant peaks located at the $(\theta, \text{ tilt})$ coordinates of $(60.0^{\circ}, -59.0^{\circ})$ and $(60.0^{\circ}, -30.0^{\circ})$. The projections of θ -tilt surface plot onto the θ and tilt plane are equivalent to the distribution of separated θ and tilt angle evaluated from the QMCF simulation, respectively. The main peaks of the distribution of θ angle at 124° and the distribution of tilt angle at 8° and -6° represent the orientation of water molecules, pointing with one of hydrogen atom to the surface of HCO₃ ion without the information of the orientation of water molecules within the hydration shell of bicarbonate's hydrogen atom.

Dynamical Properties of the Hydration Shell

Table 1 summarizes the ligand mean residence time (MRT) results evaluated by the direct method 25 for individual oxygen atoms and hydrogen and for the solvent-accessible surface of HCO_3^- ion with $t^*=0.0$ and 0.5 ps to account an exchange event. The total number of water molecules counted for individual exchange processes of the oxygens and hydrogen of HCO_3^- ion were 83 and 29, being larger than those obtained for the solvent-accessible surface (34 and 18). The total number of attempted exchange processes of individual atoms evaluated at $t^*=0.0$ ps (477 events) is identical to the value of the surface (480 events), while the total value of individual atoms obtained at $t^*=0.5$ ps is 62 and thus higher than the 31 events counted for the surface of the ion. The total number of processes needed for one successful water exchange, $R_{\rm ex}$, for individual atoms within the HCO_3^- ion is 34.4, compared to 15.3 evaluated for the solvent-accessible surface. With the standard relaxation time used

in the direct method with $t^* = 0.5 \,\mathrm{ps},^{25}$ the mean residence time (MRT) of a water ligand at a coordination site results as 1.04, 1.05, 1.36, 0.82, and 1.62 ps for O(1), O(2), O(3), H atom, and the whole HCO_3^- ion, respectively. Hydrogen bond life-times can be evaluated with $t^* = 0.0 \,\mathrm{ps}$ and result as 0.15, 0.18, 0.12, 0.07, and 0.10, respectively. The corresponding value obtained for pure water by a simulation based on the QM/MM MD formalism is 0.33 ps; these values account for each hydrogen bond making/breaking process. Poth mean residence times and hydrogen bond life-times for the individual atoms and the whole ion prove the HCO_3^- ion to weaken the solvent's structure in its vicinity. This effect is not evenly distributed, however, to all sites of the anion, and most pronounced near the H atom.

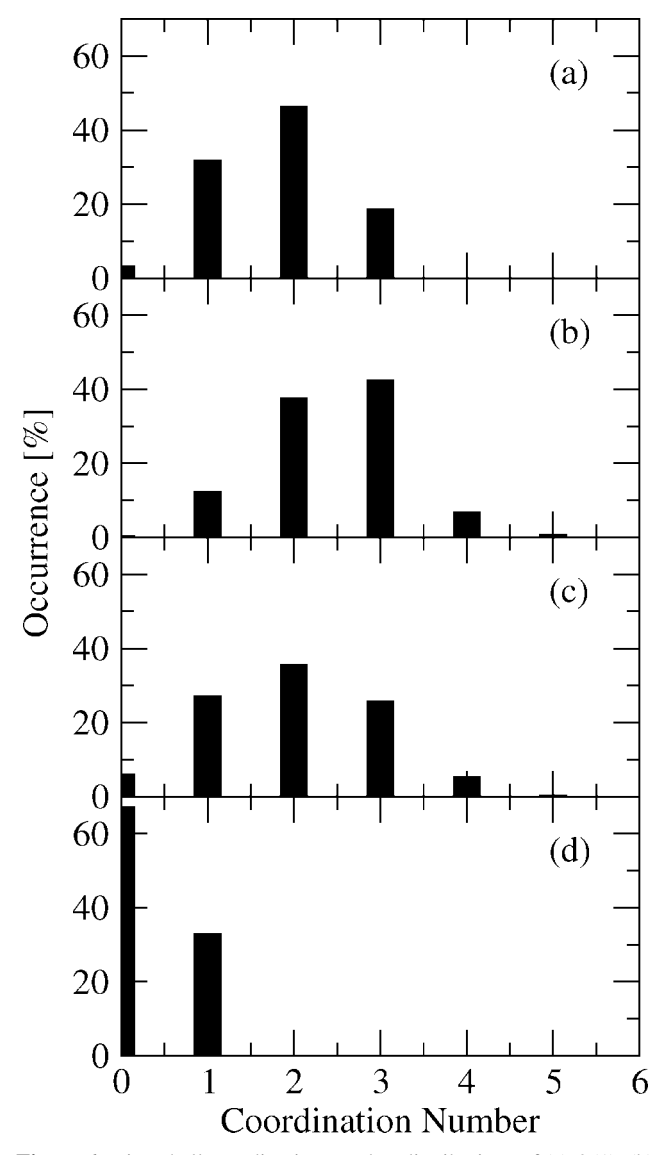


Figure 6. First shell coordination number distributions of (a) O(1), (b) O(2), (c) O(3), and (d) H atoms of bicarbonate ion obtained from the QMCF MD simulation.

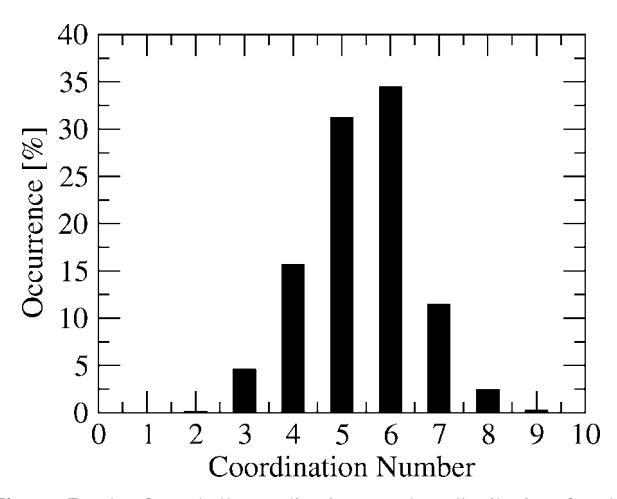


Figure 7. The first shell coordination number distribution for the solvent-accessible surface of bicarbonate ion.

Discussion and Conclusion

Assessment of the Usage of Methodological Level

The Hartree-Fock (HF) level with the selected basis sets used within the QM region of the QMCF formalism was assessed by comparing the predicted structure of the HCO₃ ion in terms of bond distances and bond angles to the available experimental data. Table 2 summarizes the structural properties of HCO₃ ion obtained from our QMCF simulation in comparison to the structures of NaHCO₃ obtained from X-ray crystallography, 4,5 a previous gasphase theoretical study⁶ and our optimized structures obtained at Hartree-Fock (HF), second-order Møller-Plesset (MP/2), coupledcluster singles and doubles (CCSD), and density functional levels (B3LYP and B3PW91), associated with Dunning double-ζ plus polarization function (DZP+) 20,21 and aug-cc-pVXZ (X = D, T, Q, and 5)^{28,29} basis sets. All bond distances between carbon and oxygens of HCO₃ ion of our QMCF simulation are very similar to those obtained from X-ray crystallography, while our distance of O(3)-H is significantly shorter. However, X-ray diffraction cannot determine the location of hydrogen atom well and we, therefore, consider our value for the liquid reliable. The similar distance reported by Jönsson et al. for the gas-phase, calculated with (9s5p)/[4s2p] basis set⁶ seems to support our viewpoint. Our gas-phase structures of bicarbonate ion optimized with and without inclusion of electron correlation predict an O(3)-H distance in the range of 0.94 to 0.97 Å, indicating the influence of correlation to be rather minor, and also indicating the reliability of our QMCF result for the ion in water. For the angles within the HCO_3^- ion, the peak of our angular distributions coincides with the optimized gas-phase structure reported by Jönsson et al., but the angles from our optimized structures in the gas phase show significant deviations from the values obtained in solution. Considering the high flexibility and thus variability of these angles, the solution values are also in fair agreement with the crystal structure. The structural parameters obtained from the QMCF simulation represent the ion in aqueous solution and are expected, therefore, to differ to some extent from both gas and solid state, due to the influence of hydration on the structure of ion. The

fair agreement of the HCO_3^- structure obtained by our calculation level with the crystal structure of NaHCO₃⁵ can be seen as a good indication toward the reliability of the HF method with the Dunning double- ζ plus polarization and diffuse functions (DZP+)^{20,21} basis sets for the investigation of structural properties of hydrated anions.

Structural Properties of the Hydration Shell

Table 3 presents the average binding energy with the percentage of basis set superposition error (BSSE) according to Boys-Bernardi procedure^{30,31} for the [HCO₃(H₂O)_n]⁻ (n = 1 to 4) clusters obtained from HF, B3LYP, MP2, and CCSD levels with DZP+ basis set. The corresponding structures are shown in Figure 9. The binding energy obtained from the HF calculations are close to the values of correlated methods (MP2 and CCSD), comparing to the overestimated energy calculated by the density functional method (B3LYP) showing again a significant weakness of the density functional theory approach for solvated ions.^{32–34} QM/MM simulations for hydrated metal ions by both HF and DFT methods have shown the advantage of *ab initio* HF as far as structure and coordination numbers are concerned.^{33,35} The percentages of BSSE also indicate the suitability of HF level associated with DZP+ basis set to investigate the aqueous bicarbonate system.

The dihedral angles determined between the hydrogen atom and three oxygen atoms within the HCO_3^- ion obtained from the optimized structures of $[HCO_3(H_2O)_n]^-$ (n=1 to 4) in Figure 9 are presented in Table 4. These dihedral angle values indicate that the number of water molecules has an influence in distorting the planarity of bicarbonate structure. The dihedral angle distribution in Figure 3 shows the absolute variation of this angle and also represents the dynamical movement of the hydrogen atom between both sides of oxygen plane agrees according to solvent effects. Our results differ from the hydrated planar HCO_3^- structure resulting from a DFT simulation using the RPBE functional.⁸ One reason for the deviation could be the small number of water molecules in

Table 1. Mean Ligand Residence Time τ in ps, Number of Accounted Ligand Exchange Events N, and Sustainability of Migration Processes to/from the First Hydration Shell $S_{\rm ex}$ Obtained from the QMCF Simulation.

	$t^* = 0.0 \mathrm{ps}$			$t^* = 0.5 \mathrm{ps}$			
	$\overline{N_{\mathrm{inv}}}^{\mathrm{a}}$	$N_{\rm ex}^{0.0}/10{\rm ps^b}$	$ au_D^{0.0 ext{c}}$	$\overline{N_{\mathrm{inv}}^{\mathrm{a}}}$	$N_{\rm ex}^{0.5}/10{\rm ps^b}$	$ au_D^{0.5\mathrm{c}}$	$R_{\rm ex}^{ m d}$
O(1)	22	124	0.15	8	19	1.04	6.5
O(2)	26	143	0.18	11	24	1.05	6.0
O(3)	26	166	0.12	8	15	1.36	11.1
Н	9	44	0.07	2	4	0.82	10.8
Surface	34	480	0.10	18	31	1.62	15.3
H_2O^e		269^{25}	$0.2,^{25}$ $0.33,^{27}$	24^{25}	2.,,	11.2^{25}	
			0.55^{26}		1.51^{27}		

^aNumber of ligand involved in the MRT evaluation according to the value of t^*

^bNumber of accounted exchange events per 10 ps lasting at least 0.0 and 0.5 ps, respectively.

^cMean residence time determined by the direct method²⁵ in ps.

^dAverage number of processes needed for one successful ligand exchange.

eValues obtained from a QM/MM-MD simulation of pure water²⁵ in ps.

Table 2. Comparison of Bond Distances and Bond Angles within HCO $_3^-$ Ion Obtained from the QMCF Simulation with the Structural Parameters Obtained from X-ray Crystallography, 4,5 the Optimized Structure of Hartree-Fock Calculations, 6 and the Optimized Structures Obtained at Hartree-Fock (HF), Second-Order Møller-Plesset (MP/2), Coupled-Cluster Singles and Doubles (CCSD), and Density Functional Levels (B3LYP and B3PW91), Associated with Various Basis Sets. 20,21,28,29

Method	$r_{\mathrm{C-O(1)}}$ (Å)	$r_{\mathrm{C-O(2)}}$ (Å)	$r_{\mathrm{C-O(3)}}$ (Å)	$r_{\mathrm{O(3)-H}}$ (Å)	∠O(1)CO(2)(°)	∠O(1)CO(3)(°)	∠CO(3)H(°)
QMCF	1.24 ± 0.08	1.25 ± 0.09	1.37 ± 0.14	0.96 ± 0.08	129 ± 12	115 ± 10	106 ± 15
X-ray ^{4,5}	1.25	1.28	1.35	1.07	126	120	103
HF^6	1.25	1.25	1.43	0.98	129	115	106
				HF			
DZP+	1.22	1.24	1.40	0.94	132	114	104
aug-cc-pVDZ	1.22	1.24	1.40	0.94	131	114	104
aug-cc-pVTZ	1.22	1.23	1.39	0.94	131	114	105
aug-cc-pVQZ	1.21	1.23	1.39	0.94	131	114	105
aug-cc-pV5Z	1.21	1.23	1.39	0.94	131	114	105
				B3LYP			
DZP+	1.24	1.25	1.45	0.97	132	113	102
aug-cc-pVDZ	1.24	1.26	1.45	0.97	132	114	102
aug-cc-pVTZ	1.23	1.25	1.45	0.96	132	113	102
aug-cc-pVQZ	1.23	1.25	1.45	0.96	132	114	102
aug-cc-pV5Z	1.23	1.25	1.45	0.96	132	114	102
				B3PW91			
DZP+	1.24	1.26	1.44	0.97	132	113	101
aug-cc-pVDZ	1.24	1.26	1.44	0.97	132	114	102
aug-cc-pVTZ	1.23	1.25	1.44	0.96	132	113	102
aug-cc-pVQZ	1.23	1.25	1.44	0.96	132	114	102
aug-cc-pV5Z	1.23	1.25	1.44	0.96	132	114	102
				MP/2			
DZP+	1.25	1.27	1.45	0.97	133	113	101
aug-cc-pVDZ	1.25	1.26	1.46	0.97	133	114	101
aug-cc-pVTZ	1.24	1.26	1.44	0.96	132	113	101
aug-cc-pVQZ	1.24	1.25	1.44	0.96	132	113	101
				CCSD			
DZP+	1.24	1.26	1.44	0.97	132	113	102
aug-cc-pVDZ	1.24	1.26	1.44	0.96	132	114	102
aug-cc-pVTZ	1.23	1.25	1.43	0.96	132	114	102

Car-Parrinello type simulations, which does not provide a proper embedding in a larger amount of solvent.

Because of the low symmetry of HCO₃⁻, the individual RDFs of each oxygen and hydrogen atom were evaluated to determine the boundary of individual hydration shells and to compare them to the data obtained for the solvent-accessible surface. The summation of the individual coordination numbers gives a value of 6.56, which is close to the coordination number of 6.9 reported by Leung et al.8 However, the integration and the coordination number obtained for the solvent-accessible surface of 6.13 and 5.41, respectively, are lower than the sum of individual coordination numbers (6.56), showing the location of some water molecules within the overlap zone of individual hydration shells. The inequality of coordination number obtained from the solvent-accessible surface RDF and CND arises from the asymmetric geometry of solvent-accessible surface and the different evaluation procedures. The integration number from HCO₃ RDF was obtained by counting the water molecules referring to all oxygens and thus to somewhat larger distance from hydrogen. The volume with the solvent-accessible radius of 3.485 Å, therefore, includes some extra water molecules beyond the hydration shell of

Table 3. Average Binding Energies in kcal/mol with the Percentage of Basis Set Superposition Error (BSSE) According to Boys-Bernardi Procedure^{30,31} in Parentheses for $[HCO_3(H_2O)_n]^-$ Clusters Obtained from HF, B3LYP, MP2, and CCSD Calculations with DZP+ Basis Set.

E _{bond} (kcal/mol)						
CCSD						
-18.7 (17.6)						
-15.3 (24.2)						
-17.0 (18.2)						
-17.4 (18.4)						
-17.0 (21.2)						
-15.6 (22.4)						
-16.4 (21.3)						
$[HCO_3(H_2O)_4]^-$						
-15.2 (21.2)						

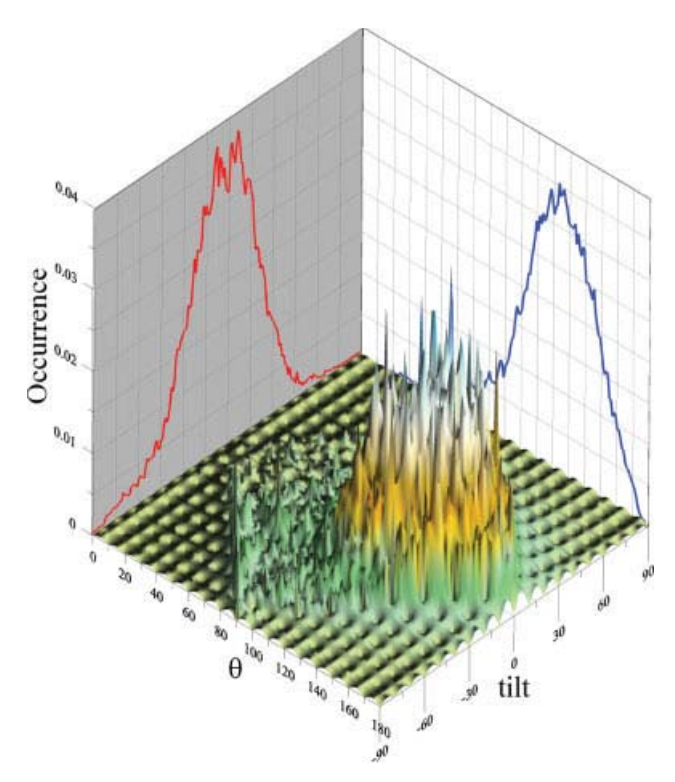


Figure 8. The θ -tilt angle surface plot of water molecules within the hydration shell of HCO_3^- ion based on the solvent-accessible surface. The projections of the surface plot onto the θ and tilt plane refer to the distribution functions of θ and tilt angle, respectively.

hydrogen atom. In the CND case, the radii of individual hydration shells were assigned in the evaluation process, and hence the coordination number obtained from the CND evaluation is slightly smaller.

The θ -tilt surface plot (Fig. 8) shows the major configuration of water molecules within the first hydration shell, utilizing one of the hydrogen atom to coordinate with the oxygen atoms of HCO_3^- ion. This plot also reveals a further orientation of water molecules with the (θ , tilt) coordinates at (60.0° , -59.0°) and (60.0° , -30.0°), representing the oxygen atom of water molecules coordinating to the hydrogen atom of HCO_3^- ion. This information is lost in the investigation of separated θ and tilt angle distribution. The different number of peaks for the orientation of water molecule suggests a weak hydration shell for the hydrogen atom of HCO_3^- ion compared with the oxygen atoms of this ion, corresponding to the coordination numbers of 0.33 for hydrogen and \sim 2 for the oxygen atoms.

Dynamical Properties of the Hydration Shell

The difference of water molecules involved in the exchange processes between the sum over individual atoms (29 molecules) and the HCO_3^- ion as an entity (18 molecules) again indicates the location of water molecules within the intersection of individual hydration shells. The corresponding difference in exchange processes (62 and 31, respectively) shows that half of the exchange

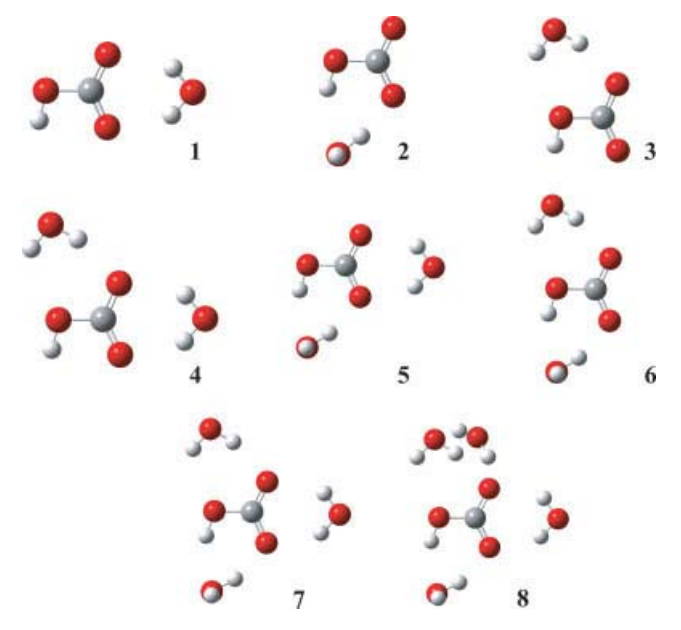


Figure 9. The structure of $[HCO_3(H_2O)_n]^-$ (n=1 to 4) clusters correspond to the structures employing as the starting configuration for the optimization with the selected theoretical levels to determine the binding energy and structural parameter.

events are migrations of water molecules between coordination sites of the HCO₃⁻ ion. All MRT values of oxygen atoms are larger than the values for the hydrogen atom, indicating the easiest exchange of water at this site of the ion. On the other hand, the smaller number of water molecules involved in the exchange processes is an evidence for a local fluctuation of hydrogen bonds to the oxygens without producing ligand exchanges in every case. This can be well recognized from a visualization provided as a short video clip (http://www.molvision.com/video clips). Although the Berendsen temperature-scaling algorithm¹⁹ requires in principle a long simulation period to sufficiently describe the phase space, a large number

Table 4. The Dihedral Angle Measured Between the Hydrogen Atom and the Plane of Three Oxygen Atoms within the HCO_3^- Ion, Corresponding to the $[HCO_3(H_2O)_n]^-$ Clusters Presented Earlier.

		Dihedral angle (°)				
Structure	HF	B3LYP	MP2	CCSD		
		[HCO ₃ (H ₂ O) ₁] ⁻				
1	0.000	0.000	0.000	0.000		
2	-0.628	-0.735	-0.757	-0.772		
3	0.000	-0.145	-0.510	-0.025		
		$[HCO_3(H_2O)_2]^-$				
4	0.004	-0.003	-0.009	-0.023		
5	-0.518	-0.459	-0.102	-0.255		
6	-0.606	-0.651	-0.908	-0.731		
		$[HCO_3(H_2O)_3]^-$				
7	-0.314	-0.400	0.875	0.230		
		$[HCO_3(H_2O)_4]^-$				
8	0.224	0.289	1.109	1.036		

of successful simulations published indicate that our simulation time of 10 ps is adequate to investigate the properties of hydrated ions, and thus also of the bicarbonate ion. Comparing results for exchange dynamics and H-bond life times for simulations of pure water²⁷ and experimental results,²⁶ the HF method seems to be the best compromise between accuracy and affordable computational effort to estimate dynamical effects as well. Although HF and the methodical problems associated with the thermostatization probably lead to slightly underestimated values, the associated errors are probably within a 10–20% range.

Summarizing all results, HCO₃ is clearly characterized as a structure-breaking ion in water. Compared with other hydrated anions studied by the same simulation technique, the simultaneous presence of different hydration sites in the low symmetry of HCO₃ ion and the higher vicinity of coordination sites distinguishes it clearly from anions with tetrahedral symmetry such as sulfate, phosphate, and perchlorate, in particular if one compares the range of mean residence times of water ligands at these hydration sites (0.82 to 1.36) with those for the aforementioned anions $(PO_4^{3-} 3.9,$ SO_4^{2-} , 2.1, and ClO_4^{-} 1.5 ps). 12 The flexibility of the HCO_3^{-} hydration structure is not only reflected in the weak and thus rapidly changing solvent binding, but it also shows a clear dependence on the location of the solvent molecules in the surrounding of the anion. To describe these effects by classical or conventional QM/MM molecular dynamics would be a most difficult task. Conventional QM/MM MD simulations would have required the construction of analytical interaction potential functions taking into account all the asymmetry of the interaction between solute and solvent, which in the case of bicarbonate would be extremely difficult and subject to many possible error sources and inaccuracies.

References

- 1. Kern, D. M. J Chem Educ 1960, 37, 14.
- 2. Silverman, D. N.; Vincent, S. H. CRC Crit Rev Biochem 1983, 14, 207.
- 3. Silverman, D. N.; Lindskog, S. Acc Chem Res 1988, 21, 30.
- 4. Sass, R. L.; Scheuerman, R. F. Acta Crystallogr 1962, 15, 77.
- 5. Sharma, B. D. Acta Crystallogr 1965, 18, 818.
- Jönsson, B.; Karlström, G.; Wennerström, H. J Am Chem Soc 1978, 100, 1658.
- Keesee, R. G.; Lee, N.; Castleman, A. W., Jr. J Am Chem Soc 1979, 101, 2599.

- 8. Leung, K.; Nielsen, I. M. B.; Kurtz, I. J Phys Chem B 2007, 111, 4453.
- 9. Rode, B. M.; Hofer, T. S.; Randolf, B. R.; Schwenk, C. F.; Xenides, D.; Vchirawongkwin, V. Theor Chem Acc 2006, 115, 77.
- Vchirawongkwin, V.; Rode, B. M.; Persson, I. J Phys Chem B 2007, 111, 4150.
- 11. Vchirawongkwin, V.; Rode, B. M. Chem Phys Lett 2007, 443, 152.
- 12. Pribil, A. B.; Vchirawongkwin, V.; Hofer, T. S.; Randolf, B. R. In Computation in Modern Science and Engineering, Proceedings of the International Conference on Computational Methods in Science and Engineering, Vol. 2, Part B; Simos, T. E.; Maroulis, G., Eds.; American Institute of Physics: New York, 2007; pp. 921.
- Pribil, A. B.; Hofer, T. S.; Randolf, B. R.; Rode, B. M. J Comput Chem 2008, 29, 2330.
- 14. Warshel, A.; Levitt, M. J Mol Bio 1976, 103, 227.
- 15. Field, M. J.; Bash, P. A.; Karplus, M. J Comput Chem 1990, 11, 700.
- 16. Gao, J. J Am Chem Soc 1993, 115, 2930.
- 17. Bakowise, D.; Thiel, W. J Phys Chem 1996, 100, 10580.
- Brooks, B. R.; Bruccoleri, R. E.; Olafson, B. D.; States, B. D.; Swaminathan, S.; Karplus, M. J Comput Chem 1983, 4, 187.
- Berendsen, H. J. C.; Postma, J. P. M.; van Gunsteren, W. F.; DiNola, A.; Haak, J. R. J Chem Phys 1984, 81, 3684.
- Dunning, T. H., Jr.; Hay, P. J. In Modern Theoretical Chemistry: Methods of Electronic Structure Theory; Schaefer, H. F., III, Ed.; Plenum Press: New York, 1977; Vol. 3; Chapter 1, pp. 1.
- 21. Dunning, T. H., Jr. J Chem Phys 1970, 53, 2823.
- 22. Stillinger, F. H.; Rahman, A. J Chem Phys 1978, 68, 666.
- 23. Bopp, P.; Janscó, G.; Heinzinger, K. Chem Phys Lett 1983, 98, 129.
- 24. Leung, K. Biophys Chem 2006, 124, 222.
- Hofer, T. S.; Tran, H. T.; Schwenk, C. F.; Rode, B. M. J Comput Chem 2004, 25, 211.
- Lock, A. J.; Woutersen, S.; Bakker, H. J. J Phys Chem A 2001, 105, 1238.
- Xenides, D.; Randolf, B. R.; Rode, B. M. J Chem Phys 2005, 122, 174506
- 28. Dunning, T. H., Jr. J Chem Phys 1989, 90, 1007.
- Kendall, R. A.; Dunning, T. H., Jr.; Harrison, R. J. J Chem Phys 1992, 96, 6796.
- 30. Boys, S. F.; Bernardi, F. Mol Phys 1970, 19, 553.
- 31. Simon, S.; Duran, M.; Dannenberg, J. J. J Chem Phys 1996, 105, 11024.
- 32. Schwenk, C. F.; Loeffler, H. H.; Rode, B. M. J Chem Phys 2001, 115, 10808
- 33. Schwenk, C. F.; Rode, B. M. J Chem Phys 2003, 119, 9523.
- Schwenk, C. F.; Hofer, T. S.; Rode, B. M. J Phys Chem A 2004, 108, 1500
- Schwenk, C. F.; Hofer, T. S.; Rode, B. M. J Am Chem Soc 2004, 126, 12786.

An *Ab Initio* Quantum Mechanical Charge Field Molecular Dynamics Simulation of a Dilute Aqueous HCl Solution

CHINAPONG KRITAYAKORNUPONG, VIWAT VCHIRAWONGKWIN, BERND M. RODE³

¹Faculty of Science, Department of Chemistry, King Mongkut's University of Technology,
Thonburi, Bangkok 10140, Thailand

²Faculty of Science, Department of Chemistry, Chulalongkorn University,
Bangkok 10330, Thailand

³Theoretical Chemistry Division, Institute of General, Inorganic and Theoretical Chemistry,
University of Innsbruck, Innrain 52a, Innsbruck A-6020, Austria

Received 19 June 2009; Revised 14 September 2009; Accepted 20 October 2009 DOI 10.1002/jcc.21469 Published online 17 December 2009 in Wiley InterScience (www.interscience.wiley.com).

Abstract: An *ab initio* quantum mechanical charge field (QMCF) molecular dynamics simulation has been performed to study the structural and dynamical properties of a dilute aqueous HCl solution. The solute molecule HCl and its surrounding water molecules were treated at Hartree-Fock level in conjunction with Dunning double- ζ plus polarization function basis sets. The simulation predicts an average H—Cl bond distance of 1.28 Å, which is in good agreement with the experimental value. The $H_{HCl}\cdots O_w$ and $Cl_{HCl}\cdots H_w$ distances of 1.84 and 3.51 Å were found for the first hydration shell. At the hydrogen site of HCl, a single water molecule is the most preferred coordination, whereas an average coordination number of 12 water molecules of the full first shell was observed for the chloride site. The hydrogen bonding at the hydrogen site of HCl is weakened by proton transfer reactions and an associated lability of ligand binding. Two proton transfer processes were observed in the QMCF MD simulation, demonstrating acid dissociation of HCl. A weak structure-making/breaking effect of HCl in water is recognized from the mean residence times of 2.1 and 0.8 ps for ligands in the neighborhood of Cl and H sites of HCl, respectively.

© 2009 Wiley Periodicals, Inc. J Comput Chem 31: 1785–1792, 2010

Key words: hydrogen chloride; hydration structure; dynamical properties; hydrogen bond; acid dissociation; proton transfer; simulation; QMCF

Introduction

It is well known that hydrogen bond formation and proton transfer of hydrogen halides in aqueous solution play an important role in a wide range of chemical and biological processes.1 Hydrogen chloride is a strong acid with $pK_a = -7$, indicating a dissociated form of hydrogen chloride in dilute aqueous solution. There are very few experiments related to the hydration structure of HCl in aqueous solution.²⁻⁶ Matrix isolation spectroscopy of HCl(H2O)_n complexes was performed, showing the nondissociated structure of HCl with $n \leq 3$, whereas proton transfer is achieved from the complex with n = 4.2 X-ray and neutron diffraction techniques were applied to evaluate the structure of the aqueous HCl acid solution at 20°C and it was found that four water molecules were required to solvate each hydronium and Cl ions in solution.3 Concentrated HCl solutions were also studied using spectroscopic and diffraction techniques, suggesting a pentagonal ring structures of HCl(H2O)6 and (HCl)2(H2O)6 in solution.⁴ Ragout-jet Fourier transform infrared spectroscopy was used to evaluate the proton vibrational dynamics in $(HCl)_m$ – $(H_2O)_n$ clusters, reporting that HCl complexes with three or more water molecules could not be assigned in the IR spectrum.⁵ Recently, X-ray absorption of aqueous HCl solution was investigated. It was found that the addition of HCl to liquid water leads to a decrease in intensity of the X-ray absorption spectrum.⁶ In addition, neutron diffraction of a highly concentrated HCl solution has been performed to determine the Eigen or Zundel complexes, but its results are not comparable to the species formation in dilute HCl solution.⁷ Numerous theoretical techniques have been applied to describe the characteristics of

Correspondence to: C. Kritayakornupong; e-mail: chinapong.kri@kmutt.

Contract/grant sponsors: Thailand Research Fund (TRF), Thailand Commission on Higher Education, Austrian Science Foundation (FWF)

HCl in aqueous solution. 4-6,8-25 An MP2/6-31+G* calculation in the continuum model of water confirmed the nondissociation of monohydrated and dihydrated HCl complexes.8 HCl on an ice surface at 190 K was studied using molecular dynamics simulations, indicating that ionic solvation processes are thermodynamically feasible. 9,10 A calculation using BLYP level of approximation with an extended basis set showed that the proton transfer takes place without transition state in the case of HCl(H₂O)₄. 11 Using the MP2 method, a nondissociated HCl complex was observed with a cyclic three-water cluster, indicating a red-shift in the HCl stretching frequency, 13 whereas the dissociated form appears to be possible when the HCl molecule was surrounded by four water molecules. 15 The MP2/ 6-311++G(d,p) level of theory was applied to describe the nondissociated form of HCl with four water molecules. 18 Upon extension of the cluster size to five water molecules, proton transferred type was shown to exist. The nondissociated form was determined as the most stable structure for the HCl(H₂O)_n (n = 1 - 3) clusters evaluated by the B3LYP/D95++(d,p) method. 19 The HCl(H2O)4 cluster resulted as an intermediate with both nondissociated and dissociated structures obtained from both the B3LYP and the MP2 method. 19,22 Car-Parrinello molecular dynamics (CPMD) simulations were performed to evaluate the dissociation and vibrational dynamics of DCl in D₂O molecules. ^{12,16,23–25} Concentrated HCl solutions (2.7 and 5.3 M) where complete dissociation has already been assumed by the composition of the system (protons, Cl ions, and water) have also been studied by CPMD simulations,26 in which the gradient-corrected BLYP functional has been used that usually leads to too rigid H-bonds and thus to too slow dynamics. The amount of solvent considered further does not provide sufficient water molecules for a full hydration of ions. Monte Carlo simulations were applied to investigate the mechanism of HCl ionization in water. 17,20 Furthermore, the vibrational spectra of aqueous HCl were evaluated in both experimental and theoretical studies. 4,5,13,19-25 The results obtained thereby showed that the number of water molecules surrounding HCl and the accuracy of approximation methods utilized play a significant role on characteristics and stability of proton transferred and proton nontransferred HCl forms in aqueous solution. Summarizing all of these results, therefore, our intentions were (i) To investigate HCl in very dilute aqueous solution, providing the possibility of full hydration (498 water molecules for one HCl molecule). (ii) To utilize an ab initio HF method in an extended QM region with the new quantum mechanical charge field (QMCF) methodology. HF is known to lead to slightly too weak H-bonds, but proved more suitable than DFT in many systems.^{27,28} (iii) To start with undissociated HCl to see, whether dissociation would occur readily.

To answer these questions, in this study, we have performed an *ab initio* QMCF molecular dynamics simulation of HCl in aqueous solution. The structure of aqueous HCl solution was evaluated in terms of radial distribution functions, coordination numbers, angular distributions, θ -angle, and tilt angle distributions. To describe the dynamical properties, the mean ligand residence times for ligand exchange processes between hydration shell of HCl and bulk and the vibrational frequency of H—Cl were also determined.

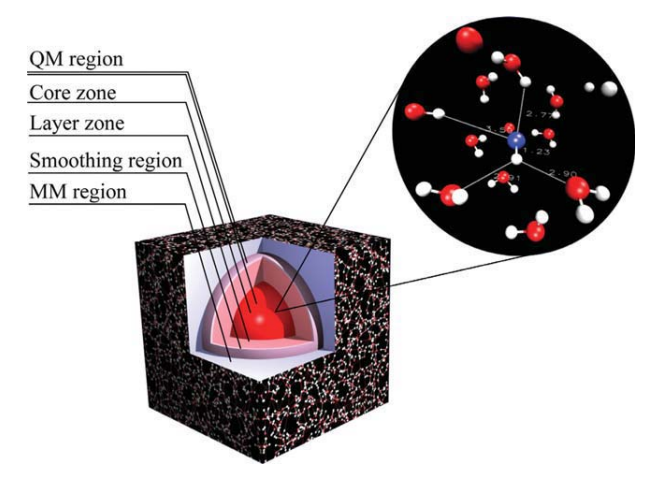


Figure 1. Definition of the quantum mechanical (QM) and molecular mechanical (MM) regions in the QMCF approach.

QMCF MD Simulation

The *ab initio* QMCF molecular dynamics technique²⁹ is similar to conventional QM/MM MD methods^{30–32} in which the system is separated into two regions, namely QM and MM regions. In the QMCF method, the QM region is enlarged to include the second hydration shell and consists of two subregions, the so-called "core region" (inner QM subregion) and the "layer region" (outer QM subregion), as shown in Figure 1. By using the QMCF method, no solute–solvent potentials are required, and an improved handling of Coulombic interactions is introduced. The calculated forces between the core region and the MM region are the major difference between the QM/MM MD and the QMCF MD simulation. In the QMCF MD simulation, the forces acting on each particle in the different regions are defined as

$$F_j^{\text{core}} = F_j^{\text{QM}} + \sum_{i=1}^{M} \frac{q_j^{\text{QM}} q_i^{\text{MM}}}{r_{ii}^2}$$
 (1)

$$F_{j}^{\text{layer}} = F_{j}^{\text{QM}} + \sum_{i=1}^{M} \frac{q_{j}^{\text{QM}} q_{i}^{\text{MM}}}{r_{ij}^{2}} + \sum_{i=1}^{M} F_{ij}^{\text{BJHnC}}$$
 (2)

$$F_{j}^{\text{MM}} = \sum_{\substack{i=1\\i\neq j}}^{M} F_{ij}^{\text{BJH}} + \sum_{i=1}^{N_{1}+N_{2}} \frac{q_{i}^{\text{QM}} \cdot q_{j}^{\text{MM}}}{r_{ij}^{2}} + \sum_{i=1}^{N_{2}} F_{ij}^{\text{BJHnC}}$$
(3)

where $F_j^{\rm core}$ is the quantum mechanical force acting on the particle j in the core region, $F_j^{\rm layer}$ is the forces acting on particle j located in the solvation layer, $F_j^{\rm MM}$ represents the forces acting on the particle j in the MM region, and M is the number of atoms in the MM region. In each simulation step, the forces in the core and layer region ($F_j^{\rm core}$, $F_j^{\rm layer}$) are calculated from the ab initio quantum mechanical treatment plus the Coulombic forces obtained from all MM atoms, whereas the forces in the

MM region $(F_j^{\rm MM})$ are obtained from the BJH-CF2 water model^{33,34} augmented by the Coulombic forces exerted by all atoms in the core region (N_1) and the layer region (N_2) , and the noncoulombic forces generated by the atoms in the layer region (N_2) . Consequently, the QM forces in the layer $(F_j^{\rm layer})$ are supplemented by the noncoulombic forces of particles in the MM region evaluated from the BJH-CF2 water model.^{33,34} The Coulombic interactions are calculated with the point charges of the atoms in the MM region and the quantum chemically evaluated partial charges on the atoms in the QM region. The charges of the particles in the MM region are incorporated via a perturbation term into the core Hamiltonian:

$$H_{\rm CF} = H_{\rm HF} + V_i'$$

$$V_i' = \sum_{i=1}^M \frac{q_j}{r_{ij}} \tag{4}$$

where q_j are the partial charges of each MM atoms obtained by Mulliken population analysis, which proved to be best compatible with the BJH-CF2 water model. The oxygen and hydrogen charges are -0.65996 and +0.32983, according to the charges of the BJH-CF2 water model utilized in the MM region.^{33,34}

In the QMCF MD simulation, solvent molecules can freely migrate between the QM and MM region. A smoothing function 35 is applied between the radii r_0 (5.7 Å) and r_1 (5.5 Å), corresponding to an interval of 0.2 Å, to ensure a continuous transition of forces at the boundary. The forces acting on each particle in the system can be defined as:

$$F_j^{\text{Smooth}} = F_j^{\text{MM}} + (F_j^{\text{layer}} - F_j^{\text{MM}}) \cdot S_{\text{m}}(r)$$
 (5)

where $F_j^{\rm MM}$ represents the force acting on the particle j in the MM region, $F_j^{\rm layer}$ is the force acting on the particle j located in the solvation layer, r is the distance of the water molecule from the chlorine atom of the solute molecule, and $S_{\rm m}$ a smoothing function.

$$S_{m}(r) = 1, for r \le r_{1}$$

$$S_{m}(r) = \frac{\left(r_{0}^{2} - r^{2}\right)^{2}\left(r_{0}^{2} + 2r^{2} - 3r_{1}^{2}\right)}{\left(r_{0}^{2} - r_{1}^{2}\right)^{3}}, for r_{1} < r \le r_{0}$$

$$S_{m}(r) = 0, for r > r_{0},$$

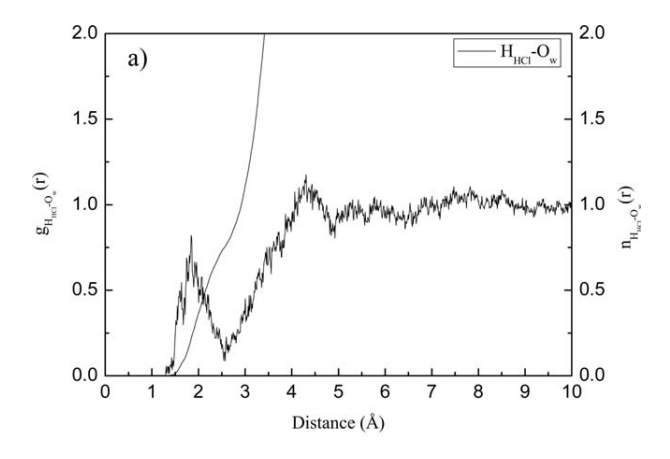
$$(6)$$

where r_1 is the inner border of the smoothing region and r_0 is the radius of the QM region. Further details of this method are given in ref. 31.

This simulation protocol used in the present work is similar to that applied in a previous simulation of aqueous HF solution³⁶ and has been successfully applied to investigate characteristics of several composite chemical species in solution.^{29,36–39} The QMCF MD simulation was performed in a periodic boundary cubic box with a side length of 24.65 Å, containing one hydrogen chloride molecule plus 498 water molecules. Temperature was controlled by the Berendsen temperature-scaling algorithm⁴⁰ with a relaxation time of 100 fs to maintain 298.15 K. The

density of the simulation was fixed at 0.997 g/cm³, corresponding to the experimental value of pure water. A predictor-corrector algorithm was used to integrate the Newtonian equations of motion with the chosen time step of 0.2 fs. The flexible BJH-CF2 water model^{33,34} including an intramolecular potential was used to elucidate the interactions between pairs of water molecules in the MM region, as it allows explicit hydrogen movements, and thus, also a smooth transition of water molecules from the OM to the MM region and vice versa. The reaction field⁴¹ was applied to correct for longrange Coulombic interactions. Cutoff distances of 5 and 3 Å were used for noncoulombic O-H and H-H interactions, respectively. The radial cutoff limit for Coulombic interactions was set to half the box length. The values of 6.0 and 11.0 Å were chosen for the diameters of the core and the layer region, respectively, and hence, the full first hydration shell and a part of the second hydration shell are included in the QM region, according to the radial distribution functions (RDF) in the equilibrated state. The TURBOMOLE 5.9 program 42-44 was used to evaluate the forces in the QM region calculated at the restricted Hartree-Fock level. Dunning double-ζ plus polarization function (DZP) basis sets^{45,46} applied for chlorine, oxygen, and hydrogen atoms. These basis sets were chosen as a suitable compromise between accuracy of the results and computational effort. Many test calculations with the DZP basis sets comparing solvent clusters with one to six water molecules by HF, B3LYP, MP2, and CSSD have shown that the error by neglecting electron correlation is very minor. 47-50 Moreover, the QM/MM simulation using the B3LYP functional have revealed deviating descriptions such as too rigid structures for solvates and H-bonded systems. 51-53 In addition, the influence of the basis set super position error (BSSE) for HCl monohydrate was also determined at several levels of theory. The lowest BSSE energy of 0.2 kcal/mol was obtained from the HF method, whereas the values of 0.5, 0.9, and 0.8 kcal/mol were evaluated from the B3LYP, MP2, and CCSD methods, respectively. These indicate that the effects of electron correlation and BSSE should have only a minor influence on quality of the QMCF simulation results. The QMCF MD simulation was equilibrated for 2 ps and total of 10 ps was performed for sampling. Simulation time had to be limited to 50,000 steps of 0.2 fs (needed to appropriately describe hydrogen movements) as these 10 ps already consume 5 months of CPU time on a 4 AMD Opteron 2.8 GHz processors high performance computer.

Velocity autocorrelation functions (VACFs) were used to determine the dynamical properties of HCl in aqueous solution. With $C_{\infty v}$ symmetry of the HCl molecule, the vibrational motion of the HCl molecule is both infrared active and Raman active. The velocities of the hydrogen atom of HCl and the oxygen atom of H₂O were projected onto a unit vector parallel to the corresponding Cl—H bond (\vec{u}_1) and $H_{\text{HCl}}\cdots O_w$ direction (\vec{u}_2) , respectively, thus the vibrational modes are the projections of the hydrogen and oxygen velocities onto the unit vectors \vec{u}_1 and \vec{u}_2 , respectively. The vibrational frequencies of the normal mode and the intermolecular $H_{\text{HCl}}\cdots O_w$ interactions were calculated by their Fourier transformations of the VACFs. The normalized VACF, C(t), is defined by



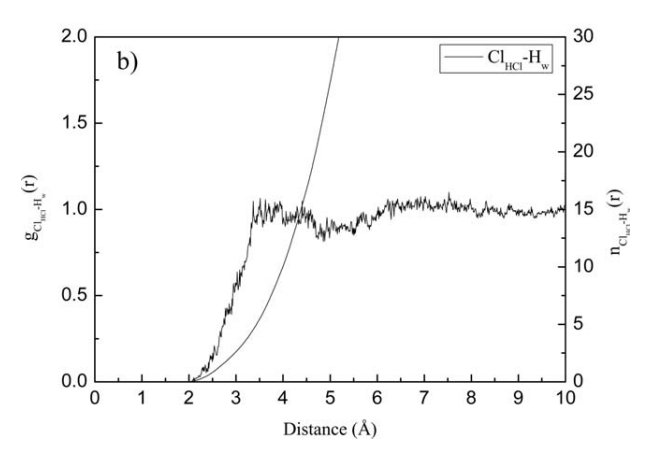


Figure 2. (a) $H_{HCl}\cdots O_w$, and (b) $Cl_{HCl}\cdots H_w$ RDFs and their corresponding integration numbers.

$$C(t) = \frac{\sum_{i}^{N_{t}} \sum_{j}^{N} v_{j}(t_{i}) v_{j}(t_{i} + t)}{N_{t} N \sum_{i}^{N_{t}} \sum_{i}^{N} v_{j}(t_{i}) v_{j}(t_{i})},$$
(7)

where N is the number of particles, N_t is the number of time origins t_i , and v_j denotes a certain velocity component of the particle j.

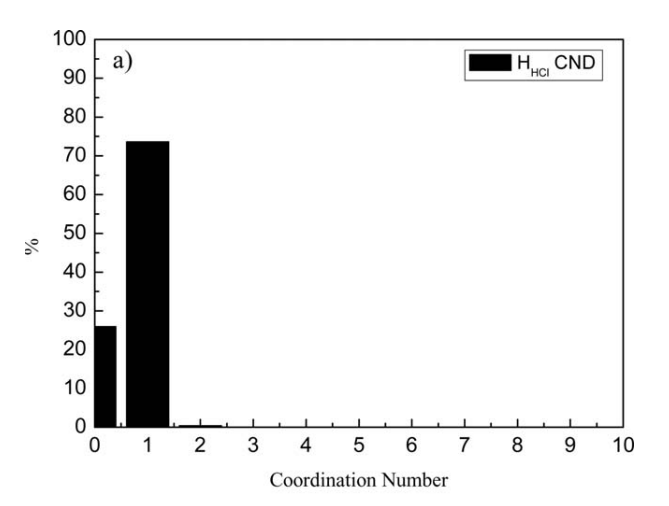
Results and Discussion

Structural Properties

The hydration structure of the HCl in aqueous solution was evaluated in terms of RDF, coordination numbers, and angular distributions. In the QMCF MD simulation, The H—Cl distance varies in the range of 1.2–1.5 Å, with an averaged value of 1.28 Å, which is in good agreement with the experimental value of 1.274 Å. 54,55 Figure 2 shows the radial distribution functions for each atom of HCl and its neighboring water molecules together with their corresponding integration numbers evaluated

from the QMCF MD simulation. The first peak in the H_{HCI}···O_w RDF characterizes the first hydration shell, located between 1.5 and 2.5 Å with a maximum value of 1.84 Å. This value is larger than that determined in the case of an aqueous HF solution (1.62 Å).³⁶ The second peak corresponding to the water ligands near the Cl atom in the first hydration shell is located at 4.30 Å. The Cl_{HCI}···H_w RDF and the corresponding integration are depicted in Figure 2b. The first Cl_{HCI}···H_w peak lies within the range of 2.0–4.0 Å, showing its maximum at 3.51 Å with additional peaks at 3.36, 3.62, and 3.93 Å. The Cl_{HCI}···H_w second peak is situated at 4.40 Å, covering distances of 4.0–4.7 Å, and corresponds to the second H atom of coordinated water molecules.

The coordination number distributions of the first hydration shell determined from the $H_{HCl}\cdots O_w$ and $Cl_{HCl}\cdots O_w$ interactions of the aqueous HCl solution are displayed in Figure 3. According to Figure 3a, a single water molecule bound to the H site of the HCl molecule is the most dominant coordination with 74%



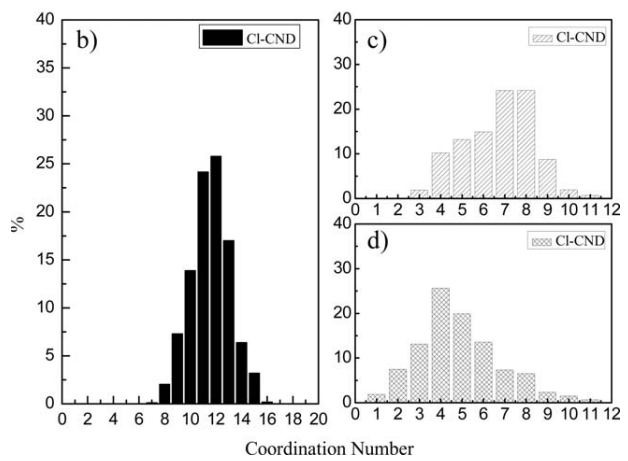


Figure 3. Coordination number distributions of (a) H and (b) Cl atoms in the first hydration shell of HCl, (c) Cl atom in immediate first shell from 0.0 to 4.2 Å, and (d) Cl atom in extended first hydration shell from 4.2 to 4.8 Å.

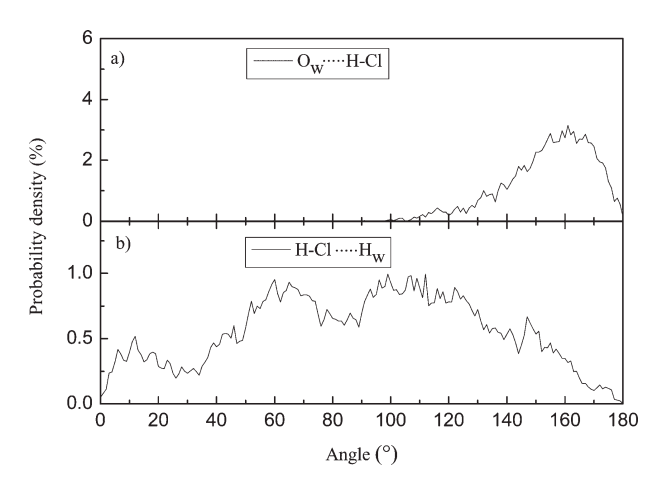


Figure 4. Distributions of (a) $O_w \cdots H_{HCl} - Cl_{HCl}$ angles and (b) $H_{HCl} - Cl_{HCl} \cdots H_w$ angles, obtained from the QMCF MD simulation.

occurrence. The Cl_{HCl}···O_w RDF displays two distinguished parts of the first hydration shell, one representing an extended first hydration shell located between 4.2 and 4.8 Å. Therefore, the coordination number distributions of the water molecules in the substructure near the Cl atom were examined and depicted in Figures 3b-3d. As shown in Figure 3c, the coordination number distribution integrated up to the distance of 4.2 Å of the first part of the Cl_{HCI}···O_w peak covers a wide range of 3-11, giving an average value of 6.7. For the extended first hydration shell, an average coordination number of 4.9 was found with a large variation in the hydration numbers ranging from 1 to 11. These findings indicate almost seven water molecules to be directly bound to the Cl site of the HCl molecule, while in average five water molecules are located in the extended first hydration shell. This shows that the frequent ligand exchange processes must occur at the Cl site, whereas the one water molecule bound to the H atom seems to be more stably coordinated.

The hydrogen bond angle between HCl and water molecule can be determined in terms of the angular distribution functions of the Ow ... HHCI - ClHCI and HHCI - ClHCI ... Hw angles in the first hydration shell. According to Figure 4a the O_w···H_{HCl}—Cl_{HCl} angular distribution has its maximum at 161° with tailing until 100° , proving the preference for linear $O_w \cdots H_{HCl} - Cl_{HCl}$ hydrogen bond arrangements. However, considerably less linearity of this hydrogen bond in the case of HCl was observed in comparison with HF, where the Ow-HHF-FHF angular distribution is situated at 170° with variation down to 100°.36 The presence of nonlinear, weak, and flexible hydrogen bonds between water and the Cl site of HCl is recognized from three dominant H_{HCl}-Cl_{HCl}···H_w peaks at 12°, 60°, and 112°, respectively. The low angle value of 12° reflects the arrangement of two hydrogen bonds in the intermediate HCl monohydrate (ClHCI···Hw and $H_{HCl} \cdots O_w$).

To further characterize the flexibility and orientation of the water molecules surrounding HCl in the first hydration shell, angle θ and tilt angle are introduced. The angle θ is the angle between the vector pointing along C_g — O_w (C_g is the center of mass of the HCl molecule) and the dipole vector of water

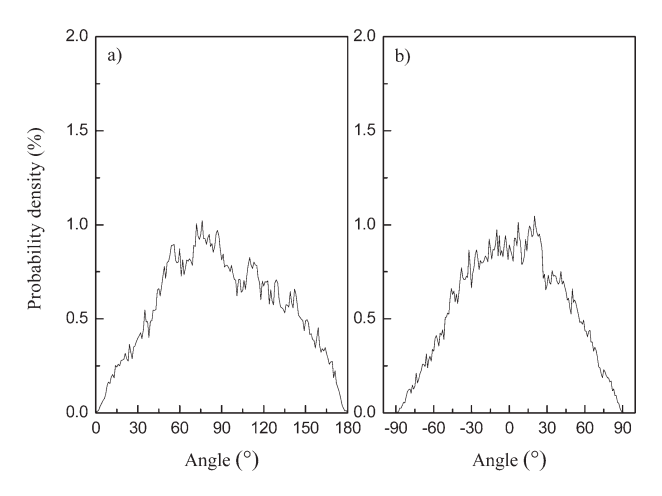


Figure 5. The θ and tilt angular distributions of water ligands near the HCl molecule.

molecule. The tilt angle is the angle between the $H_{HCl}-Cl_{HCl}$ axis and the plane defined by the O_w-H_w vectors. Figure 5 presents the θ and tilt angular distributions in the first hydration shell of HCl. The broad peak of the angle θ distribution obtained from the QMCF MD simulation has its maximum at 76° , covering a wide range of $0{\text -}180^\circ$. A similar result was also observed in the case of HF. 36 However, the maximum value of 136° evaluated for HF is much larger than that determined from HCl. The maximum value of the tilt angle for the first shell is located at 20° , and the distribution reaches 0 at $\pm 90^\circ$. Both angle distributions prove a very high flexibility of the first shell ligands' orientation.

Dynamical Properties

The vibrational frequencies of the normal mode H_{HCl} — Cl_{HCl} and the intermolecular H_{HCl} — O_w interactions were examined using the VACFs and their Fourier transformations. Figure 6

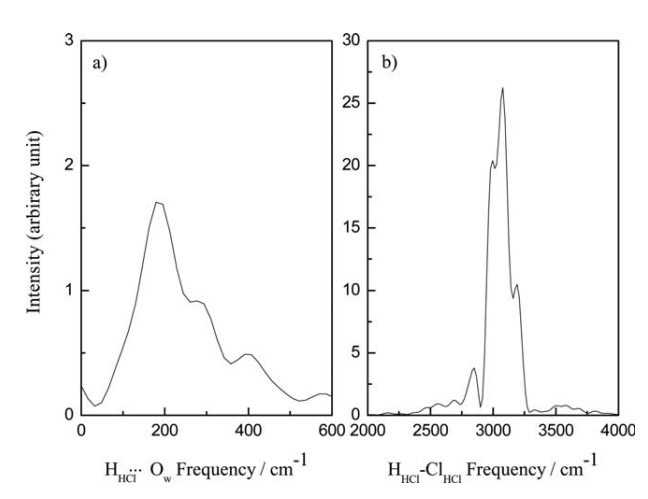


Figure 6. Power spectra of (a) $H_{HCl} \cdots O_w$ and (b) $H_{HCl} - Cl_{HCl}$ stretching modes in the first hydration shell.

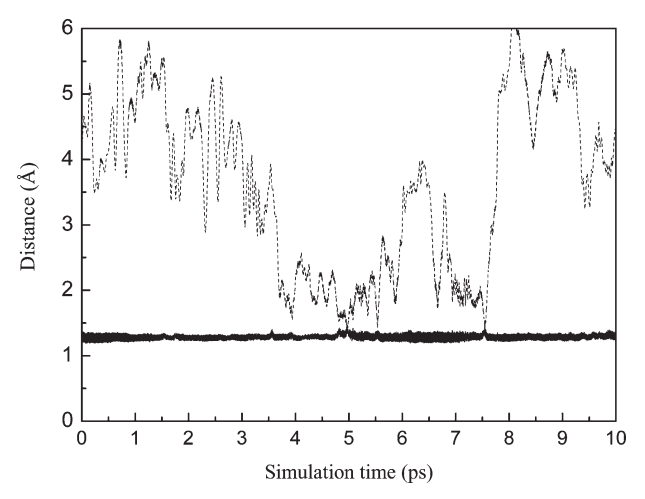


Figure 7. The $H_{HCl} \cdots Cl_{HCl}$ (solid line) and $H_{HCl} \cdots O_w$ (dashed line) distances as a function of time in the first hydration shell evaluated for the proton transfer processes.

illustrates the power spectra of the H_{HCl}···O_w and H_{HCl}···Cl_{HCl} vibrational motions in the first hydration shell obtained from the QMCF MD simulation. In Figure 6a, the maximum frequency of the H_{HCl}···O_w vibrational mode in the first hydration shell is situated at 179 cm⁻¹, with two shoulder peaks at 277 and 390 cm⁻¹. The force constant of 1.8 N/m was calculated for this frequency of the HHCI···Ow peak, which is much weaker than that obtained for the H_{HF}···O_w interaction (5.9 N/m),³⁶ but slightly stronger than the value of 1.6 N/m retrieved from the experimental O_w—H_w···O_w stretching (170 cm⁻¹).⁵⁶ This demonstrates that the acid dissociation of HCl is much more facilitated than that of HF, since the $H_{\mbox{\scriptsize HCl}}{\cdots}O_{\mbox{\scriptsize w}}$ hydrogen bond interaction is almost equally weak as the Ow-Hw···Ow interaction in pure water. For the H_{HC1} — Cl_{HC1} stretching motion, the highest value of this mode is centered at 3078 cm⁻¹, with two shoulder peaks at 2997 and 3192 cm⁻¹. The force constants evaluated for these peaks are 547.1, 518.7, and 588.4 N/m, respectively. The H_{HCl}-Cl_{HCl} stretching frequency calculated from the QMCF simulation is in reasonable agreement with the experimental harmonic vibrational frequency of 2990 cm⁻¹.57,58 In addition, the

Table 1. The Energy Parameters for the $HCl(H_2O)_4$ Clusters Calculated by Different Levels of Theory.

Method	HCl(H ₂ O) ₄ undissociated form (Hartree)	HCl(H ₂ O) ₄ dissociated form (Hartree)	$\Delta E ext{ (kcal/mol)}^a$
HF/DZP	-764.2932329	-764.2869273	3.96
BLYP/DZP ^b	_	-766.5469201	_
B3LYP/DZP ^b	_	-766.6512601	_
MP2/DZP	-765.2326384	-765.2291570	2.18
CCSD/DZP	-765.2784585	-765.2715970	4.31

^aThe relative energies of the dissociated form with that of the undissociated form.

Table 2. Mean Ligand Residence Times and Sustainability of Migration Processes to and from the First Hydration Shell of Chlorine and Hydrogen Atoms of the Hydrogen Chloride Molecule.

		t* =	$t^* = 0 \text{ ps}$ $t^* = 0.5 \text{ ps}$				
Solute	$t_{\rm sim}$	$N_{\rm ex}^0$	$ au_{ m H_2O}^0$	$N_{\rm ex}^{0.5}$	$ au_{ m H_2O}^{0.5}$	$S_{\rm ex}$	$1/S_{\rm ex}$
Cl_{HCl}	10.0	392	0.3	56	2.1	0.14	7.1
H_{HCI}	10.0	80	0.1	9	0.8	0.11	9.1
Bulk ^a	10.0	269	0.2	24	1.7	0.09	11.2

^aValues obtained from a QM/MM MD simulation of pure water. ⁵²

gas-phase value of 3153 cm $^{-1}$ for the H_{HCI} – Cl_{HCI} stretching frequency was also evaluated from the HF/DZP method to confirm that this agreement is not a coincidence. The value of 547.1 N/m estimated for the force constant in the case of HCl is much weaker than that observed for HF (819.1 N/m), ³⁶ proving less stability of the nondissociated form of HCl. It was further found that the ligand exchange processes in the H site of HCl causes the shoulder peaks in the H_{HCl} – Cl_{HCl} stretching mode.

To characterize the acid dissociation of HCl, the ionization structure of this acid has been evaluated. Figure 7 shows distributions of the H_{HCI}···Cl_{HCI} and H_{HCI}···O_w distances in the first hydration shell, exhibiting the proton migration from the chlorine atom of hydrogen chloride to oxygen of a neighboring water. The first proton migration takes place around 4.9-5.0 ps and the second one occurs during the simulation time of 7.5-7.6 ps. Another dissociation attempt observed at 5.5 ps is not completed, but almost successful. It is seen that the proton coming from HCl bound to the neighboring water forming H₃O⁺ species comes back to the Cl atom reforming the HCl molecule within the femtosecond scale. Despite the short simulation time of 10 ps, three proton migration processes were observed, which shows that dissociation can occur already on the picosecond scale in very dilute solution. In the previous CPMD simulation,16 corresponding to a higher concentration, a number of

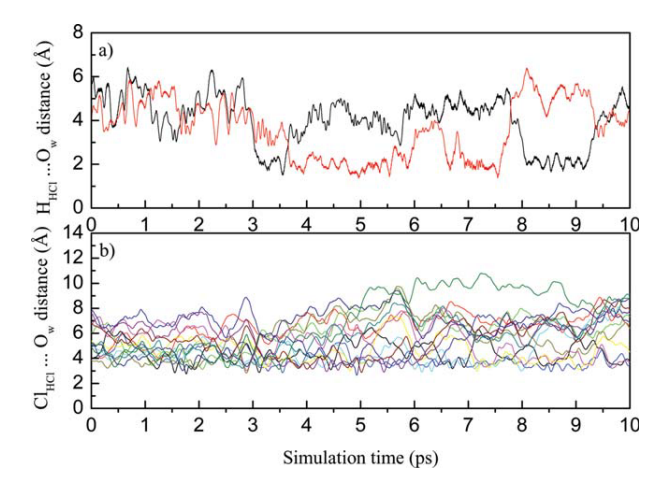


Figure 8. (a) The $H_{HCl}\cdots O_w$ and (b) the $Cl_{HCl}\cdots O_w$ distances as a function of time in the first hydration shell obtained from the QMCF MD simulation.

^bOnly the dissociated forms were observed.

error sources can be identified, partly due to the early time it has been performed, such as the use of DCl and D2O and the functionals being used, for which several problems have been identified in the meantime.⁵⁹ As previous cluster calculations (DFT and MP2)^{19,22} have already shown that DFT overrates the stability of the dissociated state, it seemed appropriate to perform new cluster calculations including HF, MP2, CCSD, and the more modern B3LYP density functional, and the results, shown in Table 1, clearly prove that DFT leads to an unjustified preference for the dissociated state. It should be emphasized, however, that the frequent attempts of proton transfer in our simulation within a few picoseconds are a clear indication that over a longer time period a number of them will be successful thus creating a sufficient number of hydronium ions. For study of full dissociation, i.e., separation of Cl and hydrated hydronium ion, a longer simulation time would have been required but on the basis of the results obtained for 10 ps one can easily predict such a dissociation process to happen.

The dynamics of ligand exchange processes at each atom of HCl were also determined by the mean residence times (MRTs) using the "direct" method. 60 The time parameters t^* of 0.0 and 0.5 ps were used, reflecting to the minimum duration of a ligand's displacement from its original coordination shell to be accounted. The number of ligand exchange processes, the MRTs, and the sustainability of migration processes from the first hydration shell are summarized in Table 2. The variations of the $H_{HCI}\cdots O_w$ and $Cl_{HCI}\cdots O_w$ distances obtained at $t^* =$ 0.5 ps in the first hydration shell are presented in Figure 8. As shown in Figure 8a, there are three exchange processes occurring at the H atom of HCl, the first one taking place at 3.5 ps and the second and the third one observed in the range of 6-7 and 7-8 ps, respectively. For the Cl site, several ligand exchange processes were found during the simulation time of 10 ps, as shown in Figure 8b. The calculated MRT values with respect to $t^* = 0.0$ and 0.5 ps for the first hydration shell located around the Cl atom are 0.3 and 2.1 ps, which are the same as those estimated for the F site of HF. 36 The values of 0.1 and 0.8 ps for t^* = 0.0 ps and t^* = 0.5 ps, respectively, were determined for the H site of HCl. These values are smaller in comparison with the aqueous HF solution (0.8 ps for $t^* = 0.0$ ps and 2.5 ps for $t^* =$ 0.5 ps),³⁶ and also smaller than that obtained from QM/MM (1.51 ps)⁵³ simulation of pure water. In the QMCF MD, hydrogen bond life times of 1.1 and 0.31 ps were evaluated for the $Cl_{HCl} - H_{HCl} \cdots O_w \quad \text{and} \quad H_{HCl} - Cl_{HCl} \cdots H_w \quad \text{hydrogen} \quad \text{bonds},$ respectively, suggesting a very different stability of these Hbonds. The average lifetime of the Cl_{HCl}-H_{HCl}···O_w hydrogen bond is higher than that observed in pure water by experiment⁶¹ (0.55 ps), and a QM/MM MD simulation (0.33 ps),⁵³ confirming the stability of this H bond. The value of 0.31 ps obtained for the H_{HCl}--Cl_{HCl}···H_w hydrogen bond is almost the same as the value of 0.36 determined for the F site of the HF molecule. The MRT values and the hydrogen bond lifetimes predicted from the QMCF MD simulation reveal that HCl in aqueous solution is simultaneously a weak structure-making and a weak structure breaking species. The sustainability coefficients S_{ex} were computed by comparing the number of all exchanges through the border of the hydration shell $(N_{\rm ex}^{0.0})$ to the number of exchanges processes lasting at least 0.5 ps $(N_{\rm ex}^{0.5})$, resulting in 0.11 and 0.14 for H and Cl sites of hydrogen chloride. The corresponding $1/S_{\rm ex}$ values are 9.1 and 7.1, suggesting that one lasting exchange process in the neighborhood of H and Cl is achieved by about nine and seven attempts to cross a shell boundary, respectively.

Conclusions

We have performed a QMCF molecular dynamics simulation to investigate the hydration structure and dynamics of the aqueous HCl solution. The calculated H—Cl bond distance and its vibrational frequency are in good agreement with the experimental observation. A relatively strong hydrogen bond at the H site of hydrogen chloride was detected, whereas weak hydrogen bonding dominates at the Cl site. The coordination number of ~7 is prevailing in the first hydration shell, augmented by about five water molecules of an extended first shell. The acid dissociation of HCl is visible from the proton transfer events observed in the QMCF MD simulation. The QMCF MD simulation shows several ligand exchange processes in the first hydration shell, which occur more frequently at the Cl site of the molecule.

Acknowledgments

Financial support for this work by the Thailand Research Fund (TRF) and Thailand Commission on Higher Education (ASEA-UNINET fellowships for C.K. and V.V.) are gratefully acknowledged and B.M.R. acknowledges support by the Austrian Science Foundation (FWF).

References

- Kirk, K. L. Biochemistry of Halogens and Inorganic Halides; Plenum Press; New York, 1991.
- 2. Amirand, C.; Maillard, D. J Mol Struct 1988, 176, 181.
- 3. Triolo, R.; Narten, A. H. J Chem Phys 1975, 63, 3624.
- 4. Agmon, N. J Phys Chem A 1998, 102, 192.
- Fárník, M.; Weimann, M.; Suhm, M. A. J Chem Phys 2003, 118, 10120.
- Cappa, C. D.; Smith, J. D.; Messer, B.; Cohen, R. C.; Saykally, R. J. J Phys Chem B 2006, 110, 1166.
- Botti, A.; Bruni, F.; Ricci, M. A.; Soper, A. K. J Chem Phys 2006, 125, 14508.
- 8. Chipot, C.; Gorb, L. G.; Rivail, J. L. J Phys Chem 1994, 98, 1601.
- 9. Robertson, S. H.; Clary, D. C. Faraday Discuss 1995, 100, 309.
- 10. Gertner, B. J.; Hynes, J. T. Science 1996, 271, 1563.
- 11. Planas, M.; Lee, C.; Novoa, J. J. J Phys Chem 1996, 100, 16495.
- 12. Laasonen, K.; Klein, M. L. J Am Chem Soc 1994, 116, 11620.
- 13. Packer, M. J.; Clary, D. C. J Phys Chem 1995, 99, 14323.
- Balbuena, P. B.; Johnston, K. P.; Rossky, P. J. J Phys Chem 1996, 100, 2716.
- Lee, C.; Sosa, C.; Planas, M.; Novoa, J. J Chem Phys 1996, 104, 7081.
- 16. Laasonen, K.; Klein, M. L. J Phys Chem A 1997, 101, 98.
- 17. Ando, K.; Hynes, J. T. J Phys Chem B 1997, 101, 10464.
- Geiger, F. M.; Hicks, J. M.; de Dios, A. C. J Phys Chem A 1998, 102, 1514.
- 19. Re, S.; Osamura, Y.; Suzuki, Y. J Chem Phys 1998, 109, 973.

- Bacelo, D. E.; Binning, R. C.; Ishikawa, Y. J Phys Chem A 1999, 103, 4631.
- Chaban, G. M.; Gerber, R. B.; Janda, K. C. J Phys Chem A 2001, 105, 8323.
- Cabaleiro-lago, E. M.; Hermida-Ramón, J. M.; Rodríguez-Otero, J. J Chem Phys 2002, 117, 3160.
- 23. Masia, M.; Forbert, H.; Marx, D. J Phys Chem A 2007, 111, 12181.
- 24. Buch, V.; Dubrovskiy, A.; Mohamed, F.; Parrinello, M.; Sadlej, J.; Hammerich, A. D.; Devlin, J. P. J Phys Chem A 2008, 112, 2144.
- 25. Lee, H.-S.; Tuckerman, M. E. J Phys Chem A 2009, 113, 2144.
- 26. Heuft, J. M.; Meijer, E. J. Phys Chem Chem Phys 2006, 8, 3116.
- 27. Rode, B. M.; Schwenk, C. F.; Tongraar, A. J Mol Liq 2003, 110, 105.
- Rode, B. M.; Schwenk, C. F.; Hofer, T. S.; Randolf, B. R. Coord Chem Rev 2005, 249, 2993.
- Rode, B. M.; Hofer, T. S.; Randolf, B. R.; Schwenk, C. F.; Xenides,
 D.; Vchirawongkwin, V. Theor Chem Acc 2006, 115, 77.
- 30. Field, M. J.; Bash, P. A.; Karplus, M. J Comput Chem 1990, 11, 700.
- 31. Gao, J. J Am Chem Soc 1993, 115, 2930.
- 32. Bakowies, D.; Thiel, W. J Phys Chem 1996, 100, 10580.
- 33. Stillinger, F. H.; Rahman, A. J Chem Phys 1978, 68, 666.
- 34. Bopp, P.; Janscó, G.; Heinzinger, K. Chem Phys Lett 1983, 98, 129.
- 35. Brooks, B. R.; Bruccoleri, R. E.; Olafson, B. D.; States, D. J.; Swaminathan, S.; Karplus, M. J Comput Chem 1983, 4, 187.
- Kritayakornupong, C.; Vchirawongkwin, V.; Hofer, T. S.; Rode, B. M. J Phys Chem B 2008, 112, 12032.
- Vchirawongkwin, V.; Rode, B. M.; Persson, I. J Phys Chem B 2007, 111, 4150.
- Fatmi, M. Q.; Hofer, T. S.; Randolf, B. R.; Rode, B. M. J Comput Chem 2007, 28, 1704.
- Hofer, T. S.; Randolf, B. R.; Shah, S. A. A.; Rode, B. M.; Persson,
 I. Chem Phys Lett 2007, 445, 193.
- 40. Berendsen, H. J. C.; Postma, J. P. M.; van Gunsteren, W. F.; DiNola, A.; Haak, J. R. J Chem Phys 1984, 81, 3684.
- 41. Adams, D. J.; Adams, E. H.; Hills, G. J Mol Phys 1979, 38, 387.
- 42. Ahlrichs, R.; Bär, M.; Häser, M.; Horn, H.; Kölmel, C. Chem Phys Lett 1989, 162, 165.

- Ahlrichs, R.; von Arnim, M. Methods and Techniques in Computational Chemistry: METECC-95; Cagliari: Sardinia, 1995.
- 44. von Arnim, M.; Ahlrichs, R. J Comput Chem 1998, 19, 1746.
- 45. Dunning, T. H., Jr.; Wadt, W. R. J Chem Phys 1989, 90, 1007.
- Dunning, T. H., Jr.; Hay, P. J. Modern Theoretical Chemistry: Methods of Electronic Structure Theory, Vol. 3; Schaefer, H. F., III, Ed.; Plenum Press: New York, 1977.
- D'Incal, A.; Hofer, T. S.; Randolf, B. R.; Rode, B. M. Phys Chem Chem Phys 2006, 8, 2841.
- Hofer, T. S.; Pribil, A. B.; Randolf, B. R.; Rode, B. M. J Am Chem Soc 2005, 127, 14231.
- Hofer, T. S.; Randolf, B. R.; Rode, B. M. Phys Chem Chem Phys 2005, 7, 1382.
- Hofer, T. S.; Rode, B. M.; Randolf, B. R. Chem Phys 2005, 312,
- Schwenk, C. F.; Hofer, T. S.; Rode, B. M. J Phys Chem A 2004, 108, 1509
- Schwenk, C. F.; Löfffler, H. H.; Rode, B. M. J Chem Phys 2001, 115, 10808.
- Xenides, D.; Randolf, B. R.; Rode, B. M. J Chem Phys 2005, 122, 174506.
- 54. Herzberg, G.; Spink, J. W. T. Z Phys 1934, 89, 474.
- Huber, K. P.; Herzberg, G.Molecular Spectra and Molecular Structure, Vol. 37; Van Nostrand Reinhold: New York, 1979.
- Franks, F. Water: A Comprehensive Treatise, Vol. 1; Plenum Press: New York, 1972.
- Shimanouchi, T. Tables of Molecular Vibrational Frequencies, Vol. 37; National Bureau of Standards: Washington, D.C., 1972.
- Chase, M. W.; Davies, C. A.; Downey, J. R.; Frurip, D. J.; McDonald, R. A.; Syverud, A. N. J Phys Chem Ref Data Suppl 1985, 14.
- Yoo, S.; Zeng, X. C.; Xantheas, S. S. J Chem Phys 2009, 130, 221102.
- Hofer, T. S.; Tran, H. T.; Schwenk, C. F.; Rode, B. M. J Comput Chem 2004, 25, 211.
- Lock, A. J.; Woutersen, S.; Bakker, H. J. J Phys Chem A 2001, 105, 1238.

RISM-SCF-SEDD Study on the Symmetry Breaking of Carbonate and Nitrate Anions in **Aqueous Solution**

Viwat Vchirawongkwin,† Hirofumi Sato,*,‡ and Shigeyoshi Sakaki^{‡,¶}

Department of Chemistry, Faculty of Science, Chulalongkorn University, Phyathai Road, Prathumwan, Bangkok 10330, Thailand, Department of Molecular Engineering, and Fukui Institute for Fundamental Chemistry, Kyoto University, Kyoto, 615-8510, Japan

Received: February 25, 2010; Revised Manuscript Received: July 1, 2010

The planarity of carbonate and nitrate anions was investigated in the gas and solution phases by means of the reference interaction site model self-consistent field spatial electron density distribution (RISM-SCF-SEDD) method. The computed optimized geometries and solvation structures are compared with the diffraction data. In the solution phase, the symmetry of carbonate anion is changed from D_{3h} to C_{3v} , whereas the planarity of nitrate anion is still retained. These are fully consistent with experimental knowledge. The classical electrostatic model was also utilized to elucidate the mechanism of the symmetry breaking. It should be emphasized that the symmetry breaking occurs not only by a specific solvent molecule attaching to the ion but by an overall electrostatic interaction between the infinite number of solvent molecules and the ion.

Introduction

Carbonate and nitrate anions are abundant and important in biological systems as well as in environmental systems. Carbonate is a ubiquitous and reactive anion that can be found in groundwater and reacts to form aqueous and solid-state complexes with the majority of metals in the periodic table. 1 Nitrate is the most fully oxidized compound of nitrogen and is therefore stable to oxidation, regarded as a potentially strong oxidizing agent. It can also be generated in the human body through the oxidation of nitric oxide, which is produced by nitric oxide synthases from L-arginine.^{2,3}

The structures of these two compounds are very similar, normally planar possessing D_{3h} symmetry with six normal modes: symmetric stretch (ν_1), out-of-plane deformation (ν_2), two doubly degenerate modes, i.e., antisymmetric stretch (ν_3) and in-plane deformation (ν_4). Rudolph and co-workers observed the v_2 mode and its overtone of carbonate ion in an aqueous solution using Raman spectroscopy, suggesting the symmetry breaking in the concentrated⁴ and dilute⁵ solutions. They also optimized the water cluster, a carbonate with two water molecules, by employing the density functional theory in the gas phase, showing the $C_{2\nu}$ symmetry.⁴ On the other hand, the far-ultraviolet resonance Raman spectroscopy indicates the planarity of nitrate ion in several polar solvents, though a very broad band of v_3 suggests that the symmetry is lowered from D_{3h} to C_{2v} or to C_s . The results of photoelectron spectroscopy suggested the first hydration consisting of three water molecules with the C_{3h} symmetry as the geometry of nitrate ion in aqueous solution.⁷ Raman results have been reported that the splitting of ν_3 vanishes for the dilute nitrate solutions.^{8–10} The recent infrared multiple photon photodissociation experiment on the $NO_3^-(H_2O)_n$ clusters (n = 1-6) observed the splitting of the ν_3 band due to the perturbation of water molecules, showing the possibility of symmetry lowering to C_1 . Pathak et al.

computed an effect of explicit water molecules on the lowering symmetry of carbonate and nitrate anion clusters. 12

The optimization of carbonate ion in aqueous solution (dielectric media) with the generalized conductor-like screening model indicates a slight effect on the geometry compared with the gaseous state.¹³ An empirical force field for the carbonate ion including the out-of-plane displacement of the carbon atom was developed to investigate the phase transition of calcite.¹⁴ The potential function with increasing the stiffness of the carbonate ion was adopted to the classical molecular dynamics (MD) simulation of calcium carbonate. 15 The recent investigations based on Car-Parrinello (CP) MD simulation provided the structural properties of hydration shell, but the symmetry breaking was not discussed. 16,17 The inclusion of an anharmonic force field in the classical MD simulation¹⁸ and a combined quantum mechanics/molecular mechanics (QM/MM) MD simulation¹⁹ of hydrated nitrate ion presented the splitting of v_3 that agrees with the spectroscopic results.

At the same time, there is no wonder that nonsymmetric solvation structure around the ion breaks its symmetry; the symmetry of the cluster model is inevitably lowered by the specific hydrating molecule. The question that we would like to raise here is whether the symmetry of the anions in aqueous solution is inherently broken or not, under an isotropic environment. If so, what is the driving force of the breaking? It should be stressed that the issue is deeply related to both the electronic structure of the anion and solvation structure around it. QM/ MM or an equivalent treatment is essentially needed.

Here we present an alternative method to the QM/MM, RISM-SCF, which is a hybrid method of integral equation theory in statistical mechanics (reference interaction site model selfconsistent field, RISM-SCF) and an ab initio electronic structure theory. 20-24 This method succeeded to investigate the structural properties of the solute and the solvation effects on the reactions in a solution phase.^{25–29} In particular, the symmetry breaking in the solvated I_3^- system was precisely discussed. 30 In this work, we applied the RISM-SCF formalism to investigate the optimized geometries of carbonate and nitrate anions in aqueous solutions. The classical electrostatic free energy calculation

^{*} To whom correspondence should be addressed. E-mail: hirofumi@ moleng.kyoto-u.ac.jp.
† Chulalongkorn University.

^{*} Department of Molecular Engineering, Kyoto University.

[¶] Fukui Institute for Fundamental Chemistry, Kyoto University.

TABLE 1: Lennard-Jones Parameters for the ${\rm CO_3}^{2-}$ and ${\rm NO_3}^-$ Anions and Water Molecule

-		
	σ/Å	ε /kcal mol ⁻¹
	Solute	
C	3.296	0.1200
N	3.150	0.1700
O	2.850	0.2000
	H_2O	
Н	1.000	0.0560
O	3.166	0.1550

based on the multipole expansion^{31,32} was also utilized as a model to understand the true nature of the symmetry breaking caused by the solvation effect.

Method

The RISM-SCF method has been outlined in detail elsewhere.20-24 Similar to the QM/MM, this method evaluates the statistical solvent distribution consistent with the electronic structure of the solute, while the electronic structure of the solute is affected by the surrounding solvent distribution. Thus, both the RISM integral equation and ab initio molecular orbital (MO) calculation must be solved in a self-consistent manner. The statistical mechanics part of the RISM-SCF method was solved with the Kovalenko and Hirata (KH) closure approximation^{33,34} to obtain the structure of the solvent on a grid of 2048 points on the radial direction, whereas the ab initio MO methods at Hartree-Fock (HF) and density functional theory, namely, Becke, three-parameter, Lee-Yang-Parr exchange-correlation functional (B3LYP), associated with the 6-311+G* basis set, 35,36 were utilized to evaluate the electronic structure of carbonate and nitrate ions in the SCF procedure, so-called RISM-SCF/ HF and RISM-SCF/B3LYP, respectively. We further employed the CCSD(T) method coupled with solvation effect (RISM-SCF/ CCSD(T)) to obtain highly accurate solvation energy. The SPC water model³⁷ with the corrected Lennard-Jones parameters of hydrogen sites ($\sigma = 1.0 \text{ Å}$ and $\varepsilon = 0.056 \text{ kcal mol}^{-1}$) was selected for solvent water in the RISM equation. Table 1 lists all parameters^{21,38,39} employed in the solution-phase calculations. The density of solvent water was set to 1 g cm⁻³ at 298.15 K.

All solution-phase calculations were performed with the RISM-SCF-SEDD (spatial electron density distribution, SEDD)²³ code implemented in GAMESS program package⁴⁰ modified by us. In the theory, the total energy of the system (\mathcal{A}) is defined as the sum of the solute potential energy and solvation free energy:

$$\mathcal{A} = \langle \Psi^{\text{solute}} | H_0 | \Psi^{\text{solute}} \rangle + \Delta \mu \tag{1}$$

where H_0 is the standard Hamiltonian of solute in a gas phase, Ψ^{solute} is the wave function of the solute obtained by solving the equation with the modified Fock operator, and $\Delta\mu$ is the solvation free energy evaluated by the KH closure equations. ^{33,34}

In order to understand the solvation effects on the symmetry breaking of anions, we also calculated the classical electrostatic free energy based on the multipole expansion with the spherical model^{31,32} of radius b from the center of mass of solute immersed in a solvent with a dielectric constant D, which was set to 80 for the solvent water.

Results and Discussion

Optimized Structures of Carbonate and Nitrate Anions in the Solution Phase. The initial geometries of carbonate and nitrate anions in both gas and solution phases were set as an

TABLE 2: Optimized Geometries of ${\rm CO_3}^{2-}$ and ${\rm NO_3}^{-}$ Anions in the Gas and Solution Phases Obtained from HF, B3LYP, RISM-SCF/HF, and RISM-SCF/B3LYP Calculations with the 6-311+G* Basis Set

	gas phase		solution	n phase
	HF	B3LYP	RISM-SCF/ HF	RISM-SCF/ B3LYP
		CO ₃ ²⁻		
$C-O_1$ (Å)	1.282	1.308	1.267	1.288
$C-O_2$ (Å)	1.282	1.308	1.267	1.288
$C-O_3$ (Å)	1.282	1.308	1.267	1.288
C- torsion (deg)	0.00	0.00	7.45	7.79
		NO_3^-		
$N-O_1$ (Å)	1.224	1.261	1.217	1.253
$N-O_2$ (Å)	1.224	1.261	1.217	1.253
$N-O_3$ (Å)	1.224	1.261	1.217	1.253
N- torsion (deg)	0.00	0.00	0.02	0.00

nonsymmetric structure and optimized without any symmetry constraint. Table 2 summaries the optimized geometries of carbonate and nitrate anions in the isolated state evaluated with the standard HF and B3LYP and the solution phase with the RISM-SCF/HF and RISM-SCF/B3LYP methods. The C— and N— torsion angles are defined to investigate the planarity of the solute as the $C-O_1-O_2-O_3$ and $N-O_1-O_2-O_3$ dihedral angles, respectively.

The geometries of both anions obtained from the HF and B3LYP optimizations in the gas phase show the equivalence of three bonds and the molecular plane described with the Cand N- torsion angles to be equal to 0.00° , possessing the D_{3h} symmetry. However, the situation is different when these anions are dissolved in water. The symmetry of carbonate ion was lowered to nonplanar structure. The C- torsions were increased to 7.45° and 7.79° for the optimized geometry obtained from the RISM-SCF/HF and RISM-SCF/B3LYP, respectively. The N- torsion of nitrate ion obtained from the RISM-SCF/HF was hardly changed by 0.02°, and the ion has retained the planarity for the RISM-SCF/B3LYP optimization. All bonds within each anion remain the equivalence in the solution phase, but they are slightly shorter than those in the gas phase by 0.015 and 0.020 Å for carbonate ion, and 0.007 and 0.008 Å for nitrate, obtained from the RISM-SCF/HF and RISM-SCF/B3LYP, respectively. These results indicate the symmetry of carbonate ion is changed from D_{3h} to C_{3v} , but nitrate ion is still as D_{3h} . Our intramolecular distances of carbonate and nitrate anions, namely, C-O_C and N-O_N, obtained from the RISM-SCF optimizations show a good agreement with the recent neutron diffraction experiments of K₂CO₃ solutions that reported the C-O_C distance of 1.3 Å⁴¹ and with the NaNO₃ solutions in which the N-O $_N$ distances vary between 1.21 \pm 0.02 and 1.24 \pm 0.02 Å, 42 respectively.

The radial distribution functions (RDFs) of solvent molecules around the solute are also obtained from the computations as shown in Figures 1 and 2. The positions of the first peaks for each anion obtained from the RISM-SCF/HF summarized in Table 3 are slightly shorter than those of RISM-SCF/B3LYP within the maximum deviation of 0.03 Å. The positions of the first hydration peaks represent the stronger interactions of water molecules with the carbonate ion than those of the nitrate ion. This result corresponds to the neutron diffraction with isotopic substitution (NDIS) of Cs_2CO_3 and $CsNO_3$ in an aqueous solution, indicating that the stronger hydrogen bonds are formed between the solvent water and carbonate ion than those formed in the nitrate ion. 43 Our results in Table 3 are also in an

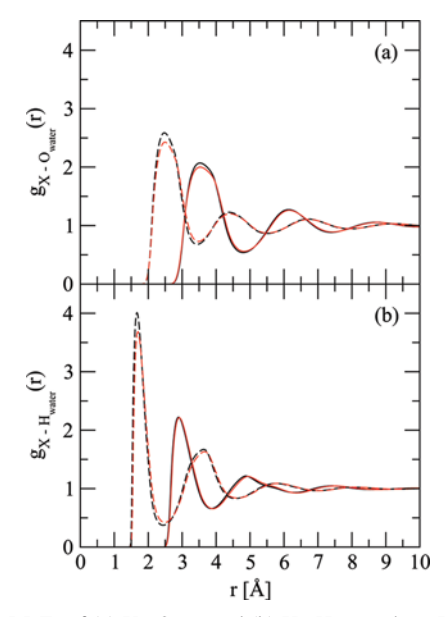


Figure 1. RDFs of (a) $X-O_{water}$ and (b) $X-H_{water}$, where X stands for the C and O sites of CO₃²⁻ ion. The black and red lines refer to the RDFs obtained from RISM-SCF/HF for the C (the black solid lines) and O (the black dashed lines) sites and RISM-SCF/B3LYP for the C (the red solid lines) and O (the red dashed lines) sites, respectively.

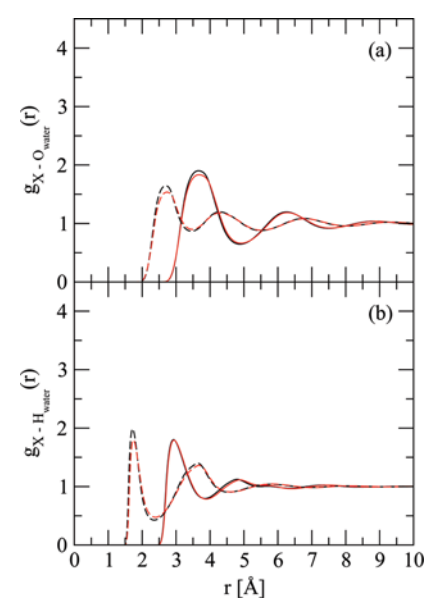


Figure 2. RDFs of (a) $X-O_{water}$ and (b) $X-H_{water}$, where X stands for the N and O sites of NO_3^- ion. The black and red lines refer to the RDFs obtained from RISM-SCF/HF for the N (the black solid lines) and O (the black dashed lines) sites and RISM-SCF/B3LYP for the N (the red solid lines) and O (the red dashed lines) sites, respectively.

agreement with the C···O_w of 3.35 Å and N···O_w of approximately 3.7 Å estimated by the neutron diffraction⁴¹ and X-ray diffraction⁴² measurements, respectively. The consistency of optimized geometries and hydration structures obtained from the RISM-SCF calculations indicate the reliability of the methods to elucidate the properties of these anions in solution phase. However, the discussion about the planarity of anions needs a further evaluation presented in the following.

Comparison of Energy Surfaces between the Gas and Solution Phases. The potential energy surfaces (PESs) in the gas phase and free energy surfaces (FESs) in the aqueous solution of carbonate and nitrate anions are plotted as a function of C- or N- torsion at the same theoretical levels employed

TABLE 3: Distance of First Hydration Peaks Obtained from the RISM-SCF Optimizations of CO₃²⁻ and NO₃⁻ Anions in the Solution Phase

	RISM-SCF/HF	RISM-SCF/B3LYP
	CO ₃ ²⁻	
$C \cdots O_w$	3.53	3.53
$C \cdots H_w$	2.90	2.91
$O_C \cdots O_w$	2.48	2.49
O_C · · · H_w	1.67	1.69
	NO_3^-	
$N \cdots O_w$	3.66	3.68
$N \cdots H_w$	2.92	2.94
$O_N \cdots O_w$	2.70	2.73
$O_N {\boldsymbol{\cdots}} H_w$	1.72	1.75

in the previous section (Figure 3). The FESs of the solution phase were constructed by moving the carbon or nitrogen atom along the principal axis, retaining the C_{3v} symmetry, and the optimization for the rest of geometrical parameters was performed to evaluate the total energy according to eq 1. The energy points of PESs in the gas phase were obtained by the single-energy calculations at the geometries adopted from each point in the FESs of the solution phase. Each relative energy with respect to the minimum is plotted in the figure.

The minimum for the carbonate and nitrate anions in the gasphase PES is located at 0.00° , corresponding to the D_{3h} symmetry structure. Whereas the FESs of nitrate anion in the solution phase have a minimum at the N- torsion of 0.00°, those of carbonate anion show double minima situated at $\pm 7.39^{\circ}$ and $\pm 7.74^{\circ}$ obtained from the RISM-SCF/HF and RISM-SCF/ B3LYP calculations, respectively. Furthermore, the RISM-SCF/ CCSD(T) method was also employed to construct the FESs at the geometry of each point on the FES of RISM-SCF/B3LYP calculations. The FES of hydrated nitrate anion showed the minimum at the N- torsion of 0.00°, whereas those of the carbonate anion again exhibited double minima located at the C-

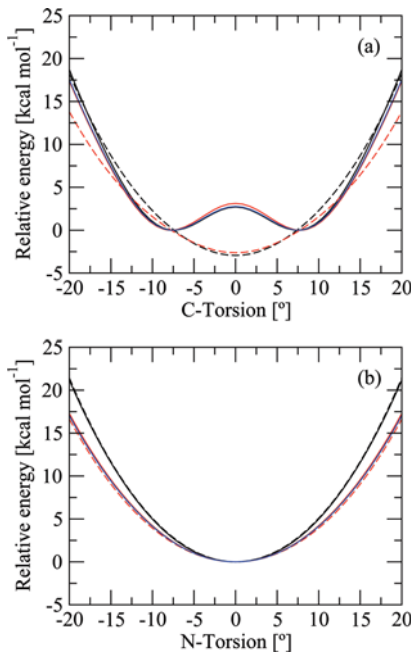


Figure 3. PESs and FESs of (a) CO₃²⁻ and (b) NO₃⁻ anions as a function of dihedral angle obtained by HF (the black dashed lines) and B3LYP (the red dashed lines) in the gas phase and by RISM-SCF/HF (the black solid lines), RISM-SCF/B3LYP (the red solid lines), and RISM-SCF/CCSD(T) (the blue solid lines) in aqueous solution.

TABLE 4: Harmonic Frequencies of CO₃²⁻ and NO₃⁻ Anions in Gas Phases

	frequency (cm ⁻¹)			
	ν_1	ν_2	ν_3	$ u_4 $
		CO ₃ ²⁻		
HF	1125	991	1498	722
B3LYP	1011	856	1311^{a}	643^{a}
$exptl^b$	1066	884	1385	684
		NO_3^-		
HF	1228	989	1567	792
B3LYP	1066	842	1378^{a}	704^{a}
$exptl^b$	1048	832	1348	718

^a Averaged values. ^b In aqueous solution (ref 4).

TABLE 5: Harmonic Force Constant and Frequency of the Out-of-Plane Mode for ${\rm CO_3}^{2-}$ and ${\rm NO_3}^-$ Anions

		$k \text{ (kcal mol}^{-1} \text{ Å}^{-2}\text{)}$	$v_{\rm g}$ or $v_{\rm s}$ (cm ⁻¹)
		CO ₃ ²⁻	
gas	HF	1420.02	991
_	B3LYP	1124.17	856
aqueous	RISM-SCF/HF	3461.29	1591
•	RISM-SCF/B3LYP	3548.21	1521
		NO_3^-	
gas	HF	1474.78	989
_	B3LYP	1078.94	842
aqueous	RISM-SCF/HF	1391.22	960
•	RISM-SCF/B3LYP	1141.02	866

torsion of $\pm 7.57^{\circ}$. The local maximum points on the FESs of hydrated carbonate anion are located at the C- torsion = 0.00°, showing the barrier of 2.71 (RISM-SCF/HF), 3.12 (RISM-SCF/B3LYP), and 2.76 (RISM-SCF/CCSD(T)) kcal mol⁻¹. These results strongly indicate that the statistical optimal geometry of carbonate is inherently C_{3v} symmetry in the solution phase. It is noted that the present result does not deny the possibility of further lowering of symmetry caused by a specific hydration of water solvents.

The fundamental frequencies are usually obtained from the Hessian method, i.e., the second-order energy gradient with respect to the nuclear coordinates, implemented in the standard ab initio MO program packages. Table 4 list the fundamental frequencies of carbonate and nitrate anions for the optimized geometries corresponding to the PESs (Figure 3). On the other hand, FES is not directly connected to the frequencies of solvated ions (ν_s), but still it might be meaningful to estimate the frequency from the curvature, especially for the out-of-plane motion (ν_2) in the solution phase.

$$\nu_{\rm s} = \sqrt{\frac{k_{\rm s}}{k_{\rm g}}} \nu_{\rm g} \tag{2}$$

was employed to evaluate the frequency from the FES curvature, where $k_{\rm g}$ and $k_{\rm s}$ are, respectively, the harmonic force constant obtained from the curve-fitting of gas and solution energy surfaces, and $\nu_{\rm g}$ is the frequency in the gas phase. These are summarized in Table 5. The significant changing of energy surfaces and k values shows a large effect on the solvation of carbonate anion and introduces strong anharmonicity. The similarity of PESs and FESs in Figure 3b for the nitrate ion in the gas and solution phase shows a moderate effect of water on the solvation.

Origin of the Symmetry Breaking. The present result suggests that the symmetry breaking of carbonate anion does

TABLE 6: Molecular Radius (*b*) and Atomic Charge Sets of CO_3^{2-} and NO_3^- Anions Obtained from the RISM-SCF Calculations at the D_{3h} Symmetry in the Solution Phase

	CO ₃ ²	ion	NO ₃	ion -
	HF	B3LYP	HF	B3LYP
<i>b</i> (Å)	2.408	2.417	2.377	2.391
e_1	1.753	1.686	1.248	1.120
e_2	-1.251	-1.229	-0.749	-0.706
e_3	-1.251	-1.229	-0.749	-0.706
e_4	-1.251	-1.229	-0.749	-0.706

occur even without specific water molecules attaching to the ion, whereas the nitrate anion does not. What is the difference between the two anions? The classical electrostatic free energy, \mathcal{W} , based on the multipole expansion with the spherical model, ^{31,32} is introduced here to clarify the difference. The expression of \mathcal{W} is

$$\mathcal{W} = \sum_{k=1}^{\nu-1} \sum_{l>k}^{\nu} \frac{e_k e_l}{D_i | \mathbf{r}_k - \mathbf{r}_l|} + \sum_{n=0}^{\infty} \frac{-(D - D_i)(n+1)G_n}{D_i b^{2n+1} [(n+1)D + nD_i]} \quad (\nu = 4) \quad (3)$$

where G_n is defined as

$$G_n = \sum_{k=1}^{\nu-1} \sum_{l>k}^{\nu} e_k e_l |\mathbf{r}_k|^n |\mathbf{r}_l|^n P_n(\cos \vartheta_{kl}) \tag{4}$$

The set of point charge $\{e_{\nu}\}$ denotes the atomic charges evaluated by the Gill et al. procedure⁴⁴ at the RISM-SCF optimized D_{3h} structure for the carbonate and nitrate anions, \mathbf{r}_k is a position vector with respect to the center of mass, and ϑ_{kl} is the angle between \mathbf{r}_k and \mathbf{r}_l . The D_i is the internal dielectric constant of molecule that equals to 1, whereas D=80 represents water solvent. $P_n(\cos\vartheta_{kl})$ are the ordinary Legendre functions. The molecular radius b was determined from the polarizable continuum model (PCM).⁴⁵ All these parameters obtained from the RISM-SCF/HF and RISM-SCF/B3LYP are summarized in Table 6.

The computed \mathcal{W} 's for the carbonate anion are plotted in Figure 4, parts a and b. The calculations were performed with different maximum orders of Legendre functions (n=0,1,2,3,4,5,10, and 20). As shown in the figures, eqs 3 and 4 properly reproduce the double-minima character corresponding to the FESs obtained from the RISM-SCF-SEDD calculations (Figure 3a). The dipole moment (n=1), represented with the red lines in the figure, seems dominate the height of the barrier in the FESs of carbonate ion. \mathcal{W} 's for the nitrate (Figure 4, parts e and f) are again identical with the FESs obtained from the RISM-SCF-SEDD calculations (Figure 3b). These results indicate this simple classical model is reasonably representing the solvation free energy profile obtained from the higher-level, coupled electronic/classical RISM-SCF-SEDD method.

In this simplified model, both of the atomic charges and geometrical coordinates are taken from the RISM-SCF-SEDD computations. A hypothetical model is thus introduced to check which contribution is responsible to the difference between the anions. W's were computed with the charge sets of the nitrate anion at the carbonate optimized geometry (Figure 4, parts c and d) and vice versa (Figure 4, parts g and h). The changing

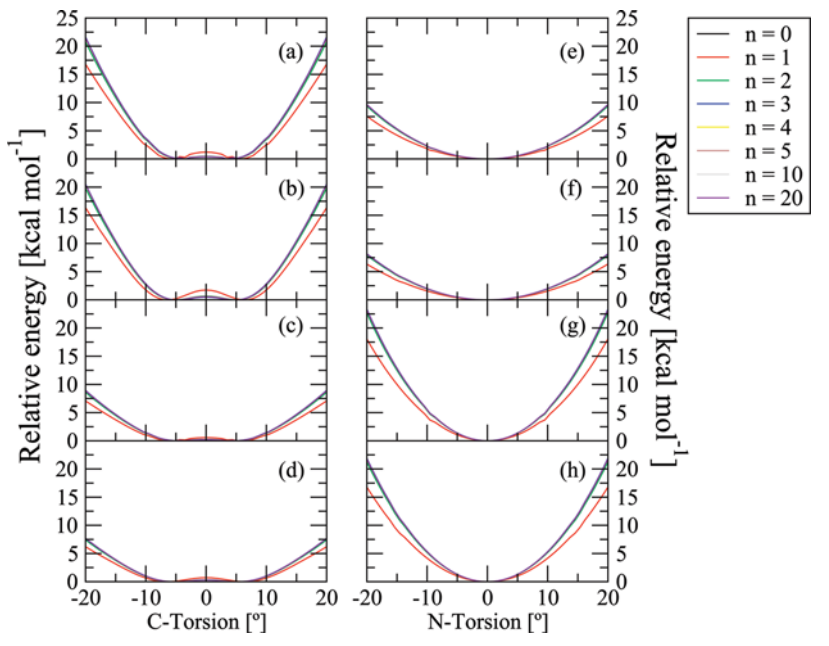


Figure 4. Classical electrostatic free energy of CO₃²⁻ ion computed with the charge sets of (a) RISM-SCF/HF and (b) RISM-SCF/B3LYP. The hypothetical sets were taken from NO₃⁻; (c) RISM-SCF/HF and (d) RISM-SCF/B3LYP (see the text). The classical electrostatic free energy of NO₃⁻ ion computed with the charge sets of (e) RISM-SCF/HF and (f) RISM-SCF/B3LYP. The hypothetical sets were taken from CO₃²⁻; (g) RISM-SCF/HF and (h) RISM-SCF/B3LYP. All of them are plotted with various multipole expansions (n = 0, 1, 2, 3, 4, 5, 10,and 20).

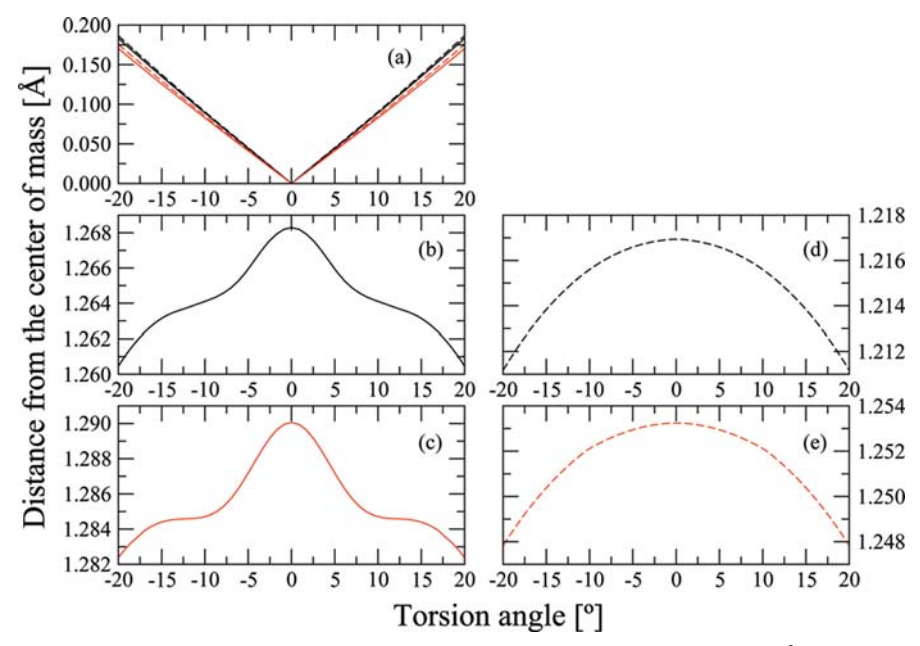


Figure 5. Distance from the center of mass to (a) carbon (black lines) and nitrogen (red lines) atoms of CO₃²⁻ and NO₃⁻ by RISM-SCF/HF (solid lines) and RISM-SCF/B3LYP (dashed lines). The same plots to oxygen of CO₃²⁻ anion by (b) RISM-SCF/HF (the black solid line) and (c) RISM-SCF/B3LYP (the black dashed line) and of NO₃⁻ anion by (b) RISM-SCF/HF (the red solid line) and (c) RISM-SCF/B3LYP (the red dashed line).

of total charge from -2 to -1 for the carbonate ion makes the curvature moderate. On the contrary, the changing of total charge from -1 to -2 for the nitrate anion raises the relative energies. But all of these figures still remain the similar pattern corresponding to the original FESs. These results suggest that the atomic and total charges are rather minor contributions on the peculiar properties of hydrated carbonate anion. The geometry of the anion is the parameter that emphasizes the contribution from the multipole expansion and makes the symmetry-broken structure stable.

To check the geometrical difference between the anions in detail, the distances between the central atom (carbon or nitrogen) and the center of mass are plotted as a function of the torsion angles (C- and N- torsion) in Figure 5a. All of them are linear functions, representing the similar behavior with the slightly larger slope obtained from the carbonate anion than that of the nitrate. This means that the stabilization in carbonate anion due to the shift of the central atom (C) is more greater than that of nitrate (N) because the distances ($|\mathbf{r}_k|$) are important to increase the attractive contribution according to the eq 4. However, the oxygen atoms play a more important role. The distance plots of oxygen with respect to the center of mass at the optimized geometry are shown for the carbonate (Figure 5, parts b and c) and for the nitrate (Figure 5, parts d and e) anions;

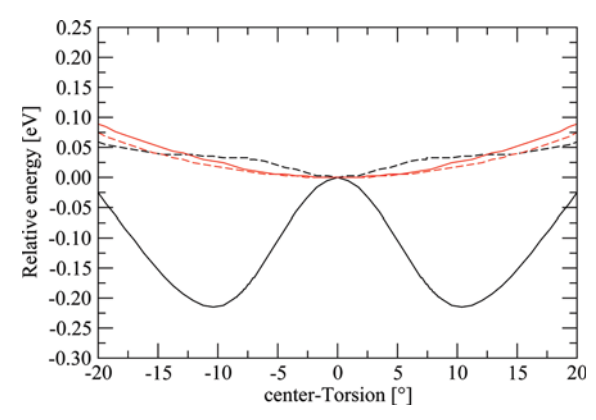


Figure 6. Orbital energy changing along the torsion. The HOMO energies are plotted with respect to the D_{3h} values: CO_3^{2-} in the gas phase (dotted black line) and in aqueous solution (solid black line) and NO₃⁻ in the gas phase (dotted red line) and in aqueous solution (solid red line).

obviously they look very different from each other. The drastic decreasing as increasing of C-O distances found in the carbonate anion around the C- torsion = 0.00° seems to be related to the character of carbonate FESs. In other words, the symmetry breaking in the carbonate is attributed to the peculiar character of the optimized geometry.

The orbital energy changing along the distortion (Walsh diagram) may provide a direct information for the present issue. Figure 6 plots the changing of the orbital energy of the highest occupied molecular orbital (HOMO) along the torsion angle. The optimized geometry in aqueous solution was adopted to plot both of the gas- and aqueous-phase values. Two nitrate curves are nondescriptive and increase as distorting from the highly symmetric geometry. However, the energy of carbonate in aqueous solution again shows a peculiar character with a minimum around 10°. It is interesting to note that the orbital energy in the gas phase monotonically increases although the same geometry was used. Hence, the above-mentioned peculiar character of the optimized geometry is attributed to the changing of orbital energy in aqueous solution. It is well-recognized that orbital energy in aqueous solution differs from the gas-phase one under the influence of the electric field from the polar solvent. Many of the deeper orbitals also show a similar trend for solvated carbonate. Presumably, the minimum is caused by an interplay between the two different contributions: one is an increasing in energy along the torsion corresponding to the gasphase behavior, the other is stabilization due to the enhancement of multipole interaction between solute and solvent.⁴⁶

Conclusion

The carbonate and nitrate anions in an aqueous solution were investigated by means of the RISM-SCF-SEDD method. The computed bond distances and RDFs show an excellent agreement with the diffraction results. 41-43 The optimized geometries of nitrate anion are in a good agreement with the experimental results, meaning that the structure retains planarity in both gas and solution phases. On the contrary, the symmetry breaking occurs in the carbonate anion in an aqueous solution from D_{3h} to $C_{3\nu}$ (or lower) losing the planarity. This phenomenon has been detected by IR and Raman spectra4 but has not been discussed in other theoretical studies. Our calculations suggest the strong anharmonicity of hydrated carbonate anion. It is important to emphasize that the symmetry is inherently broken even under the isotropic and uniform field generated by the solvent. We also employed a simple model based on the classical

electrostatic free energy calculations to clarify the effect. Although the changing of the atomic charge gives only a small effect on the profile of FESs, geometrical changing considerably affects the contribution from the multipole moments, especially the dipole moment, resulting in the main reason to break the molecular planarity of carbonate ion.

Acknowledgment. The authors express their thanks to Professor Keiji Morokuma for many helpful discussions about this work. We are also grateful to the JENESYS (Japan-East Asia Network of Exchange for Students and Youths) Programme. The Thailand Research Fund and Thailand Commission on Higher Education (MRG5280241, fellowships for V.V.) are gratefully acknowledged. The work is also financially supported in part by the Grant-in-Aid for Scientific Research on Priority Areas "Ionic Liquids" (452-20031014) and "Molecular Science of Fluctuations" (2006-21107511) as well as by the Grant-in-Aid for Scientific Research (C) (20550013).

References and Notes

- (1) Bargar, J. R.; Kubicki, J. D.; Reitmeyer, R.; Davis, J. A. Geochim. Cosmochim. Acta 2005, 69 (6), 1527-1542.
- (2) Mitchell, H. H.; Shonle, H. A.; Grindley, H. S. J. Biol. Chem. 1916, 24, 461-490.
 - (3) Benjamin, N. Ann. Zootech. 2000, 49 (3), 207-216.
- (4) Rudolph, W. W.; Fischer, D.; Irmer, G. Appl. Spectrosc. 2006, 60
- (5) Rudolph, W. W.; Irmer, G.; Königsberger, E. Dalton Trans. 2008, (7), 900-908.
- (6) Waterland, M. R.; Kelley, A. M. J. Chem. Phys. 2000, 113 (16), 6760-6773.
- (7) Wang, X.-B.; Yang, X.; Wang, L.-S.; Nicholas, J. B. J. Chem. Phys. **2002**, 116 (2), 561–570.
- (8) Chang, T. G.; Irish, D. E. *J. Phys. Chem.* **1973**, 77 (1), 52–57. (9) Zhang, Y.-H.; Choi, M. Y.; Chan, C. K. *J. Phys. Chem. A* **2004**, 108 (10), 1712-1718.
- (10) Wahab, A.; Mahiuddin, S.; Hefter, G.; Kunz, W.; Minofar, B.; Jungwirth, P. J. Phys. Chem. B 2005, 109 (50), 24108-24120.
- (11) Goebbert, D. J.; Garand, E.; Wende, T.; Bergmann, R.; Meijer, G.; Asmis, K. R.; Neumark, D. M. J. Phys. Chem. A 2009, 113 (26), 7584-
- (12) (a) Pathak, A. K.; Mukherjee, T.; Maity, D. K. J. Phys. Chem. A 2008, 112 (15), 3399-3408. (b) Pathak, A. K.; Maity, D. K. J. Phys. Chem. A 2009, 113 (48), 13443-13447.
- (13) Stefanovich, E. V.; Boldyrev, A. I.; Truong, T. N.; Simons, J. J. Phys. Chem. B **1998**, 102 (21), 4205–4208.
- (14) Archer, T. D.; Birse, S. E. A.; Dove, M. T.; Redfern, S. A. T.; Gale, J. D.; Cygan, R. T. *Phys. Chem. Miner.* **2003**, *30* (7), 416–424.
- (15) Bruneval, F.; Donadio, D.; Parrinello, M. J. Phys. Chem. B 2007, 111 (42), 12219-12227
- (16) Tommaso, D. D.; de Leeuw, N. H. J. Phys. Chem. B 2008, 112 (23), 6965-6975.
- (17) Kumar, P. P.; Kalinichev, A. G.; Kirkpatrick, R. J. J. Phys. Chem. B 2009, 113 (3), 794-802.
- (18) Ebner, C.; Sansone, R.; Hengrasmee, S.; Probst, M. Int. J. Quantum Chem. 1999, 75 (4-5), 805-814.
- (19) Tongraar, A.; Tangkawanwanit, P.; Rode, B. M. J. Phys. Chem. A **2006**, 110 (47), 12918–12926.
- (20) Ten-no, S.; Hirata, F.; Kato, S. Chem. Phys. Lett. 1993, 214 (3-4), 391-396.
- (21) Ten-no, S.; Hirata, F.; Kato, S. J. Chem. Phys. 1994, 100 (10), 7443-7453
- (22) Sato, H.; Hirata, F.; Kato, S. J. Chem. Phys. 1996, 105 (4), 1546-1551.
- (23) Yokogawa, D.; Sato, H.; Sakaki, S. J. Chem. Phys. 2007, 126 (24), 244504.
- (24) Yoshida, N.; Ishizuka, R.; Sato, H.; Hirata, F. J. Phys. Chem. B 2006, 110 (16), 8451-8458.
 - (25) Sato, H.; Hirata, F. J. Phys. Chem. A 1998, 102 (15), 2603-2608. (26) Sato, H.; Hirata, F. J. Mol. Struct. (THEOCHEM) 1999, 461-462,
- (27) Sato, H.; Sakaki, S. J. Phys. Chem. A 2004, 108 (9), 1629-1634. (28) Iida, K.; Yokogawa, D.; Sato, H.; Sakaki, S. Chem. Phys. Lett. **2007**, *443* (4-6), 264–268.
- (29) Hayaki, S.; Yokogawa, D.; Sato, H.; Sakaki, S. Chem. Phys. Lett. **2008**, 458 (4-6), 329-332.

- (30) Sato, H.; Hirata, F.; Myers, A. B. J. Phys. Chem. A 1998, 102 (11), 2065–2071.
 - (31) Kirkwood, J. G. J. Chem. Phys. 1934, 2 (7), 351-361.
- (32) Kirkwood, J. G.; Westheimer, F. H. J. Chem. Phys. 1938, 6 (9), 506–512.
- (33) Kovalenko, A.; Hirata, F. J. Chem. Phys. 1999, 110 (20), 10095–10112.
- (34) Kovalenko, A.; Hirata, F. Chem. Phys. Lett. 2001, 349 (5-6), 496-502.
- (35) Krishnan, R.; Binkley, J. S.; Seeger, R.; Pople, J. A. J. Chem. Phys. 1980, 72 (1), 650–654.
- (36) Clark, T.; Chandrasekhar, J.; Spitznagel, G. W.; Schleyer, P. V. R. *J. Comput. Chem.* **1983**, *4* (3), 294–301.
- (37) Berendsen, H. J. C.; Postma, J. P. M.; van Gunsteren, W. F.; Hermans, J. In *Intermolecular Forces*; Pullman, B., Ed.; Reidel Publishing Company: Boston, MA, 1981; pp 331–342.
- (38) Weiner, S. J.; Kollman, P. A.; Case, D. A.; Singh, U. C.; Ghio, C.; Alagona, G.; Profeta, S.; Weiner, P. J. Am. Chem. Soc. **1984**, 106 (3), 765–784.
- (39) Weiner, S. J.; Kollman, P. A.; Nguyen, D. T.; Case, D. A. *J. Comput. Chem.* **1986**, *7* (2), 230–252.
- (40) Schmidt, M. W.; Baldridge, K. K.; Boatz, J. A.; Elbert, S. T.; Gordon, M. S.; Jensen, J. H.; Koseki, S.; Matsunaga, N.; Nguyen, K. A.; Su, S.; Windus, T. L.; Dupuis, M.; Montgomery, J. A., Jr. *J. Comput. Chem.* **1993**, *14* (11), 1347–1363.
- (41) Kameda, Y.; Sasaki, M.; Hino, S.; Amo, Y.; Usuki, T. *Physica B (Amsterdam, Neth.)* **2006**, *385–386* (Part 1), 279–281.

- (42) Megyes, T.; Bálint, S.; Peter, E.; Grósz, T.; Bakó, I.; Krienke, H.; Bellissent-Funel, M.-C. *J. Phys. Chem. B* **2009**, *113* (13), 4054–4064.
- (43) Mason, P. E.; Neilson, G. W.; Dempsey, C. E.; Brady, J. W. J. Am. Chem. Soc. 2006, 128 (47), 15136–15144.
- (44) Gill, P. M. W.; Johnson, B. G.; Pople, J. A.; Taylor, S. W. J. Chem. Phys. **1992**, 96 (9), 7178–7179.
- (45) Frisch, M. J.; Trucks, G. W.; Schlegel, H. B.; Scuseria, G. E.; Robb, M. A.; Cheeseman, J. R.; Montgomery, J. A., Jr.; Vreven, T.; Kudin, K. N.; Burant, J. C.; Millam, J. M.; Iyengar, S. S.; Tomasi, J. J.; Barone, V.; Mennucci, B.; Cossi, M.; Scalmani, G.; Rega, N.; Petersson, G. A.; Nakatsuji, H.; Hada, M.; Ehara, M.; Toyota, K.; Fukuda, R.; Hasegawa, J.; Ishida, M.; Nakajima, T.; Honda, Y.; Kitao, O.; Nakai, H.; Klene, M.; Li, X.; Knox, J. E.; Hratchian, H. P.; Cross, J. B.; Adamo, C.; Jaramillo, J.; Gomperts, R.; Stratmann, R. E.; Yazyev, O.; Austin, A. J.; Cammi, R.; Pomelli, C.; Ochterski, J. W.; Ayala, P. Y.; Morokuma, K.; Voth, A.; Salvador, P.; Dannenberg, J. J.; Zakrzewski, V. G.; Dapprich, S.; Daniels, A. D.; Strain, M. C.; Farkas, O.; Malick, D. K.; Rabuck, A. D.; Raghavachari, K.; Foresman, J. B.; Ortiz, J. V.; Cui, Q.; Baboul, A. G.; Clifford, S.; Cioslowski, J.; Stefanov, B. B.; Liu, G.; Liashenko, A.; Piskorz, P.; Komaromi, I.; Martin, R. L.; Fox, D. J.; Keith, T.; Al-Laham, M. A.; Peng, C. Y.; Nanayakkara, A.; Challacombe, M.; Gill, P. M. W.; Johnson, B.; Chen, W.; Wong, M. W.; Gonzalez, C.; Pople, J. A. Gaussian 03, revision D.02; Gaussian Inc.: Wallingford, CT, 2004.
 - (46) Iida, K.; Sato, H.; Sakaki, S. J. Chem. Phys. 2009, 130, 044107.

JP101700D

Structural and Dynamical Properties and Vibrational Spectra of Bisulfate Ion in Water: A Study by *Ab Initio* Quantum Mechanical Charge Field Molecular Dynamics

Viwat Vchirawongkwin,**[†] Chinapong Kritayakornupong,[‡] and Bernd M. Rode[§]

Department of Chemistry, Faculty of Science, Chulalongkorn University, Phayathai Road, Patumwan, Bangkok 10330, Thailand, Department of Chemistry, Faculty of Science, King Mongkut's University of Technology Thonburi, Bangkok 10140, Thailand, and Theoretical Chemistry Division, Institute of General, Inorganic and Theoretical Chemistry, University of Innsbruck, Innrain 52a, A-6020 Innsbruck, Austria

Received: June 6, 2010; Revised Manuscript Received: August 2, 2010

The *ab initio* quantum mechanical charge field molecular dynamics (QMCF MD) formalism was applied to simulate the bisulfate ion, HSO_4^- , in aqueous solution. The averaged geometry of bisulfate ion supports the separation of six normal modes of the O^*-SO_3 unit with C_{3v} symmetry from three modes of the OH group in the evaluation of vibrational spectra obtained from the velocity autocorrelation functions (VACFs) with subsequent normal coordinate analyses. The calculated frequencies are in good agreement with the observations in Raman and IR experiments. The difference of the averaged coordination number obtained for the whole molecule (8.0) and the summation over coordinating sites (10.9) indicates some water molecules to be located in the overlapping volumes of individual hydration spheres. The averaged number of hydrogen bonds (H-bonds) during the simulation period (5.8) indicates that some water molecules are situated in the molecular hydration shell with an unsuitable orientation to form a hydrogen bond with the ion. The mean residence time in the surroundings of the bisulfate ion classify it generally as a weak structure-making ion, but the analysis of the individual sites reveals a more complex behavior of them, in particular a strong interaction with a water molecule at the hydrogen site.

Introduction

Bisulfate ion is produced by the first deprotonation of sulfuric acid, playing an important role to form hygroscopic aerosols in the atmosphere. 1-4 The vibrational spectra of bisulfate ion were investigated by in situ Fourier transform infrared (FTIR) spectroscopy of molecular adsorption on the surface of Pt single crystal electrodes,⁵ producing anomalous peaks from the adsorption and desorption of submonolayers of strongly bound hydrogen.^{6,7} The fundamental vibrational frequencies of HSO₄⁻ ion were also assigned within the infrared spectra of concentrated solution in the spectral region of 600-1500 cm^{-1.8} The Raman studies of aqueous NH4HSO4 solutions over a broad concentration and temperature range indicate that the bisulfate ion is the dominant species above 250 °C and possesses $C_{3\nu}$ symmetry in dilute solutions.^{9,10} The phase diagram for the NH₄HSO₄/H₂O system presented a low-temperature crystalline phase composed of NH₄HSO₄ with eight water molecules.¹¹ Although the properties of bisulfate ion have been investigated in many experiments, most theoretical treatments were only interested in the system of hydrated sulfuric acid. 12-17 This motivated our interest to investigate the vibrational spectra and the structural and dynamical properties for the HSO₄⁻ ion and its hydration shell in aqueous solution.

The specific investigation of an aqueous bisulfate system is difficult by experiment, due to a mixture of sulfate and hydronium ions produced by the second dissociation of sulfuric acid. Computer simulations have become an alternative tool to gain access to solvate microspecies properties needed for the

interpretation of experimental observations and the chemical behavior. The structural and dynamical properties of hydrated bisulfate ion are of great significance for the detailed understanding of all chemical processes of this ion in aqueous solution. However, the bisulfate ion is a composite structure difficult to access by a conventional QM/MM method, because of the complicated and asymmetric potential energy hypersurface describing the interaction between the HSO₄⁻ ion and water. An ab initio quantum mechanical charge field molecular dynamics (QMCF MD) formalism, 18,19 however, does not require an analytical solute-solvent potential, and hence, this method has already been successfully employed to investigate the structural and dynamical properties of the hydrated sulfate, 20,21 phosphate,^{22,23} perchlorate,^{22,24} and bicarbonate^{25,26} anions. In this work, the QMCF MD method was used to simulate the hydrated HSO_4^- ion in order to obtain its structure and some dynamical properties, and also the vibrational spectra of all normal modes evaluated by means of the velocity autocorrelation functions (VACFs). The structural properties for each hydration site and the overall molecular shell were obtained via radial distribution functions (RDFs), coordination number distributions (CNDs), and angular distribution functions (ADFs). The dynamics were characterized by means of ligand mean residence times (MRTs). We also evaluated structural and dynamical properties by means of the molecular approach equivalent to the "solventaccessible surface" referred to in previous work.25

Methods

The *ab initio* quantum mechanical charge field molecular dynamics (QMCF MD) formalism has been outlined in detail elsewhere. ^{18,19} Due to the inclusion of an additional quantum mechanically treated solvent *layer zone* located beyond the first hydration shell of the solute species, the QMCF method does

 $[\]mbox{\ensuremath{^{\ast}}}$ To whom correspondence should be addressed. E-mail: Viwat.V@ Chula.ac.th.

[†] Chulalongkorn University.

^{*} King Mongkut's University of Technology Thonburi.

[§] University of Innsbruck.

not require the construction of potential functions between the solute and water molecules; i.e., it avoids a time-consuming and sometimes hardly manageable task necessary in the conventional quantum mechanical/molecular mechanical molecular dynamics (QM/MM MD) formalism.^{27–30} A further advantage of the QMCF MD method is the inclusion of the point charges of the atoms in the MM region with their changing positions in the core Hamiltonian for the QM region via a perturbation term

$$V' = \sum_{i=1}^{n} \sum_{j=1}^{m} \frac{q_j^{\text{MM}}}{r_{ij}}$$
 (1)

where n is the number of atoms in the QM region, m is the number of atoms in the MM region, $q_j^{\rm MM}$ is the partial charges of these atoms according to the selected water model, and r_{ij} refers to the distance between a pair of particles in the QM (i) and MM (j) regions. On the other hand, the dynamically changing charges of QM particles, $q_i^{\rm QM}$, determined by population analysis contribute to the force on each atom j in the MM region as Coulombic forces

$$F_j^{\text{QM} \to \text{MM}} = \sum_{i=1}^n \frac{q_i^{\text{QM}} \cdot q_j^{\text{MM}}}{r_{ij}}$$
 (2)

As the conventional QM/MM MD formalism, the QMCF MD method allows the migration of water molecules between the QM and MM region. For this process, one has to apply a smoothing function³¹

$$S(r) = \begin{cases} 0 & \text{for } r > r_{\text{on}} \\ \frac{(r_{\text{off}}^2 - r^2)^2 (r_{\text{off}}^2 + 2r^2 - 3r_{\text{on}}^2)}{(r_{\text{off}}^2 - r_{\text{on}}^2)^3} & \text{for } r_{\text{on}} \le r \le r_{\text{off}} \end{cases}$$
(3)

where r is the distance of a given solvent molecule from the center of the simulation box, $r_{\rm off}$ is the radius of the QM region, and $r_{\rm on}$ is the inner border of the smoothing region. The formalism is applied to all atoms of molecules located in the smoothing region, ensuring a continuous transition and change of forces for these molecules according to

$$F_j^{\text{smooth}} = F_j^{\text{MM}} + (F_j^{\text{layer}} - F_j^{\text{MM}}) \times S(r)$$
 (4)

where $F_j^{\rm layer}$ is the force acting on a particle j located in the (outer QM) smoothing zone and $F_j^{\rm MM}$ is the force acting on a particle j in the MM region. In this context, it has to be mentioned that energy is not rigorously conserved, but the related error can be considered very minor due to the short simulation time and the large size of the quantum mechanical region.

The bisulfate solution consisted of one bisulfate ion and 496 water molecules in a cubic box of 24.67 Å with the periodic boundary condition. The density of the simulation box was 0.997 g cm⁻³, i.e., the experimental value of pure water at 298 K. The simulation was performed in the *NVT* ensemble using a general predictor-corrector algorithm with a time step of 0.2 fs. The system temperature was maintained at 298.16 K by the

Berendsen temperature-scaling algorithm³² with a relaxation time of 100 fs. The QM subregions, namely, the core and layer zone, extended to 3.5 and 6.0 Å, respectively. The quantum mechanical calculation was performed by means of the Hartree-Fock (HF) method with the Dunning double-ζ plus polarization (DZP)^{33,34} basis sets for hydrogen, sulfur, and oxygen atoms in the QM region, i.e., the same theoretical level employed in our previous study of the hydrated sulfate ion.20 The thickness of the smoothing region was chosen as 0.2 Å with the values of $r_{\rm on}$ and $r_{\rm off}$ as 5.8 and 6.0 Å, respectively, according to the radial distribution function (RDF) obtained from the equilibrated simulation. The selected water model applied to calculate the interactions between pairs of water in the MM region was the flexible BJH-CF2 model, 35,36 with cutoff distances of 3.0 and 5.0 Å for non-Coulombic interactions between H atoms and between O and H atoms, respectively. The partial charges for oxygen and hydrogen atoms in the water molecule according to the BJH-CF2 model are -0.65966 and +0.32983. This water model supports the fully flexible molecular geometries of water molecules transiting between the QM and MM region. The Coulombic interactions between the Mulliken charges on the atoms within the QM region and the point charges of water molecules according to the BJH-CF2 model are evaluated providing an electrostatic description by a dynamically charging field of point charges, which change according to the movements of atoms inside the OM region and water molecules in the MM region in the course of the simulation. This ensures the continuous adaptation of the Coulombic interactions to all polarization and charge-transfer effects within solute and surrounding solvent layers. 18,19 In addition, the reaction field method combined with the shifted-force potential technique were applied to account for long-range electrostatic potentials and forces, with a spherical cutoff limit of 12.350 Å. The system was equilibrated with the QMCF MD method for 50 000 steps (10 ps), and a further 50 000 steps (10 ps) were collected as data sampling for analyzing the structural and dynamical properties. On average, 24.8 water molecules were present in the OM region.

The structural and dynamical properties for the hydration shell of HSO₄⁻ ion were not only evaluated for individual atoms but also in a molecular manner. The molecular hydration shell of bisulfate ion was constructed by the combination of all atomic hydration spheres of the ion. The coordinating site for each water molecule to the bisulfate ion was defined by searching for the shortest distance between the oxygen atom of the water molecule and each atom within the ion.²⁵ The molecular radial distribution functions (RDFs), molecular coordination number distributions (CNDs), and molecular ligand mean residence times (MRTs) for the hydration shell of bisulfate ion are thus presented in this Article. All MRT values were evaluated by the direct method,37 counting the water exchange processes between hydration shell and bulk. The most appropriate time span to record a water displacement from its original coordination sphere as an exchange process is 0.5 ps, ^{37,38} which corresponds to the average lifetime of a hydrogen bond in the solvent.³⁹

The dynamical properties of a fluid system related to macroscopic transport coefficients can be evaluated from the velocity autocorrelation functions (VACFs), and their Fourier transformations can be interpreted as the vibrational spectra. The vibrational spectra of bisulfate ion were obtained from the VACFs using normal-coordinate analysis. 40 The normalized VACF, C(t), is defined as

$$C(t) = \frac{\sum_{i}^{N_{t}} \sum_{j}^{N} \nu_{j}(t_{i})\nu_{j}(t_{i} + t)}{N_{t}N \sum_{i}^{N_{t}} \sum_{j}^{N} \nu_{j}(t_{i})\nu_{j}(t_{i})}$$
(5)

where N is the number of particles, N_t is the number of time origins t_i , and v_j denotes a certain velocity component of the particle j. A correlation length of 2.0 ps was used to obtain the power spectra with 4000 averaged time origins.

Results and Discussion

Structural and Dynamical Properties of HSO₄⁻ Ion. Due to the dynamic motion of all atoms within the system during the simulation period, all structural parameters such as bonds, angles, and dihedral angles within the bisulfate ion required to construct the geometry of the ion were collected with their statistical deviation listed in Table 1. The averaged geometry of HSO₄ ion constructed from the structural parameters in Table 1 is shown in Figure 1. The average S=O distances vary within 0.070 Å and are slightly shorter than those in the SO₄²⁻ ion²⁰ by 0.02 Å, while the single bond of S to O(4) is significantly longer with 1.585 Å. The average O-H distance of 0.975 Å for the HSO₄⁻ ion is slightly longer than the distance of the analogous bond in the HCO_3^- ion²⁵ by ~ 0.02 Å. The bond and dihedral angles were collected in the form of angular distribution functions (ADFs). The average bond angles around the sulfur atom again indicate the similarity of terminal oxygens and the unique property of O(4). In contrast to the strong flexibility of the $\angle CO(3)H$ angle of the HCO_3^- ion,²⁵ the ∠SO(4)H ADF shows a deviation of only 9°. Our selected theoretical level, HF/DZP, for the QMCF MD simulation was validated by comparing the structural parameters with those obtained from various methods evaluated in the gas phase and solution using the polarizable continuum model (PCM).⁴² The hybrid B3LYP exchange-correlation functional coupling with the tzvp+ basis set⁴³ was employed to verify the interpretation of the spectra of photoelectron spectroscopy for the HSO₄⁻ ion;⁴¹ thus, we also utilized this basis set coupling with the Hartree-Fock (HF), B3LYP, and quadratic CI calculation including single and double substitutions (QCISD) levels to optimized the geometry of HSO₄⁻ in both phases. The HF/DZP level was also performed to investigate the effect of isotropic and uniform field generated by the PCM to the geometry of HSO₄⁻ ion. All optimized geometries in gas and solution phase were found to have C_s symmetry. The effect of PCM on the geometry of HSO₄⁻ ion presents slightly longer bonds of terminated oxygen and O(4)-H bond, and a slightly shorter S-O(4) bond. The structural parameters obtained from the QMCF MD simulation show a similar changing pattern to the PCM model but presenting a slightly stronger effect of explicit water molecules on the HSO₄⁻ ion compared with the HF/DZP results. Due to the fact that the structural parameters from the QCISD/tzvp+ optimization are within the deviation of those obtained from the QMCF MD simulation, this presents a suitability of the HF/DZP level to investigate the structural and dynamical properties of hydrated HSO₄⁻ ion.

The dihedral angle measured between the plane defined by the O(4)-S-O(1) and the hydrogen atom is one of the interesting structural characteristics, with a large deviation as shown in Table 1. The distribution of this angle within the simulation period is presented in Figure 2, showing a broad band with a main peak situated at 60° and an average dihedral

angle of 40°. This angle distribution represents the ease of rotation for the hydrogen atom around the S–O(4) bond. This result agrees with the experimental result of a free rotation of OH group, treating the bisulfate ion with the C_{3v} symmetry. ^{9,10} We also utilized this approximation to separate three modes of the OH group, namely, O–H stretching (ν (OH)), S–O–H bending (ν (OH)), and S–O–H torsional (ν (OH)), from nine normal modes of the O*–SO₃ unit. The nine normal modes of the O*–SO₃ unit in ν 0 symmetry will span the following representation:

$$\Gamma(C_{3v}) = 3a_1(R, ir) + 3e(R, ir)$$
 (6)

In the Raman and infrared spectra under C_{3v} symmetry, the spectra will be predicted as only six bands, three of them becoming doubly degenerate modes. The power spectra of these normal modes for the HSO₄⁻ ion predicted by the QMCF MD simulation are displayed in Figure 3, and the frequencies of peaks for each mode are listed in Table 2. The v_1 and v_3 modes seemed to identify the characteristic of the O*-SO3 unit in the HSO₄ ion when it was investigated by Raman and IR experiments. 8-10 The calculated frequencies of these modes are in good agreement with the experimental data, again showing the reliability of QMCF MD simulation analyzing via VACFs the vibration modes of the solute. 21,26,44,45 It is interesting that the peak at 593 cm^{-1 8} was only assigned as a characteristic frequency of HSO₄⁻ ion by Miller et al.⁴⁶ The peak of our calculation for the δ_6 mode located at 603 cm⁻¹ corresponds to the observed data, 8,46 and hence, we assigned this mode to the characteristic frequency of HSO₄⁻ ion found in the cesium bromide region. 46 We also classified the frequency at 1341 cm⁻¹ reported by Walrafen et al. as δ_4 , as the other two totally symmetric (a_1) modes at 1050 and 885 cm⁻¹ were identified as the ν_1 and ν_3 modes, respectively. However, the peak of the δ_4 mode calculated by our VACF method at 635 cm⁻¹ agrees with the assignment by Dawson et al. for this mode at 585 $cm^{-1}.10$

Our calculated spectra for the OH group present very broad bands, as shown in Figure 3B. The power spectrum of the $\nu(OH)$ mode also presents the frequency band coinciding with the the δ (OH) mode, due to the different orientation of the O-H bond for each time origin included in the evaluation of the $\nu(OH)$ mode producing the mixed modes. By our vector projection, the frequency bands of the $\nu(OH)$, $\delta(OH)$, and $\gamma(OH)$ modes are found in the region of 2573-4039, 1075-1645, and 179-928 cm⁻¹, respectively. The $\nu(OH)$ mode shows the highest peak as a strong band at 3795 cm⁻¹ and a weak band in the region 2573-3339 cm⁻¹ in agreement with the assignment by the experiments.^{8,10} The $\delta(OH)$ mode again is identified as characteristic of the OH group by the Raman and IR investigations, 8-10 and our calculated band with the peak at 1384 cm⁻¹ for this mode is in good agreement with that. The projection of H's velocities onto a unit vector perpendicular to the S-O(4)-H plane for the γ (OH) mode presents two bands with peaks at 179 and 733 cm⁻¹ for a weak and a strong band, respectively; this corresponds well with the assignment by Walrafen et al.8

The self-diffusion coefficient (D) of bisulfate ion was calculated from the center-of-mass VACF using the Green-Kubo relation⁴⁷

$$D = \frac{1}{3} \lim_{t \to \infty} \int_0^t C(t) \, \mathrm{d}t \tag{7}$$

		HF/	DZP	HF/t	zvp+	B3LY	P/tzvp+	QCISD/tzvp+	
structural parameter	QMCF MD	gas	PCM	gas	PCM	gas ⁴¹	PCM	gas	PCM
S-O(1) (Å)	1.453 ± 0.062	1.441	1.444	1.446	1.449	1.483	1.485	1.477	1.479
S-O(2) (Å)	1.455 ± 0.064	1.432	1.440	1.436	1.445	1.473	1.480	1.467	1.475
S-O(3) (Å)	1.454 ± 0.067	1.441	1.444	1.446	1.449	1.483	1.485	1.477	1.479
S - O(4) (Å)	1.585 ± 0.076	1.619	1.579	1.626	1.585	1.709	1.655	1.682	1.635
O(4)—H (Å)	0.975 ± 0.064	0.946	0.969	0.947	0.970	0.968	0.993	0.969	0.993
$\angle O(1)SO(2)$ (deg)	113 ± 7	115	114	115	114	116	114	116	114
$\angle O(1)SO(3)$ (deg)	113 ± 7	113	113	113	113	114	113	114	113
$\angle O(1)SO(4)$ (deg)	106 ± 7	104	106	104	106	104	106	104	106
\angle SO(4)H (deg)	113 ± 9	108	112	107	110	104	108	104	108
O(3)SO(1)O(2) dihedral (deg)	-131 ± 7	-136	-132	-136	-132	-137	-133	-137	-133
O(4)SO(1)O(2) dihedral (deg)	114 ± 8	112	112	112	112	110	111	110	111

60

59

60

60

TABLE 1: Structural Parameters for the Geometry of HSO₄⁻ Ion Obtained from the Averaging of Their Distributions with Their Variations

The calculated D value obtained from the QMCF MD simulation is 1.584×10^{-5} cm 2 s $^{-1}$, which is in good agreement with the experimental value of 1.385×10^{-5} cm 2 s $^{-1}$.⁴⁸ This again presents the success of the QMCF MD formalism to acquire the dynamical properties of hydrated composite solute.

 40 ± 49

59

HO(4)SO(1) dihedral (deg)

Structural and Dynamical Properties of the Hydration Shell. With the QM radius of 6.0 Å, the average number of solvent molecules inside this region was 24.8 ± 6.3 , during the simulation period. The coordinating sites of bisulfate ion consist of five atoms, namely, O(1) to O(4) and H, interacting with water molecules, and thus producing the hydration shell around this molecular solute. The structural property for each site was first evaluated by means of the radial distribution functions

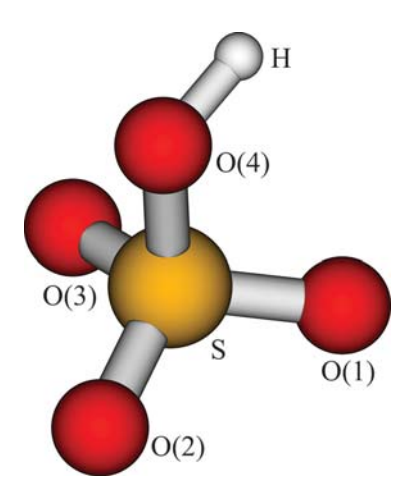


Figure 1. The averaged geometry of HSO_4^- ion constructed from the structural parameters of QMCF MD simulation presenting with the labels.

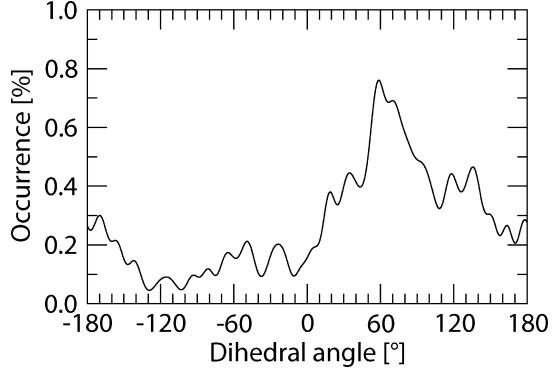


Figure 2. The distribution of H-O(4)-S-O(1) dihedral angle.

(RDFs) shown in Figure 4. The maximum and minimum distances of the hydration shell for each coordinating site obtained from the (site)-O_{water} and (site)-H_{water} are listed in Table 3. The shorter distances of a maximum and minimum for each O_s-H_{water} RDF compared to each related O_s-O_{water} RDF correspond to the orientation of water molecules pointing with hydrogen to the coordinating oxygens. Although the geometry analysis in the previous section has shown that the S-O bonds for the terminal oxygens O(1) to O(3) are almost identical, the hydration shells for each site present a different structure reflected by some variations of maximal and minimal distances in their RDFs. The RDFs of the hydration shell of O(2) represent a slightly more compact structure than those of the other two sites. With respect to the averaged geometry of HSO₄⁻ ion (see Figure 1), the O(2) site is far from the hydrogen atom so that the water molecules can hydrate this site with less perturbation from the hydrogen atom. The RDFs of O(4) atom show a more flexible hydration shell than the terminal oxygens,

60

59

60

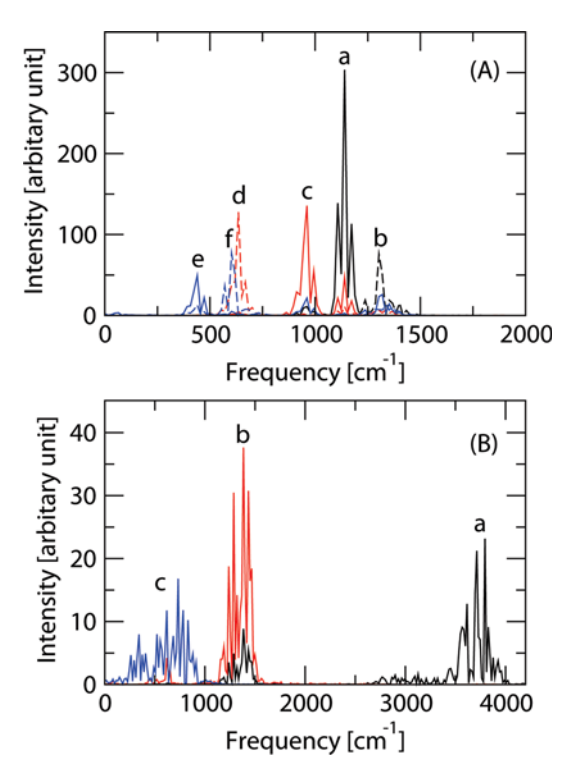


Figure 3. Power spectra of (A) the O* $-SO_3$ unit consisting of (a) ν_1 , (b) ν_2 , (c) ν_3 , (d) δ_4 , (e) δ_5 , and (f) δ_6 modes and (B) three modes for the OH group consisting of (a) ν (OH), (b) δ (OH), and (c) γ (OH) modes.

TABLE 2: Vibration Frequencies (cm⁻¹) of Highest Peak for Each Normal Mode of HSO_4^- Ion Evaluated by the VACFs of OMCF MD Simulation, Given as Values Scaled by the Factor 0.902²¹ in Parentheses

vibration mode	QMCF MD	Raman and IR
v_1 symmetric SO ₃ stretch, a_1	1140 (1028)	1050, ^a 1052, ^b 1050 ^c
v_2 asymmetric SO ₃ stretch, e	1303 (1175)	1191, ^a 1230 ^c
v_3 S $-$ (OH) stretch, a_1	961 (867)	899, ^a 898, ^b 885 ^c
δ_4 symmetric SO ₃ deformation, a_1	635 (573)	585, ^a 1341 ^c
δ_5 asymmetric SO ₃ deformation, e	440 (397)	422, ^a 417 ^c
δ_6 SO ₂ bending, e	603 (544)	593 ^c
ν (OH)	3795 (3423)	2900, ^a 3000 ^c
δ (OH)	1384 (1248)	1340, ^a 1240, ^b 1175–1250, ^c 1800 ^c
$\gamma(OH)$	733 (661)	$675 - 740^{\circ}$

 a Raman data of 3.8 mol kg $^{-1}$ NH $_4$ HSO $_4$ solution at 25 $^{\circ}$ C. 10 b Raman data of 0.876 mol kg $^{-1}$ NH $_4$ HSO $_4$ solution at 22 $^{\circ}$ C. 9 c IR data of concentrated aqueous solutions of sulfuric acid in the region 290-4000 cm⁻¹.

indicated by the flat shape and lower maximum of the O(4)—H_{water} RDF in the region assigned as hydration shell. The RDFs of H atom indicate the direction of the oxygen atom of water pointing to this site, and represent a well-defined structure by a strong peak in the H-O_{water} RDF.

The distances of the minima for each (site)—O_{water} RDF were employed to evaluate the coordination number distribution (CND) for the sites, as shown in Figure 5. Their averaged coordination numbers are also listed in Table 3 in the last column. The O(2) atom located in the far position from the hydrogen atom has the smallest coordination number among the oxygens and a significantly large average CND of O(3), again illustrating the different hydration structure for these oxygen atoms. The reasons for small deviations of the coordination numbers of the three terminated oxygen atoms are to be seen in slight deviations from the C_{3v} symmetry in the course of the simulation and the short sampling time, which would not cover sufficient orientations to include all possible configurations. Hence, the difference of 0.3 water molecules cannot be considered statistically significant. The actual effect of water molecules to each oxygen site requires further details as the average number of H-bonds, presented with the following analysis. The minimum of the O(4)-O_{water} RDF at 3.46 Å utilized to evaluate its CND also includes a part of the hydration shell of hydrogen atom. This leads to an overcounting of the coordination number for the composite molecular solute. 20,25 To clarify this problem, we again evaluated the RDF and CND for the molecular structure employing the distances of minimum for each (site)-Owater RDF as the criterion to assign the coordinating site for each water molecule shown in Figure 6. The characteristic values of molecular hydration shell and its averaged coordination number obtained from the molecular surface-water RDFs and CND are also listed in Table 3 in the last row.

The surface-O_{water} RDF presents two peaks at 1.80 and 2.90 Å in the region of 0.00-3.72 Å, corresponding to the hydration spheres of hydrogen and all oxygen atoms. The peak of O_s-O_{water} within the molecular RDF is well-defined and stronger than that in the individual O_s-O_{water} RDFs, representing more water molecules confined in the molecular hydration shell than those in the individual hydration spheres. However, the total average coordination number of 10.9 for all individual sites is larger than the average coordination number of 8.0 for the

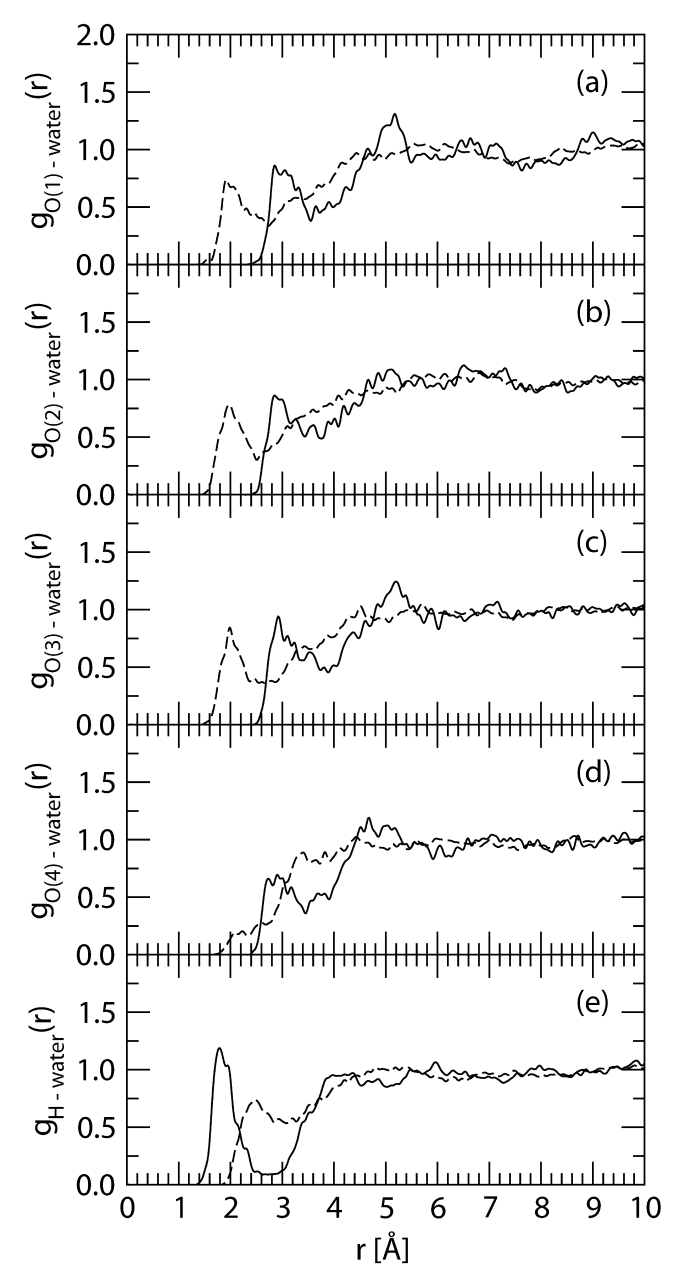


Figure 4. RDF plots of (a) O(1)-water, (b) O(2)-water, (c) O(3)—water, (d) O(4)—water, and (e) H—water; solid and dashed lines refer to the RDFs for the O and H atoms of water, respectively.

TABLE 3: Characteristic Values of the Radial Distribution Function $g_{\alpha\beta}(r)$ for Each Site of HSO_4^- Ion in the Hydration Shell Determined by the QMCF MD Simulation

coordinating site	$r_{\max}(O_{\mathrm{w}})^a$	$r_{\min}(O_{\mathrm{w}})^a$	$r_{\rm max}(H_{\rm w})^a$	$r_{\min}(H_{\mathrm{w}})^a$	n^a
O(1)	2.86	3.56	1.92	2.72	2.4
O(2)	2.86	3.44	1.98	2.52	2.1
O(3)	2.92	3.88	1.98	2.68	3.5
O(4)	2.90	3.46	2.22	3.34	1.9
Н	1.78	2.64	2.48	3.08	1.0
surface	1.80, 2.90	2.42, 3.72	2.10	3.72	8.0

 $^{^{}a}$ $r_{
m max}$ and $r_{
m min}$ are the distances of the maximum and minimum of $g_{\alpha\beta}(r)$ for the hydration shell in Å, and n is the averaged coordination number of the shell, respectively.

molecular hydration shell, showing an overcounting of \sim 3 water molecules, due to the overlap of individual hydration spheres as observed also in the hydration structures of sulfate20 and bicarbonate²⁵ ions.

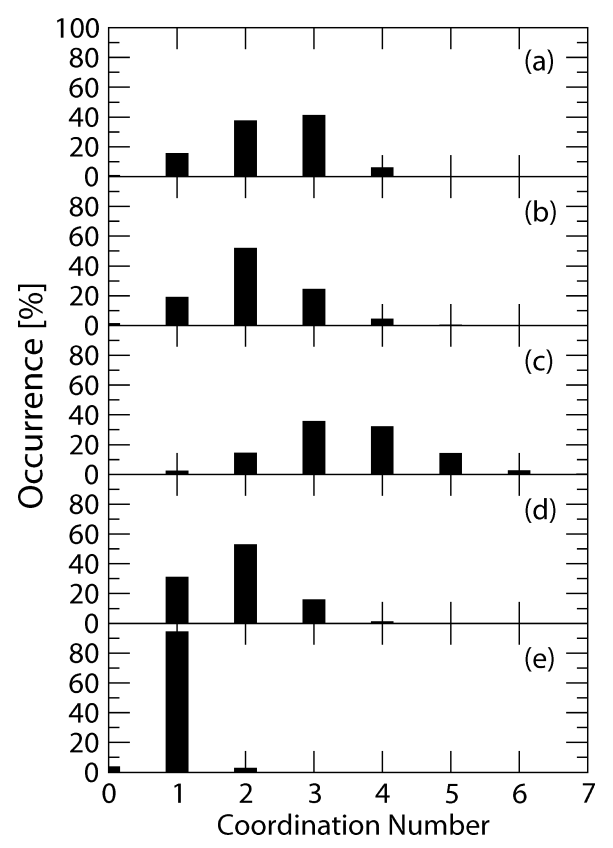


Figure 5. Hydration shell coordination number distributions of (a) O(1), (b) O(2), (c) O(3), (d) O(4), and (e) H atom of bisulfate ion.

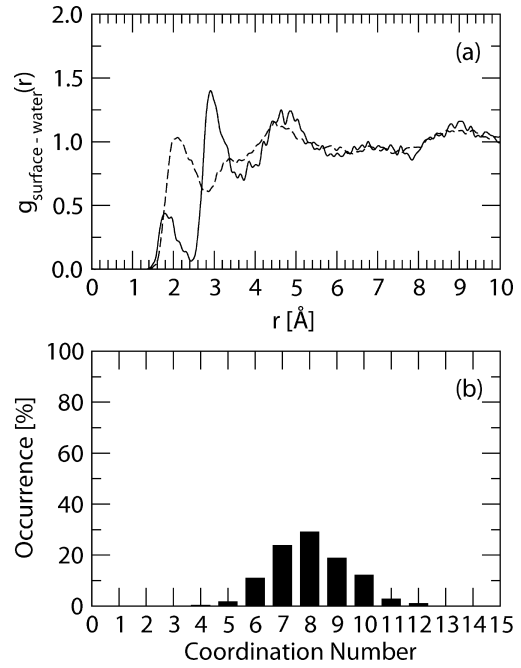


Figure 6. (a) Molecular RDF plots of HSO_4^- ion obtained from the QMCF MD simulation evaluated by means of the combination of spheres; solid and dashed lines refer to the RDFs for the O and H atoms of water, respectively. (b) The molecular hydration shell coordination number distribution of the HSO_4^- ion.

The orientation of water molecules in the individual hydration spheres was investigated by means of the angular distribution function (ADF) of $O_w-H_w\cdots$ (site) angles, shown in Figure 7. These ADFs show a similar pattern with two peaks located at ca. 60 and 160°, corresponding to the two hydrogens of

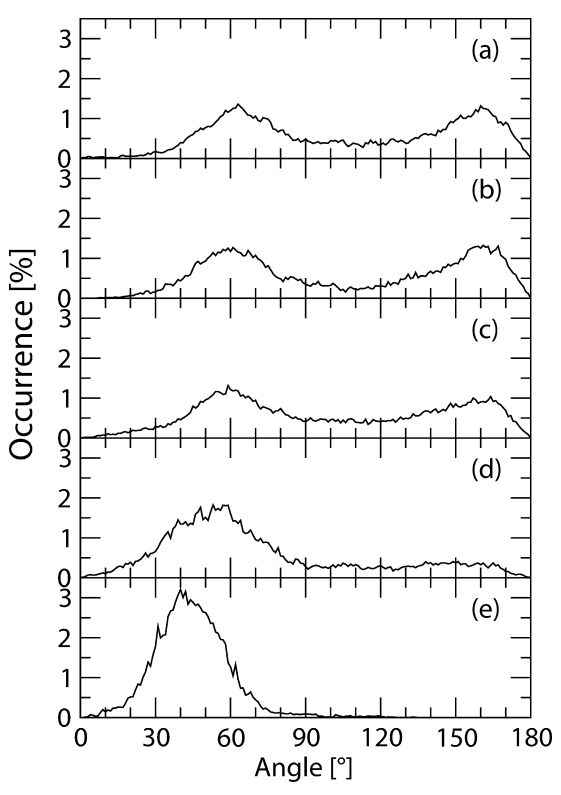


Figure 7. O_w - H_w -···(site) ADFs for (a) O(1), (b) O(2), (c) O(3), (d) O(4), and (e) H atom of HSO_4^- ion.

hydrating water molecules. The H_{water} atom pointing to the terminal oxygen sites is represented by the large angles. The ADF of O(4) displays a different orientation of hydrating water molecules with a high probability of small angles and very low probability of large angles, indicating that most of the H_{water} atoms do not point to this site.

According to the dynamical movements of all atoms within the system, the number of H-bonds between the bisulfate ion and the hydrating water molecules fluctuates during the simulation period. Since the definition of H-bond has been expressed in two different ways, namely, an energetic and a geometric criterion, 49,50 we utilized the structural criterion depending on the cutoff parameters (distances $R_{\rm HO}^{\rm (c)}$ and $R_{\rm OO}^{\rm (c)}$ and angle $\phi^{\rm (c)}$) in analogy to water-dimethyl sulfoxide mixtures⁵¹ and hydrated bicarbonate ion. ²⁶ The cutoff distances $R_{HO}^{(c)}$ and $R_{OO}^{(c)}$ for each oxygen site were obtained from the corresponding (Os-Hwater and O_s-O_{water}) RDFs, while the cutoff parameters for the hydrogen site employed the distances of the first boundary in the H-O_{water} and O(4)-O_{water} RDFs, respectively. The angle $\phi^{(c)}$ was set to 30°. The number of H-bonds as a function of time for each site is shown in Figure 8, presenting an average number of H-bonds of 1.5 \pm 0.8, 1.5 \pm 0.8, 1.6 \pm 0.8, 0.4 \pm 0.5, and 0.9 \pm 0.3 for the O(1), O(2), O(3), O(4), and H sites, respectively. The smaller average number of H-bonds compared with the corresponding average coordination number for each hydration site indicates that some water molecules located in the hydration shell actually coordinate with the bisulfate ion, while others have an unsuitable orientation to form an H-bond. The slight difference of the average number of H-bonds for the O(1), O(2), and O(3) again presents the identical characteristics of these sites, corresponding to the $C_{3\nu}$ symmetry. This difference for the O(4) site (ca. 1.5 molecules) clarifies the inclusion of extra water molecules from the hydration shell of the H site, and proves a weak interaction with water molecules at this site. The average number of H-bonds (5.8) compared

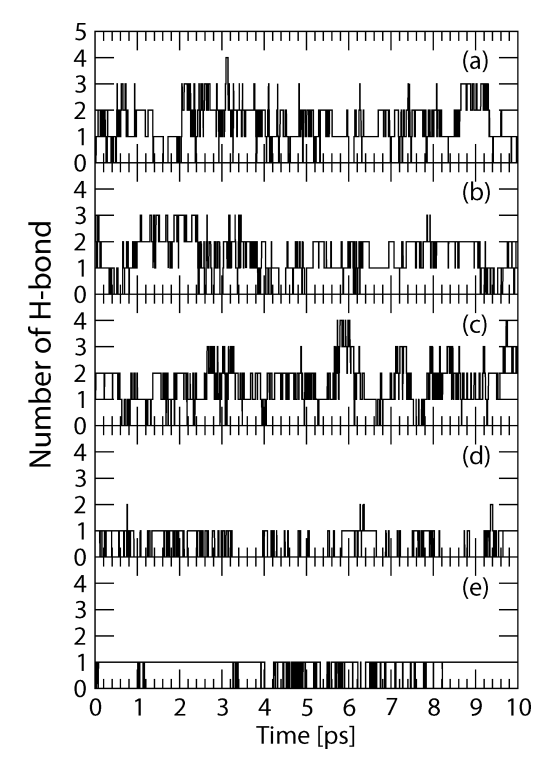


Figure 8. Number of hydrogen bonds between (a) O(1), (b) O(2), (c) O(3), (d) O(4), and (e) H atom of HSO₄⁻ ion and water molecules within the hydration shell during 10 ps of the QMCF MD simulation.

with the average coordination number (8.0) for the molecular ion shows that \sim 2 water molecules are located in the molecular hydration shell without forming H-bonds to the bisulfate ion, however.

The dynamical properties of water molecules hydrating the bisulfate ion were investigated by the ligand mean residence time (MRT) evaluated by the direct method,³⁷ from the average number of water molecules in the hydration shell during the simulation and from the number of exchange events for two time parameters $t^* = 0.0$, defined as the minimum duration of a ligand displacement from its original shell to account for an exchange process. t^* was set to 0.5 ps in accordance with the average lifetime of a hydrogen bond, ³⁹ whereas $t^* = 0.0$ counts all exchange attempts. All MRT values for individual oxygen and hydrogen sites were summarized in Table 4. The total number of water molecules counted for individual exchange processes of all oxygens and hydrogen were 90 and 37, being larger than those counted for the molecular hydration shell (33 and 19). The total number of attempted and lasting exchange processes of individual atoms evaluated at $t^* = 0.0$ ps (576) events) and $t^* = 0.5$ ps (73 events), respectively, are also higher than the 410 and 39 events counted by the molecular approach, which avoids counting water molecules within the intersection of individual hydration spheres. The difference in exchange processes (73 and 39, respectively) shows that half of the exchange events are actually migrations of water molecules between the coordinating sites of HSO_4^- ion, similar to the HCO₃⁻ system.²⁵ The number of processes needed for one successful water exchange, $R_{\rm ex}$, for the terminal oxygen atoms indicates a weak interaction with the water molecules in their vicinity compared to the hydrogen site. The peculiar value of $R_{\rm ex}$ for the O(4) site stems from the partial inclusion of the hydration sphere of the hydrogen site. The standard relaxation time used in the direct method with $t^* = 0.5$ ps leads to the MRT of water ligands at the coordination sites, while the

TABLE 4: Mean Ligand Residence Time τ in ps, Number of Accounted Ligand Exchange Events N, and Total Number of Processes Needed for One Successful Water Exchange $R_{\rm ex}$ **Obtained from the QMCF Simulation**

	$t^* = 0.0 \text{ ps}$			$t^* = 0.5 \text{ ps}$			
	$N_{ m inv}^a$	$N_{\rm ex}^{0.0}$ / 10 ps ^b	$ au_{ m D}^{0.0~^c}$	$N_{ m inv}^a$	$N_{\rm ex}^{0.5}/10 {\rm ps}^b$	$ au_{ m D}^{0.5^c}$	$R_{\rm ex}^{d}$
O(1)	17	118	0.20	10	19	1.27	6.2
O(2)	19	131	0.17	8	21	1.04	6.2
O(3)	25	160	0.22	12	24	1.47	6.7
O(4)	22	110	0.17	5	7	2.72	15.7
Н	7	57	0.17	2	2	4.95	28.5
surface	33	410	0.19	19	39	2.02	10.5
H_2O^e		269^{37}	$0.2,^{37}$ 0.33^{38}		24^{37}	$1.7,^{37}$ 1.51^{38}	11.2^{37}
H_2O^f		131^{52}	$0.2,^{52}$ 0.55^{39}		20^{52}	1.3^{52}	6.5^{52}

^a Number of ligands involved in the MRT evaluation according to the value of t*. b Number of accounted exchange events per 10 ps lasting at least 0.0 and 0.5 ps, respectively. EMean residence time determined by the direct method³⁷ in ps. ^d Average number of processes needed for one successful ligand exchange. e Values obtained from a QM/MM-MD simulation of pure water^{37,38} in ps. ^f Values obtained from a QMCF MD simulation of pure water⁵² in

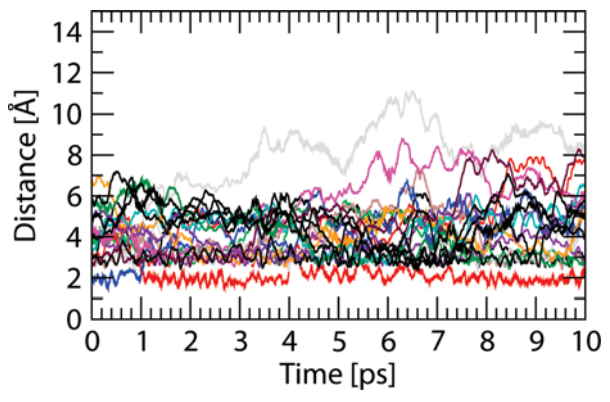


Figure 9. Distance plot of the molecular anion sites and oxygen atom of water as a function of time during the QMCF MD simulation period.

hydrogen bond lifetimes can be estimated with $t^* = 0.0 \text{ ps.}^{25,37}$ The corresponding value obtained from the simulation of the pure water system based on the QM/MM MD formalism is 0.33 ps; the $t^* = 0.0$ values account for each hydrogen bond making/ breaking process.³⁸ Both mean residence times and hydrogen bond lifetimes for the individual sites and the molecular ion as a whole prove HSO₄⁻ as a weak structure-making ion. This effect is not evenly distribution to all sites of the ion but most pronounced near the hydrogen site, as shown in Figure 9. This plot presents the distances of all water molecules within the molecular hydration shell measured from each coordinating site. After an exchange of water molecules binding to the hydrogen site at 1.0 ps, the water molecule retained the interaction with this site until the end of sampling time. Structure breaking/ making is commonly regarded as a property related to the dynamics of the water molecules in the surrounding of a solute. If it was defined only as a structural effect, any kind of solute would break some H bonds of the solvent and hence its structure. However, in a dynamical sense, structure making means the formation of a layer of solvent molecules around the solute with lower mobility, while structure breaking would mean that the surrounding solvent molecules are more mobile than the solvent molecules in the bulk. Although the Berendsen temperaturescaling algorithm³² requires in principle a long simulation period to sufficiently describe the phase space, a large number of successful simulations published indicate that our simulation time of 10 ps is adequate to reproduce well the properties of hydrated ions, and thus also of the bisulfate ion. Comparing results for exchange dynamics and H-bond life times for simulations of pure water 38 and experimental results 39 the HF method seems to be a good compromise between accuracy and affordable computational effort to estimate dynamical effects as well. Although HF and the methodical problems associated with the thermostatisation probably lead to slightly underestimated values, the associated errors are probably within a 10-20% range.

As HSO₄⁻ ion is still a fairly strong acid in water, a dissociation process could be expected to be observable. However, this is a function not only of the thermodynamics but also of the kinetics, and even in the case of a much stronger acid, namely, HCl, despite a number of attempted proton transfers within 10 ps of simulation, no full proton transfer could be observed.⁴⁵ There is no doubt that, over a much longer simulation time, such a process would occur, however.

Conclusion

Our QMCF MD simulation results for hydrated bisulfate ion are well compatible with the Raman and IR experiments, assuming C_{3v} symmetry.^{9,10} The vector projection of each vibration mode coupling with the VACF calculations gives the vibrational frequencies in good agreement with the experimental observations, especially of the characteristic modes. \hat{s}^{-10} These results again indicate the success and reliability of our approach to investigate the properties of composite hydrated anions. 20-26 The HSO₄⁻ ion is characterized as a weakly structure-making ion in aqueous solution, slightly weaker than the sulfate ion.²⁰ The hydrogen site forms a significant hydration structure characterized by a strong H-bond with one water. This stronger interaction of the hydrogen site of the HSO₄⁻ ion compared to that of the HCO₃⁻ ion reflected by the mean residence times of water ligands at the hydrogen site of 4.95 for the HSO₄⁻ and 0.82 for HCO₃⁻²⁵ clearly demonstrates the higher acidity of HSO₄⁻. The water molecules hydrating the bisulfate ion have a high mobility, reflected by rapidly changing binding sites and orientations while forming and breaking H-bonds with the ion. To describe these effects by classical or conventional QM/MM molecular dynamics would be a most difficult task, as it would have required the construction of analytical interaction potential functions taking into account all the asymmetry of the interaction between solute and solvent, which in the case of bisulfate would be difficult and subject to many possible error sources and inaccuracies.

Acknowledgment. Generous financial support by the Austrian Science Foundation (FWF) and ASEA-UNINET, the Thailand Research Fund and Thailand Commission on Higher Education (fellowships for V.V. and C.K.), Faculty of Science, Chulalongkorn University (RES A1 B1-19 for V.V.), and Center for Petroleum, Petrochemicals and Advanced Materials, Chulalongkorn University are gratefully acknowledged.

References and Notes

- (1) Calhoun, J. A.; Charlson, R. J.; Bates, T. S. *Geophys. Res. Lett.* **1991**, *18*, 1877–1880.
- (2) Charlson, R. J.; Schwartz, S. E.; Hales, J. M.; Cess, R. D.; Coakley, J. A., Jr.; Hansen, J. E.; Hofmann, D. J. Science **1992**, 255, 423–430.
- (3) Laaksonen, A.; Talanquer, V.; Oxtoby, D. W. Annu. Rev. Phys. Chem. 1995, 46, 489–524.
 - (4) Bianco, R.; Hynes, J. T. Acc. Chem. Res. 2006, 39, 159-165.
- (5) Faguy, P. W.; Marinković, N. S.; Adžić, R. R. Langmuir 1996, 12, 243–247.

- (6) Clavilier, J. J. Electroanal. Chem. 1980, 107, 211-216.
- (7) Faguy, P. W.; Marinkovic, N.; Adzic, R. R.; Fierro, C. A.; Yeager, E. B. *J. Electroanal. Chem.* **1990**, 298, 245–262.
- (8) Walrafen, G. E.; Dodd, D. M. *Trans. Faraday Soc.* **1961**, *57*, 1286–1296
- (9) Rudolph, W. Z. Phys. Chem. 1996, 194, 73-95.
- (10) Dawson, B. S. W.; Irish, D. E.; Toogood, G. E. J. Phys. Chem. **1986**, 90, 334–341.
- (11) Imre, D. G.; Xu, H.; Tang, I. N.; McGraw, R. J. Phys. Chem. A 1997, 101, 4191–4195.
- (12) Re, S.; Osamura, Y.; Morokuma, K. J. Phys. Chem. A 1999, 103, 3535–3547.
 - (13) Ding, C.-G.; Laasonen, K. Chem. Phys. Lett. 2004, 390, 307-313.
- (14) Choe, Y.-K.; Tsuchida, E.; Ikeshoji, T. J. Chem. Phys. 2007, 126, 154510.
- (15) Anderson, K. E.; Siepmann, J. I.; McMurry, P. H.; VandeVondele, J. J. Am. Chem. Soc. **2008**, *130*, 14144–14147.
- (16) Hammerich, A. D.; Buch, V.; Mohamed, F. Chem. Phys. Lett. 2008, 460, 423-431.
- (17) Kakizaki, A.; Motegi, H.; Yoshikawa, T.; Takayanagi, T.; Shiga, M.; Tachikawa, M. *THEOCHEM* **2009**, *901*, 1–8.
- (18) Rode, B. M.; Hofer, T. S.; Randolf, B. R.; Schwenk, C. F.; Xenides, D.; Vchirawongkwin, V. *Theor. Chem. Acc.* **2006**, *115*, 77–85.
- (19) Hofer, T. S.; Pribil, A. B.; Randolf, B. R.; Rode, B. M. Ab Initio Quantum Mechanical Charge Field Molecular Dynamics: A Nonparametrized First-Principle Approach to Liquids and Solutions. In *Combining Quantum Mechanics and Molecular Mechanics. Some Recent Progresses in QM/MM Methods*; Sabin, J. R., Brändas, E., Eds.; Academic Press: San Diego, 2010; Vol. 59, pp 213–246.
- (20) Vchirawongkwin, V.; Rode, B. M.; Persson, I. J. Phys. Chem. B **2007**, 111, 4150–4155.
- (21) Vchirawongkwin, V.; Rode, B. M. Chem. Phys. Lett. 2007, 443, 4152–157.
- (22) Pribil, A. B.; Vchirawongkwin, V.; Hofer, T. S.; Randolf, B. R. Structure and Dynamics of Composite Anions in Aqueous Solution. Computation in Modern Science and Engineering, Proceedings of the International Conference on Computational Methods in Science and Engineering; American Institute of Physics (AIP): New York, 2007; pp 921–923.
- (23) Pribil, A. B.; Hofer, T. S.; Randolf, B. R.; Rode, B. M. *J. Comput. Chem.* **2008**, *29*, 2330–2334.
- (24) Pribil, A. B.; Hofer, T. S.; Vchirawongkwin, V.; Randolf, B. R.; Rode, B. M. Chem. Phys. **2008**, 346, 182–185.
- (25) Vchirawongkwin, V.; Pribil, A. B.; Rode, B. M. J. Comput. Chem. **2010**, *31*, 249–257.
- (26) Vchirawongkwin, V.; Kritayakornupong, C.; Ruangpornvisuti, V.; Rode, B. M. *THEOCHEM* **2009**, *913*, 236–239.
 - (27) Warshel, A.; Levitt, M. J. Mol. Biol. 1976, 103, 227-249.
- (28) Field, M. J.; Bash, P. A.; Karplus, M. J. Comput. Chem. 1990, 11, 700–733.
 - (29) Gao, J. J. Am. Chem. Soc. **1993**, 115, 2930–2935.
 - (30) Bakowise, D.; Thiel, W. J. Phys. Chem. 1996, 100, 10580–10594.
- (31) Brooks, B. R.; Bruccoleri, R. E.; Olafson, B. D.; States, B. D.; Swaminathan, S.; Karplus, M. *J. Comput. Chem.* **1983**, *4*, 187–217.
- (32) Berendsen, H. J. C.; Postma, J. P. M.; van Gunsteren, W. F.; DiNola, A.; Haak, J. R. *J. Chem. Phys.* **1984**, *81*, 3684–3690.
- (33) Dunning, T. H., Jr.; Hay, P. J. In *Gaussian Basis Sets for Molecular Calculations*; Schaefer, H. F., III, Ed.; Plenum Press: New York, 1977; Vol. 3, Chapter 1, pp 1–27.
 - (34) Dunning, T. H., Jr. J. Chem. Phys. 1970, 53, 2823–2833.
- (35) Stillinger, F. H.; Rahman, A. J. Chem. Phys. 1978, 68, 666–670.
- (36) Bopp, P.; Janscó, G.; Heinzinger, K. Chem. Phys. Lett. 1983, 98, 129-133.
- (37) Hofer, T. S.; Tran, H. T.; Schwenk, C. F.; Rode, B. M. J. Comput. Chem. **2004**, 25, 211–217.
- (38) Xenides, D.; Randolf, B. R.; Rode, B. M. J. Chem. Phys. 2005, 122, 174506.
- (39) Lock, A. J.; Woutersen, S.; Bakker, H. J. J. Phys. Chem. A 2001, 105, 1238–1243.
 - (40) Bopp, P. Chem. Phys. 1986, 106, 205-212.
- (41) Wang, X.-B.; Nicholas, J. B.; Wang, L.-S. J. Phys. Chem. A 2000, 104, 504–508.
- (42) Frisch, M. J. et al. *Gaussian 03*, revision E.01; Gaussian, Inc.: Wallingford, CT, 2004.
- (43) Godbout, N.; Salahub, D. R.; Andzelm, J.; Wimmer, E. Can. J. Chem. 1992, 70, 560–571.
- (44) Kritayakornupong, C.; Vchirawongkwin, V.; Hofer, T. S.; Rode, B. M. J. Phys. Chem. B 2008, 112, 12032–12037.
- (45) Kritayakornupong, C.; Vchirawongkwin, V.; Rode, B. M. J. Comput. Chem. **2010**, *31*, 1785–1792.

- (46) Miller, F. A.; Carlson, G. L.; Bentley, F. F.; Jones, W. H. *Spectrochim. Acta* **1960**, *16*, 135–235.
- (47) McQuarrie, D. A. Statistical Mechanics; Harper & Row: New York,
- (48) CRC Handbook of Chemistry and Physics, 90th ed.; Lide, D. R., Ed.; CRC Press/Taylor and Francis: Boca Raton, FL, 2010.
- (49) Sceats, M. G.; Rice, S. A. J. Chem. Phys. 1980, 72, 3236–3247.
- (50) Mezei, M.; Beveridge, D. L. J. Chem. Phys. 1981, 74, 622–632.
 (51) Luzar, A.; Chandler, D. J. Chem. Phys. 1993, 98, 8160–8173.
- (52) Randolf, B. R.; Hofer, T. S.; Rode, B. M. Unpublished results.

JP105181N

Determination of Structure and Dynamics of the Solvated Bisulfide (HS⁻) Ion by ab Initio QMCF Molecular Dynamics

Chinapong Kritayakornupong,**,† Viwat Vchirawongkwin,‡ and Bernd M. Rode§

Department of Chemistry, Faculty of Science, King Mongkut's University of Technology Thonburi, Bangkok, 10140 Thailand, Department of Chemistry, Faculty of Science, Chulalongkorn University, Bangkok, 10330 Thailand, and Theoretical Chemistry Division, Institute of General, Inorganic and Theoretical Chemistry, University of Innsbruck, Innrain 52a, A-6020 Innsbruck, Austria

Received: May 27, 2010; Revised Manuscript Received: August 13, 2010

The hydration structure of the bisulfide (HS⁻) ion in dilute aqueous solution was characterized by means of an ab initio quantum mechanical charge field (QMCF) molecular dynamics simulation at the Hartree–Fock level employing Dunning double- ξ plus polarization function (DZP) basis sets. An average H–S bond distance of 1.35 Å resulted from the simulation and a hydration shell located at 2.42 Å $S_{HS}^-\cdots H_w$ and 3.97 Å HS⁻ distances, respectively. At the sulfur site, the average coordination number is 5.9 \pm 1.1, while the value for the hydrogen site is 9.2 \pm 1.6. The calculated $H_{HS}^--S_{HS}^-$ stretching frequency of 2752 cm⁻¹ obtained from the QMCF MD simulation is in good agreement with that reported from the Raman spectrum (2570 cm⁻¹) only if a scaling factor of 0.89 is applied. The stability of the nondissociated HS⁻ structure is reflected by the force constants of 436.1 and 4.5 N/m determined for the $H_{HS}^--S_{HS}^-$ and $H_{HS}^-\cdots O_w$ bonds, respectively. A weak structure-making effect of the hydrated HS⁻ ion results from the mean residence times of 1.5 and 2.1 ps of coordinated water molecules at the sulfur and hydrogen sites of the HS⁻ ion, respectively.

1. Introduction

The chemistry of sulfide ions is an interesting area, not only in the fundamental chemistry and electrochemistry of numerous salts1 but also in atmospheric pollution as a constituent of the sulfur cycle,² petroleum hydrodesulfurization processes, as well as paper and pulp industries. In aqueous solution, bisulfide (HS⁻) ion can be obtained from the dissolved hydrogen sulfide (H₂S) with a suggested pK_1 value of 7.01,³ while the subsequent dissociation of the bisulfide leads to the sulfide (S2-) ion, characterized by large experimental values of pK_2 in the wide range 12.5-18.5.4-11 For example, Stephens and Cobble⁵ presented a value of 13.78, Licht et al.8 reported a value of 17.1, and Migdisov et al.9 selected a value of 17.4 at 25 °C. All of these indicate that HS- exists as a major species in aqueous H₂S solution, while minor activities of S²⁻ only occur in extremely high ionic strength solutions.8 In general, HS⁻ acts as a Lewis base, whereas H2S can behave as a Lewis base or acid. Due to the dominance of bisulfide ion in aqueous solution, several experiments confirmed that the bisulfide ion acts as the initial species to form metal hydrosulfide in the precipitation of metal sulfide from solution, which is of great environmental interest. 12,13 To our knowledge, no structural analysis of the HSion in aqueous solution has been performed by experimental techniques, only the H-S vibrational frequency of 2570 cm⁻¹ was determined by Raman spectroscopy.7 For theoretical investigations, there have been a few calculations aimed at the structure and stability of [H₂S(H₂O)]_n clusters, ¹⁴⁻¹⁸ which are not directly relevant for the solvated HS⁻ ion.

Recently, the quantum mechanical charge field (QMCF) molecular dynamics simulation approach has been developed, ¹⁹

presenting a suitable tool to investigate composite and asymmetrical ions in aqueous solution, $^{20-23}$ since the first and second hydration layers are included in the quantum mechanical treatment. In our previous publications, 21,22 structural and dynamical properties of aqueous HF and HCl solutions were successfully studied using this technique. Therefore, it was of great interest to characterize the hydration structure as well as the dynamical behavior of the analogous HS $^-$ compound with its extremely weak acid behavior in aqueous solution by employing the QMCF MD methodology.

In the present work, an ab initio quantum mechanical charge field molecular dynamics simulation at the Hartree–Fock level was performed for a system consisting of one HS $^-$ ion plus 498 water molecules. To characterize the hydration structure of the hydrated HS $^-$ ion, numerous structural parameters such as radial distribution functions, coordination numbers, angular distributions, θ angle, and tilt angle distributions were determined. The vibrational frequency of the H–S bond was determined to compare it with the experimental value, while the $H_{\rm HS}^-\cdots O_{\rm w}$ vibrational mode was calculate to describe the hydrogen bond strength between solute and water molecules. Subsequently, dynamics of ligand exchange processes between hydration shell of the HS $^-$ ion and bulk were analyzed on the basis of the mean residence times.

2. QMCF MD Simulation

The quantum mechanical charge field (QMCF) molecular dynamics simulation^{19,24} is a technique based on a partitioning scheme similar to conventional QM/MM MD methods,^{25–27} which divides the system into two parts (QM and MM regions) where different levels of theory are appropriately applied. In the QMCF technique, the QM region using the ab initio quantum mechanical calculation is extended to include the second hydration shell and also splits into two subregions, which are

^{*} Corresponding author. Fax: +66(2)470-8962. E-mail:chinapong.kri@kmutt.ac.th.

[†] King Mongkut's University of Technology Thonburi.

^{*} Chulalongkorn University.

[§] University of Innsbruck.

the core region containing the solute and the first solvation shell and the solvation layer containing only solvent molecules. In addition, the QMCF technique describes the Coloumbic interactions of the solute with bulk solvent molecules by quantum chemically evaluated partial charges of the atoms in the QM region and the point charges of the atoms in the MM region. The charges of the MM particles also enter as a perturbation term into the core Hamiltonian:

$$H_{\rm CF} = H_{\rm HF} + V_i^{'} \tag{1}$$

$$V_i = \sum_{j=1}^M \frac{q_j}{r_{ij}} \tag{2}$$

where q_j are the partial charges of each atom in the MM region as defined in the used water model BJH-CF2, ^{28,29} i.e., -0.65966 and +0.32983 for oxygen and hydrogen, respectively. Consequently, the forces acting on each particle in the different regions are defined as

$$F_j^{\text{core}} = F_j^{\text{QM}} + \sum_{i=1}^M \frac{q_j^{\text{QM}} q_i^{\text{MM}}}{r_{ii}^2}$$
 (3)

$$F_{j}^{\text{layer}} = F_{j}^{\text{QM}} + \sum_{i=1}^{M} \frac{q_{j}^{\text{QM}} q_{i}^{\text{MM}}}{r_{ii}^{2}} + \sum_{i=1}^{M} F_{ij}^{\text{BJHnC}}$$
(4)

$$F_{j}^{\text{MM}} = \sum_{\substack{i=1\\i\neq j}}^{M} F_{ij}^{\text{BJH}} + \sum_{\substack{i=1}}^{N_{1}+N_{2}} \frac{q_{i}^{\text{QM}} \cdot q_{j}^{\text{MM}}}{r_{ij}^{2}} + \sum_{\substack{i=1}}^{N_{2}} F_{ij}^{\text{BJHnC}}$$
(5)

where F_j^{core} , F_j^{layer} , and F_j^{MM} are the forces acting on particle jsituated in the core region, the solvation layer, and the MM region, respectively. M is the number of atoms in the MM region. In each simulation step, the ab initio quantum mechanical forces in core and layer regions (F_i^{core} and F_i^{layer}) are evaluated in conjunction with the Coulombic forces obtained from all particles in the MM region. The non-Coulombic forces between the core particles and the MM particles are neglected, justified by the distance between the core and the MM region of at least 3 Å, while the QM forces in the layer (F_i^{layer}) are supplemented by the non-Coulombic forces of particles in the MM region according to the BJH-CF2 water model.^{28,29} Consequently, the forces in the MM region (F_i^{MM}) are determined by the BJH-CF2 water model^{28,29} augmented by the Coulombic forces exerted by all particles in the core region (N_1) and the layer region (N_2) , and the non-Coulombic forces (F_{ii}^{BJHnC}) generated by the particles in the layer region (N_2) .

During the QMCF MD simulation, the migration of solvent molecules between the QM and MM region can occur frequently. To ensure a continuous transition of forces at the boundary, the forces acting on each particle in the system can be defined as

$$F_j^{\text{Smooth}} = F_j^{\text{MM}} + (F_j^{\text{layer}} - F_j^{\text{MM}}) \cdot S_{\text{m}}(r)$$
 (6)

where F_j^{MM} and F_j^{layer} are the forces acting on the particle j in the MM region and located in the solvation layer, respectively,

r is the distance of the water molecule from the sulfur atom of the HS⁻ ion, and S_m is a smoothing function,³⁰

$$S_{\rm m}(r) = 1 \qquad \text{for } r \le r_1$$

$$S_{\rm m}(r) = \frac{(r_0^2 - r^2)^2 (r_0^2 + 2r^2 - 3r_1^2)}{(r_0^2 - r_1^2)^3} \quad \text{for } r_1 < r \le r_0$$

$$S_{\rm m}(r) = 0 \qquad \text{for } r > r_0$$

$$(7)$$

where r_1 is the inner border of the smoothing region and r_0 is the radius of the QM region. Further details of the method are presented in refs 19 and 24.

The QMCF MD simulation of the bisulfide ion in aqueous solution was performed in a 24.7 Å \times 24.7 Å \times 24.7 Å periodic boundary cubic box, consisting of one HS⁻ ion plus 498 water molecules. The canonical NVT ensemble was controlled by the Berendsen temperature-scaling algorithm³¹ using a relaxation time of 100 fs to keep the temperature at 298.15 K. The density of the simulation was fixed at 0.997 g cm⁻³, corresponding to the experimental value of pure water at this temperature. The time step of the predictor-corrector algorithm was set to 0.2 fs, enabling an explicit description of hydrogen movements. The flexible BJH-CF2 water model^{28,29} for the MM region also enables explicit hydrogen movements, thus ensuring a smooth transition of water molecules between QM and MM region. Cutoff distances of 5 and 3 Å were used for non-Coulombic O-H and H-H interactions, respectively. The radial cutoff limit for Coulombic interactions was set to half the box length and the reaction field³² was applied to correct for long-range Coulombic interactions. The radius of the core region was chosen as 3.0 Å with the layer region ranging from 3.0 to 5.7 Å in which the smoothing function³⁰ was applied between r_0 (5.7 Å) and r_1 (5.5 Å). The TURBOMOLE 5.9 program^{33–35} was employed to evaluate the forces in the QM region calculated at the restricted Hartree-Fock (RHF) level. Dunning double- ζ plus polarization function (DZP) basis sets³⁶⁻³⁸ were applied for sulfur, oxygen, and hydrogen atoms. A methodical test was performed for a comparison of the geometric parameters obtain from the HF method optimization of $[HS(H_2O)_n]^-$ (n = 0-6)clusters with and without diffuse functions of the DZP basis set. It was found that the average H-S distances determined by the HF/DZP+ method are slightly shorter by \sim 0.002 Å than those evaluated from the HF/DZP method. In addition, the H-S distance in the [HS(H₂O)₄]⁻ cluster is 1.3333 Å calculated from the HF/DZP method, which is in good agreement with that evaluated from the MP2/6-31+G(d,p) method (1.33 Å). ¹⁶ These prove that the diffuse functions can be neglected. The initial configuration was taken from the simulation of the HF molecule. After equilibration of 6 ps, a 10 ps run was used for sampling. To ensure that true equilibrium had been established, the sampling trajectory was separately evaluated for the first and second 5 ps. The simulation protocol applied in this work is similar to that utilized in previous simulations of aqueous HF and HCl solutions.21,22

Similar to the HF and HCl molecules, the HS $^-$ ion has the $C_{\infty\nu}$ symmetry, indicating that vibrational motion of the HS $^-$ ion is both infrared- and Raman-active. Velocity autocorrelation functions (VACFs) were evaluated to gain access to the vibrational spectrum of the HS $^-$ ion in aqueous solution. The velocity of the hydrogen atom was projected onto a unit vector parallel to the corresponding S $^-$ H bond ($\vec{\mathbf{u}}_1$), while the vibrational mode ν is the projection of the hydrogen velocity onto the unit vector $\vec{\mathbf{u}}_1$. The vibrational frequencies of the normal

10

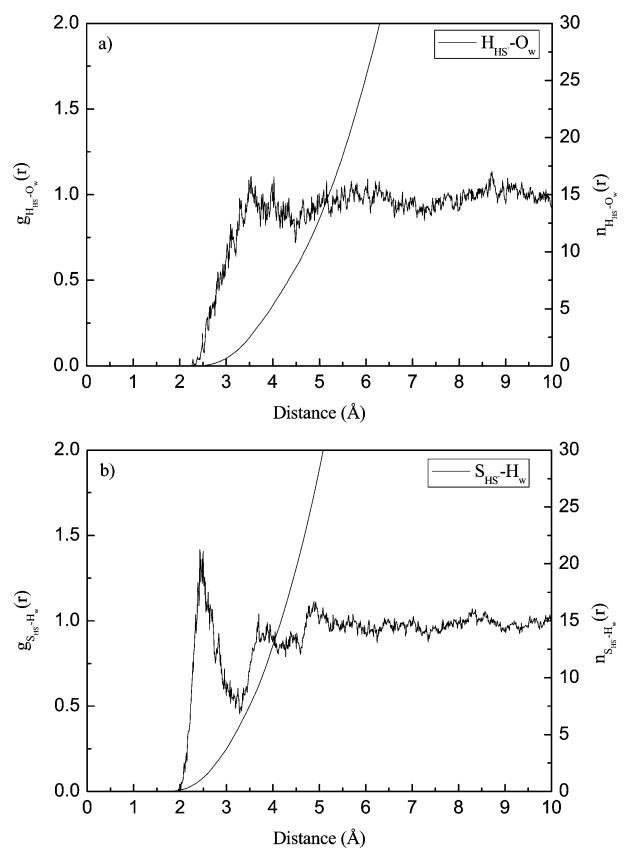


Figure 1. (a) H_{HS}-···O_w and (b) S_{HS}-···H_w RDFs and their corresponding integration numbers.

mode and the intermolecular H_{HS}-···O_w interactions were calculated by their Fourier transformations of the velocity autocorrelation functions (VACFs). The normalized VACF, C(t), is defined by

$$C(t) = \frac{\sum_{i}^{N_{t}} \sum_{j}^{N} \nu_{j}(t_{i}) \ \nu_{j}(t_{i} + t)}{N_{t}N \sum_{i}^{N_{t}} \sum_{j}^{N} \nu_{j}(t_{i}) \ \nu_{j}(t_{i})}$$
(7a)

where N is the number of particles, N_t is the number of time origins t_i , and v_i denotes a certain velocity component of the particle j. The power spectrum of C(t) was determined using a correlation length of 2.0 ps.

3. Results and Discussion

3.1. Structural Properties. To describe the structural properties of the HS- ion in aqueous solution, several hydration parameters such as radial distribution functions (RDF), coordination numbers, and angular distributions were determined. An averaged H-S bond distance of 1.35 Å was evaluated for HS⁻ in water. Figure 1 illustrates the radial distribution functions for both atoms of the HS⁻ ion and their neighboring water molecules together with the corresponding integration numbers. The first broad $H_{HS}^{-}\cdots O_{w}$ peak corresponding to the hydration shell is peaking \sim 4 Å, covering a wide range of 2.1–4.6 Å. Weak intermediate peaks at 3.2 and 3.6 Å correspond to water molecules near the H of the HS^- ion. As the mean $H_{HS}^- \cdots O_w$ distance \sim 4 Å is much larger than the $H_{HF}\cdots O_w$ and H_{HCl}···O_wdistances of 1.62 and 1.84 Å observed in aqueous

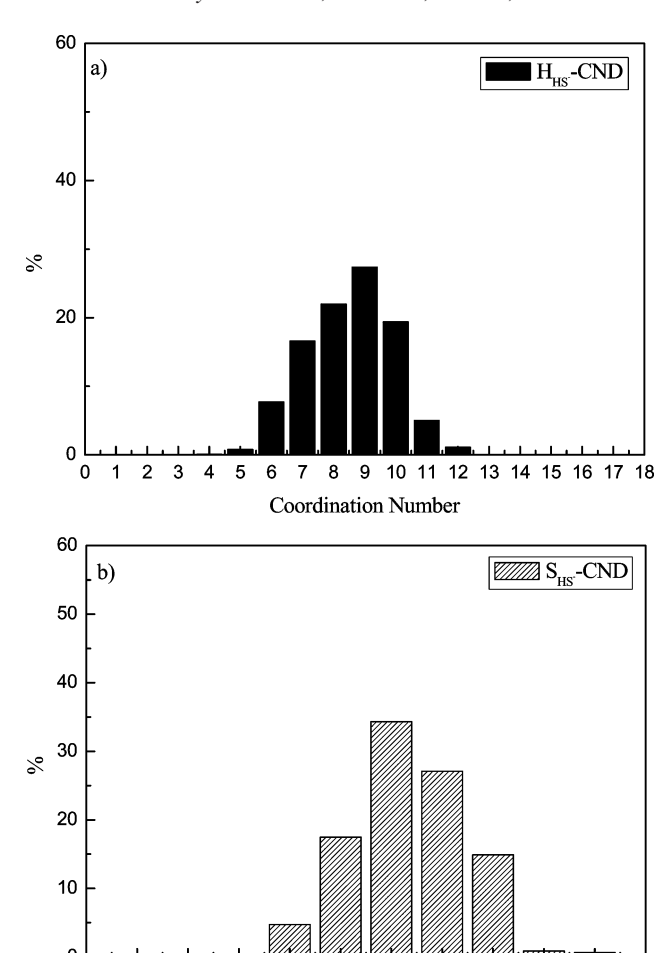


Figure 2. Coordination number distributions of (a) H (up to 4.5 Å) and (b) S (up to 4.0 Å) atoms in the first hydration shell of the HS

Coordination Number

HF and HCl solutions, respectively, 21,22 the extremely weak acidity of the H atom and thus its inability to form stable hydrogen bonds is clearly recognized. As visible in Figure 1a, the minimum between the first shell and bulk is far from the baseline, indicating frequent water exchanges and a very weak separation of the hydration shell from bulk. Figure 1b presents the S_{HS}-···H_w RDF and the corresponding integration. The first sharp S_{HS}-···H_w peak is centered at 2.42 Å, reflecting that the water molecules in the first hydration shell bind much more strongly to the sulfur site than to the hydrogen site. According to Figure 1b, a second S_{HS}-···H_w peak within the range 3.2-4.0 Å with its maximum at \sim 3.7 Å can be assigned to the distance between sulfur atom and the second hydrogen atom of coordinated water molecules in the hydration shell.

The hydration shell coordination number distribution determined from the H_{HS}-···O_w interactions of the HS⁻ ion in aqueous solution is shown in Figure 2a. A variation between 5 and 12, with 9 being the most dominant species is obtained from the simulation. As shown in Figure 2b, the coordination number distribution of the $S_{HS}^{-}\cdots O_w$ interactions covers a narrower range of 4-10 with an average value of 5.9 ± 1.1 . These results confirm the assumption of a very weak water coordination at the hydrogen site of the HS⁻ ion. To see whether a true equilibrium has been established, the first and the second half of the sampling trajectory were analyzed separately and listed in Table 1. The results prove that there is only a minor

TABLE 1: Coordination Numbers for the Hydration Shell of the HS⁻ Ion Evaluated for Sulfur and Hydrogen Sites, and in a Molecular Manner

simulation time (ps)	CND-S	CND-H	CND-HS
0-5	5.9 ± 1.1	9.3 ± 1.6	10.2 ± 1.6
5-10	5.8 ± 1.0	9.0 ± 1.5	9.9 ± 1.5
0-10	5.9 ± 1.1	9.2 ± 1.6	10.0 ± 1.7

difference between both parts, which also gives a confidence limit for the overall results.

To further detail the hydrogen bond interactions of the HS⁻ ion in aqueous solution, the angular distribution functions of the $O_w\cdots H_{HS^-}-S_{HS^-}$ and $H_{HS^-}-S_{HS^-}\cdots H_w$ angles in the first hydration shell were examined as depicted in Figure 3. Both of these extend over almost the whole range from 0° to 180°, with a clear preference of nonlinear, almost rectangular H bonds. This result is in strong contrast to the cases of $O_w\cdots H-X$ bonds of HF $(170^\circ)^{21}$ and HCl $(161^\circ)^{.22}$ The $H_{HS^-}-S_{HS^-}\cdots H_w$ angle peaking at $\sim 100^\circ$ is smaller but not so different from the $H_{HF}-F_{HF}\cdots H_w$ and $H_{HCl}-Cl_{HCl}\cdots H_w$ angles of 116° and 112°. 21,22

3.2. Dynamical Properties. On the basis of the velocity autocorrelation functions (VACFs) and their Fourier transformations, the vibrational frequencies of the normal mode H_{HS}-- S_{HS^-} and the intermolecular $H_{HS^-}\cdots O_w$ interactions were analyzed. The power spectra of the $H_{HS^-}\cdots O_w$ and $H_{HS^-}-S_{HS^-}$ vibrational modes of the hydrated ion obtained from the simulation are presented in Figure 4. As shown in Figure 4a, the maximum frequency of the H_{HS} - \cdots O_w vibrational mode in the first hydration shell is centered at 285 cm⁻¹, with two shoulder peaks at 204 and 383 cm⁻¹, corresponding to the force constants of 4.5, 2.3, and 8.2 N/m, respectively. The calculated force constant of 4.5 N/m obtained from the H_{HS}-···O_w frequency is slightly weaker than the value of 5.9 N/m determined from the H_{HF}···O_w interaction.²¹ However, it is much stronger than that of 1.6 N/m evaluated from the experimental O_w-H_w···O_w stretching frequency of 170 cm⁻¹ in pure water.³⁹ This indicates a preference of the nondissociated structure of the HS⁻ ion, which was also observed in the case of HF.21 The intramolecular HHS--SHS- stretching mode obtained from the QMCF MD simulation is centered at 2752 cm⁻¹ (a value of 2449 cm⁻¹ is obtained, if the intramolecular frequency is scaled by the standard factor of 0.8940-42 for Hartree-Fock results), which is in reasonable agreement with the experimental evaluation by Raman spectroscopy (2570 cm⁻¹). The deviation can be explained by the high concentration

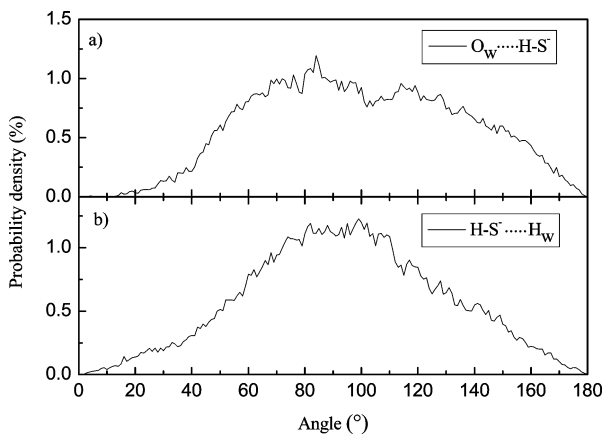


Figure 3. Distributions of (a) $O_w \cdots H_{HS^-} - S_{HS^-}$ angles and (b) $H_{HS^-} - S_{HS^-} \cdots H_w$ angles, obtained from the QMCF MD simulation.

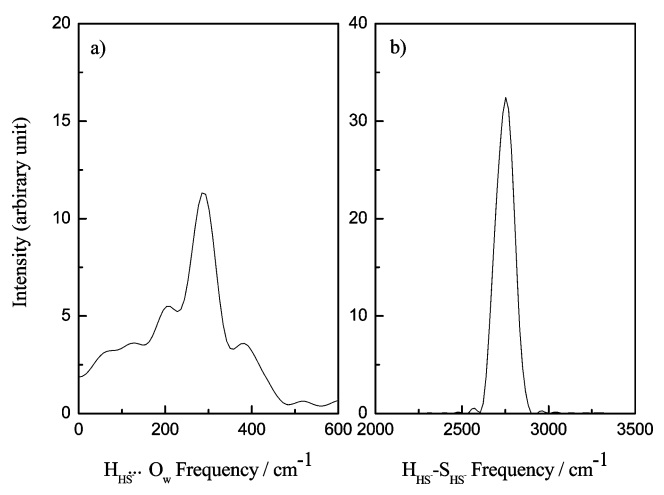


Figure 4. Power spectra of (a) H_{HS} - \cdots O_w and (b) H_{HS} - $-S_{HS}$ -stretching modes in the first hydration shell.

TABLE 2: Mean Ligand Residence Times and Sustainability of Migration Processes to and from the First Hydration Shell of Sulfur and Hydrogen atoms of the Bisulfide ion

		$t^* = 0 \text{ ps}$		$t^* = 0.5 \text{ ps}$		
solute	$t_{\rm sim}$	$N_{\rm ex}^0$	$ au_{ m H_2O}^0$	$N_{\rm ex}^{0.5}$	$ au_{ m H_2O}^{0.5}$	$R_{\rm ex}$
S _{HS} -	10.0	190	0.3	40	1.5	4.8
H_{HS}^-	10.0	900	0.1	43	2.1	20.0
bulk ^a	10.0	131	0.2	20	1.3	6.5

^a Values obtained from a QMCF MD simulation of pure water. ⁴⁴

of perchlorate solution employed in the Raman study⁷ and/or the inaccuracy of the Hartree—Fock method and the relatively small basis set. The force constant of 436.1 N/m for the H_{HS} — S_{HS} —bond confirms the stability of the HS—ion in water.

Additional information about the solution dynamics was obtained in terms of the mean residence times (MRTs), corresponding to ligand exchange processes in the first hydration shell of the HS⁻ ion and determined by the "direct" method⁴³ for both sulfur and hydrogen sites of the HS⁻ ion. The number of ligand exchange processes, the mean residence times, and the number of attempts needed for a sustainable ligand migrating from the hydration shell as revealed by the use of both time parameters t^* 0.0 and 0.5 ps are listed in Table 2. As shown in Table 2, only 43 ligand exchange processes lasted longer than 0.5 ps at the hydrogen site of the HS⁻ ion during the simulation time of 10 ps, while 900 exchange attempts were recorded for $t^* = 0.0$ ps. The calculated MRT values for the hydrogen site are 0.1 ps and 2.1 for $t^* = 0.0$ and 0.5 ps, respectively. The MRT value of 2.1 ps is considerably larger than that of pure water determined from a QMCF simulation (1.3 ps)⁴⁴ and HCl (0.8 ps),²² but it is slightly smaller than that of HF (2.5 ps).²¹ At the sulfur site, the MRT values of 0.3 and 1.5 ps for $t^* =$ 0.0 and 0.5 ps were obtained, corresponding to 190 and 40 exchange processes, respectively. As the result, the mean residence time for the water ligands located around the sulfur atom is shorter than that evaluated for the fluorine (2.1 ps) and chlorine (2.1 ps) sites of HF and HCl, respectively, 21,22 suggesting weak hydrogen bond interactions at the sulfur site of the HS⁻ ion. For the evaluation of hydrogen bond, the distances of 4.0 and 4.5 Å for hydrogen and oxygen atoms of water molecules and angle of >120° were applied to define hydrogen bonds between HS⁻ and water molecules. Hydrogen bond life times estimated for the $S_{HS}-H_{HS}-\cdots O_w$ and $H_{HS}--S_{HS}-\cdots H_w$ hydrogen bonds are 0.23 and 0.26 ps, respectively. The average

lifetime of the S_{HS}--H_{HS}-···O_w hydrogen bond is much smaller than that determined by experimental investigation of pure water (0.55 ps), 45 and a QMCF MD simulation (0.33 ps). 44 The value of 0.26 ps of the H_{HS} - $-S_{HS}$ - \cdots H_w hydrogen bond is also smaller than the corresponding values of 0.36 and 0.31 ps for HF and HCl. These results reflect once more a very weak hydrogen bond between the HS⁻ ion and its neighboring water molecules in the hydration shell. According to the MRT values and the hydrogen bond lifetimes obtained from the QMCF MD simulation, the HS⁻ ion in aqueous solution behaves as weak structuremaking species.

4. Conclusion

A detailed description on hydration structure and dynamics of the HS- ion in aqueous solution could be obtained using a QMCF MD simulation. The H_{HS} - $-S_{HS}$ - vibrational frequency predicted from the QMCF MD simulation is in reasonable agreement with the experiment, while very weak hydrogen bonding between the bisulfide ion and its neighboring water molecules was recognized. These data confirm the preference of nondissociated HS⁻ in aqueous solution. As expected, ligand exchange processes in the hydration shell occur frequently at both sites of the HS⁻ ion.

Acknowledgment. Financial support for this work by the Thailand Research Fund (TRF) and Thailand Commission on Higher Education (ASEA-UNINET fellowships for C.K. and V.V.) are gratefully acknowledged and B.M.R. acknowledges support by the Austrian Science Foundation (FWF). V.V. acknowledges additional support by Faculty of Science, Chulalongkorn University (Grant Number RES A1 B1-19).

References and Notes

- (1) Light, T. S. Ion-Selective Electrodes; National Bureau Standards Special Publication no. 314; NBS: Washington, DC, 1969; p 371.
- (2) Wayne, R. P. Chemistry of Atmospheres, 2nd ed.; Clarendon Press: Oxford, U.K., 1991; Chapters 1 and 5.
- (3) Barbero, J. A.; McCurdy, K. G.; Tremaine, P. R. Can. J. Chem.
 - (4) Licht, S.; Manassen, J. J. Electrochem. Soc. 1987, 134, 918.
 - (5) Stephens, H. P.; Cobble, J. W. Inorg. Chem. 1971, 10, 619.
- (6) Gigenbach, W. *Inorg. Chem.* **1971**, *10*, 1333. (7) Meyer, B.; Ward, K.; Koshlap, K.; Peter, L. *Inorg. Chem.* **1983**,
 - (8) Licht, S.; Forouzan, F.; Longo, K. Anal. Chem. 1990, 62, 1356.
- (9) Migdisov, A. A.; Williams, A. E.; Lakshtanov, L. Z.; Alekhin, Y. V. Geochim. Cosmoschim. Acta 2002, 66, 1713.
- (10) Schoonen, M. A.; Barnes, H. L. Geochim. Cosmoschim. Acta 1988,
 - (11) Eckert, W. J. Electrochem. Soc. 1998, 145, 77.

- (12) Kolthoff, L.; Moltzau, D. Chem. Rev. 1935, 17, 293.
- (13) Luther, I., G. W.; Richard, D. T.; Theberge, S.; Olroyd, A. Environ. Sci. Technol. 1996, 30, 671.
 - (14) McCarthy, V. N.; Jordan, K. D. Chem. Phys. Lett. 2006, 429, 166.
- (15) Joshi, R.; Ghanty, T. K.; Naumov, S.; Mukherjee, T. J. Phys. Chem. A 2007, 111, 2362.
- (16) Lee, C.; Sosa, C.; Planas, M.; Novoa, J. J. Chem. Phys. 1996, 104, 7081.
- (17) Planas, M.; Lee, C.; Novoa, J. J. J. Phys. Chem. 1996, 100, 16495. (18) Smith, A.; Vencent, M. A.; Hillier, I. H. J. Phys. Chem. 1999, 103, 1132
- (19) Rode, B. M.; Hofer, T. S.; Randolf, B. R.; Schwenk, C. F.; Xenides, D.; Vchirawongkwin, V. Theor. Chem. Acc. 2006, 115, 77.
- (20) Vchirawongkwin, V.; Pribil, A. B.; Rode, B. M. J. Comput. Chem. 2010, 31, 249.
- (21) Kritayakornupong, C.; Vchirawongkwin, V.; Hofer, T. S.; Rode, B. M. J. Phys. Chem. B 2008, 112, 12032.
- (22) Kritayakornupong, C.; Vchirawongkwin, V.; Rode, B. M. J. Comput. Chem. 2010, 31, 1785.
- (23) Frick, R. J.; Hofer, T. S.; Pribil, A. B.; Randolf, B. R.; Rode, B. M.
- J. Phys. Chem. A 2009, 113, 12496. (24) Hofer, T. S.; Pribil, A. B.; Randolf, B. R.; Rode, B. M. Ab Initio Quantum Mechanical Charge Field Molecular Dynamics-A Nonparameterized First-Principle Approach to Liquids and Solutions; Academic Press,
- Elsevier Inc.: Amsterdam, 2001; Vol. 59. (25) Field, M. J.; Bash, P. A.; Karplus, M. J. Comput. Chem. 1990, 11, 700
 - (26) Gao, J. J. Am. Chem. Soc. 1993, 115, 2930.
 - (27) Bakowies, D.; Thiel, W. J. Phys. Chem. 1996, 100, 10580.
 - (28) Stillinger, F. H.; Rahman, A. J. Chem. Phys. 1978, 68, 666
- (29) Bopp, P.; Janscó, G.; Heinzinger, K. Chem. Phys. Lett. 1983, 98,
- (30) Brooks, B. R.; Bruccoleri, R. E.; Olafson, B. D.; States, D. J.; Swaminathan, S.; Karplus, M. *J. Comput. Chem.* **1983**, *4*, 187. (31) Berendsen, H. J. C.; Postma, J. P. M.; van Gunsteren, W. F.; DiNola,
- A.; Haak, J. R. J. Chem. Phys. 1984, 81, 3684.
- (32) Adams, D. J.; Adams, E. H.; Hills, G. J. Mol. Phys. 1979, 38, 387.
- (33) Ahlrichs, R.; Bär, M.; Häser, M.; Horn, H.; Kölmel, C. Chem. Phys. Lett. 1989, 162, 165.
- (34) Ahlrichs, R.; von Arnim, M. Methods and Techniques in Computational Chemistry: METECC-95; Cagliari: Sardinia, 1995
 - (35) von Arnim, M.; Ahlrichs, R. J. Comput. Chem. 1998, 19, 1746.
 - (36) Magnusson, E.; Schaefer, H. F., III. J. Chem. Phys. 1985, 83, 5721.
 - (37) Dunning, T. H., Jr.; Wadt, W. R. J. Chem. Phys. 1989, 90, 1007.
- (38) Dunning, T. H., Jr.; Hay, P. J. Modern Theoretical Chemistry: Methods of Electronic Structure Theory; Schaefer, H. F., III, Ed.; Plenum Press: New York, 1977; Vol. 3.
- (39) Franks, F. Water: a Comprehensive Treatise; Plenum Press: New York, 1972; Vol. 1.
 - (40) Scott, A. P.; Random, L. J. Phys. Chem. 1996, 100, 16502.
- (41) Grev, R. S.; Janssen, C. L.; Schaefer, H. F., III. J. Chem. Phys. **1991**. 95. 5128.
 - (42) DeFrees, D. J.; McLean, A. D. J. Chem. Phys. 1985, 82, 333.
- (43) Hofer, T. S.; Tran, H. T.; Schwenk, C. F.; Rode, B. M. J. Comput. Chem. 2004, 25, 211.
 - (44) Randolf, B. R.; Hofer, T. S.; Rode, B. M. Unpublished results.
- (45) Lock, A. J.; Woutersen, S.; Bakker, H. J. J. Phys. Chem. A 2001, 105, 1238.

JP104856Q